Assimilation of snow information into a cold regions hydrological model

A Dissertation Submitted to the College of Graduate and Postdoctoral Studies
In Partial Fulfillment of the Requirements
For the Degree of Doctor of Philosophy
In the Department of Geography and Planning
(Centre for Hydrology)
University of Saskatchewan
Saskatoon, Canada

by

Zhibang Lv

Permission to use

In presenting this thesis in partial fulfilment of the requirements for a Postgraduate degree from the University of Saskatchewan, I agree that the Libraries of this University may make it freely available for inspection. I further agree that permission for copying of this thesis in any manner, in whole or in part, for scholarly purposes may be granted by the professor or professors who supervised my thesis work or, in their absence, by the Head of the Department or the Dean of the College in which my thesis work was done. It is understood that any copying or publication or use of this thesis or parts thereof for financial gain shall not be allowed without my written permission. It is also understood that due recognition shall be given to me and to the University of Saskatchewan in any scholarly use which may be made of any material in my thesis.

Disclaimer

Reference in this thesis/dissertation to any specific commercial products, process, or service by trade name, trademark, manufacturer, or otherwise, does not constitute or imply its endorsement, recommendation, or favouring by the University of Saskatchewan. The views and opinions of the author expressed herein do not state or reflect those of the University of Saskatchewan, and shall not be used for advertising or product endorsement purposes.

Requests for permission to copy or to make other uses of materials in this thesis/dissertation in whole or part should be addressed to:

Head of the Department of Geography and Planning
117 Science Place
University of Saskatchewan
Saskatoon, Saskatchewan S7N 5C8 Canada

OR

Dean
College of Graduate and Postdoctoral Studies
University of Saskatchewan
116 Thorvaldson Building, 110 Science Place
Saskatoon, Saskatchewan S7N 5C9 Canada

Abstract

Spring and summer snowmelt runoff from the Canadian Rocky Mountains recharge many rivers and hence provide critical water supplies for a large portion of the population in western Canada. Because of the complex topography and vegetation conditions, the sparse network of observations of climate and snow properties, and the low quality of atmospheric model products, data assimilation (DA) is a potentially useful tool to improve the forecasting and prediction of snow properties and streamflow. To achieve better snowpack and streamflow estimations using DA, this research aims to: 1) evaluate the usefulness of SNODAS SWE data in Canada, and determine the influence of processes missing from the SNODAS model on the accuracy of SNODAS SWE, 2) explore the possibility of using remotely sensed data for detecting snow interception in forest canopies, 3) assimilate *in situ* measured and remotely sensed snow interception data into CRHM and assess their influence on the simulation of snow interception losses, 4) determine the optimal method to assimilate *in situ* snow measurements into the CRHM for prediction of basin snowpacks and streamflow.

The results illustrate: 1) missing snow processes (blowing snow transport and canopy snow interception and sublimation) in the SNODAS snow model contribute substantially to its overestimation of SWE, 2) canopy intercepted snow can be detected by optical remote sensing data (NDSI and NDVI), 3) automated snow depth data measured from an adjacent forest and clearing can be used in a mass budget to accurately quantify snow interception loss, and assimilation of *in situ* measured and remotely sensed snow interception information can all improve simulations of snow interception timing and magnitude, 4) assimilating *in situ* SWE and snow depth into CRHM generally improves the simulation of snowpack properties and streamflow, but the results varied among different assimilation schemes. A better SWE simulation through DA does not always lead to better prediction of streamflow. The advanced snow interception measurement and DA techniques presented here deepens the understanding of cold regions hydrological DA and improve the capacity to forecast and predict the hydrology of headwater river basins in the Canadian Rockies and other similar regions.

Acknowledgments

The thesis could not have been possible without the assistance of a variety of people and organizations. First and foremost, I would like to thank my supervisor, Dr. John Pomeroy, for giving me this opportunity to study in Canada and for his guidance and support throughout. I want to thank my committee: Dr. Xulin Guo, Dr. Warren Helgason, Dr. Alain Pietroniro, and Dr. Robert Patrick for their insightful comments that improved this research. I am also thankful to Dr. Barton Forman for serving as my external examiner.

I would like to thank the financial support from China Scholarship Council and the logistic support from Nakiska Ski Resort and Fortress Mountain Ski Resort. I am grateful to "May" Xiujuan Guan and Angus Duncan for helping me with the field work. Thank you to "Logan" Xing Fang for support in the CRHM model and field data collection. Thank you to Joni Onclin and Phyllis Baynes, who povided me travel and logistic support during my program. Many thanks to all the research scientists, postdoctoral fellows, technicians, and graduate students from the Centre for Hydrology for their friendly companion and insightfull scientific feedback.

This PhD was full of ups and downs, the company and support from my family and friends made this journey delightful. I would like to thank all my friends for the unforgettable memories and the help they provided. Thank you to my parents and brother, who always believing and always being there for me. My dear wife, Ning, for always by my side for the moments with tears and laughters, and for understanding every bit of my frustrations. I know this would have been much more difficult without your love and support, thank you.

Table of Contents

List of Tables

List of Figures

List of Abbreviations

4DVAR: Four-Dimensional VARiational data assimilation

AMSR-E: Advanced Microwave Scanning Radiometer for EOS

ARHYTHM: ARctic HYdrological and THermal Model

AVHRR: Advanced Very High Resolution Radiometer

BERMS: Boreal Ecosystem Research and Monitoring Sites

BRDF: Bidirectional Reflectance Distribution Function

BT: Brightness Temperature

CC: Circular Cut spruce forest

CLASS: Canadian LAnd Surface Scheme

CV: Coefficient of Variation

CRHM: Cold Regions Hydrological Model

DA: Data Assimilation

DEM: Digital Elevation Model

DSM: Digital Surface Model

EKF: Extended Kalman filter

EnKF: Ensemble Kalman filter

FLAASH: Fast Line-of-sight Atmospheric Analysis of Hypercubes

FMSL: Fortress Mountain Snow Laboratory

FR: Fisera Ridge

FRNF: Fisera Ridge North Facing slope

FRRF: Fisera Ridge Ridge Top

FRSF: Fisera Ridge South Facing slope

GCM: General Circulation Model

GCP: Ground Control Point

GEM: Global Environmental Multiscale

HM: Hay Meadow

HRU: Hydrological Response Unit

KF: Kalman Filter

LaF: Larch Forest

LAI: Leaf Area Index

LF: Level Forest

LiDAR: Light Detection And Ranging

LPP: Lodgepole Pine forest

LST: Land Surface Temperature.

MB: Model Bias

MCRB: Marmot Creek Research Basin

MESH: MEC-Surface & Hydrology

MEMLS: Microwave Emission Model of Layered Snowpacks

MF: Mixed Forest

MODIS: Moderate Resolution Imaging Spectroradiometer

MODSCAG: MODIS Snow Covered-Area and Grain size retrieval algorithm

NDFSI: Normalized Difference Forest Snow Index

NDSI: Normalized Difference Snow Index

NDVI: Normalized Difference Vegetation Index

NF: North Facing slope

NOAA: National Oceanic and Atmospheric Administration

NOHRSC: National Operational Hydrologic Remote Sensing Center

NRMSE: Normalized Root Mean Square Error

NSE: Nash-Sutcliffe Efficiency

NSM: NOHRSC Snow Model

NWP: Numerical Weather Prediction

OA: Old Aspen

OJP: Old Jack Pine

OL: Open Loop

PF: Particle Filter

PM: Passive Microwave

PRACTISE: Photo Rectification And ClassificaTIon SoftwarE

PV: Proportion of Vegetation

RGB: Red-Green-Blue

RT: Ridge Top

RMSE: Root Mean Square Error

SAR: Synthetic Aperture Radar

SAST: Snow-Atmosphere-soil transfer

SCA: Snowcovered Area

SCRB: Smith Creek Research Basin

SD: Standard Deviation

SDC: Snow Depletion Curve

SEA: Solar Elevation Angle

SFB: South Facing slope Bottom

SFT: South Facing slope Top

SHE: Système Hydrologique Européen

SNODAS: SNOw Data Assimilation System

SRM: Snow Runoff Model

SWE: Snow Water Equivalent

UC: Upper Clearing

UofS: University of Saskatchewan

USGS: United States Geological Survey

VIC: Variable Infiltration Capacity

VV: Vista View

CHAPTER 1: Introduction

1.1 Background

Snow is a critical but temporary land surface component of cold regions. Snowmelt runoff is the main water resource of many rivers and hence provides essential water supply for agriculture, industry, and domestic use over a large portion of the Earth's surface. The high albedo of snow also changes global energy budgets through reflecting large portion of solar radiance directly back to the atmosphere. Because of climate change, the timing and extent of snowcover as well as snowmelt runoff have faced great changes in many regions during the past few decades (Bavay et al., 2009; Horton et al., 2006; Krogh and Pomeroy, 2018; Musselman et al., 2017; Rasouli et al., 2014; Rasouli et al., 2015; Stewart, 2005). Feedbacks from these changes also contribute to further climate change (Groisman and Davies, 2001). Therefore, determining the timing and extent of snowcover is not only crucial for the present but also critical for future global water security.

The Canadian Rockies form the headwaters of major rivers that provide essential water supply for large portions of western Canada and the northwestern United States. The complex topography, land cover, and hydrological processes and sparse meteorological and snowpack observations result in challenges for assessing snowcover extent and snowmelt runoff magnitude and timing. NOAA's National Operational Hydrologic Remote Sensing Center's (NOHRSC) SNOw Data Assimilation System (SNODAS) provides the only high resolution snow products for these areas (Carroll et al., 2001). However, the accuracy of these products and the influence of their snow model's structure on the accuracy of these products have not yet been explored in Canada.

Needleleaf forests cover a large portion of the Canadian Rockies, and the snow interception by and sublimation from the forest canopy greatly influence snow accumulation under the canopy (Ellis et al., 2010). Many researchers have developed snow interception measurement approaches that can measure canopy snow interception quantitatively or qualitatively. However, these measurements are confined in single-tree or small catchment scales (Friesen et al., 2015). This makes large-scale validation of snow interception model simulation impossible. The potential of using satellite remote sensing data to detect forest canopy snow interception has not been explored.

Observations and modelling are two approaches for determining the time and magnitude of snow on the ground or on the canopy. However, despite their merits, they each have drawbacks. Observations typically have limited spatial coverage (automatic stations) or low repeat frequency (satellite sensor), whereas models are simplified

representations of the real world, and their simulation results are highly influenced by the quality of input data, correctness of the model and the veracity of model parameterizations (Figure 1-1). In mountainous area, complex topography and vegetation condition limited the spatial representations of climate station data. Considering the sparse distribution of observation stations in many regions, the products from climate models can be the only forcing data available to run the hydrological models. However, these climate model products typically have relatively low accuracy and are of lower spatial resolution than the hydrological models they run. This has triggered the necessity of data assimilation (DA), which merges the advantage of observation (e.g., relatively higher accuracy) and modelling (e.g., low cost and consistent at reasonable spatial and temporal scales), for better simulation of snow on the ground and under forest canopies (Liu et al., 2012).

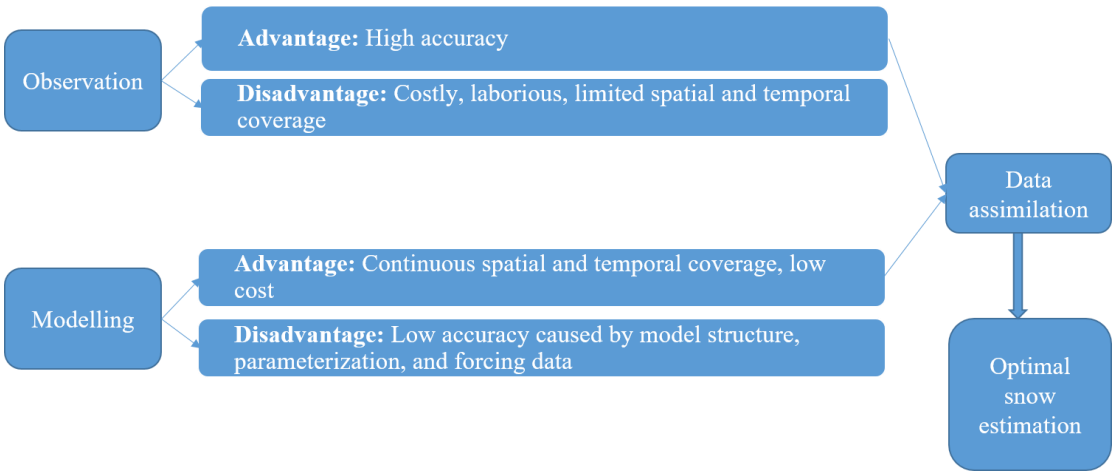

Figure 1-1. Advantages and disadvantages of observation and modelling in cold regions hydrology research.

Many snow DA studies have been conducted in cold regions around the world. However, most of the research has been done with simpler models (Bergeron et al., 2016; Franz et al., 2014; Slater and Clark, 2006; Stigter et al., 2017). The potential influence of DA on multilayer, physically based models that contain a full suite of snow redistribution and ablation processes still needed to be explored (Magnusson et al., 2017). Further, those studies were mainly focussed on the assimilation of snow depth (Kumar et al., 2014; Stigter et al., 2017), snow cover fraction (Andreadis and Lettenmaier, 2006; Rodell and Houser 2004), and SWE (Franz et al., 2014; Liston and Hiemstra, 2007). The assimilation of canopy intercepted snow information has not been studied. Assimilations of ground snowpack and canopy snow information from *in situ* or remotely sensed measures into the multilayer, physical models that contain a full suite of snow redistribution and ablation processes are believed to have great potential to benefit the accurate estimation of snowpack and snowmelt runoff in mountain headwater drainage basins.

1.2 Literature review

The literature review provides an overview of detailed features of snow interception on the forest canopy, cold regions hydrological modelling, and DA.

1.2.1 Snow interception in coniferous forests

Snowmelt is the main spring to early summer water resource for many rivers in cold regions. The amount of water that can be recharged to rivers in these regions is strongly controlled by the accumulation of the seasonal snowpack, which is affected by various factors such as sublimation and redistribution. In open areas, snowfall which reaches the ground can be redistributed by wind and sublimated from snow that is transported as blowing snow (Pomeroy et al., 1993). In needleleaf forests, redistribution is controlled by the canopy interception (Nakai et al., 1994; Pomeroy and Gray, 1995). Snow is first intercepted in the canopy, and remains there for a few hours to tens of days, and then leaves the canopy mainly through falling to the ground, sublimation, and meltwater drip (Hedstrom and Pomeroy, 1998; Pomeroy et al., 1998b; Suzuki and Nakai, 2008). These processes can reduce the SWE on the ground under the canopy compared to that in a clearing. Kuz'min (1960) reported that the mean SWE under the pine and spruce forests were 5%–35% and 10%–60% lower than in nearby open areas in Russia. Pomeroy and Schmidt (1993) found that in the midwinter in Canadian boreal forests, 60% of the snowfall was intercepted, and the sublimation of intercepted snowfall can reach 30% of the annual snowfall. Storck et al. (2002) conducted experiments with weighing lysimeters, cut-tree and manual snow surveys in the Umpqua National Forest in USA; they found approximately 60% of the annual snowfall was intercepted by the canopy during the study period. Therefore, understanding and quantifying the processes related with interception is important for the water resource management of cold regions.

1.2.1.1 Interception of snow and subsequent sublimation, melt and unloading

Snow interception is a complex process that is affected by various factors. Miller (1964) stated that the amount of snow that can be intercepted in a forest is mainly controlled by three factors: canopy morphology, wind speed, and air temperature. The snow interception accumulation rate is controlled by the interception efficiency of canopy branches. This interception efficiency deceases with the increase of wind speed, air temperature, density of intercepted snow, and elastic rebound of snow crystals whilst increases with the increase of canopy density, snow crystal size, and horizontal cross-sectional areas of branches (Gubler and Rychetnik, 1991; Pomeroy and Schmidt, 1993; Schmidt and Gluns, 1991; Schmidt and Pomeroy, 1990). Schmidt and Gluns (1991) found that interception efficiency of a branch increased and then decreased with increasing snowfall event size. However, Hedstrom and Pomeroy (1998) found that interception efficiency declines with increasing snowfall in the cold boreal forest. This

contrast may be caused by the scaling issue between individual tree and forest stand interception efficiencies. Interception efficiencies vary between deciduous and coniferous trees. Kuz'min (1960) reported that the SWE under the deciduous forests is not much different from that of neighboring open areas but quite different from that of the coniferous forests. There are difference in collection efficiency between coniferous trees. Satterlund and Haupt (1970) assessed two tree species with considerable morphological differences and found that there was difference in the intercepted snow amount between different tree species.

As mentioned above, intercepted snow leaves the canopy mainly through three ways: falling to the ground, sublimation, and meltwater drip (Andreadis et al., 2009; Hedstrom and Pomeroy, 1998; Suzuki and Nakai, 2008). Sublimation is the process that the snow on the canopy becomes vapour and directly goes back to atmosphere (Schmidt, 1991). The percentage of sublimation snow in total interception varies from location to location. Lundberg and Halldin (1994) studied the sublimation of intercepted snow by a weighted hanging-tree method and found that the sublimation rate can reach 3.3 mm per 24 h in a spruce canopy. They claimed that the most important factors that affect sublimation are relative humidity, aerodynamic resistance, wind speed, and intercepted mass. Lundberg et al. (1998) used the gamma ray attenuation data to measure the sublimation of intercepted snow on a forest canopy in Scotland. They found that more than 30% of intercepted snow can be sublimated. Pomeroy et al. (1998b) measured and modeled the intercepted snow sublimation in the southern boreal forest in central Canada. The found the intercepted snow sublimation rate can up to 3 mm/day for the full-size jack pine. They observed the sublimation of intercepted snow account for 13%, 31%, and 40% of annual snowfall in mixed spruce–aspen, mature pine, and mature spruce, respectively. Nakai et al. (1999a, 1999b) studied the sublimation of intercepted snow in a cool-temperate maritime climate in Japan; they found that the sublimation efficiency increases with the increase of the ratio between the snow-covered area and crown projection area. Parviainen and Pomeroy (2000) coupled the snow interception and sublimation algorithms from Pomeroy et al. (1998b) to the Canadian Land Surface Scheme (CLASS). They tested the model at two jack pine stands for two snowfall events and found the coupled sublimation model can predict the intercepted snow sublimation losses well and the sublimation rate can reach to 0.76 mm for the mature jack pine stand. Storck et al. (2002) used a large lysimeter and cutting trees to measure the sublimation of intercepted snow. They found that when temperature remained below the freezing point after snowfall, sublimation is dominant in the release processes, and the observed maximum sublimation rate was 4.3 mm SWE per 7 hours. However, the sublimation rate was too trial in the maritime mountainous climates as meltwater drip and unloading are the dominant intercepted snow removal processes. Montesi et al. (2004) conducted a study on the sublimation of intercepted snow in the U.S. They put one cut subalpine fir and an artificial conifer at two elevations. They found that sublimation rates were very large when the lower-elevation site had warmer temperatures, lower relative humidity, and higher wind speed. Around 20%–30% of

total snowfall was sublimated on the canopy during the research period. Suzuki and Nakai (2008) studied the sublimation in a coniferous plantation forest and found that almost 26% of the total snowfall was sublimated to the atmosphere and most of it was from canopy intercepted snow.

Sublimated snow does not contribute to the streamflow of the basin, but that unloaded through falling and meltwater drip does. Mass release of intercepted snow occurs as a result of mechanical wind effects or snow melt. These processes are controlled by the adhesion of the snow to the tree branches (Andreadis et al., 2009). Hedstrom and Pomeroy (1998) found that the unloading of intercepted snow is mainly controlled by the unloading rate coefficient and time after snow load. Meltwater drip is rare in the low-temperature midwinter continent environments. Kittredge (1953) measured the meltwater drip of the forest canopy in Sierra Nevada and found that meltwater drip rarely happened in the forest, and the percentage of meltwater drip was only 2% of the total snowfall. However, in some maritime forest areas, the meltwater drip can be relatively large. Stock et al. (2002) studied the removal of intercepted snow in a maritime mountain in the U.S. They found that when temperature is high, sublimation seldom happens, and the removal of intercepted snow is dominated by falling and meltwater drip. The meltwater percentage can reach 72%, and the falling can reach 28% of the unloading of intercepted snow. The intercepted snow meltwater drip amount can be modelled by introducing a threshold ice-bulb temperature in which the intercepted snow is all unloaded when exceeded for certain amount of time (Ellis et al., 2010; Gelfan et al., 2004)

1.2.1.2 Measurement of snow interception

Because of the complexity of the interception process and irregular shape of trees, direct measurement of the intercepted snow is difficult. Mass budgeting, which compares the difference in the increases of snow accumulations between the forest floor and a nearby clearing or open area over the course of a snowstorm or a snow season, is a common method to determine the amount of intercepted snow for snow storm or the snow loss caused by snow interception and sublimation for a snow season (Pomeroy and Schmidt, 1993). The increase in snow accumulation can be determined by precipitation gauges (e.g., Koivusalo and Kokkonen, 2002), automated SWE measurements (e.g., Lundberg et al., 1998; Floyd and Weiler, 2008), and snow survey (e.g., Hedstrom and Pomeroy, 1998).

To directly measure the snow interception, some early researchers knocked the snow off from a branch or tree and weighed it (Goodell, 1959; Miller, 1964). But this method is labourious and time consuming and only provides interception magnitude at a point scale for a single storm. To continuously measure snow interception, a cut tree branch (e.g. Schmidt and Gluns, 1991), a whole tree (e.g. Pomeroy and Schmidt, 1993; Storck et al., 2002), or artificial structures (e.g., boards in Floyd and Weiler, 2008; artificial tree in Schmidt et al., 1988) can be connected to a lysimeter to measure the weight

change during the interception processes. These methods mentioned above are capable of providing good measurements for point scale, but it is challenge to scale this point data up to a catchment or regional scale. Martin et al. (2013) used a trunk compression sensor installed in a living tree to measure the interception magnitude during a storm. However, this method is still a prototype and does not work when the tree freezes in cold weather.

Larger scale snow interception measurements can be obtained through signal attenuation approaches. Lundberg et al. (1998) used emitted gamma ray attenuation to measure snow interception along a path length (35 m) through a forest stand as intercepted snow impacts the attenuation of gamma rays emitted from a radioactive source. Magnusson (2006) explored the usage of active impulse radar system in measuring snow interception and found intercepted snow affects radar signal attenuation. These methods can measure snow interception at larger scale than a single tree. However, the footprint of the sensors they used still restricts usage of these methods in catchment or regional scales for snow interception measurement.

Optical photography has been used to detect the presence of intercepted canopy snow based on the fact that snow has much higher reflectivity than tree canopy. Tennyson et al. (1974) first tried using a time-lapse movie camera to develop a snow load index to represent the canopy snow load. Pomeroy and Schmidt (1993) modeled the intercepted snow sublimation based on the sublimation algorithm and the relationship between digital-camera imagery derived snowcovered area in the canopy and snow mass on a weighed hanging tree. Floyd and Weiler (2008) used a time-lapse digital camera to measure the canopy snowcovered area (ratio of snow-covered pixels to total pixel on canopy in the image) for rain-on-snow events. Parajka et al. (2012) used a time-lapse camera to detect the intercepted snow on a canopy and compared this detected canopy snow information to the simulation of the snow interception model developed by Hedstrom and Pomeroy (1998). Garvelmann et al. (2013) used a 45-camera time-lapse network to record the canopy snow coverage and timing of interception and unloading in several mesoscale catchments. Although the optical photography is able to provide relative magnitude and timing of interception, which can be used to validate a snow interception model's performance (Parajka et al., 2012; Stähli et al., 2009), its usage is still confined at small catchment scales. Snow interception measurements at regional or global scales have not been found in the literature.

1.2.1.3 Modeling of Snow interception

Many models were developed by researchers to simulate the snow interception processes. Most of them determine the snow interception using the initiate snow load, the snowfall rate, and the maximum snow storage capacity of the canopy, which is determined by air temperature, fresh snow density, and canopy coverage. The very first model that was developed for snow interception simulation was proposed by Satterlund and Haupt (1967). They studied the snow interception of two coniferous tree species

(Douglas fir and white pine) and found that snow interception follows the classical law of autocatakinetic growth. Their general equation for snow interception was:

$$I_s = S/[1+e^{-k(P-P_0)}] \quad (1.1)$$

where I_s is the interception storage, S is the storage capacity of the canopy, k is a constant that express the interception storage rate, P and P_0 are accumulated snowfall and snowfall at the time of the most rapid storage, respectively. In this model, k has to be determined for each tree species.

Hedstrom and Pomeroy (1998) found that Satterlund and Haupt's model did not describe observed snow interception in the boreal forest. They developed a model that included more general tree canopy parameterizations such as leaf area index (LAI) and canopy cover. They assumed that the interception efficiency increases when canopy density increases but deceases with canopy snow load increasing and unloading increases with time. For a snowstorm, the snow interception before unloading is given by:

$$I_{HP} = (L^* - L_0)(1 - e^{-mP}) \quad (1.2)$$

where I_{HP} is the canopy interception load before the beginning of unloading, L^* is maximum snow the canopy can hold, L_0 is the initial canopy snow load at the beginning of the storm, e is the base of the natural logarithm, P is the snowfall, m is a proportionality factor that can be derived from the following equation:

$$m = \frac{C_P}{L^*} \quad (1.3)$$

where C_p is the maximum plan area of the snow-leaf contact per unity area of ground and it's value can be determined by:

$$C_P = \frac{C_C}{1-\frac{C_C uH}{wJ}} \quad (1.4)$$

where C_c is the canopy cover, u is the wind speed, H is the canopy height, w is the vertical velocity of a snowflake falling through the gap in the canopy, and J is the mean forest canopy downwind distance.

The L^* in Equation 1.2 can be calculated by the following equation:

$$L^* = MS * LAI \quad (1.5)$$

where LAI is the leaf area index of the canopy, MS is the maximum snow load per unit branch area and it can be determined by:

$$MS = \bar{S}(0.27 + \frac{46}{\rho_S}) \quad (1.6)$$

where value of $\bar{S}$ should be 6.6 and 5.9 kg/m^2 for pine and spruce, respectively, ρ_s is the fresh snow density.

Many researchers borrowed the concept or equations from the Hedstrom and Pomeroy (1998) model for their snow interception models (e.g. Bartlett et al., 2006; Gelfan et al., 2004).

Andreadis et al. (2009) developed a series of models to simulate the snow accumulation and ablation processes in forested environments. They incorporated the air temperature influence on canopy snow interception and their snow interception (I_A) at a given time step is:

$$I_A = fP_s \quad (1.7)$$

where I is the intercepted snow water equivalent during a time step, f is the efficiency of snow interception (0.6), and P_s is the snowfall over the time step. Snow interception on the canopy will continue until it reached its maximum interception capacity (B).

$$B = L_r * m * (LAI) \quad (1.8)$$

where B is the maximum interception capacity, LAI is the single-sided leaf area index of the canopy, m is determined by the observations of maximum snow interception capacity, and L_r is the leaf area ratio and it can be calculate by a step function of air temperature (Andreadis et al., 2009),

$$\begin{aligned} Lr &= 4.0 && T_a > -1\ ^\circ c \\ Lr &= 1.5T_a + 5.5 && -1\ ^\circ c \leq T_a < -3\ ^\circ c \\ Lr &= 1.0 && T_a \leq -3\ ^\circ c \end{aligned} \quad (1.9)$$

With the development of remote sensing, more and more detailed canopy structure metrics are available and hence some researchers incorporated them into their recent models (Moeser et al., 2015; Roth and Nolin, 2019). Moeser et al. (2015) assumed that canopy interception is mainly controlled by the log-transformed canopy structure variables (mean distance to canopy (x1, unit: m), canopy closure (x2), total open area (x3, unit: m^2)) and snowstorm event size. The interception amount (I_m) of a snowstorm is given by:

$$I_M = \frac{I_{Mmax}}{1+e^{-0.3(P-13.3)}} \quad (1.10)$$

where I_{Mmax} is the interception storage capacity and it can be determined by:

$$I_{Mmax} = m1(x1) + m2(x1)^2 + m1(x2) + m2(x2)^2 + m1(x3) + m2(x3)^2 + b \quad (1.11)$$

Most snow interception models were developed in continental snow climates and the influence of air temperature was not found important for most models. Working in the Pacific Northwest, Roth and Nolin (2019) developed a model that incorporated both temperature and detailed canopy structure in their snow interception model. The interception amount (I_R) of a storm is given:

$$I_R = P^{\zeta} \quad (1.12)$$

where ζ is the Roth parameter that controlled by air temperature and canopy structure:

$$\zeta = 0.04 * T_a - 0.75 * G_z + 1.56 \quad (1.13)$$

where G_z is the ratio of median gap length to change in height of the canopy.

This model was tested against the models from Hedstrom and Pomeroy (1998), Andreadis et al. 2009, and Moeser et al. (2015) in both a maritime and continental snow climate. The results illustrated that this model outperformed all other models in the maritime climate site, where canopy snow is more sensitive to the relatively high winter air temperature. In the continental snow climate (Marmot Creek Research Basin, Alberta), the model from Hedstrom and Pomeroy (1998) still obtained the best results.

1.2.2 Hydrological modelling in cold regions

Modelling is an important aspect of research on cold regions hydrology since it helps to understand the present condition of water cycling and shows us past and future situations. Many hydrological models were developed to simulate the mass and energy balance of cold regions snow processes: such as Variable Infiltration Capacity (VIC) (Wood et al., 1992), NOHRSC Snow Model (NSM) (Carroll et al., 2001), and Cold Regions Hydrological Modelling platform (CRHM) (Pomeroy et al., 2007). Anderson (1973) described a snow accumulation and ablation model–SNOW-17. SNOW-17 is a conceptual index model using air temperature as the only index for the determination of energy balance and snow grain size. This model does not simulate the snow redistribution by canopy interception and wind but can simulate most of the processes happening within a snow pack, although only two inputs (temperature and precipitation) are required. In the 1980s, the Danish Hydraulic Institute, SOGREAH (France) and the

Institute of Hydrology (UK) developed the Système Hydrologique Européen (SHE) model (Abbott et al., 1986, Beven et al., 1980). It is a physically based distributed model that simulates eight processes (e.g., snowfall and snowmelt) in every grid point. This model is highly spatially detailed, so it requires large amounts of data inputs and complex parameter estimation. Its canopy interception component is based on the rainfall interception model developed by Rutter et al. (1971) in which the water storage on the canopy is determined by the amount of intercepted water minus evaporation and drainage. Wood et al. (1992) introduced the VIC model to link with general circulation models (GCMs) to simulate land surface hydrology over large areas. The VIC model needs estimation of the infiltration parameter, the evaporation parameter, and the base flow recession coefficient. The authors compared the stream discharge results of this model and GCM land surface schemes and found that the simulation of VIC model was closer to measured streamflow. With the development of this model, many cold regions snow processes such as snow interception and blowing snow transport have been included in it. Wigmosta et al. (1994) described the distributed hydrology-vegetation model to simulate the mass and energy balance of evaporation, transpiration, snow accumulation and melt, and runoff generation. Canopy evapotranspiration was calculated by a two-layer (overstory and understory) Penman–Monteith approach. Snow accumulation and ablation were modelled using an energy balance approach that includes the topographical and vegetation effects. The upgraded version–the Distributed Hydrology Soil Vegetation Model (DHSVM) now is capable of simulating the snow interception and release in the forest canopy. Sun et al. (1999) developed a simple snow-atmosphere-soil transfer (SAST) energy balance physically based snow model. This model divides the snow pack up to three layers, depending on snow depth, and simulates crucial physical processes occurring in each layer such as snow compaction, heat conduction, snow grain evolution, and snow melting. However, this model can not simulate the snow interception and sublimation in forest and the blowing snow transport and sublimation in the open areas. Kuchment et al. (2000) developed a distributed physical model to simulate the snowmelt and rainfall runoff generation in permafrost regions. This model includes algorithms for simulating snowcover formation and melt, evaporation, thawing of the ground, basin water storage dynamics, and flow on the land surface, subsurface and channels. The important feature of this model is that it accounts for the effects of the depth of thawed ground on the water balance between surface and subsurface layers. Kuchment et al. (2000) took a three-step calibration approach to the model and found that the main parameters and accuracy of the model was improved after that. Gelfan et al., (2004) added snow interception and sublimation process to this model. Zhang et al. (2000) developed the arctic hydrological and thermal model (ARHYTHM), for simulation of the arctic region's hydrological processes. This model uses physical equations to present snowmelt, evapotranspiration, subsurface flow and overland flow. Moreover, a degree-day method was used to simulate snow melt when there is not enough data for utilizing the energy balance method. Another physically based model, NSM (Carroll et al., 2001) is a distributed multi-layer snow model. The model borrowed the snow surface temperature solution

from Tarboton and Luce (1996) and the snow thermal dynamics for energy and mass fluxes algorithms from Jordan (1990). It computes the snowpack and soil properties (SWE, internal energy, thickness, temperature, and water content) for three snow layers and two soil layers separately. However, because the model is spatially uncoupled, it does not simulate the transport of blowing snow even though it simulates the sublimation of blowing snow. Another important process that missing in the NSM is the forest canopy snow interception and sublimation. Pietroniro et al. (2007) coupled the atmospheric model, land-surface scheme and a hydrological routing scheme into the MEC Surface and Hydrology (MESH) system. They conducted numerical prediction experiments in the Great Lakes basin in North America and found that MESH is able to provide a deeper understand of different land-surface schemes' performances and reliable ensemble hydrological forecasts for the research area.

As mentioned above, many models have been developed for hydrological simulation in the cold regions, but most of them do not include the snow interception in the forests and the blowing snow transport in the open areas. However, these two processes are the main factors that control the snow redistribution in most cold regions. Therefore, selecting a model that can simulate all important snow processes is the top priority for hydrological modelling in the cold regions.

1.2.2.1 Cold Regions Hydrological Model platform (CRHM)

The CRHM platform was developed by Environment Canada, the University of Wales, Aberystwyth and the Centre for Hydrology, University of Saskatchewan. Compared to the models mentioned above, CRHM has a more complete range of hydrological processes (Table 1-1) for cold regions such as the Canadian Rockies (Pomeroy et al., 2007). Users of CRHM can construct their own model by selecting the modules from the CRHM module library or even add their own module to the platform based on input data availability, research scale and interest. The basic spatial simulation unit of CRHM is the hydrological response unit (HRU) that is mainly defined by basin topography, hydrography, and vegetation. A detailed description of CRHM was provided by Pomeroy et al. (2007) and recently updated (Fang and Pomeroy, 2016; Pomeroy et al., 2016).

Table 1-1. Cold regions hydrological models and snow processes they simulate.

Model name	Interception and sublimation	Snow albedo	ET	Blowing snow	Frozen soil infiltration	Snow melt	Flow
SNOW-17	NO	YES	YES	NO	NO	TI	NO
VIC	YES	YES	YES	YES	YES	EB or TI	YES
SHE	NO	YES	YES	NO	NO	EB	YES
DHVSM	YES	YES	YES	NO	NO	EB	YES
ARHYTHM	NO	YES	YES	NO	NO	EB or TI	YES
SAST	NO	YES	YES	NO	NO	EB	NO
MESH	YES	YES	YES	YES	YES	EB	YES
NSM	NO	YES	NO	NO	NO	EB	YES
Runoff model (Kuchment et al.,2000; Gelfan et al., 2004)	YES	YES	YES	YES	YES	EB	YES
CRHM	YES	YES	YES	YES	YES	EB	YES

(YES and NO denote whether the model can simulate the process or not. EB indicates Energy balance. TI means Temperature Index.)

1.2.3 Data assimilation

1.2.3.1 Principles of Data Assimilation

DA is an approach to integrating the data from a variety of sources, resolutions, and accuracies with model predictions to improve deterministic model accuracy (McLaughlin et al. 2005). In other words, DA methods are designed to merge observation data, including *in situ* and remote sensing data, with estimates from hydrological models. By combining these complementary information sources, a more objective estimate of the actual state of a natural system can be gained. In a DA process,

various mathematical methods are used to quantify observational and hydrological model errors, and the model states are then updated through an optimal combination of observation and model simulation (Moradkhani, 2008). Reichle (2008) used a simple DA system to illustrate the basic concept. This study assumed that in a specific time window, there will be a model-simulated variable m with error variance (uncertainty) x^2 and observation o with error variance y^2. Then, one can use an objective function J to present the misfit among the true state z, the model estimate m and the observation o. After minimization of J with respect to z yields, a z^* can be obtained, which is the least-squares estimate of z, presented by m, o, x^2 and y^2. Now, a $K = x^2 / (x^2 + y^2)$ is introduced, where K is the Kalman gain; $0 \leq K \leq 1$ (Reichle, 2008). Then, z^* can be calculated by m, o and K. The model states can then be updated using K.

DA is mainly used to solve three problems in hydrological modelling (Liu et al., 2012). The first one is that of updating states, in which observations are assimilated into models to update the state variables. The second one is optimization or calibration. Instead of using observations to directly update the model state variables, this DA strategy using observations to estimate or optimize model parameters to achieve optimal simulation. The third one is error updating, in which DA is used to estimate the difference between model forecast and observation and use this difference to revise the future predictions of the model. This type of DA is widely used in operational practice. For example, this DA may helps the forecaster to decide whether or not to release a warning according to recent information on errors in the model outputs.

1.2.3.2 Data Assimilation Methods

There are many DA methods, such as simple direct insertion and various Kalman filters. Different methods use their own algorithms to calculate K. At the very beginning, hydrologists used the direct insertion approach in the DA process. In this process, the model state is directly replaced by the observation when and where an observation is available. Liston et al. (1999), Pan et al. (2003) and Rodell et al. (2004) used this approach to replace their model states by *in situ* and remotely sensed observations in their snow property studies and DA systems. This approach is time saving and easily implemented. However, the assumption on which this approach is based—that the observation is perfect, and the model output has no value—is too simple and, in most cases, far from the reality since the model performance may sometimes be even better than that of the observation (Sun et al., 2004). Later DA approaches, which have developed various sophisticated and better algorithms to determine the uncertainty of model estimates and observations, combine the advantages of both of these resources (Liu et al., 2012; Reichle et al., 2008).

Traditional Kalman filters (KF) update the model state variables when an observation is shown and explicitly compute the error covariances through an additional matrix equation that propagates error information from one time step to the next (Reichle, 2008). This method performs well when the error of the model and observations are

both Gaussian distributed and mutually independent and temporally uncorrelated, but the model needs to be linear. The nonlinear version of the Kalman filter is extended Kalman filter (EKF), which can be used in nonlinear models. However EKF cannot be used for nonlinear models and in a large study area because its error covariance integration requires large computational capability (Reichle et al., 2002). The alternative method is the ensemble Kalman filter (EnKF), which can perform better since it avoids the complex integration of the state error covariance matrix by propagating an ensemble of states through a Monte Carlo approach from which the required covariance information is obtained at the time of the update (Reichle et al., 2002).

According to the updating frequency of state variables, DA algorithms can be divided into two groups: filter (sequential) and smoothing (batch) algorithms (Reichle, 2008). Filter algorithms update model state variables and compute the error covariance immediately when an observation is available. Such algorithms include direct insertion, traditional Kalman filter, EKF, EnKF, and particle filter methods. Smoothing algorithms, such as the four-dimensional variational DA (4DVAR), update the model state variables over a designated time interval. In this situation, the model state variables are not updated by a single observation as in the filter algorithm but by several observations. For this algorithm, one must consider the time dimension of the observation, and the error covariance must be calculated implicitly.

1.2.3.3 Data Assimilation Applications in Cold Regions Hydrology

Hydrological models for application to cold regions are developed in part to simulate the snow processes and eventually estimate basin streamflow discharge using various snow properties, including SWE, snow depth, and snowcovered area (SCA). With development of remote sensing concepts and technology, these snow properties can be measured in various temporal scales, spatial scales, and degrees of accuracy and thus provide a useful data resource for snow data assimilation systems.

SCA is an important snow parameter since it represents the horizontal extent and distribution of a snowpack. However, SCA is difficult to measure directly by traditional surface-based methods because of the large extent of snow cover. Fortunately, measurement of SCA became available with remote sensing technology as snowcover presence can be easily estimated from visible wavelengths. Especially in recent years, researchers developed algorithms (e.g., MODSCAG, Painter et al., 2009) to calculate the sub-pixel snowcover to overcome the problem caused by low resolution. SCA can be used for hydrological model DA in two ways. One approach is to directly assimilate SCA data to a model as the SCA is a state variable of the hydrological model. Clark et al. (2006) assimilated the MODIS SCA data to their conceptual snow model, which uses temperature index methods to simulate the accumulation and ablation of snowpacks, by using the EnKF method. They found that assimilation of SCA data improved the estimate of streamflow. Nagler et al. (2008) used the SCA data retrieved

from MODIS and SAR to update the snow runoff model (SRM) though a simple DA scheme. Results of their research showed that the runoff estimates updated by the combination of two sets of remote sensing data were superior to those obtained by using a single set of data. Another way is to retrieve SWE from SCA and then assimilate the SWE to a hydrological model when SCA is not the state variable of the model. Rodell and Houser (2004) developed a simple rule-based method for assimilating the MODIS SCA data to their model. Their rule is that if the model-simulated SWE is zero and the MODIS SCA fraction is more than 40%, then 5 mm SWE was added to the model, and if the model-simulated SWE is not zero and the MODIS SCA fraction is less than 10%, then the model SWE is removed, and the model SWE is unchanged under other situations. They found that both assimilated and control simulations contained errors, but assimilated simulations had a higher accuracy. Zaitchik and Rodell (2009) developed a more sophisticated model based on the rule of Rodell and Houser. They used an image up to 72 hours ahead to constrain the model simulation. This new algorithm improved SCA simulation performance at global scales when compared to the simple method of Rodell and Houser (2004). SWE can also be estimated from SCA by using the Snow Depletion Curve (SDC) (Gomez–Landsea and Rango, 2002). However, SDCs are heavily influenced by basin specifics such as topographical and meteorological conditions. Furthermore, different study areas need specific SDCs to fulfill the accuracy requirements. Andreadis and Lettenmaier (2006) used a simple SDC model to retrieve the SWE data from MODIS SCA data and then assimilated these SWE data to the VIC macroscale hydrological model by using EnKF. Validation by using the *in situ* SWE showed that this assimilation improved model performance. Kuchment et al. (2010) used MODIS-derived SCA to constrain a physically based snowpack model (Gelfan et al., 2004) parameters by comparing the model results to the ground-based point observations. They found that the streamflow simulation became more accurate thereafter. SCA is usually measured by optical remote sensors, which are heavily influenced by the weather condition. The optical remote sensors cannot penetrate cloud; this creates more uncertainty in the assimilation when more cloud covers the remote sensing image. Andreadis and Lettenmaier (2006) only used images with relatively low cloud cover (less than 20%). However, this also considerably reduced the amount of observation data, which could be used in DA.

SWE is the most important output of cold regions hydrological model simulation and hence is the most interesting input data for data assimilation. It can be estimated by both *in situ* measurements and remote sensing measurements. Liston and Hiemstra (2007) assimilated both ground-based and remotely sensed SWE data in a snow-evolution modeling system (SnowModel). The results showed that assimilation improved the SWE distribution of the model simulation, and the updated SWE was distributed more realistically than that estimated using observation data alone. With remote sensing technology, SWE can be obtained indirectly from SCA as mentioned previously and directly from microwave sensors. One of the advantages of microwave remote sensing (active or passive) is that it is not influenced by weather conditions.

However, microwave remote sensing data has its own disadvantages that limit its usage in hydrological DA. Most active microwave sensors (which emit signals and then collect the reflected energy) are airborne and thus have a small coverage area, low repeat frequency and high expense. Passive microwave data have relatively coarse resolution (e.g., AMSR-E, 25 km) since passive microwave sensors collect the low-energy microwaves emitted from the surface, rendering the passive microwave data only available in low spatial resolution. Low-resolution land surface DA is not suitable for the relatively high spatial resolution needs of physical hydrological modeling. Another disadvantage of AMSR-E data is that its algorithm is heavily influenced by snow grain size, snow depth, and liquid water content of the snow pack (Zaitchik and Rodell, 2009). These factors make the AMSR-E data unreliable for snow DA (Andreadis and Lettenmaier, 2006).

Some researchers also used land surface radiance data collected by satellite and ground-based sensors to update model-simulated SWE or snow depth by using an observation operator, which transfer the radiance to SWE or snow depth (Dechant and Moradkhani, 2011; Durand et al. 2009). Durand et al. (2009) assimilated ground-based passive microwave (PM) sensor-measured radiance into the SAST energy balance snow physics model using the EnKF method. They found that the snow depth bias was reduced from −53.3cm to −7.3 after DA. Dechant and Moradkhani (2011) used the brightness temperature (BT) data from AMSR-E to update the SNOW17 and the microwave emission model for layered snow pack (MEMLS) using the EnKF approach. The results showed that the flow estimate of the model was improved by DA. Toure et al. (2011) assimilated ground-based PM sensor-measured radiance into the snowpack energy and mass model-CROCUS using the EnKF method. CROCUS is more sophisticated than the SAST model as it divides the snowpack up into 50 layers and has 100 state variables. The ability to accurately simulate SWE and snow depth by CROCUS was largely improved after DA.

1.2.3.4 SNODAS

NOAA's NOHRSC developed and operates the SNODAS project (Carroll et al., 2001). SNODAS provides ~1 km spatial resolution and daily snow products for the conterminous USA since 1 October 2003 and for southern Canada since 1 December 2009. They assimilate ground-based snow data and remotely sensed data, such as NOHRSC Airborne Gamma SWE data and NOAA GOES/AVHRR snowcover data, into the NSM. The meteorological driving data used to force NSM is 1 km^2 resolution data, which were downscaled from a 13 km^2 resolution Numerical Weather Prediction (NWP) model (RUC2) product. The DA method used in the SNODAS project is the simple nudging method, which is also known as Newtonian Relaxation Procedure. In this assimilation procedure, the differences between model simulation and observation are first computed in each point. Second, the differences are interpolated into model grids. Third, the differences are divided by 6 to get a mean hourly nudging field for the last 6 hours. Lastly, the model is re-run for the last 6 hours, and the model estimate at

the end of each hour is nudged by using the nudging field produced in the last step (Carroll et al., 2006). The daily 30 arc-second resolution SNODAS products are archived by NOHRSC and are openly available to researchers from all over the world for various modelling and research purposes.

Clow et al. (2012) evaluated SNODAS SWE and snow depth data in the Rocky Mountains, Colorado, USA using independent ground-based snow survey measurements including snow depth and density in headwater basins. They found that the accuracy of SNODAS data in forested areas was higher than in alpine areas. In forested areas, the SNODAS explains 77% and 72% of the variance of SWE and snow depth, respectively, whereas it explains only 30% and 17% of the variance of SWE and snow depth, respectively, in alpine areas. Clow et al. (2012) developed a simple wind redistribution adjustment method for SNODAS data. This method reduced the RMSE of SNODAS snow depth and SWE data from 37 cm and 12 cm to 23 cm and 6 cm, respectively. The researchers also claimed that the SNODAS product is a reliable input data resource for moderate- and large-scale hydrological models. SNODAS has not been evaluated in Canada in any published study.

1.3 Research Gaps

From this literature review, the following research gaps were found in the research of snow interception measurement and snow information DA in the cold regions hydrology community.

1) Despite its potential utility as a snow data product, there has been no published validation of the US NWS SNODAS SWE data in Canada. Further, the influence of processes missing from the SNODAS NSM model, such as canopy interception and blowing snow transport, on the accuracy of the model has not been explored.
2) Canopy intercepted snow can have an extremely important influence on snow accumulation under needleleaf forests that cover much of the Northern Hemisphere. Snow interception observations have been limited to time-lapse camera photography, radiation attenuation and weighed hanging trees - research has not focussed on using satellite data to detect snow interception despite the potential benefits of frequent and large areal coverage.
3) Snow data assimilation research has mainly focussed on assimilating surface snowpack information. However, with the development of snow interception remote sensing, the potential benefits of assimilating snow interception data to cold regions hydrological models can now be explored.
4) Many modern hydrological models applied in cold regions now contain the full suite of snow redistribution and ablation processes. However, most snow data assimilation research has been conducted using simple conceptual models that lack these processes. As a result, the influence of assimilating snowpack properties on the performance of physically based models is not well known.

1.4 Objectives

Based on the research gaps identified, the research proposed here is aimed at improving snow information assimilation techniques and thus the simulation accuracy of snowpack properties on the ground and the forest canopy and streamflow. The specific research objectives are as follows:

1) Evaluate the accuracy of SNODAS SWE predictions in Canada, by comparing them to snow survey data in various landscape types, and determining the influence of processes missing from the SNODAS model on the accuracy of SNODAS SWE.
2) Explore the possibility of using of remotely sensed data for detecting intercepted snow presence on needleleaf forest canopies at the basin scale.
3) Assimilate ground-based and remotely sensed snow interception data into CRHM and assess their influence on the simulation of snow interception losses.
4) Determine the best methods to assimilate in situ snow measurements into a CRHM model that includes snow redistribution by wind and forest and ablation processes on complex terrain and evaluate how well assimilation of point snow observations improves the prediction of basin snowpack and streamflow.

1.5 Organization of chapters

This thesis consists of an introduction, four chapters that each address one research objective, and a summary chapter that synthesizes all of the research. Chapter 1 introduces the study background, research gaps, and objectives. Chapter 2 describes the validation of SNODAS SWE data in western Canada and the importance of including snow interception and blowing snow transportation in hydrological simulations in these regions (Objective 1). Chapter 3 illustrates the approach for detecting snow interception on needleleaf forest canopies using satellite remote sensing data (Objective 2). Chapter 4 addresses methods and the influence of assimilation of ground-observed and remotely sensed snow interception data into CRHM (Objective 3). Chapter 5 explores the ways to assimilate ground-based snowpack properties into a mountain CRHM model and evaluates the effects of this assimilation on snowpack and streamflow simulations (Objective 4). Chapter 6 summarizes all the findings of the preceding chapters and discusses the contributions and limitations of the present study.

CHAPTER 2: Evaluation of SNODAS Snow Water Equivalent in Western Canada and assimilation into a cold regions hydrological model

Status: submitted to Water Resources Research on April 11, 2019

Citation: Lv, Z., Pomeroy, J.W., and Fang, X., 2019. Evaluation of SNODAS Snow Water Equivalent in Western Canada and assimilation into a cold regions hydrological. Water Resources Research. in review.

Author Contributions: Zhibang Lv and John Pomeroy conceptualized this research. Zhibang Lv designed and performed simulations, conducted analysis, and wrote the manuscript. John Pomeroy provided data, helped with the idea formulation, and provided useful comments with regards to the content, structure and writing of the manuscript. Xing Fang helped with model construction, field data collection, and manuscript revision.

2.1 Preface

Snow water equivalent (SWE) is one of the most important physical properties of a snowpack. The US National Weather Service's Snow Data Assimilation System (SNODAS) provides snow products at high spatial (~1 km^2) and temporal (daily) resolution for the contiguous USA and southern Canada. However, the accuracy of these products and the influence of their snow model's structure on the accuracy of these products have not yet been explored in Canada.This study is aiming to: 1) evaluate the SNODAS SWE product in the boreal forest, prairie, and Rocky Mountains of western Canada against extensive snow survey measurements, 2) demonstrate that simulation of SWE in these environments where SNODAS has substantial errors can be achieved by assimilating SNODAS SWE data into a physically based Cold Region Hydrological Modelling (CRHM) platform, and 3) bias correct SNODAS.

2.2 Introduction

Snow is a crucial water resource in cold regions where much of the precipitation falls as snow and the main portion of annual streamflow runoff is generated by snowmelt (Doesken and Judson, 1996; Gray and Male, 1981). Therefore, accurately monitoring snow processes such as snowfall, accumulation, redistribution, sublimation, and melt along with tracking snow properties such as depth, density, and water equivalent are necessary and important for ecology, agriculture, forestry, industry, and other human activities. Snow water equivalent (SWE) is one of the most important physical properties of a snowpack, as it combines the information of snow depth and density to provide the amount of available water within the snowpack (Pomeroy and Gray, 1995).

One way to determine the SWE of a snowpack is by observation (e.g., field survey and remote sensing monitoring). However, ground observations typically do not provide enough information because they usually measure the SWE with limited spatial support or temporal resolution. But remote sensing SWE observations using microwaves have very coarse spatial resolution and limited ability to measure deep snow, redistributed snow, and snow under forest canopies (Derksen et al., 2003; Frei et al., 2012; Kinar and Pomeroy, 2015; Nolin, 2010; Peterson and Brown, 1975; Pulliainen and Hallikainen, 2001; Tait, 1998). In addition, hydrological models can simulate SWE continuously over a wide geographic range at various spatial scales for fine temporal resolution. However, these are simplified representations of reality, whether empirical or physical, and simulation quality relies on accurate forcing data and parameterization (Knoche et al., 2014; Vrugt et al., 2007). Due to these observation and model simulation problems, data assimilation, which is widely used in atmospheric and oceanic sciences, has been introduced to hydrology to improve SWE estimation in recent decades (Andreadis and Lettenmaier, 2006; Liston et al., 1999; Liu et al., 2012).

To provide better estimates of snow cover and associated snow properties in the USA, NOAA's National Operational Hydrologic Remote Sensing Center (NOHRSC) has developed the SNOw Data Assimilation System (SNODAS) project (Barrett, 2003). SNODAS provides fine spatial and temporal scale snow products for the conterminous USA since October 2003 and southern Canada since December 2009. There are three main components in SNODAS: data ingestion and downscaling of meteorological information from Numerical Weather Predication (NWP) models, a physically based NOHRSC Snow Model (NSM) that simulates snow mass and energy balance, and a data assimilation component that updates snowpack estimates using various ground-based and satellite observational data.

NSM (Carroll et al., 2001) is a distributed multi-layer snow model which borrowed the snow surface temperature solution from Tarboton and Luce (1996) and the snowpack thermal dynamics and energy and mass flux algorithms from Jordan (1990). It computes snowpack and soil properties (SWE, internal energy, thickness, temperature, and water

content) for three snow layers and two soil layers separately. However, as the model is spatially uncoupled, it does not simulate blowing snow transport fluxes even though it simulates the sublimation of blowing snow following Pomeroy et al. (1993). Other important processes missing from the NSM are the forest canopy snow interception, unloading, drip and sublimation processes. The NWP data that force the NSM were downscaled from Rapid Update Cycle (RUC2). The system is also capable to utilizing the Mesoscale Analysis and Prediction System (MAPS) data sets when RUC2 data are not available.

The daily 30 arc-second resolution SNODAS products are archived by NOHRSC and are openly available to researchers from all over the world for various modelling and research purposes. Many researchers have used SNODAS data in their research as it is the only data set that provides real-time spatially distributed snow properties in North America (Vuyovich et al., 2014). In hydrology research, SNODAS data have been used to validate remotely sensed SWE data (Azar et al., 2008; Tedesco and Narvekar, 2010; Vuyovich et al., 2014), been used to evaluate hydrological model performance (Artan et al., 2013; Barlage et al., 2010; Rittger et al., 2011), and been used for model calibration in ungauged basins (Boyle et al., 2014). SNODAS data have also been applied to the field of ecology, to study wildlife habitats and populations (Kays et al., 2008; Millington et al., 2010).

Although SNODAS data have been used in a wide variety of research, there are only a few studies that have validated their accuracy. SNODAS assimilates most available observations and rarely leaves other ground truth data for its evaluation. Anderson (2011) conducted a SNODAS validation in a watershed near Boise, Idaho, USA by using snow survey data and found that SNODAS underestimated SWE on the ground at most times and locations. Clow et al. (2012) evaluated SNODAS SWE and snow depth data in the Colorado Rocky Mountains, USA by using independent, ground-based snow survey data and water balance calculations in headwater basins. They found the accuracy of SNODAS data in forested areas was higher than in alpine areas, with SNODAS capturing 77% and 72% of variation of SWE and snow depth in forested areas but only 30% and 17% variation of SWE and snow depth in alpine areas. Schneiderman et al. (2013) found SNODAS SWE estimation fitted to snow survey SWE data performed better than that using two temperature index models in the Catskill Mountain region of New York State, USA. Hedrick et al. (2015) compared snow depth change data sets derived from SNODAS and LiDAR in northern Colorado and found that there was a reasonably strong correlation between two data sets, but the differences between two data sets were great in some locations. Dozier et al. [2016] suggested that SNODAS overestimates SWE during the melt period, possibly because of over-reliance on snow pillows which can overmeasure SWE during melt. They also noted that where elevational ranges are large, SNODAS can underestimate SWE at higher elevations due to assimilation of lower elevation snow pillow data. In Canada, despite the use of SNODAS by provincial water management and flood forecasting agencies, there has

not been validation and application research of the SNODAS product. The SNODAS assimilation frequency for the Boreal Ecosystem Research and Monitoring Sites (BERMS), Smith Creek Research Basin (SCRB), and Marmot Creek Research Basin (MCRB) areas are relatively low (Fall et al., 2014), and the impact of this low frequency on the accuracy of SNODAS SWE is unknown.

The objectives of this research are therefore 1) to evaluate SNODAS SWE data in various Canadian environments such as mountains, prairies, and boreal forest by comparing model products to historical snow survey data, 2) to demonstrate that simulation of SWE in these environments where SNODAS has substantial errors can be achieved by assimilating SNODAS SWE data into a physically based Cold Region Hydrological Modelling (CRHM) platform, and 3) to bias correct SNODAS.

2.3 Study area and data

The Boreal Ecosystem Research and Monitoring Sites (BERMS), Smith Creek Research Basin (SCRB), and Marmot Creek Research Basin (MCRB) represent three important landscapes in Western Canada: boreal forests, prairies, and mountains, respectively (Figure 2-1). These research sites were operated as part of the Changing Cold Regions Network (DeBeer et al., 2015) and have excellent quality and well documented snow surveys and site characteristics. A brief introduction of these sites is included here together with landscape and elevation range information of the snow survey transects and the corresponding SNODAS grid cells in the three sites (Table 2-1).

Table 2-1. Summary of landcover and elevation range of snow survey transects with corresponding SNODAS grid cells at all survey locations in western Canada.

Site	Location	Transects	Samples	Transects/Grid cell elevation range (m)	Grid cell main Landscapes (Percentage (%)/Samples)
BERMS	OJP	1	25	509-510/508-512	Coniferous forest (100/25)
	OA	1	25	509-510/508-511	Deciduous forest (100/25)
	FEN	1	25	482-483/481-486	Fen (100/25)
SCRB	LR-3	2	25,25	528,528/527-529	Grassland(9/0),Stubble(63/25), Wetland(15/13),Woodland(13/12)
	LR-6	2	25,25	529,529-530/525-530	Grassland(10/0),Stubble(64/25), Wetland(17/5),Woodland(9/20)
	SCR-2	3	25,25,10	525-526,524-525, 524-525/522-528	Grassland(15/25),Stubble(46/25), Wetland(27/0),Woodland(12/10)
	SCR-6	3	25,25,25	524,524,524/521-530	Grassland(36/25),Stubble(39/25), Wetland(13/14),Woodland(12/11)
	SC-1	2	25,25	510-511,511-512/509-515	Grassland(2/25),Stubble(71/25), Wetland(14/0),Woodland(13/0)
MCRB	HM	1	35	1430-1431/1422-1448	Forest (74/0)/Clearing(26/35)
	UC	2	30,30	1834-1846,1830-1852/1737-1872	Clearing(16/30),Forest(84/30)
	LF	1	11	1503-1509/1435-1560	Clearing(12/0),forest(88/11)
	VV	1	30	1939-1950,1930-1939/1850-2022	Clearing(30/20),Forest(70/10)
	FR	3	10,15,30	2286-2306,2302-2308, 2280-2306/2230-2508	north face slope (23/10),ridge top(14/15),south face slope(31/20), Larch forest under south face slope (32/10)

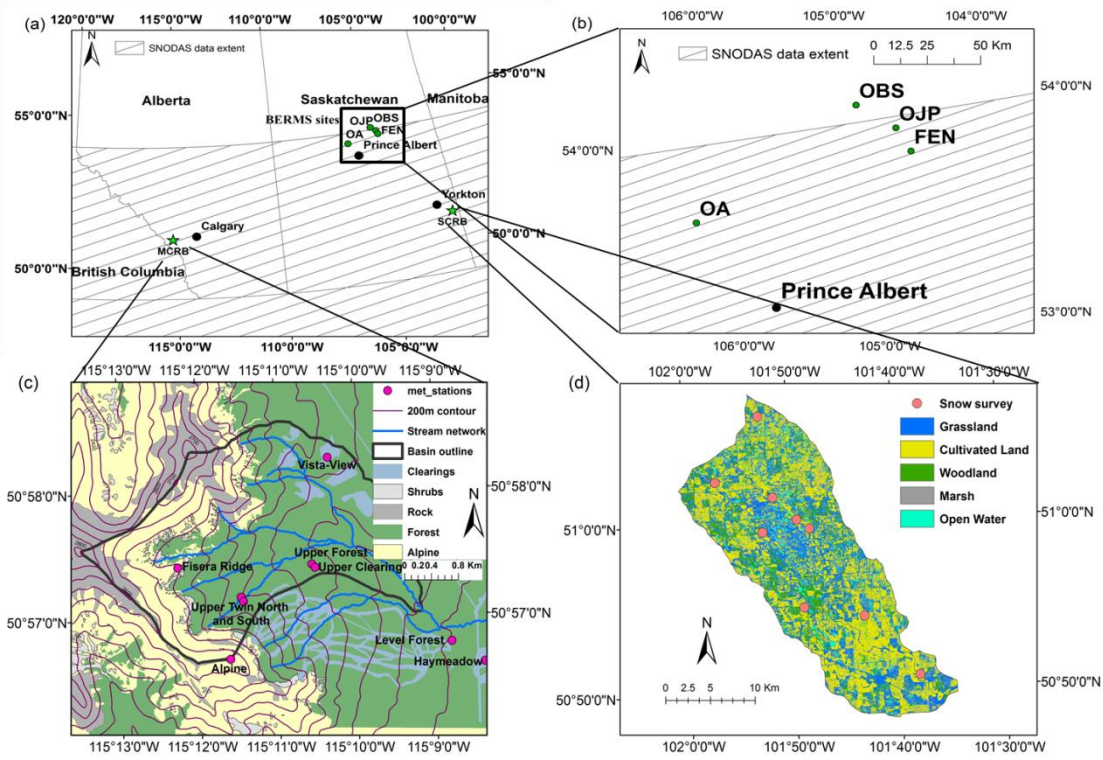

Figure 2-1. Study locations: (a) Marmot Creek Research Basin (MCRB), Smith Creek Research Basin (SCRB) and three Boreal Ecosystem Research and Monitoring Study (BERMS) sites, all in Canada. (b) The extent of SNODAS data and BERMS site locations. (c) Landcover and meteorological stations in MCRB, Alberta, Canada. (d) Landcover types and snow survey locations in SCRB, Saskatchewan, Canada.

2.3.1 Boreal Ecosystem Research and Monitoring sites

The BERMS area is located in the southern Boreal Forest within the mid-Boreal Upland and Boreal Transition ecoregions, north of Prince Albert, Saskatchewan, Canada. It is a follow-on to the Boreal Ecosystem-Atmosphere Study (BOREAS) (Nichol et al., 2000) that aimed to determine the long-term water, carbon, and energy exchanges between the atmosphere and boreal forest. Seven flux tower sites are located in various landcover types in BERMS (Barr et al. 2012). Snow survey data from four sites were available for the study period. Old Black Spruce (OBS) was excluded from the analysis as it is located outside of the extent of SNODAS data. The other three sites were chosen for this study based on precipitation measurements, snow survey data availability, and SNODAS data extent (Figure 2-1b). These sites are the needleleaf Old Jack Pine (OJP, 53°54`N, 104°41`W, elevation 570 m), deciduous Old Aspen (OA, 53°38`N, 106°12`W, elevation 600 m), and Fen (FEN, 53°57`N, 105°57`W, elevation 525 m). OJP is located in a mature jack pine forest. The landscape is relatively flat (mean slope 2% to 5%) with a 13.5 m mean canopy height and 1.9 to 2.2 winter leaf area index (Baldocchi et al., 1997; Nichol et al., 2000). This type of environment experiences substantial snow

interception losses (Pomeroy and Gray, 1995). The vegetation type of OA is mostly pure stands of mature trembling aspen overstory with heights from 18 to 22 m and a winter LAI of 0.72 and 2-m hazelnut understory with winter LAI of 0.33 (Hogg et al., 1997; Barr et al., 2004). Pomeroy and Gray (1995) showed that snow accumulation in aspen forests closely matched cumulative snowfall in the cold boreal winter. The FEN site is located in an approximately 4000 m long and 450 m wide patterned fen surrounded by black spruce and jack pine forest. Bog birch shrubs at 0.5–1.5 m height and widely scattered, stunted deciduous tamarack trees are the main vegetation types in this site (Nichol et al., 2000; Sukyer et al., 1997). Because of its sparse vegetation cover, it can be subject to snow redistribution by wind.

Researchers from Environment and Climate Change Canada (ECCC) and the Global Institute for Water Security, University of Saskatchewan conducted snow surveys on a transect around each site, one to three times per winter month. This was done using an ESC30 snow sampling tube to measure density and a ruler for depth following methods outlined by Pomeroy and Gray (1995). Along each 100-m transect, 25 depth measurements were taken at equal interval, with a density sample taken at every fifth depth measurement point. Average snow depth and density were used to calculate the mean SWE at each site. From the 2010 to 2015 water year, 89 mean SWE values were surveyed at three sites.

2.3.2 Smith Creek Research Basin

SCRB is located approximately 60 km southeast of Yorkton, Saskatchewan, Canada in the parkland ecoregion of the Canadian Prairies (Figure 2-1d). It has an area of approximately 393 km^2 and a relatively level landscape, with average slopes ranging from 2 to 5% and elevation ranging from 490 to 548 m (Fang et al., 2010). The major landscape types of SCRB are cultivated cropland, pasture, native grassland, natural wetland, and deciduous woodland. Because snow is heavily redistributed by wind from one landscape to another during winter in this environment (Pomeroy et al., 1993; Fang and Pomeroy, 2009), 13 transects were chosen to represent the major landscapes (i.e., grassland, grain stubble, roadside ditch, woodland, and wetland) at survey sites throughout the whole basin. Each transect contained 25 snow sample points with a 5-m interval. Snow depth was measured at each point and snow density was measured every fifth depth measurement using the ESC30 snow tube. Mean SWE was calculated from average snow depth and snow density following Pomeroy and Gray (1995). There were 67 mean SWE values from these transects within the 2010 to 2012 water year at SCRB (Pomeroy et al., 2014). Precipitation data from two meteorological stations, which were separately operated by University of Saskatchewan (UofS station) and ECCC (Langenburg station), located inside the SCRB were available for this research.

2.3.3 Marmot Creek Research Basin

MCRB (50°57`N, 115°09`W) is located in the Front Ranges of the Canadian Rocky Mountains (Figure 2-1c) and has an area of approximately 9.4 km^2 including three upper sub-basins: Cabin Creek, Middle Creek, and Twin Creek, as well as a lower confluence sub-basin. The elevation of MCRB ranges between 1450 m and 2825 m. The main landcovers are dense needleleaf lodgepole pine in the lower elevations; deciduous alpine larch, shrubs, grasses, needleleaf Engelmann spruce, and sub-alpine fir in the middle upper elevations; and talus and bare rocks occupy in the high alpine region (DeBeer and Pomeroy, 2009). The basin has been treated with large clearcuts and small forest clearings in the needleleaf forest zone (Ellis et al., 2013). There are substantial snow interception losses from needleleaf forests (Ellis et al., 2010) and wind redistribution of snow from alpine ridges and windward slopes to sheltered slopes and treeline forests (MacDonald et al., 2010). The average annual precipitation in MCRB is approximately 900 mm, which increases with elevation. The precipitation can reach 1140 mm at the regions above treeline where 60%–75% of it falls as snow (DeBeer and Pomeroy, 2009). Snow usually accumulates from November to March and starts to melt in later April or early May. Ten permanent meteorological stations have operated since 2005 at various locations throughout the basin (Figure 2-1c). These stations continuously collect short and long-wave radiation, air temperature, humidity, wind speed, and snow depth. Precipitation is measured with Alter-shielded Geonor weighing precipitation gauges at the Hay Meadow, Upper Clearing, and Fisera Ridge stations and is corrected for wind-induced undercatch (Smith, 2007).

Snow surveys have been conducted at the Upper Clearing (UC), Vista View (VV), Fisera Ridge (FR), Level Forest (LF), and Hay Meadow (HM) sites regularly since 2007. The survey method is same as that for SCRB with varied transect lengths. There are 348 mean SWE values from transect for SNODAS validation in MCRB for the 2010 to 2015 water years.

2.4 Methodology

SNODAS data from October 2010 to September 2015 was downloaded and processed to extract SWE, precipitation, snowmelt runoff under the snowpack, blowing snow sublimation, and snowpack sublimation for all study sites. SNODAS SWE data was compared to ground snow survey data to evaluate its point scale accuracy in all three areas. In MCRB, SNODAS SWE was also compared with a CRHM simulation to assess accuracy at the basin scale. The accuracy of a snow data assimilation system is mainly controlled by two factors: model simulation accuracy and data assimilation accuracy and frequency. The main factors influencing model simulation accuracy are driving force, parameters, and model structure. Both blowing snow transportation and canopy snow interception simulations are missing in the SNODAS NSM model. Precipitation

data is the only available driving force in the archived SNODAS data sets, and data assimilation can be determined by using a water balance calculation (see section 2.4.1). Therefore, the influence of these factors on accuracy of SNODAS SWE data was also examined. CRHM was forced by the SNODAS precipitation and locally observed climate data to evaluate the importance of two missing snow processes by turning one or both off in the model. Then a CRHM simulation, forced by SNODAS precipitation, mimicked SNODAS by turning off modules of both processes in CRHM and adding the estimated assimilation. Lastly, SNODAS assimilation amount was assimilated into a comprehensive CRHM snow model, forced by SNODAS precipitation and locally observed climate variables was used to show the impact of correcting the model. The main works of this chapter are shown in Figure 2-2 and the details are provided in the rest of Section 2.4.

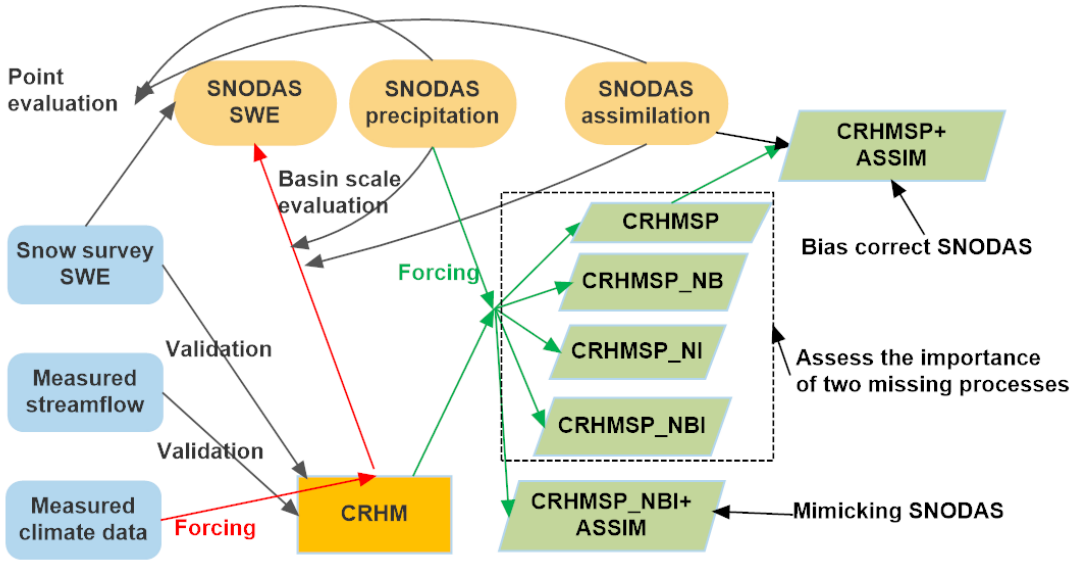

Figure 2-2. Work flow of the research in Chapter 2. CRHMSP is a complete CRHM model forced by SNODAS precipitation and local observed other climate variables. CRHMSP_NB is a CRHM model that without blowing snow transport simulation forced by SNODAS precipitation and local observed other climate variables. CRHMSP_NI is a CRHM model, forced by SNODAS precipitation and local observed other climate variables, without snow interception simulation. CRHMSP_NBI is a CRHM model, forced by SNODAS precipitation and local observed other climate variables, without both blowing snow transport and snow interception simulation. CRHMSP_NBI is a CRHM model, forced by SNODAS precipitation and local observed other climate variables, without both blowing snow transport and snow interception simulation. CRHMSP_NBI+ASSIM is a CRHM model, forced by SNODAS precipitation and local observed other climate variables, without both blowing snow transport and snow interception simulation but inlcluding SNODAS assimilation. CRHMSP+ ASSIM is a complete CRHM model, forced by SNODAS precipitation and local observed other climate variables, inlcluding SNODAS assimilation.

2.4.1 Determination of assimilation in SNODAS

In addition to SWE, SNODAS also provides daily cumulative precipitation (rain and snow), snowmelt runoff at the base of snowpack, sublimation from snowpack, and sublimation of blowing snow data for each pixel. Although there is no available information on when assimilation happens and how much SWE were assimilated at each time-step in the SNODAS system, these variables together can be used to compute the snowpack water balance to estimate assimilation. In the NSM simulation, single-day SWE should equal SWE of the previous positive snowfall minus snowmelt runoff and sublimation under condition without any data assimilation. If there is considerable differences between these two data sets, assimilation must be the cause. Therefore, Equation 2.1 was used in this research to determine the assimilation amount in SNODAS system.

$$\text{Assim} = \text{SWE}_i - (SWE_{i-1} + S - SM - BSS - SPS) \quad (2.1)$$

where Assim is the assimilation amount, SWE_i denotes SWE on the i^{th} day of year, S is snowfall, SM is snowmelt runoff, BSS is blowing snow sublimation, and SPS is snowpack sublimation.

2.4.2 Spatial representation of snow survey data

In model or remote sensing validation research, ground truth and target data should have the same spatial resolution. To satisfy this requirement for validation of SNODAS data, previous researchers conducted their snow surveys in an approximately 1-km^2 area to represent the SNODAS grid cell (Anderson, 2011; Clow et al., 2012). In the present research, however, historical snow survey data were used and a perfect matching of scale was not possible. Transect lengths of the snow surveys are usually 100 to 125 m, such that the survey area only represents a small part of the 30 arc-second SNODAS grid cell. SWE distribution is highly varied in different landcovers because of the snow redistribution caused by wind in open environments and needleleaf canopy interception (Liston et al., 2007; Pomeroy et al., 1993; Pomeroy et al., 1998a; Pomeroy and Gray, 1995). This makes a direct comparison between the historical snow survey data and the correspondent SNODAS data challenging in areas with complex terrain or heterogeneous landcovers.

For each site in BERMS, topography is flat and land cover is primarily uniform. The mean SWE from each survey site can represent the SWE of the larger area around that site. Therefore, the observed mean SWE of each site was directly compared to the extracted SNODAS SWE data at BERMS sites.

In SCRB, snow surveys at one site contain several transects that represent the dominant landscapes or surveys have one transect covering several landscapes. The present

research assumes that the SWE in each landscape type is regionally consistent in this flat area and that snow surveys of about 125 m in length can represent SWE over a larger area in that landscape type, following the stratified snow sampling methods of Steppuhn and Dyck (1974). The following equation was used to upscale the snow survey data to ~1 km^2:

$$SWE_{1K} = \sum_{i=1}^{n}(SWE_i * W_i) \quad (2.2)$$

where SWE_{1K} is the upscaled, approximately ~1 km^2 observed SWE, SWE_i is the observed SWE at i^{th} landscape type, W_i is the fractional coverage weight of the i^{th} landscape type and is the result of the area of i^{th} landscape type divided by ~1 km^2. The area of each landscape type was calculated from a 30 m landcover map at each site.

MCRB has highly heterogeneous landcover and complex terrain. The Steppuhn and Dyck (1974) method might not be suitable for upscaling the ground snow survey to the SNODAS pixel scale. The snow surveys in MCRB contain samples from most landscapes around each site, but they might not be sufficient to cover the elevation range, slope and aspect within each SNODAS cell. Various approaches were developed to upscale point snow survey data to catchment scale based on the influence of elevation, slope, aspect, radiation, vegetation condition, wind effect, and other factors on snow distribution (Elder et al., 1991; Harshburger et al., 2010; López-Moreno and Stähli, 2008). However, Grünewald et al. (2013) found the influence of elevation, slope, slope, and sheltering index on snow depth distribution was weak in MCRB. These factors explained less than 30% of local snow depth variation. There is no existing optimal method to upscale 150 m snow survey transect data to the SNODAS cell level (approximately 582×926 m) in MRCB, and developing a new approach is beyond the scope of this research. Thus, the snow survey transects SWE data from different landscapes were directly compared to the corresponding SNODAS cell SWE.

2.4.3 Point scale comparison

To examine the influence of missing processes (i.e., blowing snow transport and canopy interception) in the NSM on SNODAS accuracy, the observed and SNODAS SWE were compared using linear regression at different landscape types (i.e., forest and clearings, leeward and windward slopes) in all three research sites. The root mean square error (RMSE, Equation 2.3), correlation coefficient (R^2, Equation 2.4), and model bias (MB, Equation 2.5) between the two data sets were also calculated to evaluate accuracy.

$$RMSE = \sqrt{\frac{\sum_{i=1}^{n}(Xo_i - Xs_i)^2}{n}} \quad (2.3)$$

$$R^2 = 1 - \frac{\sum_i (X_O - X_S)^2}{\sum_i \left(X_O - \overline{X}_O\right)^2} \quad (2.4)$$

$$MB = \frac{\sum Xs}{\sum Xo} - 1 \quad (2.5)$$

where Xs and Xo are SNODAS SWE and observed SWE, respectively, and $\overline{Xo}$ is the average of observed SWE.

Time series of SNODAS SWE were created and compared to the observed SWE at sites where observed precipitation was available. Cumulative SNODAS and observed precipitation as well as the amount of data assimilation were also included in the time series to assess the influence of these factors on SNODAS accuracy.

2.4.4 CRHM model and basin scale comparison

The Cold Regions Hydrological Modelling platform (CRHM) is a system to assemble hydrological models developed for Canadian and other cold environments. It can create distributed physically based hydrological models, which use the concept of the Hydrological Response Unit (HRU) as the basic unit for modelling. HRUs are conceptual landscape groups, which are subdivisions of the basin based on the elevation, slope, aspect, vegetation cover, soils, and other hydrological or biophysical characteristics. CRHM has various modules to simulate the snow processes of each HRU. Users can construct their own model by selecting modules from the CRHM module library based on input data availability, research scale, and predictive variable of interest. These modules can be used to interpolate meteorological data and to simulate rainfall and snowfall interception, snow redistribution, snow sublimation, snow albedo decay, canopy transmittance, snow energy and mass balance, evaporation, snowmelt, snowcover depletion, infiltration, soil moisture, flow and storage of the surface and subsurface, and streamflow routing. Pomeroy et al. (2007) provide a full description of CRHM. For the basin scale comparison in MCRB, the CRHM model configuration by Fang et al. (2013) was used here. The main modules used in the project are: 1. the Radiation module (Garnier and Ohmura, 1970) was used to calculate theoretical global radiation, and direct and diffuse solar radiation including to slopes. 2. The Albedo module (Verseghy, 1991) was used to simulate the snow albedo change due to the snow condensation, melt, and snowfall throughout the winter. 3. The SNOBAL module (Marks et al., 1998) was used to simulate the mass and energy balance of snowpack. 4. The Canopy module (Ellis et al., 2010) was used to estimate forest canopy interception of rainfall and snowfall and sub-canopy shortwave and longwave radiation. 5. The Blowing Snow module (Pomeroy and Li, 2000) was used to simulate the blowing snow transportation and sublimation. Details on the modules used, model setup, and parameterization are described in several recent publications (Fang et al., 2013; Fang and Pomeroy, 2016; Pomeroy et al., 2016).

The output of the SNODAS system predicts behaviour at the centre of each grid cell, which is assumed to represent the whole pixel for hydrological purposes. This assumption is valid in flat terrain (e.g. BERMS and SCRB) but may not be appropriate for complex terrain such as that found in MCRB. In light of this, SNODAS SWE in

MCRB was also evaluated by the CRHM simulated SWE data at the basin scale. This simulation used the observed forcing data in MCRB to run the CRHM model (hereafter referred to as ObsMet). First, ObsMet-simulated SWE was compared to snow survey data at several sites to assess the ability of CRHM to predict the timing and magnitude of snow accumulation and depletion at a point scale. Second, ObsMet-simulated streamflow was compared to streamflow observations at the basin outlet to evaluate the ability of CRHM to predict the surface and subsurface hydrological processes for streamflow generation timing, snow accumulation and depletion at the basin scale. Third, the ObsMet-simulated SWE for the whole basin was compared to the averaged SNODAS SWE in MCRB. The resolution of SNODAS SWE data is 30 arc-seconds and as MCRB is located at 51° N, each SNODAS grid cell covers approximately 0.54 km^2 area at that latitude. There are 30 SNODAS grid cells overlapping MCRB, and the average SNODAS SWE in MCRB was calculated based on areal-weighted SWE of each cell. RMSE_m (Equation 2.6) and MB_m (Equation 2.7) were calculated to compare the SNODAS and ObsMet-simulated SWE. RMSE_m and MB_m have the same algorithm with RMSE and MB, but they show the comparison between two model simulations. The assimilation amount, cumulative SNODAS precipitation, and observed precipitation data were included in the time series of SNODAS and ObsMet simulated SWE to examine their influence on SNODAS SWE accuracy in MCRB.

$$RMSE\_m = \sqrt{\frac{\sum_{i=1}^{n}(Xm1_i - Xm2_i)^2}{n}} \tag{2.6}$$

$$MB\_m = \frac{\sum Xm1}{\sum Xm2} - 1 \tag{2.7}$$

where xm1 and xm2 denote the SWE simulated by SNODAS and ObsMet.

2.4.5 Mimicking SNODAS simulations using CRHM

One possible cause for the presumable error in SNODAS SWE is the structure of the NSM embedded in SNODAS system. The NSM is spatially uncoupled such that it does not consider the spatial redistribution of snow by wind even though it includes blowing snow sublimation following Pomeroy and Li (2000). NSM also does not calculate canopy snow interception and sublimation in forested regions (Carroll et al., 2001; Jordan, 1990; Tarboton and Luce, 1996). These model limitations might cause SNODAS to overestimate local SWE in MCRB, due to the presence of both windy open alpine and dense evergreen forest landcovers. Thus, one simulation was generated from an incomplete CRHM model in which blowing snow transportation and canopy interception modules were turned off but used observed precipitation in MCRB (hereafter the ObsMet_NBI).

Another possible reason for the presumable SNODAS SWE error is an inaccurate driving force. To determine the influence of an inaccurate driving force and missing processes on SNODAS SWE quality, five simulations were conducted in MCRB by replacing observed precipitation with SNODAS precipitation in the forcing data to run

CRHM with different configurations of missing processes. These were compared to ObsMet and SNODAS SWE. The first four simulations are: 1) a complete CRHM model (CRHMSP), 2) an incomplete CRHM model with blowing snow transportation module turned off (CRHMSP_NB), 3) an incomplete CRHM model without the canopy snow interception module (CRHMSP_NI), and 4) an incomplete CRHM model with both blowing snow transportation and canopy snow interception modules turned off (CRHMSP_NBI). To make a simulation that closely matches the SNODAS system, a fifth simulation was conducted by incorporating data assimilation into the CRHMSP_NBI simulation. The assimilation amount used in the SNODAS system for MCRB was used to update the CRHMSP_NBI simulated SWE based on a nudging method. In the nudging process, the updated SWE equals simulated SWE plus the assimilation amount greater or lesser than zero. This simulation is referred to as CRHMSP_NBI+ASSIM hereafter. If the CRHMSP_NBI+ASSIM simulated SWE can closely match SNODAS SWE, then CRHM is able to mimic the SNODAS NSM model.

2.5 Results and discussions

2.5.1 SNODAS accuracy at point scale

2.5.1.1 Boreal Forest

The mean SWE of each site was compared to the extracted SNODAS SWE data (Figure 2-3). The SNODAS SWE explained 64%, 71%, and 31% of variability of SWE at the OA, OJP, and FEN, respectively, with RMSE of 45.53 mm, 57.5 mm, and 77.4 mm, suggesting good correlation between the SNODAS and measured SWE in the OA and OJP sites but not in the FEN. SNODAS overpredicted SWE at all sites with a degree of overestimation that varied from 17% to 83%. The results indicate that among sites at BERMS, SNODAS works best at OA, is related to measurements but with a moderate positive bias at OJP, and is poorly related to measurements at FEN. These results can be explained by physical inference. In the needleleaf jack pine forest, ground snow accumulation is attenuated by canopy interception and sublimation losses of roughly 1/3 of winter snowfall (Hedstrom and Pomeroy, 1998; Pomeroy et al., 1998b; Pomeroy et al., 2002); snow interception and sublimation of intercepted snow are not represented in the SNODAS model simulation. Pomeroy et al. (2002) found that the ratio of forest to clearing snow accumulation was negatively related to winter LAI and canopy density of forests. However, the influence of canopy interception on snow accumulation under deciduous forest canopies is very small to negligible (Kuz'min, 1960; Pomeroy and Gray, 1995). This explains why SNODAS works better in the OA site, which is surrounded by deciduous aspen, than in OJP which is located under needleleaf canopies.

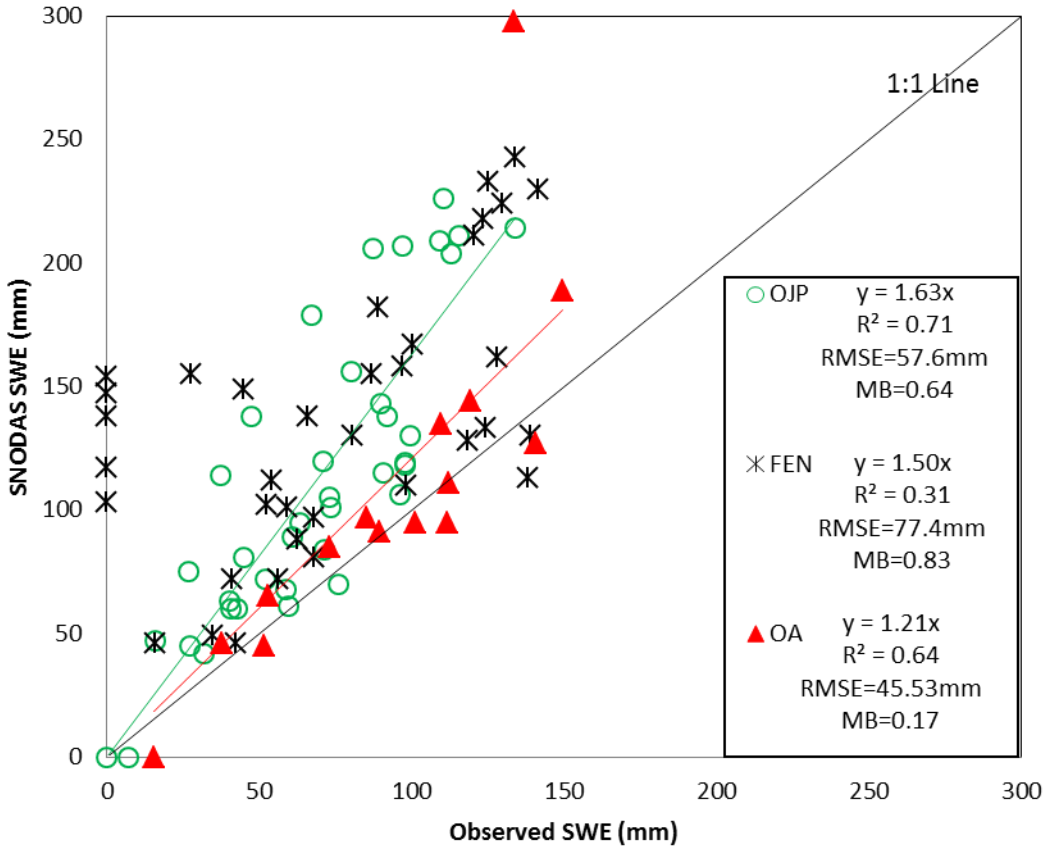

Figure 2-3. Comparison of observed and SNODAS-predicted SWE for water years 2011-2015 at BERMS sites (Saskatchewan, Canada) along with linear fits for old jack pine (OJP; green line) and old aspen (OA; red line) sites to a 1:1 relationship (black line). The fen (FEN) site has no significant linear fit.

Another factor that affects snow accumulation on the ground is blowing snow transport from open to sheltered sites (Pomeroy and Li, 2000). This is also missing in the SNODAS model even though it calculates blowing snow sublimation loss. Blowing snow transport is an important process controlling snow accumulation in open areas such as FEN (Pomeroy and Gray, 1995). Mid-winter ablation events in boreal forest clearings that are driven by advection of turbulent energy, can result in lower mid-winter snow accumulation in clearings such as the FEN, but not under the forest canopy with relatively stable and sheltered conditions in this region (Pomeroy and Granger, 1997). Additionally snowmelt in clearings is approximately three times faster than that under the canopy in this region (Pomeroy and Granger, 1997). Therefore in later the season the clearings are usually bare, but SNODAS was unable to represent this. This explains why five data points from FEN are located in the Y axis in Figure 2-3 – by this time of year there was no snow observed in the FEN but SNODAS still showed a snowpack in its simulation. Sub-canopy melt energetics are not represented in SNODAS. In addition to wind redistribution being a problem for SNODAS in open Colorado sites discovered by Clow et al. (2012), this study revealed more factors

causing SNODAS's poor performance in the open area of the Canadian boreal forest. The combination of wind redistribution, mid-winter ablation, and canopy effects on radiation and turbulent transfer explain why the SWE accuracy in the FEN site is the lowest amongst the three BERMS sites.

The cumulative precipitation data from SNODAS and observations at three sites were calculated to understand the effect of precipitation data quality on SNODAS SWE accuracy (Figure 2-4). SNODAS precipitation was close to observed precipitation in the 2011 water year, while SNODAS overestimated precipitation by 37–76% in all other water years. The SNODAS SWE accuracy varied among the five water years at each site. At OJP and FEN sites, SNODAS SWE agreed very well with observations in the 2011 water year, while the difference between the two data sets was larger in the other four water years. SNODAS SWE was in good agreement with observation at site OA except for during the 2013 water year. This means precipitation played a major role in the SNODAS SWE accuracy in this area in some years while precipitation bias was high. However, the missing processes were important every year, including those when the forcing precipitation bias was low. Besides precipitation data quality, assimilation also contributes to SNODAS SWE accuracy. There were several noticeable assimilations at these sites from the 2013 to 2015 water years, and SNODAS SWE accuracy increased after assimilations. In the 2013 water year, SNODAS had the highest precipitation bias among all years and there was assimilation at OJP and FEN but not at OA. Even though the SNODAS precipitation in this year was similar in all three sites, the RMSE between SNODAS and observed SWE was 164.3 mm for OA; higher than that of OJP (100.2mm) and FEN (61mm). However, in the years when assimilation occurred in all sites, OA had the highest accuracy. In the 2015 water year, for example, RMSE between SNODAS and observed SWE was 21.7 mm for OA; much lower than that in OJP (70.6 mm) and FEN (64.9mm). This suggests that missing model structure (i.e. canopy interception process at OJP and missing blowing snow transport at FEN) played bigger role in SNODAS SWE accuracy than did assimilation. The data assimilation frequency for this region was extremely low (less than once a year on average during the 2011 to 2015 water years) (Figure 2-4). This is much lower than in mountainous areas in the US (https://www.nohrsc.noaa.gov/pro/earth/archive.html). With such low frequency, erroneous precipitation data and the incomplete model structure of NSM together contribute more to the poor SNODAS performance in this region than does assimilation. Overall for BERMS sites, the main cause of the poor performance of SNODAS SWE was the high overestimation bias in SNODAS precipitation data in 2012–2015 water years (Figure 2-4). The major cause for SNODAS SWE accuracy was the missing processes in SNODAS model when SNODAS precipitation data bias was low. In all, the influence of erroneous precipitation data is important but only for certain years, while that of missing processes is important every year.

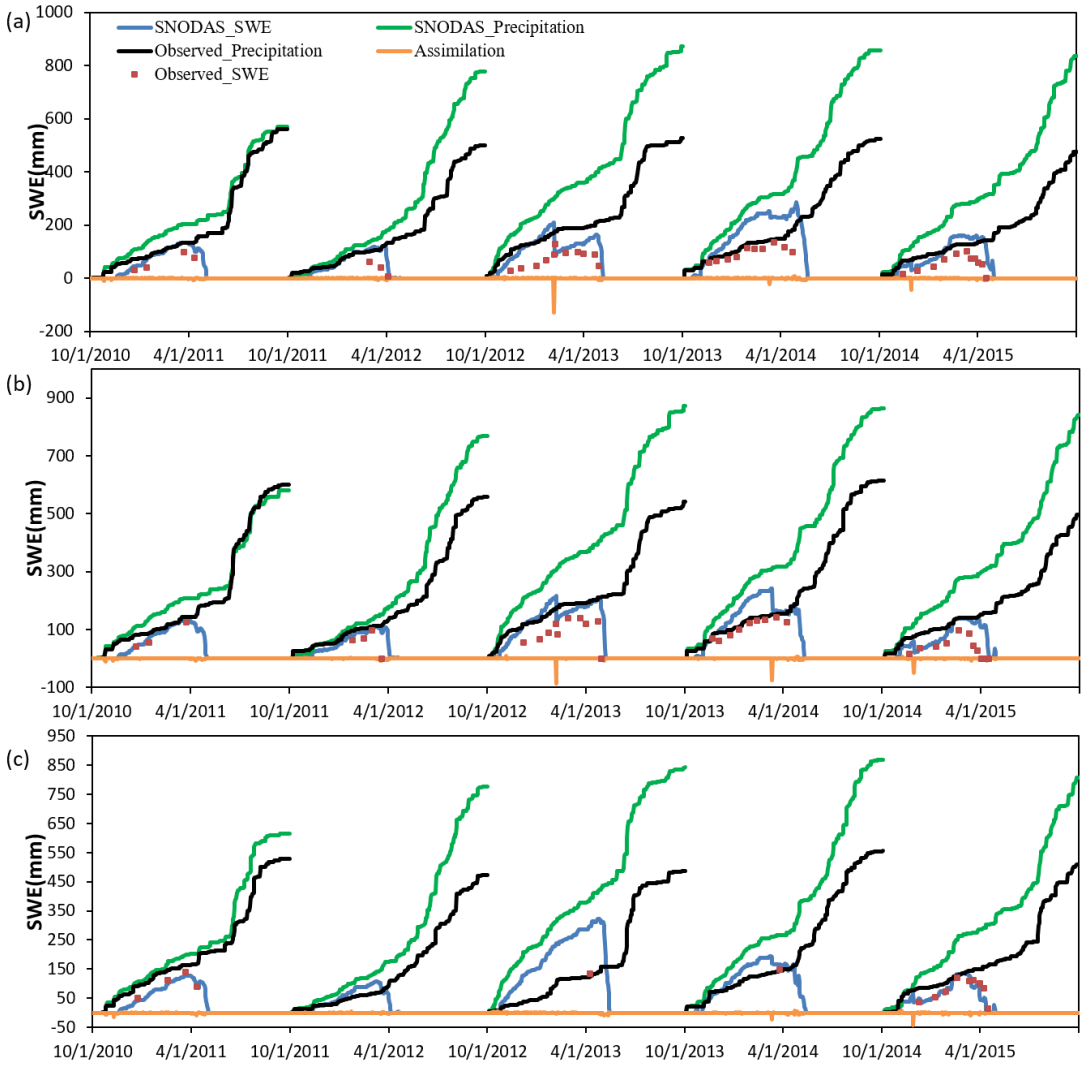

Figure 2-4. Time series comparisons of observed and SNODAS SWE and precipitation at BERMS sites for (a) old jack pine (OJP), (b) fen (FEN), and (c) old aspen (OA) sites in Saskatchewan, Canada.

2.5.1.2 Prairie

Upscaled snow survey data were compared to SNODAS predicted SWE at SCRB (Figure 2-5a). An R^2 of 0.001 with relatively large RMSE (46.5 mm) and MB (0.27) indicates that the SNODAS SWE is not correlated with observed SWE in this case. This may be largely due to a SNODAS NSM model structural defect. The spatial variation of winter SWE in the prairie environment is primarily explained by wind redistribution (Fang and Pomeroy, 2009; Pomeroy et al., 1993; Pomeroy and Li, 2000), but there is no blowing snow transport simulation in the SNODAS NSM. To verify the influence of this missing process, the SNODAS SWE was also directly compared to snow survey transect data across landscapes (Figure 2-5b). SNODAS overestimated SWE in grassland, stubble field, and wetland sites where is blowing snow occurs with an RMSE of 54.6 mm, 46.6 mm, and 35.4 mm and MB of 0.52, 0.48, and 0.32, respectively. In blowing snow sink areas, such as woodlands and river channels, SNODAS

underestimated SWE on with negative MB (–0.33 and –0.38 for woodland and river channel, respectively) and larger RMSE (120.4 mm and 132.1 mm). The R^2 between SNODAS and observed SWE at all landscapes are lower than 0.3. This means it is challenging for SNODAS to capture the spatial distribution of SWE in the Canadian prairie without simulation of blowing snow transportation.

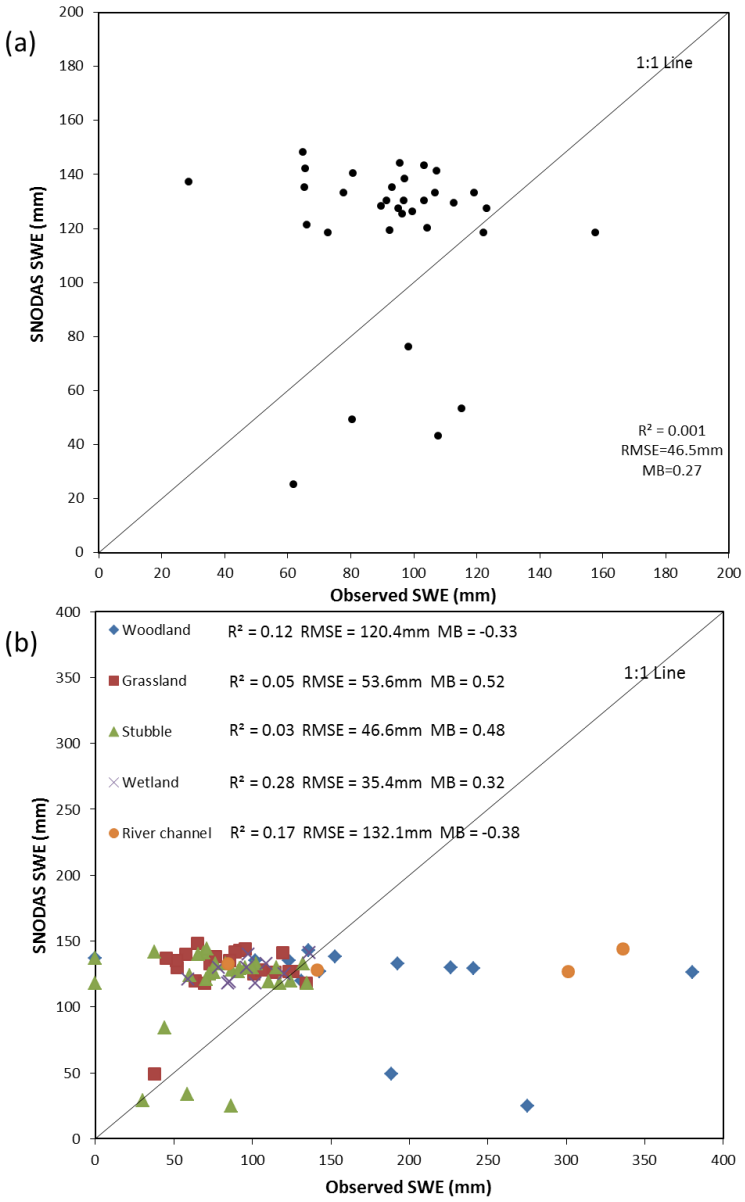

Figure 2-5. Comparison of observed and SNODAS-predicted SWE at Smith Creek Research Basin, Saskatchewan, Canada for water years 2011-2015.

Observed and SNODAS-estimated precipitation were similar between two sites for all water years. SNODAS overestimated the precipitation at both sites for all water years with variable overestimation rate. In the 2011 water year, SNODAS overestimated the precipitation by only 21% and 9% at UofS and Langenburg stations, respectively

(Figure 2-6). However, SNODAS overestimated precipitation at these two sites by 78% to 132% in other water years. In addition to SNODAS precipitation accuracy, assimilation affects SNODAS SWE accuracy at both sites. SNODAS greatly overestimated precipitation at both sites in the 2013 water year, but the RMSE between SNODAS and observed SWE was 31.9 and 39.6 mm for UosS and Langenburg. This was much lower in 2013 than in other years with only exception in Langenburg for 2012 (59 and 65.7 mm for 2011 and 64.8 and 22.34 mm for 2012). This is attributed to a noticeable assimilation on February 8, 2013 at both sites. However, there were only few noticeable assimilations in SCRB during the study period. This resulted in that NSM simulation being the major factor influencing the accuracy of SNODAS products in this area.

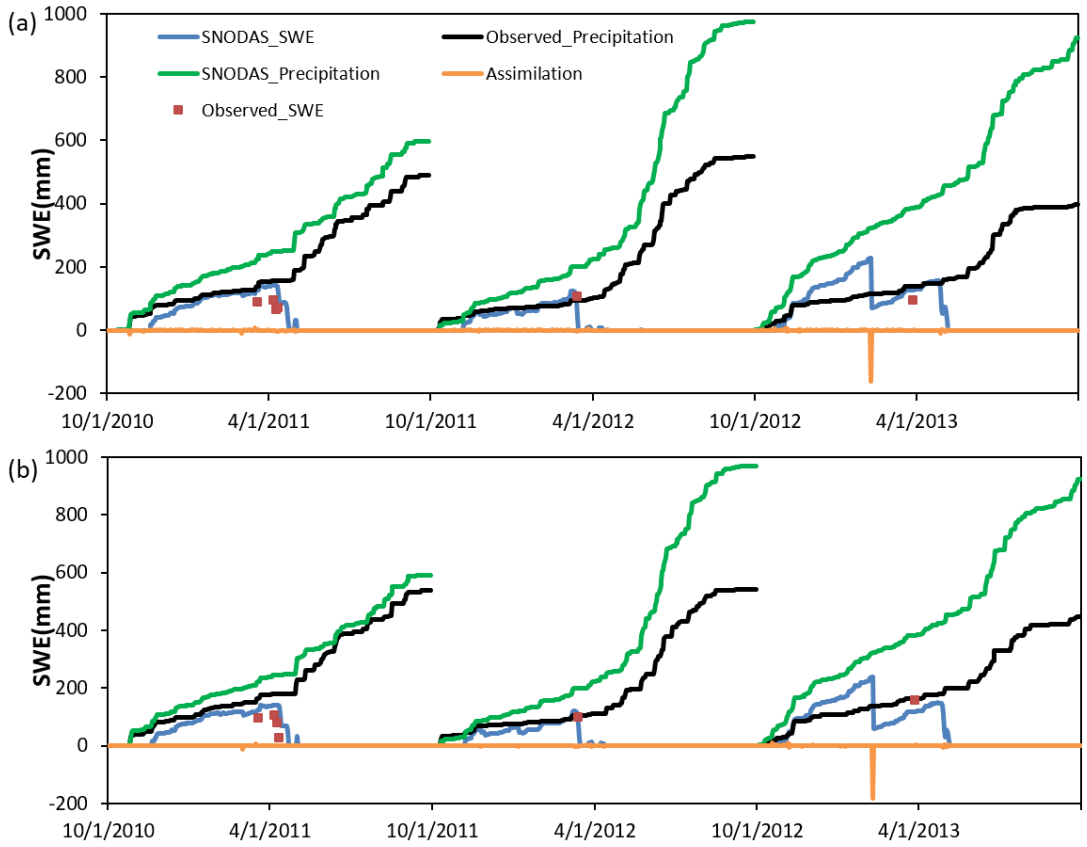

Figure 2-6. Time series comparisons of observed and SNODAS predicted SWE and precipitation at two meteorological stations at SCRB sites: (a) University of Saskatchewan station, and (b) Langenburg station.

2.5.1.3 Canadian Rockies

In MCRB, observed SWE was compared to SNODAS SWE in three landscape groups. Figure 2-7a shows the comparison of SNODAS and observed SWE from all samples from coniferous forests and clearings in MCRB. SNODAS SWE was not correlated to SWE observations for either forest or clearing land cover types, with R^2 values of 0.26 and 0.20, respectively.

SNODAS greatly overestimated SWE at both landscapes with MB of 4.76 in forests and 1.79 in clearings. SNODAS SWE accuracy was lower in forests than in clearings as the RMSE between SNODAS and observed SWE was 374.8 mm and 323.9 mm, respectively. Poorer SNODAS SWE accuracy at forest sites, especially the high SWE overestimation, is likely partially attributed to the structure of the SNODAS NSM, which lacks simulation for canopy snow interception that, in turn, affects sub-canopy snow accumulation and ablation.

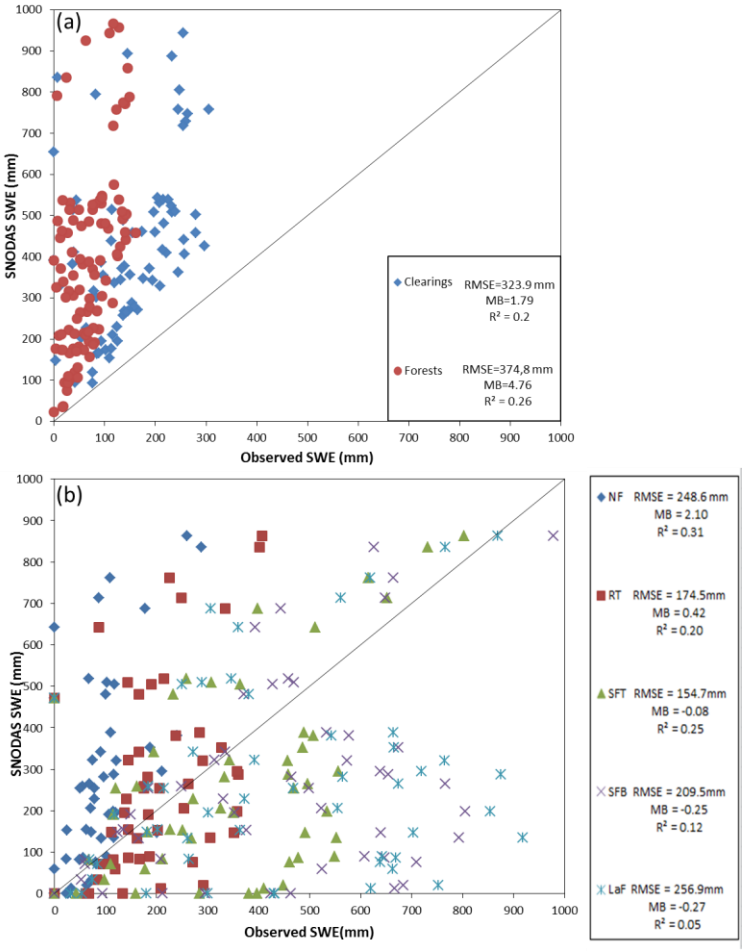

Figure 2-7. Comparison of snow surveyed SWE and SNODAS-predicted SWE across various landscapes at Marmot Creek Research Basin: (a) displays the Clearings and Forests site and (b) shows the alpine slopes around Fisera Ridge (NF: north facing slope, RT: ridge top, SFT: South facing slope top, SFB: South facing slope bottom, LaF: larch forests at bottom of south facing slope).

In addition, clearings at MCRB are relatively small and are surrounded by dense forest. Snow accumulation at them should have minimal impact from missing blowing snow and forest canopy interception processes in SNODAS. This means theoretically SNODAS SWE should closely match forest clearing observations. However, SNODAS overestimated SWE in clearings with relatively high MB and RMSE. This is likely due to a precipitation error that drives SNODAS NSM in MCRB.

Cumulative precipitation from the SNODAS models, observations as well as SNODAS

assimilation were included to determine their influence on SNODAS SWE accuracy (Figures 2-8a and 2-8b). SNODAS and observed precipitation were comparable in 2011 and 2012 water years with MB of –0.15 and 0.17, respectively, while SNODAS overestimated precipitation in other years with MB of 0.41 in 2013, 1.64 in 2014 and 1.48 in 2015. RMSE between SNODAS and observed SWE were much lower in 2011 and 2012 water years than other years at both forest and clearing sites. Using Upper Clearing as an example, RMSE were 181.6 mm, 139.9 mm, 264.7 mm, 505.2, and 247.2 for 2011 to 2015 water years in order. Assimilation clearly plays a negative role in SNODAS SWE accuracy at this site in the 2011 and 2012 water years. The cumulative SNODAS and observed precipitation were almost identical before the peak SWE in 2011 and 2012 water years at Upper Clearing, but there was still over 100 mm RMSE between SNODAS and observed SWE. This is explained by the total assimilation of 162.6 mm and 102.1 mm in the SNODAS system before peak SWE for 2011 and 2012 water years at this pixel.

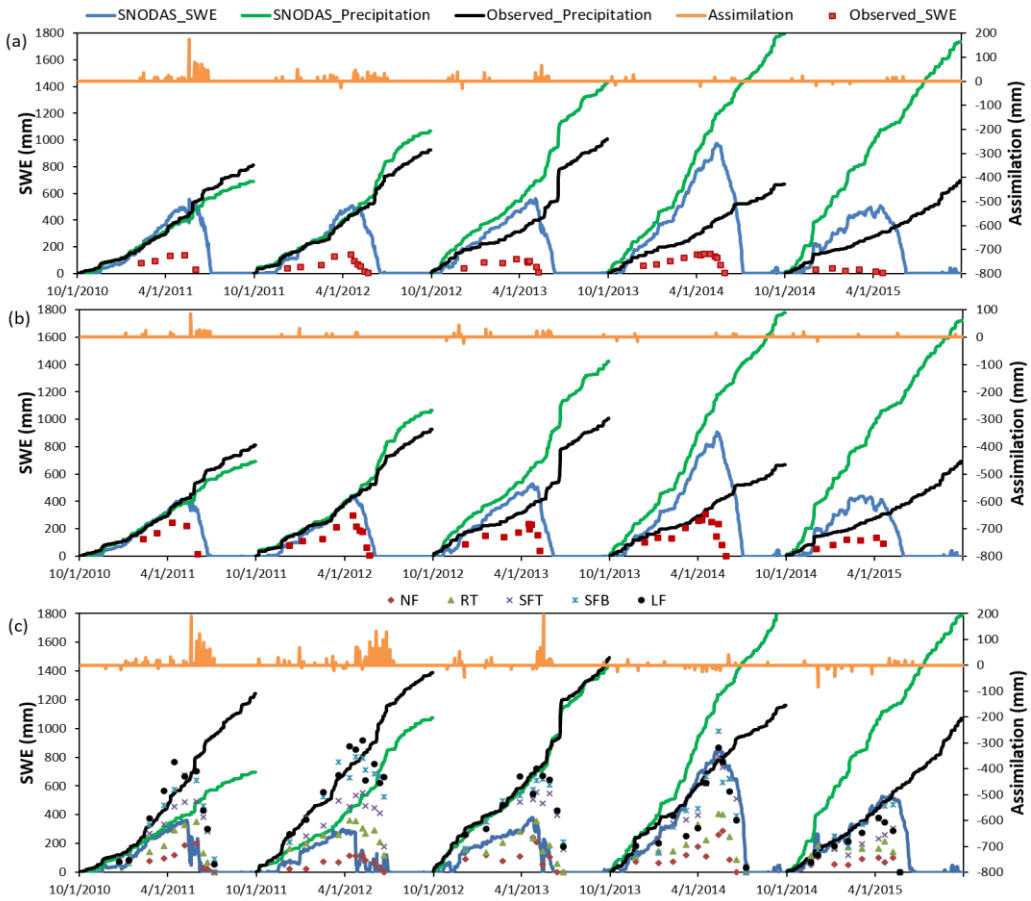

Figure 2-8. Time series comparisons of observed and SNODAS-predicted SWE and precipitation at two meteorological stations in Marmot Creek Research Basin, Alberta, Canada. (a) is the upper forest site, (b) is the upper clearing site, and (c) shows the alpine slopes around Fisera Ridge (NF: north facing slope, RT: ridge top, SFT: South facing slope top, SFB: South facing slope bottom, LaF: larch forests at bottom of south facing slope).

At FR, snow was usually redistributed from the windward areas (north-facing slope (NF) and ridge top (RT)) and deposited on the leeward areas (south-facing top slope (SFT), south-facing bottom slope (SFB), and larch forest (LaF)) (Figure 2-7b). SNODAS SWE accuracy was low in all five areas with RMSE higher than 150 mm. SNODAS tends to overestimate SWE in windward areas but underestimate the SWE at leeward sites. MB values in windward areas are positive (2.1 and 0.42 for NF and RT, respectively) but are negative at leeward areas (–0.1, –0.25, and –0.27 for SFT, SFB, and LaF, respectively) (Figure 2-7b). This is likely attributed to missing blowing snow transportation simulation in the SNODAS NSM model.

Time series of SNODAS and observed SWE were compared to assess the SNODAS precipitation data influence on SNODAS SWE accuracy at FR (Figure 2-8c). SNODAS underestimated precipitation by 44% and 22% in the 2011 and 2012 water years, respectively, which caused SNODAS to underestimate SWE for all sites except for NF. In the 2014 and 2015 water years, SNODAS overestimated precipitation at FR by 57% and 67%, and this led to the overestimation of SWE in all five areas. Although the overestimation of SNODAS precipitation in the 2015 water year was higher than that in 2014, RMSE of SWE was lower in 2015 than in 2014 as a result of a few more significant cases of assimilation in which SWE was reduced in the 2015 water year.

2.5.2 CRHM evaluation

To evaluate the reliability of CRHM, the ObsMet-simulated SWE was compared to snow survey data at a middle elevation mature coniferous forest (Upper Forest) and clearing (Upper Clearing), and alpine open slopes and deciduous forests for 2011 to 2015 water years (Figure 2-9). ObsMet captured the magnitude and timing of SWE for most years at the coniferous forest and clearing sites (Figures 2-9 a-b). RMSE ranged from 22.5 mm to 78.5 mm with a five-year mean value of 50 mm for the forest, and from 30.9 mm to 78.2 mm with a five-year mean value of 53.5 mm for the clearing (Table 2-2). MB were relatively low, with five-year mean values of 0.37 and –0.16 for the forest and clearing, respectively. In the alpine area, ObsMet captured the SWE by simulating a blowing snow sequence from source to sink areas (Figures 2-9 c-g) with five-year mean RMSE ranging from 106 to 180.4 mm and five-year mean MB from –0.1 to 1.19 (Table 2-2). Although RMSE in the alpine area is much higher than that in the forest, it is still acceptable because the SWE magnitude in the alpine area is usually much higher. Evaluation of SWE at a landscape point scale indicates that CHRM is capable of predicting snow accumulation and ablation at various landscapes with reasonable accuracy.

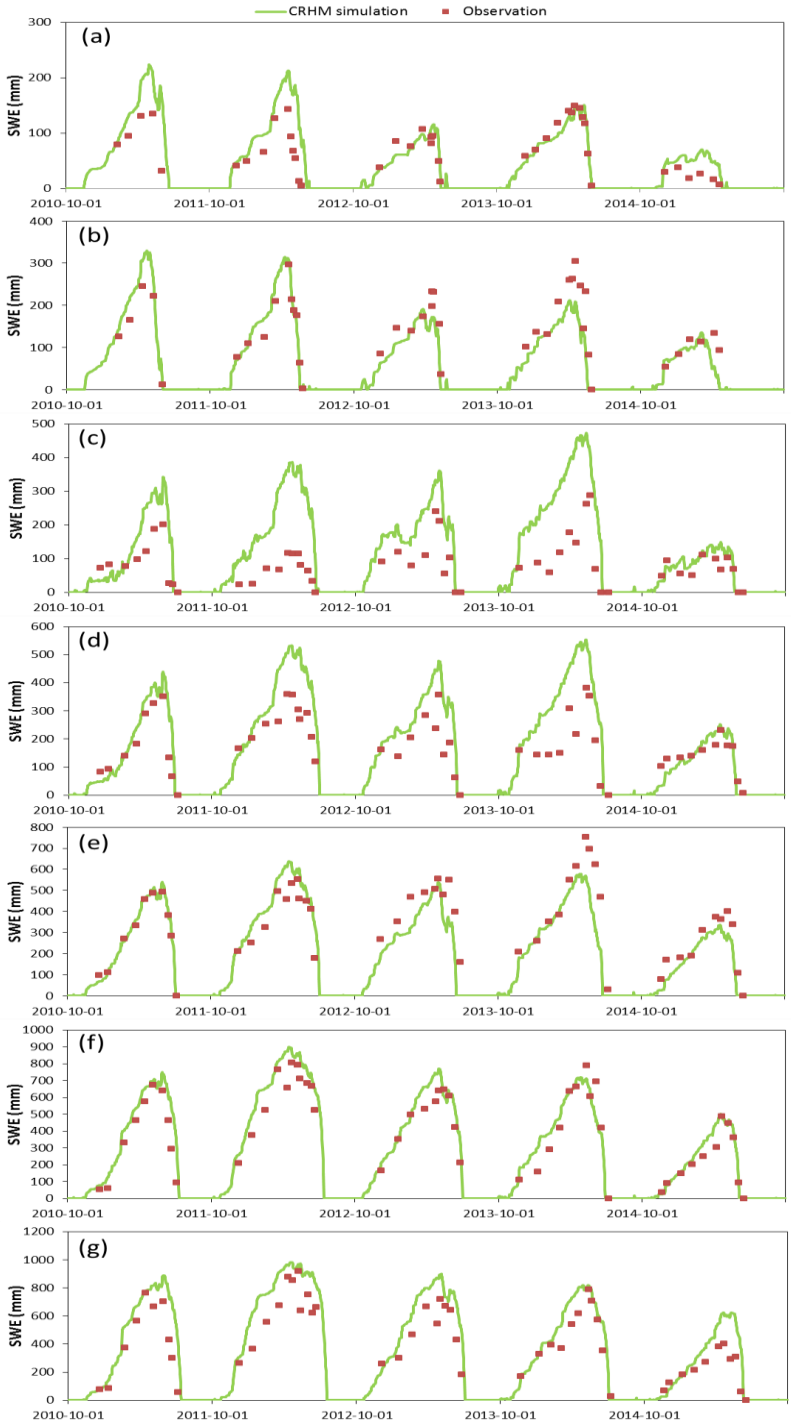

Figure 2-9. Comparison of observed and ObsMet-simulated SWE at Marmot Creek Research Basin, Alberta, Canada: (a) upper forest, (b) upper clearing, and Fisera Ridge sites: (c) north facing slope, (d) ridge top, (e) south facing slope top, (f) south facing slope bottom, (g) larch forest.

Table 2-2. Statistics comparing observed and ObsMet-simulated SWE at Marmot Creek Research Basin sites in Alberta, Canada: Upper Forest (UF), Upper Clearing (UC), and Fisera Ridge, which contains the north facing slope (NF), ridge top (RT), south facing slope top (SFT), south facing slope bottom (SFB), and larch forest (LaF) sites.

	UF		UC		NF	
	RMSE	MB	RMSE	MB	RMSE	MB
All	50.0	0.37	53.5	-0.16	139.87	1.19
2011	78.5	0.68	39.8	0.19	89.3	0.65
2012	75.9	0.97	30.9	0.002	202.0	2.89
2013	22.5	0.11	46.8	-0.23	98.1	0.83
2014	24.7	-0.04	78.2	-0.33	181.2	1.41
2015	29.8	1.22	51.7	-0.24	36.0	0.26

	RT		SFT		SFB	
	RMSE	MB	RMSE	MB	RMSE	MB
All	125.2	0.47	106.0	-0.10	107.3	0.14
2011	79.8	0.30	22.8	0.03	125.8	0.29
2012	155.2	0.53	94.2	0.20	112.5	0.16
2013	117.6	0.56	128.5	-0.25	92.4	0.14
2014	170.1	0.77	151.9	-0.23	126.5	0.02
2015	39.7	-0.01	75.6	-0.23	56.1	0.12

	LaF	
	RMSE	MB
All	180.4	0.31
2011	218.2	0.43
2012	196.3	0.27
2013	189.3	0.33
2014	115.9	0.18
2015	167.6	0.44

To assess the ability of CRHM to simulate the hydrology at the basin scale, the ObsMet-simulated basin outflow was compared to the streamflow measurements at the MCRB basin outlet for 2011 to 2015 water years (Figure 2-10). The simulated daily average streamflow agreed well with the observations and annual RMSE ranged from 0.08 to 0.39 m^3/s with an average of 0.18 m^3/s for these five water years. The MB of daily streamflow ranged from –0.27 to 0.25 with five-year mean value of –0.06. This suggests that CRHM is capable of simulating the timing and magnitude of surface and subsurface processes for streamflow generation in MCRB.

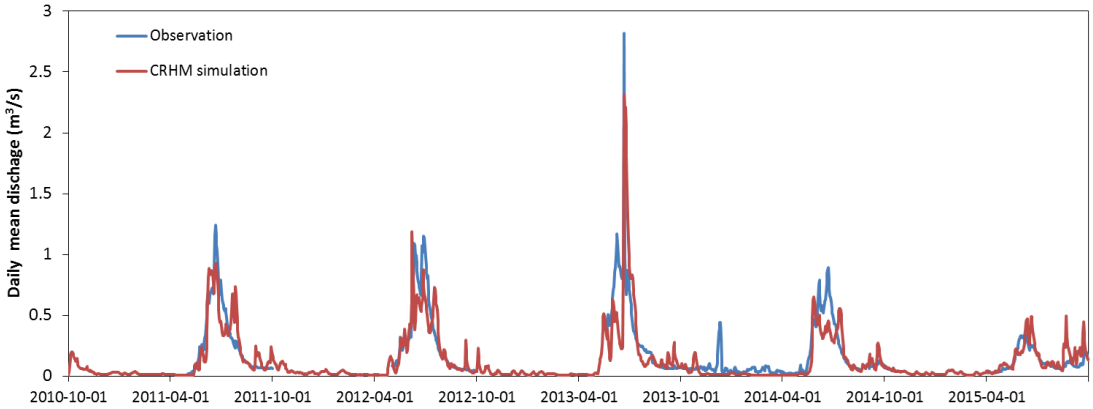

Figure 2-10. Comparison of observed and ObsMet-simulated daily mean discharge at the Marmot Creek Research Basin, Alberta, Canada outlet.

2.5.3 SNODAS performance at basin scale

To assess SNODAS SWE prediction quality at the basin scale, the MCRB basin mean SNODAS SWE was compared to the ObsMet-simulated basin average SWE for 2011 to 2015 water years (Figure 2-11). SNODAS SWE was much higher than ObsMet SWE for these five years; overestimation of SNODAS SWE ranged from 37% to 327% (five-year mean = 135%) when compared to ObsMet-simulated SWE. The RMSE between SNODAS and ObsMet -simulated SWE was also high, ranging from 66.75 to 302.34 mm (mean = 180.01 mm).

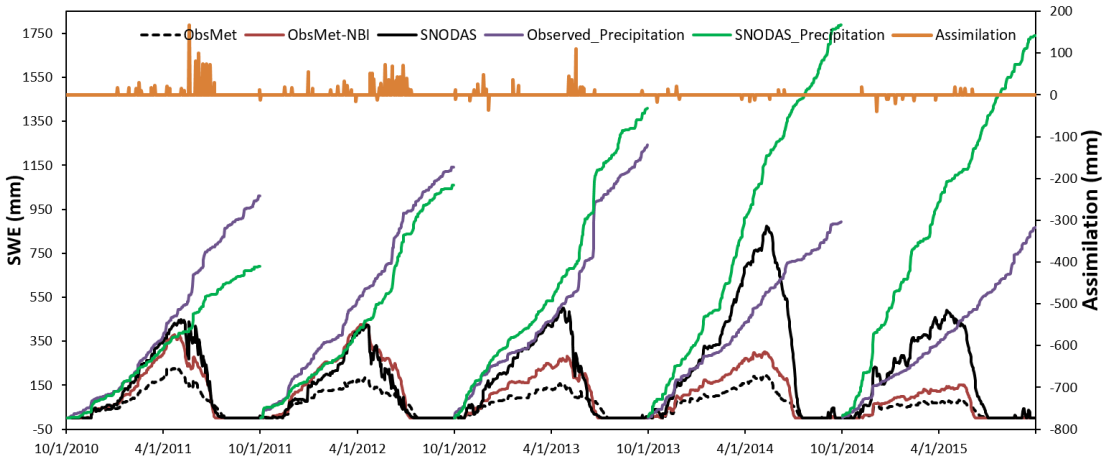

Figure 2-11. Comparisons of SNODAS, ObsMet and ObsMet_NBI-simulated basin average SWE, SNODAS and observed precipitation, and data assimilation magnitude in SNODAS at Marmot Creek Research Basin, Alberta, Canada.

To examine the effect of SNODAS precipitation on SNODAS SWE accuracy, the whole basin cumulative precipitation from SNODAS and observations were compared for each water year (Figure 2-11). The basin average SNODAS precipitation was calculated

by averaging the precipitation data from each MCRB pixel. The basin average observed precipitation was calculated by interpolating the precipitation measured from three Geonor gauges at MCRB using the observed precipitation gradient at a range of elevations throughout the basin (Fang et al., 2013). The accuracy of SNODAS precipitation data at MCRB was low during the five-year study period (mean RMSE = 371 mm and mean MB = 0.37) with variable error in different water years. SNODAS underestimated precipitation data at MCRB for with MB for water year 2011 of –0.24 and 2012 of –0.15. The RMSE between SNODAS and observed precipitation was 152.1 and 95.4 mm for 2011 and 2012 water years, respectively. SNODAS did not consistently underestimate precipitation for all five years, its overestimation ranged from 18% to 145% for the 2013 to 2015 water years. For 2013 to 2015 water years, SNODAS overestimated precipitation only by 18%, 95%, and 145%, but SNODAS SWE was 117%, 230%, and 327% higher than CRHM simulated SWE (Table 2-3). The accuracy of SNODAS SWE is strongly influenced by the accuracy of the precipitation data, however precipitation data is not the only contributor to errors.

Table 2-3. RMSE_m and MB_m between SWE that simulated by various simulations, and RMSE and MB between observed (Ob_P) and SNODAS (SNODAS_P) precipitation at Marmot Creek Research Basin, Alberta, Canada.

		SNODAS			SNODAS_P	
		RMSE_m	MB_m		RMSE	MB
All	CRHM	180.01	1.35	Ob_P	371.79	0.37
2011		89.68	0.63		152.09	-0.25
2012		66.75	0.37		95.35	-0.15
2013		140.09	1.17		116.79	0.18
2014		302.34	2.30		518.68	0.95
2015		196.35	3.27		613.68	1.45
		CRHM_NBI			CRHMSP_NBI+ASSIM	
		RMSE_m	MB_m		RMSE_m	MB_m
All	CRHM	66.58	0.50	SNODAS	41.10	0.07
2011		57.95	0.38		22.76	0.02
2012		103.08	0.72		49.58	0.22
2013		59.50	0.47		42.20	0.09
2014		59.15	0.43		41.55	0.01
2015		33.54	0.46		44.26	0.08
		CRHMSP			CRHMSP_NI	
		RMSE_m	MB_m		RMSE_m	MB_m
All	CRHM	132.13	0.57	CRHMSP	45.05	0.21
2011		46.04	-0.31		29.86	0.26
2012		60.91	-0.50		39.11	0.50
2013		33.49	0.31		34.68	0.20
2014		198.68	1.41		67.30	0.18
2015		202.25	3.38		44.68	0.14
		CRHMSP_NBI			CRHMSP_NB	
		RMSE_m	MB_m		RMSE_m	MB_m
All	CRHM	210.01	1.23	CRHMSP	57.25	0.22
2011		46.92	-0.06		19.32	0.08
2012		34.09	-0.17		22.15	0.15
2013		104.27	0.83		41.20	0.18
2014		312.53	2.32		69.03	0.20
2015		329.73	5.35		95.22	0.31
		CRHMSP+ASSIM			CRHMSP_NBI	
		RMSE_m	MB_m		RMSE_m	MB_m
All	CRHM	109.71	0.79	CRHMSP	91.77	0.42
2011		42.24	0.28		45.60	0.36
2012		41.57	0.19		58.07	0.66
2013		79.66	0.74		72.84	0.39
2014		192.44	1.40		121.23	0.38
2015		115.40	1.94		129.09	0.45

The lack of blowing snow transport and canopy snow interception simulations in the SNODAS NSM is another factor that leads to overestimation of basin SWE in MCRB. To verify this, a CRHM simulation (ObsMet_NBI) with two process modules turned off was run with local observed driving forces. The ObsMet_NBI simulated SWE was much higher than that by the complete model ObsMet (Figure 2-11). Compared to ObsMet simulated SWE, ObsMet_NBI overestimated SWE in MCRB on average by 50% for five water years with annual overestimation ranging from 38% to 72%. Compared to ObsMet, ObsMet_NBI increased peak SWE 1.44 to 1.83 times (mean = 1.6 times) during the five water years. This indicates that the missing blowing snow transport and canopy snow interception simulations in SNODAS are other major factors causing the SNODAS SWE overestimation in MCRB.

Impact of assimilation frequency and magnitude on SNODAS SWE accuracy was also analyzed (Figure 2-11). There were approximately 91 data assimilations related to water balance calculations in MCRB in SNODAS system for 2011 to 2015 water years. Assimilation was more frequent in first three water years (19 times and 798.7 mm in total for 2011, 31 times and 848.4 mm in total for 2012, and 19 times and 384.4 mm in total for 2013) than the latter two water years (10 times and –17.1 mm in total for 2014, 12 times and –34.4 mm in total for 2015). Assimilations before peak SWE in 2014 and 2015 water years were mainly negative, with more negative total assimilation amount in 2014 (–99 mm) than in 2015 (–31.4 mm). This leads to much lower SNODAS peak SWE in 2014 despite similar SNODAS precipitation in both years.

2.5.4 Mimicking SNODAS simulations using CRHM

To quantify the contribution of erroneous precipitation, model structure shortcomings, and SNODAS data assimilation accuracy in MCRB, five CRHM simulations with different model structure were run for 2011 to 2015 water years. Then, observed precipitation was replaced by SNODAS-predicted precipitation for the model forcing data (Figure 2-12). 1. CRHMSP was a complete CRHM model that simulates all processes. 2. CRHMSP_NB was a CRHM model without blowing snow transport simulation. 3. CRHMSP_NI was a CRHM model with canopy interception simulation turned off. 4. CRHMSP_NBI was the CRHM model with neither blowing snow transport or canopy snow interception. 5. CRHMSP_NBI+ASSIM was the CRHM model without either blowing snow transport or canopy snow interception, but with assimilation derived from the water balance calculation added. Compared to ObsMet, overprediction of CRHMSP SWE (five-year mean = 57%) was directly related to overestimation of SNODAS precipitation data (five year mean MB = 0.37). When compared with ObsMet SWE, CRHMSP underestimated SWE in MCRB by 31% and 50% for 2011 and 2012, which can be explained by MB of –0.25 in 2011 and –0.15 in 2012 for SNODAS precipitation. Overestimation of CRHMSP SWE in other water years ranged from 31% to 338% compared to ObsMet SWE, which is related to overestimated precipitation with MB ranging from 0.18 to 1.45. Compared to CRHMSP,

CRHMSP_NB overpredicted basin SWE by 8.1% to 31.5% for 2011 to 2015 water years with five-year mean overprediction by 22.0%. For the CRHMSP_NI simulation, the simulated basin SWE was 1.14 to 1.5 times (five-year mean = 1.21 times) of CRHMSP simulated SWE for 2011 to 2015 water years. With both blowing snow transportation and canopy interception simulations turned off, CRHMSP_NBI simulated much more SWE than CRHMSP ranging from 36% to 66% (five-year mean = 42%). One possible source of this annual variation may be the changing climate conditions among water years.

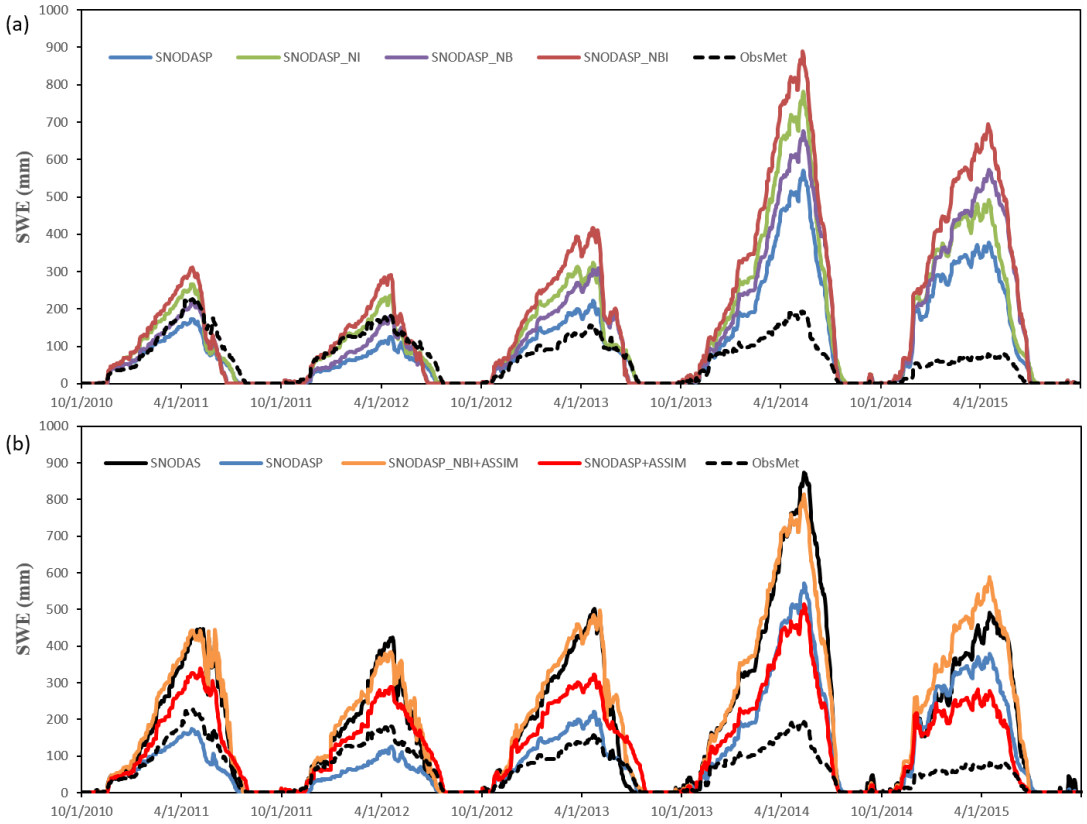

Figure 2-12. Comparison of SNODAS and ObsMet SWE to simulations driven by SNODAS precipitation at Marmot Creek Research Basin, Alberta, Canada. a) shows the influence of snow interception and blowing snow transport simulations on basin SWE. b) illustrates importance of incorporating snow interception and blowing snow transport processes in the simulation.

On average, blowing snow transport and canopy interception accounted for approximately 35% of snow loss in MCRB, with annual snow loss ranging from 24% to 49% for 2011 to 2015 water years. Without simulating these two processes, the simulated peak SWE increased by 57%, while the increase in peak SWE varied for different years ranging from 32% to 88%. These results highlight the importance of including the two processes when modelling the snowpack of the Canadian Rockies.

Although CRHMSP_NBI sbimulated SWE was closer to SNODAS SWE than other

simulations demonstrated above, it was still far from matching SNODAS SWE. This is because SNODAS SWE contains influence of data assimilation. Thus, a fifth simulation CRHMSP_NBI+ASSIM (Figure 2-12 b) was conducted, in which the assimilation derived from the water balance calculation was added to CRHMSP_NBI simulation. CRHMSP_NBI+ASSIM was comparable to SNODAS with 1% to 22% more SWE estimated for the 2011 to 2015 water years and a five-year mean of 7% overestimation. The five-year mean RMSE_m was 41.1 mm, with annual RMSE_m ranging from 22.7 mm to 49.6mm for the 2011 to 2015 water years. This difference can be explained by the different parameters and driving forces (other than precipitation) used in the two models. This indicates that, besides the two missing processes, CRHM shares similar model structure with the SNODAS NSM, and is able to mimic the SNODAS system.

Simulated SWE from CRHMSP, CRHMSP_NBI and CRHMSP_NBI+ASSIM was compared to ObsMet to quantify the influence of precipitation, missing processes, and data assimilation on SNODAS SWE accuracy (Table 2-3). The RMSE_m caused by inaccurate precipitation was 132.1 mm in all and varied across years from 33.5 to 202.3 mm. Two missing processes in the model introduced another 103.9 mm of RMSE_m across five water years. It increased the RMSE_m in most years except 2011, in which RMSE_m decreased 7.9 mm, as missing processes simulation compensated for underestimated precipitation that year. After data assimilation, the mean RMSE_m of CRHMSP_NBI+ASSIM simulated SWE reduced to 193.2 mm during the five water years. In all, data assimilation contributed positively to SNODAS accuracy but the influence was varied among water years. It decreased the RMSE_m by 2.6 and 107.3 mm in the 2014 and 2015 water year, respectively. However, in the 2011, 2012, and 2013 water years, data assimilation increased the RMSE_m by 43.9, 64.0, and 48.2 mm, respectively. This indicates that data assimilation did not always improve the accuracy of SNODAS SWE at MCRB. This might be a result of using inaccurate snow observation data in the SNODAS data assimilation system. The details of snow observations used for SNODAS assimilation in this area during these years were not explored. Snow-pillow measurement sites in the Canadian Rockies are commonly located in small level clearings at medium elevations and are not representative of areas with dense forests and varying topographic exposure to radiation and wind (Pomeroy and Gray, 1995; Pomeroy et al., 2002). If data from such sites are used to nudge the SNODAS product, then additional uncertainty occasionally may be spatially propagated (Dozier et al., 2016). Information about the type of data used for SNODAS data assimilation would be beneficial to researchers and water resources managers.

2.5.5 Assimilating SNODAS into CRHM

SNODAS overestimated SWE at all sites in three Canadian environments for 2011 to 2015 water years. This overestimation was caused by overestimated precipitation and missing components to the SNODAS model structure. Data assimilation can compensate for this problem in many places. However, the frequency of data

assimilation in the boreal forest and prairie was very low — once or twice a year. Although the assimilation frequency is higher in the Canadian Rockies (18 times a year on average), more frequent data assimilation does not always make for better results. To correct SNODAS SWE bias one must fix the problems of missing processes and precipitation prediction. The complete CRHM model (CRHMSP) can solve the problem of missing processes. Although the assimilation data in the Canadian Rockies is not always correct, it is believed the precipitation problem can be partially solved after assimilation into the CRHMSP simulation. Therefore, a simulation that contains assimilation data calculated from the water balance into CRHMSP model might be able to correct some of the bias of SNODAS SWE (CRHMSP+ASSIM).

The SWE simulated by CRHMSP+ASSIM is shown in Figure 2-12 b. Compared to the original SNODAS data, CRHMSP+ASSIM improved SWE accuracy after assimilation into CRHM in MCRB. The RMSE_m between CRHMSP+ASSIM and ObsMet for five water years dropped to 109.7 mm from 180.0 mm with annual improvement ranging from 25.2 mm to 110 mm. Overestimation in CRHMSP+ASSIM SWE, when compared to ObsMet SWE, also decreased from 1.35 to 0.79 for five water years with seasonal decreases ranging from 0.18 to 1.33. This indicates that assimilation of SNODAS into CRHM has the potential to improve the SWE accuracy of SNODAS SWE even though the problem caused by erroneous precipitation cannot be completely solved. Compared to simulations that only incorporated missing processes into SNODAS (i.e., CRHMSP), adding the data assimilation (i.e., CRHMSP+ASSIM) only decreased the RMSE_m of SWE by 22.4 mm. It improved the accuracy of all water years except 2012 (Table 2-3).

In a data assimilation system, product accuracy is heavily reliant on two factors: model simulation and assimilation. In a region like MCRB where there are no frequent and reliable data resources for assimilation, a correct model structure is much more important than data assimilation. Therefore, there are two recommendations to the SNODAS system team from the present research. Recommendation 1 is to incorporate blowing snow transportation and forest canopy interception into the SNODAS NSM. Although making the gridded model spatially coupled with two process simulations can reduce computational efficiency and add complexity of parameterisation and input data, this can nevertheless improve product accuracy in regions with infrequent and unreliable assimilation input data. Recommendation 2 is to increase the assimilation of snow information into snow modelling in Canada in whatever platform is used.

2.6 Conclusions

This study evaluated this product in three western Canadian environments; the boreal forest, prairie, and Rocky Mountains. In the boreal forest region, SNODAS worked very well in deciduous forest stands, less well in the mixed deciduous and needleleaf forests, and poorly in an open, windswept fen. On the prairies, the SNODAS predicted SWE was not correlated with observed SWE, and the RMSE and MB of prediction

were relatively high. These suggest that the SNODAS poorly captures spatial variation of SWE in the open, wind-redistributed Canadian prairie environment. In the Rocky Mountains, SNODAS data quality varied from year to year, and SNODAS overestimated measured SWE on the ground at all sites in all years as the precipitation that drove SNODAS NSM model overestimated actual precipitation.

In MCRB, a well-studied headwater basin in Canadian Rockies, SNODAS SWE accuracy was evaluated by comparing it to the CRHM physically based hydrological model. CRHM was also used to identify sources of SNODAS error by mimicking the SNODAS system with different model configurations. This indicated that the accuracy of SNODAS SWE data is greatly influenced by: 1) missing blowing snow transport and canopy interception and sublimation processes in the mass balance calculation, and 2) erroneous precipitation in the SNODAS NSM. The data assimilation in the SNODAS system in MCRB does not always improve simulations. To compensate for this, a method to correct SNODAS SWE by assimilating it into CRHM with a full set of snow processes was developed. The results show that this approach can improve the accuracy of SNODAS SWE. An additional benefit is that the CRHM assimilation process downscales the SNODAS data to the HRU scale that permits multi-scale snow and hydrological modelling. Overall, the results show promise for assimilation-based bias correction of SNODAS data products for basins in Canada with sparse precipitation measurements and the ability to use these products to estimate peak SWE at different spatial scales. To improve the SNODAS SWE accuracy, especially in the regions with sparse reliable input data for assimilation, two recommendations are also provided to the NOHRSC SNODAS team: 1) two missing snow redistribution processes should be added to the NSM, and 2) increase the assimilation of snow information into snow modelling in Canada in whatever platform is used.

CHAPTER 3: Detecting intercepted snow on mountain needleleaf forest canopies using satellite remote sensing

Status: Published online June 12, 2019

Citation: Lv, Z. and Pomeroy, J.W., 2019. Detecting intercepted snow in the coniferous forest canopies by using satellite remotely sensed data. Remote Sensing of Environment, 231. doi:10.1016/j.rse.2019.111222.

Author Contributions: Zhibang Lv conceptualized this research, designed and performed experiments, collected data, conducted analysis, and wrote the manuscript. John Pomeroy provided equipment and financial resources for the field campaign, discussion of the concept, methodology and results, and useful comments with regards to the content, structure and writing of the manuscript.

3.1 Preface

Snow interception by cold region needleleaf forest canopies is a crucial process that controls local snow accumulation and redistribution. Various ground-based methods exist to measure intercepted snow, however no research has focused on detecting canopy snow using satellite observations, which can contribute to large scale snow interception model validation and data assimilation to cold regions hydrological forecasting models. After analyzing the importance of snow interception to basin SWE in the previous chapter, it was clear that development of a method to detect snow interception using satellite remote sensing could be beneficial for cold regions hydrological modelling. The aims of this research are to: 1) examine the influence of canopy snow on four selected remote sensing indices (NDSI, NDVI, albedo, and LST), 2) determine the influence of different forest conditions on these indices when snow is present and absent on the canopy, and 3) develop an approach for canopy snow detection and compare its results to a model simulation.

3.2 Introduction

Snow accumulation and ablation processes in evergreen forests are largely influenced by snow interception in the canopy (Nakai et al., 1994, Pomeroy and Gray, 1995). In coniferous forests, some snowfall is first intercepted in the canopy, and then exits the canopy primarily through unloading, melt dripping, or evaporation and sublimation (Hedstrom and Pomeroy, 1998; Suzuki and Nakai, 2008). This process makes the snow water equivalent (the mass of the snowpack per unit area, expressed as an equivalent depth of water in mm, SWE) in forests significantly different from nearby open areas. Various research indicates that up to 60% of the annual snowfall could be intercepted and the sublimation of intercepted snow could reach up to 40% of the annual snowfall (Kuz'min, 1960; Pomeroy and Schmidt, 1993; Storck et al., 2002). Interception itself is influenced by various factors including air temperature (Miller, 1964), wind (McNay et al., 1988; Woods et al., 2006), snowfall magnitude (Boon, 2009), elevation (D'Eon, 2004), slope and aspect (Golding and Swanson, 1986), and canopy structure (Hedstrom and Pomeroy, 1998; Pomeroy et al., 2002). Intercepted snow affects energy partitioning in the canopy though changes to the canopy surface temperature and resistance and hence the direction and magnitude of sensible heat flux and Bowen ratio (Parviainen and Pomeroy, 2000; Pomeroy et al., 2008; Suzuki and Nakai, 2008). Therefore, determining the magnitude, processes and timing of snow interception has drawn a great deal of interest from cold regions land surface process and hydrological research communities (Essery et al., 2003; Friesen et al., 2015; Gelfan et al., 2004).

Because of the complexity of the interception process and irregular shape of tree crowns, direct measures of regional snow interception are difficult. Usually, the amount of intercepted snow can be indirectly assessed by comparing precipitation measured on the surface under the canopy and the surface of nearby clearings, open areas or above canopy (Kittredge, 1953; Koivusalo and Kokkonen, 2002; Winkler et al., 2005). The seasonal interception loss is usually determined from the peak SWE difference between forests and nearby clearings or open areas (Bales et al., 2011; Koivusalo and Kokkonen, 2002; Lundberg et al., 1998; Winkler et al., 2005). Various approaches have used a weighed-tree (e.g., Lundberg, 1993; Pomeroy and Schmidt, 1993,) or branch, with one direct method being to remove the snow from a branch or tree by knocking the snow off and weighing it (Goodell, 1959; Miller, 1964). However, this latter method is laborious and time consuming and only provides intercepted snow amount at a single point for a single moment in time. To continuously measure snow interception, a cut tree branch (Schmidt and Gluns, 1991) or a whole tree (Storck et al., 2002) can be connected to a lysimeter. The hanging-tree method, in which a living tree is cut and suspended on a tower with its weight continuously measured, has been widely used in various research projects at different locations (Lundberg et al., 1998; Harding and Pomeroy, 1996; Hedstrom and Pomeroy, 1998; Montesi et al., 2004; Pomeroy and

Schmidt, 1993; Suzuki and Nakai, 2008). A complication of this method is that the cut tree dries through the season and hence it is hard to determine its tare weight. Some artificial structures are used to replicate a branch (e.g., boards in Floyd and Weiler, 2008) or a tree (e.g., artificial tree in Schmidt et al., 1988). Although these structure's tare weights are stable, their structures are quite different from a real tree. For instance, the elasticity and therefore angle and shape of a real tree branch changes with temperature (Schmidt and Pomeroy, 1990), a property lacking in artificial trees or snowboards. A further problem with cut trees and artificial structures is that their thermal and longwave radiance characteristics are different from a living tree and this makes the unloading process different from real trees. To avoid cutting the tree, Friesen et al. (2008) developed a trunk compression sensor to measure the tree weight change during a storm to determine the intercepted rain amount. Martin et al. (2013) adopted this method in snow interception measurement as a prototype. Another possible method that does not require cutting the tree is to measure sway frequency. Papesch (1984) found that the intercepted snow reduces sway frequency of tree, and this can be quantified. Although those methods provide good measures of a single branch or a whole tree interception, like all other methods, it is challenge to scale this point data up to a catchment or regional scale. Signal attenuation approaches are also used in snow interception measurement by using equipment such as a emitted gamma ray attenuation (Lundberg et al., 1998), active impulse radar system (Magnusson, 2006) or passive cosmic ray sensor (Zreda et al., 2012). The principle behind these methods is that the intercepted snow will impact the attenuation of gamma rays emitted from a radioactive source in the first case, signal attenuation, in the second case, and speed or counts of neutrons, in the third case over a defined time. Although these methods can measure snow interception at larger scale than a single tree, their scale still restricted by the footprint of the sensors they use and in the case of gamma ray emission, the technique is now considered too dangerous to use because of human health concerns.

Because snow has much higher reflectivity than the tree canopy, optical photography has been used by several researchers to detect the intercepted canopy snow. Tennyson et al. (1974) used a time-lapse movie camera to develop a snow load index to represent the canopy snow load and study the importance of snow interception in an uneven-aged Ponderosa Pine forest in east-central Arizona. Using a fractal relationship for intercepted snow, Pomeroy and Schmidt (1993) modeled the relationship between digital-camera imagery derived snowcovered area in the canopy and snow mass on a tree branch. Floyd and Weiler (2008) developed a time-lapse camera system to measure the snow accumulation and ablation dynamics during rain on snow event. A digital camera was included in this system to measure the canopy snowcovered area (ratio of snow-covered pixels to total pixel on canopy in the image) during and after a storm. Garvelmann et al. (2013) used a 45-camera time-lapse network to study snow processes in several mesoscale catchments. Their results indicate that the canopy snow coverage and timing of interception and unloading can be clearly recorded. Stähli et al. (2009) used human visual inspection in the field or a photograph of a forest to determine the

snow interception level in their study of the importance of snow interception on the coniferous forest radiation processes. Parajka et al. (2012) used a time-lapse camera to detect the intercepted snow on a canopy. Their results agreed well with the simulation of the snow interception model developed by Hedstrom and Pomeroy (1998). Although time-lapse cameras are able to provide the relative magnitude and timing of interception, which could be used to validate the snow interception model performance (Parajka et al., 2012; Stähli et al., 2009), they have has only been used at small scales and are difficult to use for regional or global scales.

Satellite remote sensing has been used in various large scale snow properties studies (see Nolin, 2010, or Frei et al., 2012, for reviews). To the authors' knowledge however, no research has been focused on the canopy intercepted snow detection. Various remote sensing indices have been developed to monitor changing of landscape. The Normalized Difference Snow Index (NDSI) has been widely used in snow cover monitoring in the remote sensing community since it was developed (Dozier, 1989; Hall et al., 1995). Because the forest canopy can obstruct the reflected visible and infrared information from snow on the ground under it, the NDSI method has a much lower accuracy in detecting ground snow in forested regions (Klein et al., 1998; Wang et al., 2015; Wang et al., 2018). Niemi et al. (2012) and Heinilä et al. (2014) studied the forest canopy influence on snow reflectance behaviour in Finland using mast-borne and airborne spectrometers, respectively. Results of both studies show that NDSI increased with snow on the canopy when compared to snow-free canopies. On the other hand, Normalized Difference Vegetation Index (NDVI), which is widely used in vegetation monitoring studies, decreases when snow is present on the canopy (Heinilä et al., 2014; Niemi et al., 2012). Snow has a much higher albedo than most of other land surface objects, especially compared to the forest canopy. However, whether canopy snow changes albedo or not is not well agreed upon in the literature. Pomeroy and Dion (1996) examined the amount of intercepted snow on a Jack Pine canopy, the canopy shortwave and net radiation exchange in the boreal forest of central Saskatchewan, Canada. They found no relationship between the amount of intercepted snow and canopy albedo. However, Leonard and Eschner (1968) measured albedo above a red pine plantation in New York, USA and found the albedo increased up to 0.20 when the canopy was covered by snow, and it decreased to summer values after snow removed from the canopy. Yamazaki et al. (1996) found a nonlinear relationship between canopy snow load and forest albedo in Japan. This concurred with the results of Kuusinen et al. (2012), who found that the presence of snow on the canopy can increase the boreal Scots pine forest albedo by more than 0.2, on average. But this increase only happens when more than half of the canopy was covered by snow. Temperature might be another indicator of snow presence on the canopy as the temperature of snow-free forest canopy is usually higher than snow and atmosphere temperature on a sunny day (Musselman and Pomeroy, 2017; Pomeroy et al., 2009). Nakai et al. (1999b) found the canopy surface temperature is usually lower than air temperature when snow fully covers the canopy, while the opposite is true when the canopy is snow-free. Lundquist and Lott

(2008) used near-surface soil temperatures as an indicator of snow presence on the ground, and found higher variation when the ground is snow free. This finding should be applicable to the canopy as well. Because of the low thermal conductivity, high albedo and high longwave emissivity of snow, its psychrometric cooling during sublimation and upper limitation of 0 ºC, snow-covered canopies should have a lower daily temperature variation than snow-free canopies.

NDSI, NDVI, albedo, and Land Surface Temperature (LST) can be derived from most optical and thermal satellite sensors. This suggests that detection of intercepted snow over large scales using satellite remote sensing data is possible. The main goal of this research is to determine the potential to use satellite data to detect intercepted snow on forest canopies. The specific objectives are to: 1) examine the influence of canopy snow on four selected remote sensing indices (NDSI, NDVI, albedo, and LST), 2) determine the influence of different forest conditions on these indices when snow is present and absent on the canopy, and 3) develop an approach for canopy snow detection and compare its results to a model simulation. The methods developed are expected to provide a new source of validation data for a large-scale snow interception model simulation and input data for future snow interception data assimilation into hydrological and land surface forecasting models.

3.3 Materials and methods

3.3.1 Study area

The study area of this research is Marmot Creek Research Basin (MCRB, 50°57`N, 115°09`W), located in the Front Ranges of the Canadian Rockies in Alberta, Canada (Figure 3-1). MCRB is approximately 9.4 km^2 in area with an elevation range from 1700 m to 2825 m. Average annual precipitation in MCRB varies from 660 mm at low elevations to 1140 mm at high elevations above tree line and 60% to 75% of precipitation falls as snow (DeBeer and Pomeroy, 2009). The main land covers in MCRB are continuous stands of Lodgepole Pine, Engelmann Spruce, and Douglas Fir in the low to middle elevations; Larch, Engelmann Spruce, Sub-alpine Fir, shrubs, and grasses are dominant at upper elevations; talus and bare rocks are the main land-cover in the highest elevations (DeBeer and Pomeroy, 2009). Seven permanent meteorological stations have been established in various locations in MRCB since 2005 for continuously observing soil moisture, soil temperature, snow depth, short and long wave radiation, air temperature, humidity, and wind speed. Three Alter-shielded Geonor weighing precipitation gauges were mounted in low, middle, and high elevation bands to measure precipitation and the measurements were corrected for wind-induced undercatch (Smith, 2009). Approximately 65% of the basin is covered by forest and the sublimation of intercepted snow in the mid-elevation forest can return up to 60% of the annul snowfall directly back to the atmosphere (Ellis et al., 2010). MCRB includes four sub-basins: Cabin Creek, Middle Creek, Twin Creek, and Confluence which have

undergone different forest management. To study the influence of forest removal on local hydrology in the 1970s, two experiments were conducted with treatments in two sub-basins with the third one left as a control (Rothwell et al., 2016). In 1974, 50% of the forest area in the Cabin Creek sub-basin was clear-cut in six large blocks. In 1977–1979, around 3000 small circular openings (12.2 m to 18.3 m in diameter) were cut in a "honeycomb" pattern in Twin Creek sub-basin. The total circular opening area accounted for 50% of the forest area of this sub-basin. After 40 years, small trees are scattered in both types of clearings. These management treatments give the forests a large range of canopy cover that makes the basin a good site for the current research. Two airborne LiDAR data collection sessions were conducted in August 2007 and March 2008 in MRCB. High resolution (1 m) topographic information (Digital Elevation Model (DEM), aspect, and slope) and forest canopy data (canopy coverage and Digital Surface Model (DSM, i.e., first return of Lidar data)) is available from these observations.

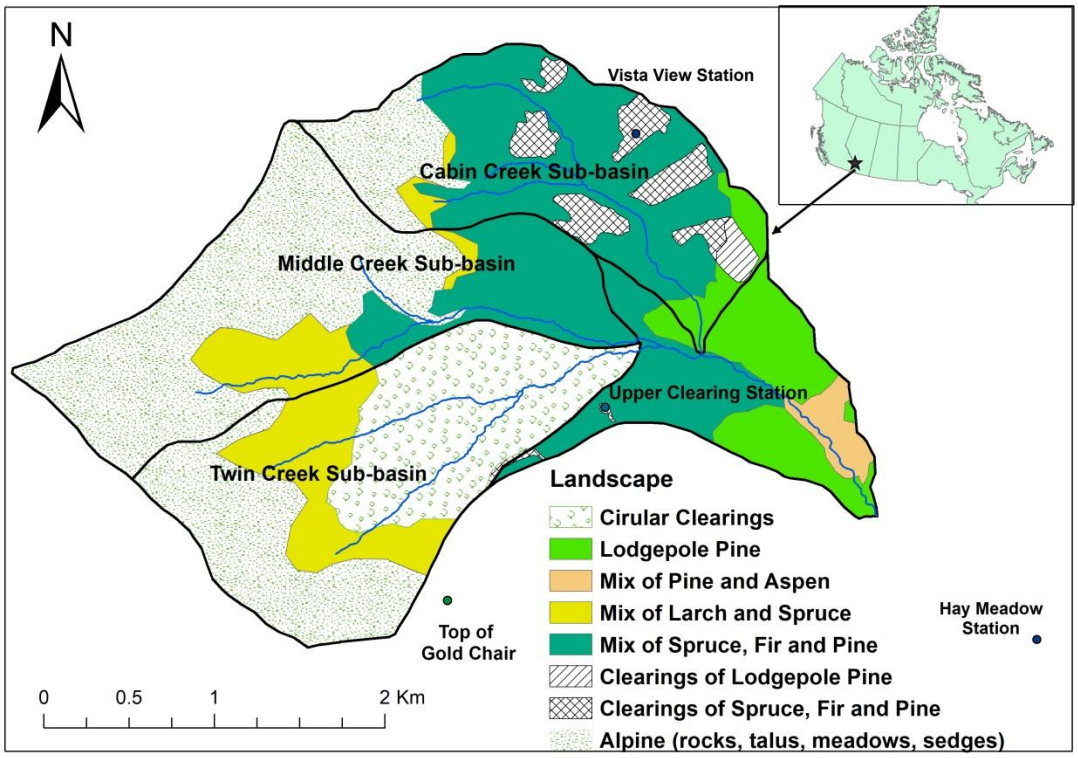

Figure 3-1. Land cover, stream network, and main sub-basins of Marmot Creek Research Basin, Alberta, Canada.

3.3.2 Time-lapse photography and processing

To collect ground truth data of snow interception, a time-lapse camera (Wingscapes TimelapseCam) with a 43° field of view was mounted on the top of the Gold Chair-lift at the Nakiska ski resort beside MRCB from March 2015 to June 2016. It took hourly, day-time images for most of the forest area in MCRB (Figure 3-2a). The "Photo

Rectification And ClassificaTIon SoftwarE" ("PRACTISE"; Härer et al., 2013) was used to derive the canopy snowcover information from the time-lapse photography. PRACTISE is used to derive micro-scale snowcover information. The input into PRACTISE are time-lapse pictures, DEM, and several camera parameters (position, offset height, roll, lens focal length, sensor height and width, photo pixel row and column numbers, and target position (middle point of photo) in the photo). The output of the routine is the image with canopy snowcover information that is used as verification of if the canopies were snowcovered.

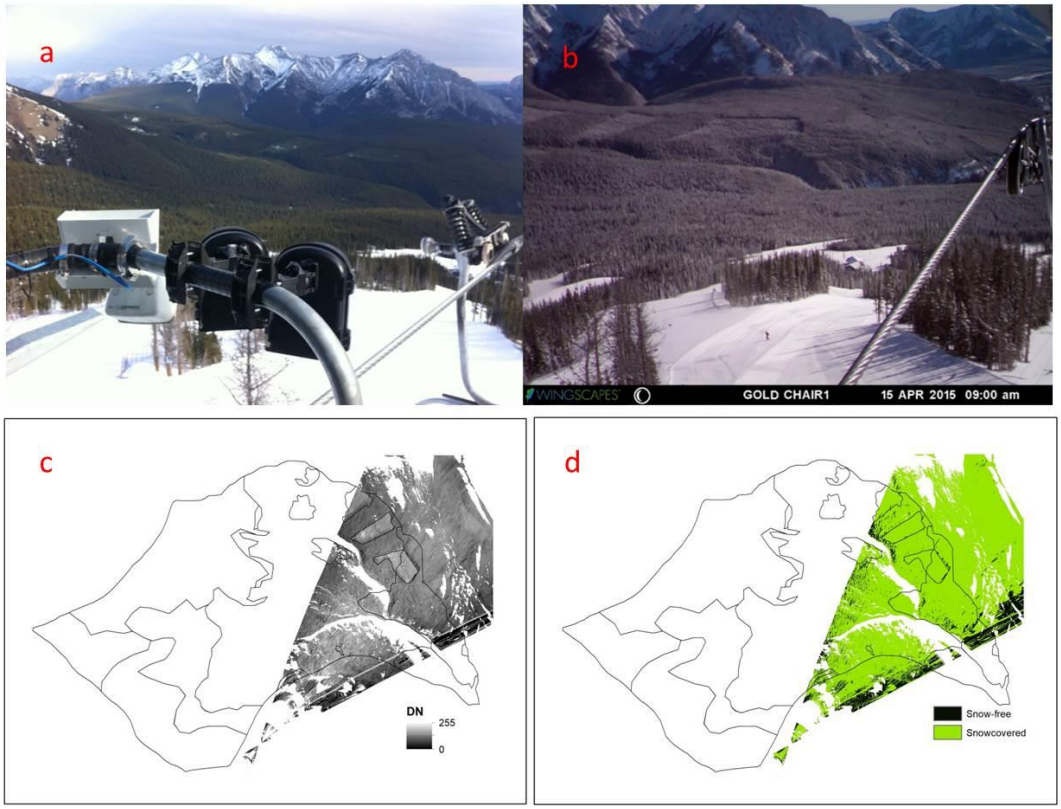

Figure 3-2. (a) Two cameras mounted on the Gold Chair lift of Nakiska ski resort, (b) picture taken by the right camera on 15 April, 2015, (c) the picture after georectification, (d) the georectified picture after classification.

PRACTISE includes four modules. The first generates a "viewshed" by identifying the visible pixels of the DSM from the camera position. Input data for this module are the 1-m resolution DSM of MCRB and surrounding area plus the camera position. The second module georectifies all visible DSM pixels, by an animation and rendering technique (Watt and Watt, 1992) that generates a 2-D virtual camera image of DSM that also contains the 3-D information of each pixel. Once rendered, the camera RGB values are assigned to the 2-D virtual image of DSM. In the end, the pixels contain RGB values that are retransformed to a 3-D position. The third module optionally assesses Ground Control Points (GCPs) and it is only activated if the precise camera or target position is

unknown. In this study, sixteen GCPs were chosen to minimize the georectification error caused by the lack of precision in the target position. The fourth module classifies snowcover using two classification approaches with different levels of complexity. The first is based on threshold values that need to be manually set for each image based on analysing RGB values of snow and other objectives. This method is laborious but relatively accurate. The second is an automatic snow classification routine developed by Salvatori et al. (2011). This method is time-saving and is suitable for long term image processing, but with reduced accuracy. The threshold method was chosen in this research due to its stability and high accuracy. The classification threshold for RGB value was set to 50 to determine whether or not the pixel is snowcovered in the image following a study by Garvelmann et al. (2013). Because the RGB value is highly influenced by illumination conditions, the RGB value for one object may vary on different days. Using the ski lift cable from each image as a reference, an RGB adjustment was calculated for all images before classification. RGB value of all other images was adjusted to the April 15, 2015 image according to the RGB ratio of the lift cable between two images. Figure 3-2b, c, and d show an original time-lapse photo, the georectified photo, and classified canopy snowcover, respectively.

After classification, a canopy snow-coverage index, which is the ratio of snowcovered to total pixels from the oblique time lapse photographs, was calculated and aggregated to 30 m × 30 m areas corresponding to Landsat image pixel locations in MRCB. This canopy snow-coverage index is not the real ratio of snowcovered area in the canopy, but it is the snow-coverage of that part of the canopy that is captured in the photographs and so its value is highly influenced by camera position, view angle and distance between camera and objective (Garvelmann et al., 2013). A detailed land cover map of the basin was used to mask out the non-forested areas, which were excluded from the following analyses.

3.3.3 Landsat image and its processing

3.3.3.1 NDSI and NDVI

Fifty-six Landsat 5 TM and Landsat 8 OLI scenes from 2007 to 2016 were used in this research according to image availability and cloud cover conditions (cloud cover less than 5% in MCRB). On the 56 images, 22 of them are from Landsat 8 and 34 of them are from Landsat 5. These geometrically corrected images are available from the United States Geological Survey (USGS) website (http://earthexplorer.usgs.gov/). Atmospheric correction was conducted in ENVI using the FLAASH algorithm. NDSI (Equation 3.1) and NDVI (Equation 3.2) of each image were calculated using Raster Calculator tool in ArcGIS 10.2:

$$NDSI = \frac{B_{Green} - B_{SWIR}}{B_{Green} + B_{SWIR}} \quad (3.1)$$

$$NDVI = \frac{B_{NIR} - B_{Red}}{B_{NIR} + B_{Red}} \quad (3.2)$$

where B_{Green} is the reflectance of green band (band 2 for Landsat 5 TM and Band 3 Landsat 8 OLI); B_{SWIR} is the reflectance of short wave infrared band (band 5 for Landsat 5 TM and Band 6 Landsat 8 OLI); B_{NIR} is the reflectance of near infrared band (band 4 for Landsat 5 TM and Band 5 for Landsat 8 OLI); B_{Red} is the reflectance of red band (band 3 for Landsat 5 TM and Band 4 for Landsat 8 OLI).

3.3.3.2 Shortwave albedo

Because of the inability to sample the intrinsic reflectance anisotropy of land surface caused by a narrow sensor field-of-view, directly retrieving an accurate spectral albedo value using Landsat images is not possible (Roy et al., 2014). Shuai et al. (2011) developed a method that combining the MODIS Bidirectional Reflectance Distribution Function (BRDF) product and Landsat images to obtain a more reliable spectral albedo. However, this method only works on snow-free surfaces. Developing a reliable snow surface shortwave albedo (hereafter referred to as albedo) retrieving method for Landsat 8 imagery is beyond the scope of this research. The focus here is to study albedo change caused by snow interception but not albedo magnitude itself. Therefore, the methods developed by Liang (2000) and Ke et al. (2016) were used to retrieve the land surface albedo. Landsat 5 TM land surface albedo was calculated following the method proposed by Liang (2000) using the following equation:

$$\alpha = 0.356\alpha_1 + 0.130\alpha_3 + 0.373\alpha_4 + 0.085\alpha_5 + 0.072\alpha_7 - 0.0018 \quad (3.3)$$

where α_1, α_3, α_4, α_5, and α_7 represent narrowband band albedo of Landsat 5 TM band 1, 3, 4, 5, and 7, respectively.

Landsat 8 OLI land surface albedo was calculated using the method introduced by Ke et al. (2016) using:

$$\alpha = 0.130\alpha_1 + 0.115\alpha_2 + 0.143\alpha_3 + 0.180\alpha_4 + 0.281\alpha_5 + 0.108\alpha_6 + 0.042\alpha_7 \quad (3.4)$$

where α_1, α_2, α_3, α_4, α_5, α_6, and α_7 represent land surface reflectance of Landsat 8 OLI band 1, 2, 3, 4, 5, 6, and 7, respectively.

Landsat derived albedo data was validated by albedo data measured *in situ* from the Hay Meadow site located in MRCB (Figure 3-1). The Hay Meadow site was chosen because it is flat open ground and its land cover was unique and constant through the winter. The measured albedo represents the 30 m area corresponding to one Landsat image pixel while the topography and land cover of other sites in MRCB are more complex.

3.3.3.2 LST

Different from previous Landsat missions, the Landsat 8 TIRS sensor divided the thermal infrared radiance measurement into two bands (Band 10 and 11). Both Jiménez-Muñoz et al. (2014) and Yu et al. (2014) reported that Band 10 provides more accurate estimates of LST. Yu et al. (2014) compared several LST retrieval methods from Landsat 8 TIRS and they found that the radiative transfer equation-based method had better accuracy than either the split-window algorithm or the single channel method. The LST is defined as:

$$LST = \frac{C_1}{\lambda ln\left(\frac{C_2}{\lambda^5\left(R-I^{\uparrow}-\tau(1-\varepsilon)I^{\downarrow}\right)/\tau\varepsilon}+1\right)} \tag{3.5}$$

where C_1 and C_2 are constants with the value 14387.7μm·K and 1.19104×10^8W·μm^4·m^{-2}·sr^{-1}, respectively, λ is the effective wavelength of the thermal band in um (band 6 and band 10 for Landsat 5 and Landsat 8, respectively), R is the thermal band at sensor radiance, $I^{\uparrow}$,$I^{\downarrow}$, and τ are upwelling path radiance, downwelling path radiance, and channel atmospheric transmittance of thermal band respectively and their values are given by the on-line NASA Atmospheric Correction Parameter Calculator (Barsi et al., 2003). The land surface emissivity, ε, is determined using a simple and popular NDVI-based method (Momeni and Saradjian, 2007; Sobrino et al., 2004; Valor and Caselles, 1996; Van de Griend and Owe, 1993; Yu et al., 2014). This method typically assumes there are only two objects on the land surface, green vegetation and soil. However, snow may be present on or under the canopy in this study, thus a modified NDVI-based method is used in this research to determine the land surface emissivity in different cases:

(1) NDVI<0.2

When the NDVI value of a pixel is less than 0.2, the pixel is assumed to be non-vegetated. If the NDSI value of this pixel is equal to or higher than 0.4, the pixel is considered covered by snow and its emissivity is assumed to be emissivity of snow. Otherwise, the land cover of this pixel is assumed to be pure soil and its emissivity is calculated from red band reflectance through an empirical relationship.

(2) 0.2≤NDVI≤0.5

Under these conditions, land cover is assumed to be a mix of either snow and vegetation or bare soil and vegetation. NDSI has poor accuracy in determining snow cover on the forest floor, so the Normalized Difference Forest Snow Index (NDFSI, Equation 3.7), that has greater accuracy in determining snow cover under a coniferous canopy (Wang et al., 2015), is used to determine if snow is present. If NDFSI is equal or higher than 0.4, the land cover is assumed to be the mixture of snow and vegetation, otherwise, it is assumed to be composed of bare soil and vegetation. The pixel proportion of vegetation (PV) was calculated from the NDVI

value and it is used to calculate land surface emissivity.

(3) NDVI>0.5

Pixel has a NDVI value higher than 0.5 is assumed to be fully covered by vegetation and its emissivity equals to emissivity of vegetation.

The modified NDVI-based method is summarized as:

$$\varepsilon = \begin{cases} \varepsilon_{\text{snow}} & \text{NDVI} < 0.2 \quad \text{NDSI} \geq 0.4 \\ a - b * \alpha_4 & \text{NDVI} < 0.2 \quad \text{NDSI} < 0.4 \\ \varepsilon_v PV + \varepsilon_{\text{snow}}(1 - PV) + C & 0.2 \leq \text{NDVI} \leq 0.5 \quad \text{NDFSI} \geq 0.4 \\ \varepsilon_v PV + \varepsilon_{\text{soil}}(1 - PV) + C & 0.2 \leq \text{NDVI} \leq 0.5 \quad \text{NDFSI} < 0.4 \\ \varepsilon_v + C & \text{NDVI} > 0.5 \end{cases} \quad (3.6)$$

where $\varepsilon_{\text{snow}}$, $\varepsilon_{\text{soil}}$, and ε_v denote to emissivity of snow (0.9904), soil (0.9668), and vegetation (0.9863), respectively. Their values were calculated from the MODIS UCSB (University of California, Santa Barbara) emissivity library. The values for a and b are constants, given as 0.973 and 0.047, respectively. C is the effect of land surface on the geometrical distribution and internal reflection. The calculation methods of PV and C refer to Sobrino et al. (2004) or Yu et al. (2014). NDFSI is calculated as:

$$NDFSI = \frac{B_{NIR} - B_{SWIR}}{B_{NIR} + B_{SWIR}} \quad (3.7)$$

Landsat derived LST data was also validated by the *in situ* measured land surface temperature data from the Hay Meadow site.

3.3.4 FLIR thermal camera measurement

Although Landsat measures regional LST, it only shows LST for a single time of each measuring day. To evaluate the influence of canopy snow on canopy temperature variation in a day, *in situ* high resolution temperature measures are needed. In this research, an FLIR T650S thermal camera was used to measure the surface temperature of forest canopy and nearby open ground snow through the day. Due to logistics, a Engelmann Spruce and Subalpine Fir coniferous forest in Fortress Mountain Snow Laboratory (FMSL, 50°82`N, 115°21`W) that is located approximately 10 km to the south-east from MRCB was chosen as the measurement location. Measurement dates were April 21 and April 26, 2016 and FMSL was partially cloudy on both days. Snow was intercepted on the forest canopy on April 26 while the forest canopy was snow-free on April 21 (Figure 3-3). Measurement started at approximately 9:30 a.m. and ended at 4:00 p.m. local time on each day and the camera was in time-lapse mode with measurement frequency of one image per 15 minutes. Images were processed using

FLIR ResearchIR software and the average temperature of canopy and nearby open ground snow surface at each time step were extracted. Because of the uncertainty from various factors, such as air temperature, relative humidity, emissivity, and instrument error, temperatures measured using thermal infrared cameras often contain errors (Muniz et al., 2014). Following the method used in Harder et al. (2018), the possible error of FLIR-measured temperature was corrected by comparison to observations from two factory-calibrated Apogee SI-111 infrared radiometers, mounted on the nearby meteorological station to measure snow surface and canopy temperatures that were also measured in the thermal images.

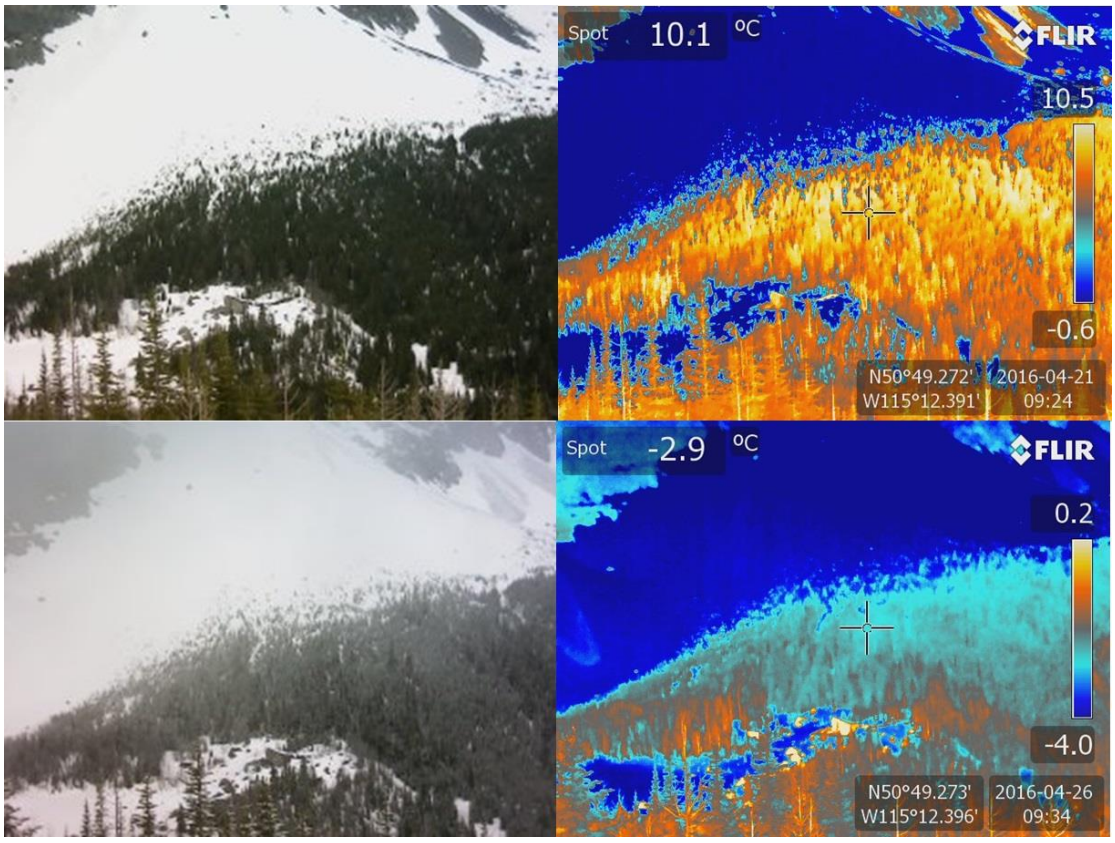

Figure 3-3. RGB (left) and thermal (right) images taken by a thermal camera for April 21 (upper) and April 26, 2016 (lower) at the Fortress Mountain Snow Laboratory.

3.3.5 Cold Regions Hydrological Modelling platform

The Cold Regions Hydrological Modelling platform (CRHM) was used to create model to simulate forest canopy snow interception, sublimation, and unloading in MCRB. CRHM is an object-oriented, flexible modelling platform through which researchers can choose a wide range of basin spatial configurations, spatial and temporal resolutions, and hydrological process modules for custom models that are suitable for the research scale, data availability, and objective interests for simulation. A detailed description of CRHM is provided by at Pomeroy et al. (2007; 2016b). The basic spatial simulation

unit of CRHM is the hydrological response unit (HRU) which is mainly defined by basin topography, hydrography, and vegetation. According to elevation, aspect, slope, drainage, and forest cover, MCRB was divided into 36 HRUs (12 in Cabin Creek sub-basin, 7 in Middle Creek sub-basin, 9 in Twin Creek sub-basin, and 8 in Confluence sub-basin) and 22 of them located in the forested area following Fang et al. (2013). Fourteen modules were assembled by CRHM to create a model to simulate the flux and state of water mass and energy in MCRB. These modules are: observation module, solar radiation modules (Gray and Landine, 1988; Garnier and Ohmura, 1970), longwave radiation module (Sicart et al., 2006), albedo module (Verseghy, 1991), canopy module (Ellis et al., 2010), blowing snow module (Pomeroy and Li, 2000), Snobal energy-balance snowmelt module (Marks et al., 1998), net radiation module (Granger and Gray, 1990), infiltration module (Ayers, 1959; Zhao and Gray, 1999), evaporation module (Granger and Gray, 1989; Granger and Pomeroy, 1997; Priestley and Taylor, 1972), hillslope module (Dornes et al., 2008; Fang et al., 2010), routing module (Chow, 1964). The major parameters of the canopy module, which is the most relevant module for this study and which simulates canopy snow interception and its unloading, melt and sublimation, are canopy albedo, leaf area index (LAI), maximum canopy snow interception load, ice bulb threshold temperature that controls snow unloading as solid or melt in liquid form, and temperature and wind speed measurement height. These parameters were set according to field measurements or following the research of Ellis et al. (2010) and Fang et al., (2013). The detailed function and parameterization of other modules are described by Ellis et al. (2010), Pomeroy et al. (2012), and Fang et al., (2013). The CRHM model was forced by the locally observed air temperature, relative humidity, soil temperature, wind speed, incoming shortwave radiation, and precipitation from seven weather stations and three precipitation gauges. The temperature and precipitation were interpolated from these stations to the 36 HRUs based on the environmental lapse rate and observed precipitation gradients by the observation module. The model ran at an hourly time step from October 2007 to September 2016. With dense surface observations for model input data and good characterization of model parameters from field research, CRHM usually simulates snowpack accumulation and depletion under the forest canopy quite well at MCRB (Fang et al., 2013). Ellis et al. (2010) found that CRHM-simulated canopy intercepted snow load agreed well with measurements from a weighed, suspended tree in the basin. Although direct validation of snow interception simulations at the basin scale is not possible due to lack of measurement techniques, these findings suggest that CRHM can simulate snow interception well in MCRB.

3.3.6 Data analysis

Landsat 8 images from April 8, April 15, November 25, and December 27, 2015 were used to study the influence of canopy snow on NDSI, NDVI, albedo, and LST because clear canopy snowcover information from time-lapse photos was available on these four days. Table 3-1 shows the statistics of forest canopy snow-coverage index derived

from time-lapse camera data. Over 99% and 95% of canopies were snow-free on April 8 and December 27 while more than 99% of the canopies had snow-coverage greater than 50% on April 15 and November 25. Solar elevation angle (SEA) has a positive influence on NDSI (Niemi et al., 2012), and a negative influence on NDVI and albedo (Warren, 1982; Pomeroy and Dion, 1996; Sesnie et al., 2012). Therefore, the April 8 image was paired with April 15 (hereafter the spring group) while November 25 was paired with December 27 (hereafter the winter group) to eliminate the influence of the SEA on those indices. The closest snowfall event (~10 mm) occurred over the evening and afternoon of the day before April 15 and November 25, while less than 4 mm snowfall occurred four and three days before April 8 and December 27, respectively. The release of intercepted snow is controlled by temperature, slope/aspect, wind speed, and time since interception and is spatially heterogeneous. Snow intercepted on south-facing slopes normally unloads, melts or sublimates faster than that intercepted on the north-facing slopes (Ellis et al., 2013; Garvelmann et al., 2013). Although the time-lapse camera used here only obliquely views the south side of trees, the short time between the end of snow storm and the Landsat satellite image and cold, calm conditions during this time restricted sublimation, melting or unloading of intercepted snow. Therefore, it was assumed that the canopy snow-coverage index measured by the time-lapse camera represented the areal canopy snowcover on the four selected dates. This assumption may not be applicable on other dates with different conditions. Most of the forest floor and clearing were snow-covered in all four days according to the snow survey data. The snow on the forest floor for the spring group was shallow and dense with snow depth less than 11 cm, while the snow depth on forest floor of winter group was approximately 30 cm. Snow depth in the clearings was approximately 50 cm for April 8, November 25, and December 27, while April 15 had less snow with approximately 20 cm depth (Table 3-2). Pixels located on the forest edge, by roads or trails, or at time-lapse photo boundaries were excluded from analyses to minimize mixed-pixel effects.

Table 3-1. Canopy snow-coverage conditions derived from time-lapse photography at four selected dates. First column indicates the partition of each category. The rest of the columns state the percentage (%) of the pixels having a canopy snow-coverage index within each corresponding category.

Canopy snow-coverage	08-Apr(%)	15-Apr(%)	25-Nov(%)	27-Dec(%)
0	99.29	0	0	95.07
>0&≤0.1	0.64	0.07	0.07	0.07
>0.1&≤0.2	0.07	0	0.07	2.8
>0.2&≤0.3	0	0.07	0.14	1.43
>0.3&≤0.4	0	0.21	0.36	0.28
>0.4&≤0.5	0	0.07	0.36	0.07
>0.5&≤0.6	0	0.42	0.5	0
>0.6&≤0.7	0	1.79	0.86	0.14
>0.7&≤0.8	0	4.73	1.86	0.07
>0.8&≤0.9	0	8.17	2.44	0.07
>0.9&≤1	0	84.47	93.34	0

Table 3-2. Solar elevation angle (SEA), air temperature, closest storm date and snow fall amount in MCRB as well as basic ground snow conditions (SWE and snow depth (SD)) in two main forested sites – Vista View (VV) and Upper Clearing (UC) in MCRB on four selected dates.

Date		April 8, 2015	April 15, 2015	November 25, 2015	December 27, 2015
SEA (^{0})		44.74	47.32	16.61	13.58
Closest Storm Date		April 4, 2015	April 14, 2015	November 24, 2015	December 24, 2015
Air temperature(^{0}C)		3.35	0.48	-12.3	-9.03
Snow Fall(mm)		4.15	10.97	8.72	1.79
UC	Forest SWE(mm)/SD(cm)	16.1/6.8	6.8/1.6	56.7/35	63.44/29.7
	Clearing SWE(mm)/SD(cm)	133.9/44.9	93.1/22.2	86/57.8	139.51/56.29
VV	Forest SWE(mm)/SD(cm)	30.9/11	17.1/2.8	78/30.7	68.22/26.78
	Clearing SWE(mm)/SD(cm)	114.3/39.6	44.6/14.3	102/54.6	118.32/54.12

The canopy snow-coverage index from time-lapse photos was compared to NDSI, NDVI, and albedo derived from the remote sensed images to determine the possible relationship between canopy snow-coverage and those three indices. The forest was subdivided into four categories according to forest type (circular cut spruce forest (CC), clearings with recovered small tree (clearing), untreated pure Lodgepole Pine forest (LPP), and mixed forest (MF) of Spruce, Fir, and Lodgepole Pine) to measure the response of NDSI, NDVI, and albedo to intercepted snow under different forest conditions. Average forest canopy coverage of CC, Clearing, LPP, and MF are 39.8%, 19.7%, 55.9%, and 54.9%, respectively. Landsat image pixels were classified to snowcovered or snow-free canopy according to canopy snow coverage from time-lapse

camera. A pixel was determined to be snowcovered when snow-coverage was higher than 0.5, and *vice versa*. NDSI, NDVI, and Albedo of canopy under snowcovered and snow-free conditions were compared amongst four forest types to determine the influence of canopy snow on those indices. The Lidar derived 1 m DEM, aspect, slope, and forest canopy cover data were scaled up to 30 m resolution to match Landsat image pixel size and location. To determine the cause of variation in NDSI, NDVI, and albedo, a multiple linear regression was conducted against the daily influence of elevation, aspect, slope, and forest canopy cover. The differences of NDSI, NDVI, and albedo from a snow-free canopy to a snowcovered canopy were calculated for each pixel. A multiple linear regression analysis was conducted to determine the relationship between changes in these indices and SEA, topography, and canopy coverage.

Unlike the other three indices, LST is highly influenced by elevation and so it is difficult to compare the LST variation at a basin scale. Given this, the clearing where the Vista View station is located and the mixed forest around it were chosen to determine the influence of canopy snow on LST to minimize to influence of elevation. The LST of clearing, forest, and open ground snowcover in the alpine in the same elevation range were compared to observed air temperature (2.26 m above ground) from the Vista View station for the four chosen days to determine the influence of canopy snow on canopy temperature. The FLIR thermal camera measured canopy and snow surface temperature in FMSL was compared to air temperature measured at a nearby meteorological station to see the influence of canopy snow on canopy temperature diurnal variation.

3.4 Results

3.4.1 Canopy snow effect on NDSI

Figure 3-4(a) shows the comparison of canopy snow-coverage index derived from time-lapse photos and NDSI derived from Landsat images. The results indicate that canopy snow-coverage index and NDSI were not highly correlated directly, but that canopy snowcover did influence NDSI. When the canopy was snow-free, the NDSI varied from near -1 to 0.8. As the canopy snow-coverage index increased, the lower boundary of NDSI range also increased. When canopy snow-coverage index was greater than 50%, the NDSI was distributed from 0.5 to 0.8. Canopy snow clearly increased the magnitude of NDSI and reduced its areal variation. Although the coefficient of determination between NDSI and canopy snow coverage was 0.67, the relationship between those two indices was not linear as over 90% of the samples had canopy snow-coverage index of either 0 or 1 but their NDSI were widely distributed. One possible reason for this is that for each pixel, NDSI provides information from snow on the canopy and snow on the ground that can be seen through tree canopy gaps. Two pixels may have same canopy snow-coverage index, while the snow on the ground that can be seen may be different because of variation in the forest canopy coverage. This explains why NDSI ranged from -0.9 to 0.8 even though the canopy snow-coverage index was zero for all pixels.

This also indicates that a different threshold must be used for different forest conditions if NDSI is to be used to detect regional canopy snow-coverage.

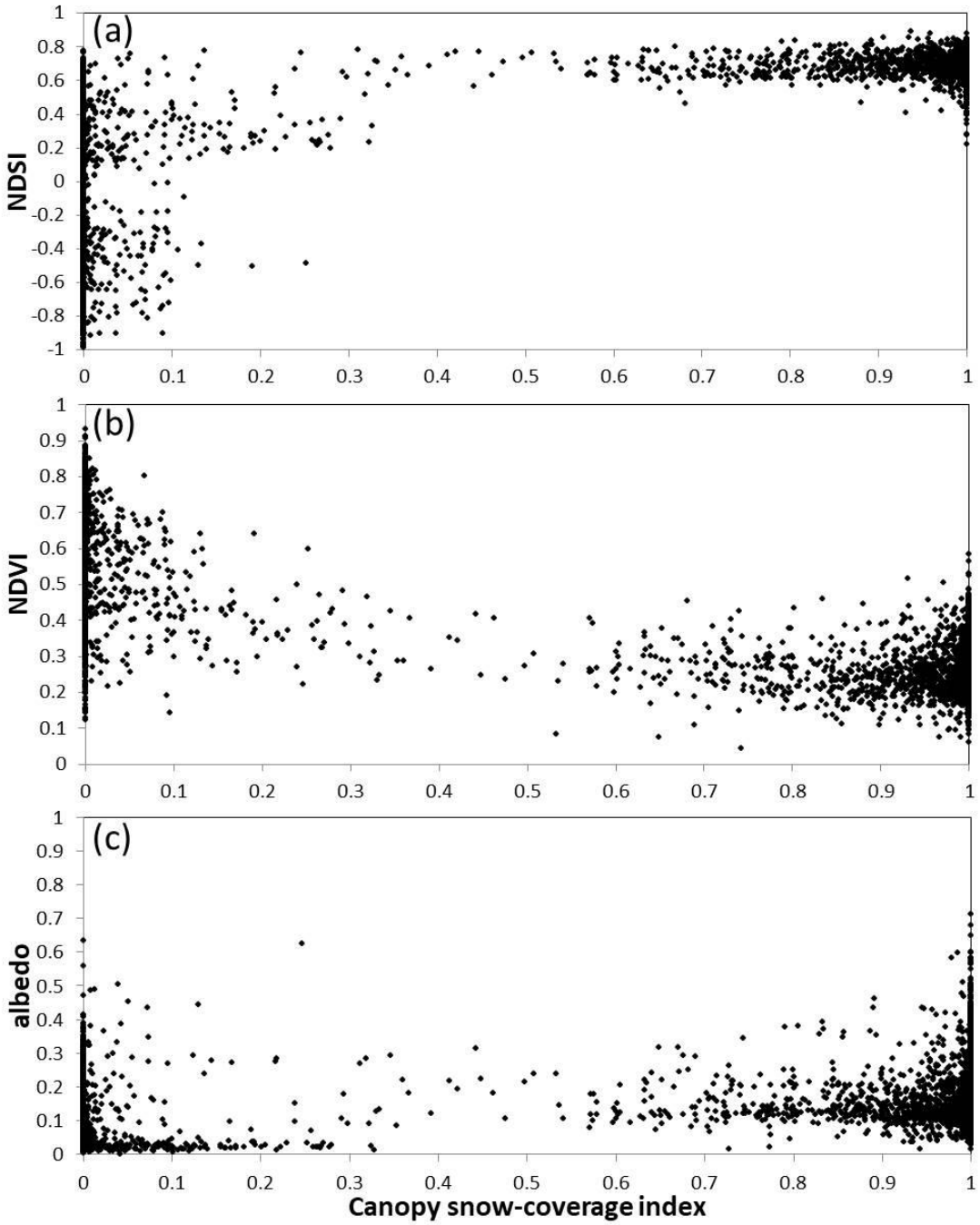

Figure 3-4. Comparison of time-lapse photo derived canopy snow-coverage index and NDSI (a), NDVI (b) and albedo (c), for four selected days in Marmot Creek Research Basin. No significant relationship was found between canopy snow-coverage index and the three indices.

Figure 3-5 (a) illustrates NDSI values for all sample points in four forest types under snowcovered and snow-free canopy conditions. In each forest condition sample points were sub-divided into two groups, spring and winter, to minimize the influence of SEA

on the indices. The presence of snow on the canopy increased the NDSI for all pixels in the four forest types. NDSI values in all forest types were similar when snow was intercepted on the canopy; the value of CC and Clearing was slightly higher than LPP and MF. However, the NDSI difference between different forest types was large when the canopies were snow-free. In Clearing, the canopy snow-free NDSI values ranged from -0.07 to 0.77 and half of them were greater than 0.4 (Figure 3-6). The NDSI ranged from 0.66 to 0.85 (mean = 0.79) when there was snow on the canopies. There was no clear divide between snow-covered and snow-free canopy NDSI in Clearing. The NDSI difference between two scenarios was 0.39 and it was the smallest among all the forest types. In CC forest, NDSI ranged from 0 to 0.65 (mean = 0.26) when canopies were snow-free. On the canopy snow-free days, NDSI was concentrated from 0.57 to 0.89 (mean = 0.71). Canopy snow increased the NDSI in CC by 0.45. The average canopy coverages of LPP and MF forests were very close, so the NDSI response to canopy cover for those two forest types were similar. With the influence of dense forest canopy, the NDSI in LPP and MF never reached 0.2 and was as low as -0.9 when canopies were snow-free even though most of the ground beneath the canopy was fully snowcovered. Most of the NDSI values in LPP and MF were higher than 0.4 when canopies were snowcovered. Canopy snow increased NDSI by 1.04 and 1.13 for LPP and MF to 0.63 and 0.67. Intercepted snow decreased the NDSI variation in all forest types as the standard deviation of NDSI was significantly reduced when canopies were snowcovered. There was no overlap between snowcovered and snow-free canopy NDSI value in LPP and MF but few samples overlapped in CC and more samples overlapped in Clearing.

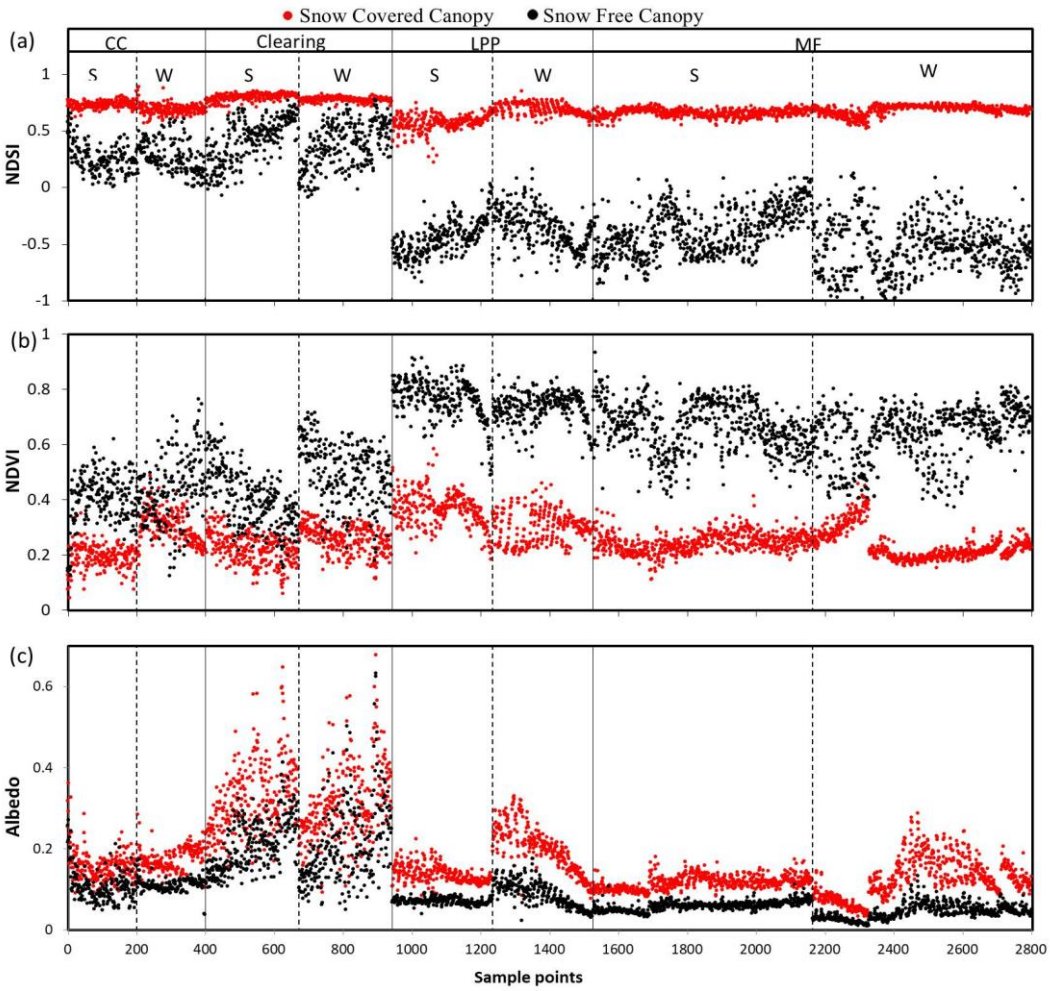

Figure 3-5. Landsat images derived NDSI (a), NDVI (b) and albedo (c) of sample points when snow is present (red dot) and absent (black dot) on the canopy for four forest conditions. 'S' and 'W' denote spring and winter groups, respectively.

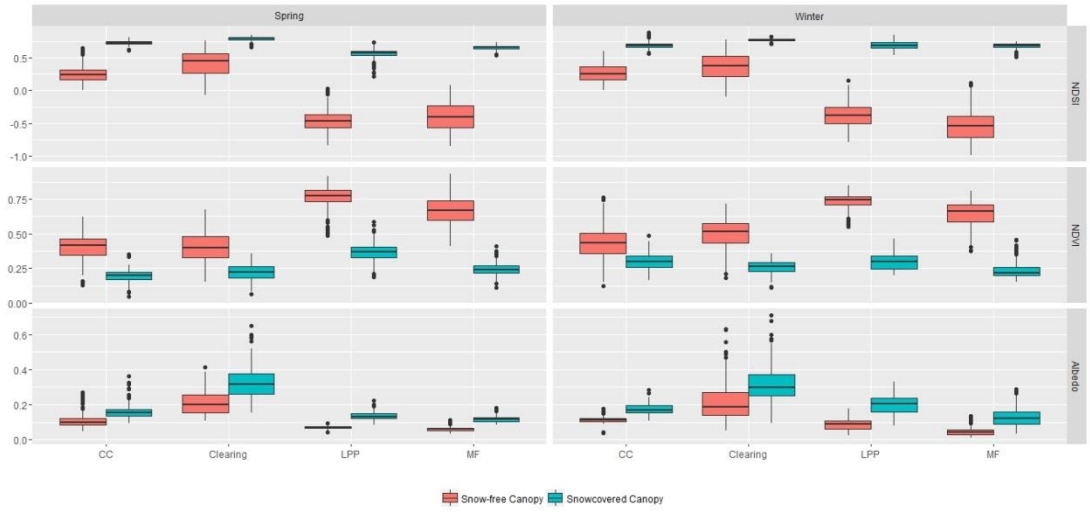

Figure 3-6. Distribution of NDSI, NDVI, and albedo values for snow-covered and snow-free canopies by forest type. Spring and winter groups are defined in the text.

NDSI values were negatively related to the forest canopy coverage under any snow cover condition (Figure 3-7). The coefficient of determination (r^2, $p < 0.05$) of the linear relationship between NDSI and canopy snow coverage ranged from 0.24 to 0.65 on the four selected dates. The slope of the relationship was much higher when the canopy was snow-free than when the canopy was snow-covered. With the increase of forest canopy coverage from 0 to 0.7, the NDSI decreased from 0.75 to −1 when the canopy was snow-free. However, when the canopy was covered by snow NDSI declined by less than 0.2 when forest canopy coverage increased by the same amount. The change of NDSI from snow-free to snowcovered canopy increased with increasing of forest canopy coverage.

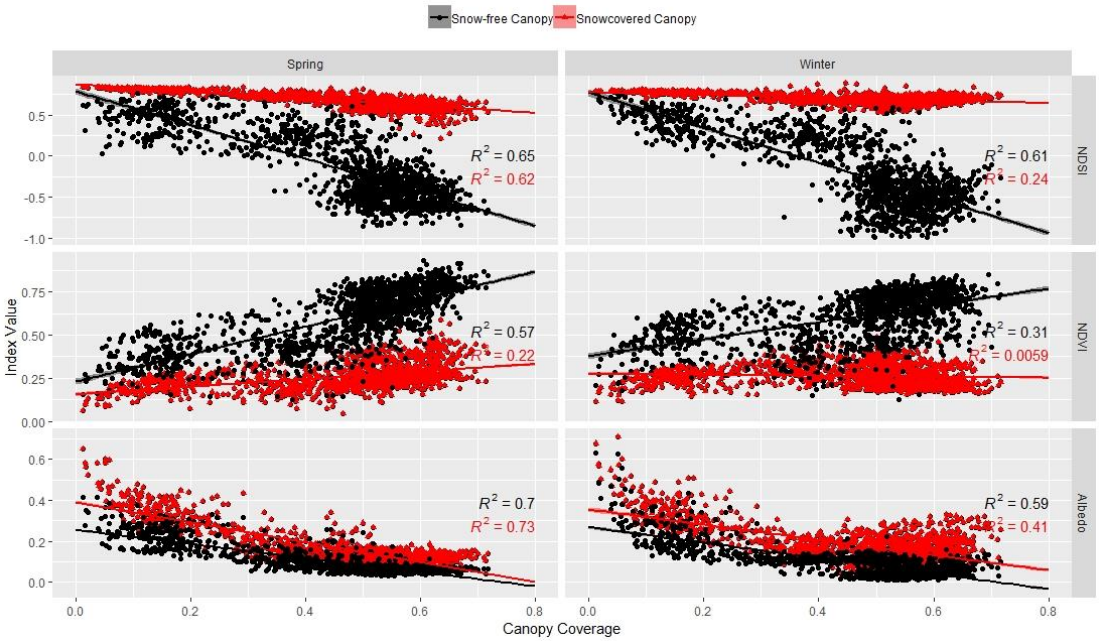

Figure 3-7. Influence of canopy snow on the relationship between forest canopy coverage and Landsat derived three indices (NDSI, NDVI, and albedo). Spring and winter denote the data from spring group and winter group, respectively.

The results of multiple linear regression analysis indicate that NDSI variation was highly related to topography (elevation, slope, and aspect) and forest canopy coverage. Elevation has a positive effect on NDSI, while other factors' effects are negative. The coefficient of determination ($p<0.05$) between NDSI and the four factors were 0.78, 0.67, 0.48, and 0.66 for April 8, April 15, November 25, and December 27, respectively (Table 3-3). Snow-free canopies had higher r^2 than snowcovered canopies. This is because when the canopy was snow-free, the NDSI value only shows snow information on the forest floor; topography and forest canopy coverage have a strong influence on forest floor snow accumulation. However, when the canopy was snowcovered, NDSI provides snow information both on the ground and on the canopy. The snow on the canopy reduced the variation of total snowcover of each pixel and hence the influence

of the four factors on NDSI. However, those four factors still explain the 48% to 67% of the variation of NDSI when canopies were snowcovered.

Table 3-3. Coefficient of determination of multiple linear regression among three indices with topography and canopy coverage in selected dates. P-Value < 0.05 for all r^2.

Date	NDSI	NDVI	albedo
08-Apr	0.78	0.72	0.79
15-Apr	0.67	0.38	0.82
25-Nov	0.48	0.20	0.70
27-Dec	0.66	0.49	0.67

The results of multiple linear regression analysis between an NDSI increase from snow-free and snowcovered canopies and elevation, slope, aspect, canopy coverage, and SEA illustrate that these five factors explain 62% of variation in the NDSI increase (Table A.2). Canopy coverage is the most important factor that influences the NDSI increase amount and it contributes half the effect whilst topography (elevation, slope, and aspect together) contributes the other half. SEA has very limited influence on the NDSI increase when compared to other factors. Topography and canopy coverage are the main factors that influence the magnitude of snow interception. This implies there might a good relationship between amount of snow interception and NDSI increase.

3.4.2 Canopy snow effect on NDVI

The relationship between NDVI and canopy snow-coverage index is shown in Figure 3-4 (b). NDVI was distributed from 0.2 to 0.8 when canopies were snow-free while the upper boundary of the NDVI range decreased with increasing of canopy snow-coverage. The distribution of NDVI shrank to the values between 0.1 and 0.5 when canopy snow-coverage index was higher than 50%. The presence of canopy snow decreased the NDVI value and variation. Although the coefficient of determination between NDVI and snow coverage was 0.67, most of the sample had a 0 or 1 canopy coverage and the corresponding NDVI was highly variable. NDVI reflects the greenness of objects in the pixel. When there was no snow on the canopy, its value was highly dependent on the forest canopy coverage. Although snow may block some of the greenness of canopies, when canopies were snowcovered, NDSI still relies on canopy coverage. This explains why the NDVI may differ between two pixels even though their canopy snow-coverages are the same.

The NDVI comparison between snowcovered and snow-free canopies for different forest types is shown in Figure 3-5 (b). The presence of snow significantly reduced the NDVI value of majority of the samples in all four forest types. The average NDVI value of snowcovered canopy for each forest were similar in their values of MF and LPP and

were slightly higher than that in CC and Clearing. Canopy snow-free NDVI for four forest types were quite different and the NDVI decrease in LPP and MF was much greater than that in CC and Clearing. The canopy snow decreased the mean NDVI for MF, LPP, CC, and Clearing by 0.41, 0.41, 0.17, and 0.21, respectively (Figure 3-6). For MF and LPP forests, although there were several samples located in the overlap region, the snow-free canopy NDVI ranged from 0.41 to 0.93, while the snowcovered canopy NDVI was clustered between 0.11 and 0.59. In CC and Clearing, NDVI was distributed from 0.12 to 0.76 (mean = 0.44) when the canopy was snow-free. NDVI was concentrated from 0.05 to 0.5 (mean = 0.24) when snow was present on the canopy. Under both forest types, there was large overlap from 0.2 to 0.4 inside of which both snowcovered and snow-free scenarios had sample points. Therefore, it was hard to determine an NDVI threshold to detect the canopy snow in CC and Clearing. The canopy snow decreased the mean NDVI from 0.65, 0.75, 0.42, and 0.45 to 0.24, 0.34, 0.25, and 0.24 for MF, LPP, CC, and Clearing, respectively. The presence of snow on the canopy also reduced the variation of areal NDVI for all four forest types as this snow make the reflectance of the land surface more homogeneous, dropping both the standard deviation and CV values.

NDVI was positively related to forest canopy coverage when the forest canopy was snow-free (Figure 3-7). The r^2 in spring (0.57) was higher than in winter (0.31). Canopy snow coverage decreased the slope and r^2 of the relationship between NDVI and forest canopy coverage. With snow on the canopy, this relationship became weak with a slightly negative slope and an extremely small r^2 (0.006) in winter. The change of NDVI between snow-free and snowcovered canopies increased with increasing forest canopy coverage in both winter and spring.

The results of multiple linear regression analysis indicated that NDVI variation was strongly related to elevation, slope, aspect, and forest canopy coverage when canopies were snow-free. This relationship was weak when snow was intercepted by the canopy. Elevation and slope had negative effects on NDVI, while the effects of aspect and canopy coverage were positive. The coefficients of determination between NDVI and the four factors were 0.72, 0.38, 0.20, and 0.49 for April 8, April 15, November 25, and December 27, respectively (Table 3-3). When canopies were snow-free, NDVI was mainly controlled by forest canopy coverage. Topography influenced NDVI by controlling the snow on the forest floor. However, when canopies were covered in snow, the snow blocked the greenness of the forest canopy and reduced the influence of canopy coverage on NDVI. New fallen snow made the snow on the forest floor more homogeneous so that influence of topography was also weaker.

Multiple linear regression analysis between the NDVI change and elevation, slope, aspect, canopy coverage, and SEA shows that these five factors explain 50% of the variation of NDVI decreases (Table A.2). Canopy coverage was the most import factor that influenced the decrease in NDVI and it explained 37% of the variation individually.

Topographic factors had limited influence on NDVI decrease individually, but together they explained 32% of the variation of the NDVI decrease. SEA had very limited effect on the magnitude of NDVI decrease when compare to other factors. Thus, the main factors that control the NDVI decrease are topography and forest canopy coverage.

3.4.3 Canopy snow effect on albedo

Figure 3-8 (a) shows the comparison of observed and Landsat derived albedo for the grassland Hay Meadow site. This shows that the observed and Landsat derived albedo were highly correlated. The coefficient of determination was approximately 0.95 and the RMSE between the two data sets was 0.05. Therefore, the Landsat derived albedo can be used for this research in MRCB.

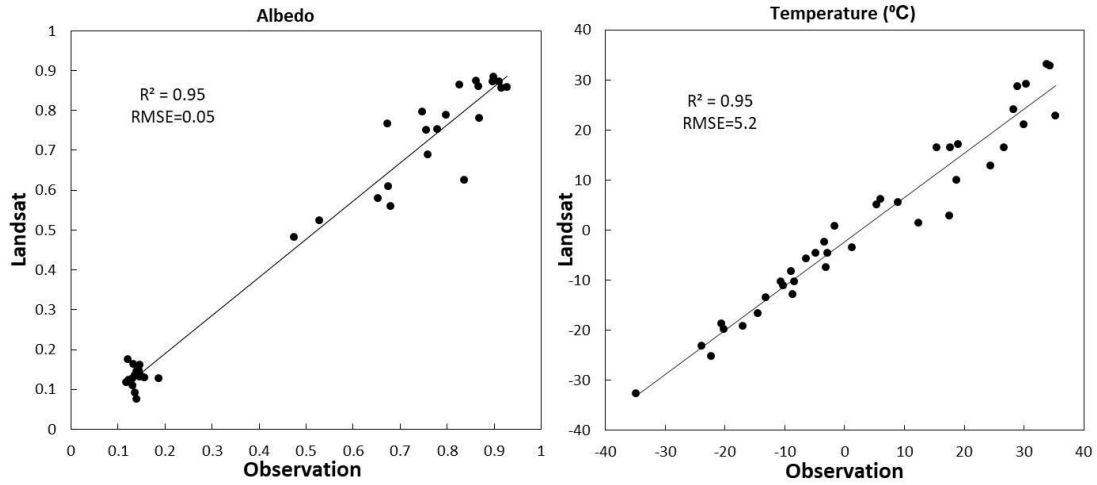

Figure 3-8. Comparison of observed and Landsat derived albedo (a) and land surface temperature (b).

Figure 3-4 (c) shows the relationship between albedo and canopy snow-coverage index. Albedo was largely distributed from 0.05 to 0.4 when the canopies were snow-free. The increasing canopy snow-coverage index had almost no influence on albedo before it reached 50% coverage. When canopy snow-coverage exceeded 50%, the distribution of albedo ranged largely from 0.1 to 0.5. Most of the samples were clustered at the canopy snow-coverage index of 0 or 1 and the albedo values that correspond to those two values were highly varied. The presence of canopy snow slightly increased the albedo and also increased its variation. The coefficient of determination between albedo and canopy snow-coverage index was 0.18.

Figure 3-5 (c) shows the snowcovered and snow-free canopy albedo for all the samples in the four forests. Canopy snow increased the albedo for most samples and the albedo was highly varied whether the canopies were snow covered or not. Amongst all the land coverss, Clearing had the highest albedo variation when the canopies were snow-covered and snow-free. The albedo was scattered from 0.08 to 0.48 (mean = 0.19) when the canopies were snow-free while it ranged from 0.13 to 0.60 (mean = 0.30) when

canopies were snowcovered (Figure 3-6). The albedo for rest of the forest types were much lower when compare to Clearing and rarely higher than 0.3. The mean values of albedo for CC were 0.11 and 0.17 when the canopies were snow-free and snow-covered, respectively. Albedo in spring was much higher than in winter in the CC and some samples with a snowcovered canopy in winter even had lower albedo than the sample from snow-free canopies from spring. Due to the low SEA and complex terrain, most winter samples of the CC were located in shade (Marsh et al., 2012). The shading effect lowered the reflectance and the albedo in this region. The canopy snow-free albedo for LPP and MF was concentrated around 0.05 to 0.17 (mean = 0.10 and 0.09), respectively. Canopy snow increased the albedo for LPP and MF by 0.08 and 0.06. Albedo variation in winter was much higher than in spring whether the canopies were snowcovered or not for those forests. The reason for this is twofold. First, some of the samples in LPP and MF were located in shade in winter because of the low SEA, so their albedo values were lowered by reduced reflectance. Second, for those who were not in the shade, their value was increased by the negative effect of SEA on albedo. Therefore, the albedo is highly influenced by topography and SEA.

The relationship between albedo and forest canopy coverage was negative for all dates (Figure 3-7). The r^2 of this relationship ranged from 0.41 to 0.73. Canopy snow coverage slightly increased the slope and r^2 of the relationship in spring. However, in winter, the r^2 decreased and there was no clear change in the slope of the relationship. This indicates that although albedo is related to forest canopy coverage, unlike NDSI and NDVI, the change of albedo from snow-free to snowcovered canopy is independent of the change in forest canopy coverage.

Multiple linear regression analysis demonstrated that albedo distribution in the study area in the four selected dates was highly controlled by topography and forest canopy coverage. The coefficient of determination between albedo and elevation, slope, aspect, and canopy coverage were 0.79, 0.82, 0.70, and 0.67, respectively (Table 3-3). The increase of albedo from snow-free to snow-covered canopy was albedo controlled by these factors and SEA. Those five factors together explain 49% of variation of the albedo increase (Table A.2). Slope aspect was the most important factor among them; it explained 22% of the variation.

3.4.4 Canopy snow effect on LST

Figure 3-8 (b) shows the comparison of *in situ* measured and Landsat derived LST from the Hay Meadow site. The observed and Landsat derived LST were highly agreed with each other with a coefficient of determination greater than 0.95 and the RMSE of 5.2 °C between the two data sets. The greatest differences were from samples with temperatures higher than 0 °C. Data sets agree with each other very well when the temperature was below the freezing point.

The temperature of the forest canopy, clearings, and snow surfaces in the alpine area were compared to air temperature measured at 2.62 m above ground at the Vista View station (Figure 3-9). The average temperature of forest canopy was lower than that of clearing in April 8 and April 15 whilst the opposite was true in November 25 and December 27. Also, the temperature differences between forest and clearing were small (within ±1 °C) for all four selected dates. There appeared to be no clear temperature difference between forest and clearing in MRCB whether or not snow was on the canopy. One reason for this could be the spatial resolution of Landsat 8 LST data (100 m). Its radiance may not be sensitive to the relatively small clearings. Another possible reason is that the clearings have small trees growing in them, which makes their thermal radiance similar to forest areas. The forest and clearing temperature were lower than air temperature but higher than snow surface temperature irrespective of canopy snow presence. The air temperature was approximately 2.5 °C on both April 8 and April 15. The forest canopy temperature was approximately -2.1 °C, which was close to open ground snow surface temperature of -3.4 °C, when snow was on the canopy, while it was 0.2 °C when the canopy was snow-free. The same patterns were found during winter. The presence of canopy snow decreased the canopy temperature hence the temperature difference between canopy and snow surface was smaller when canopy was covered by snow. The temperature difference between canopy and snow surface for April 8, April 15, November 25, and December 27 was 4.1 °C, 2.4 °C, 2.3 °C, and 2.7 °C, respectively. Without snow on the canopy, the forest canopy tends to warm up by solar radiation on sunny days. This explains why the temperature difference between the canopy and snow surface was higher when canopy was snow-free. However, in the winter, the difference between two scenarios was relatively small when compared to spring. This is probably due to the solar elevation angle (very low in winter in this region) and sun rise (late). In winter, there was not enough energy and time to have warmed up the forest when Landsat 8 passed the study region (approximately 11:00 am local time) compared to spring.

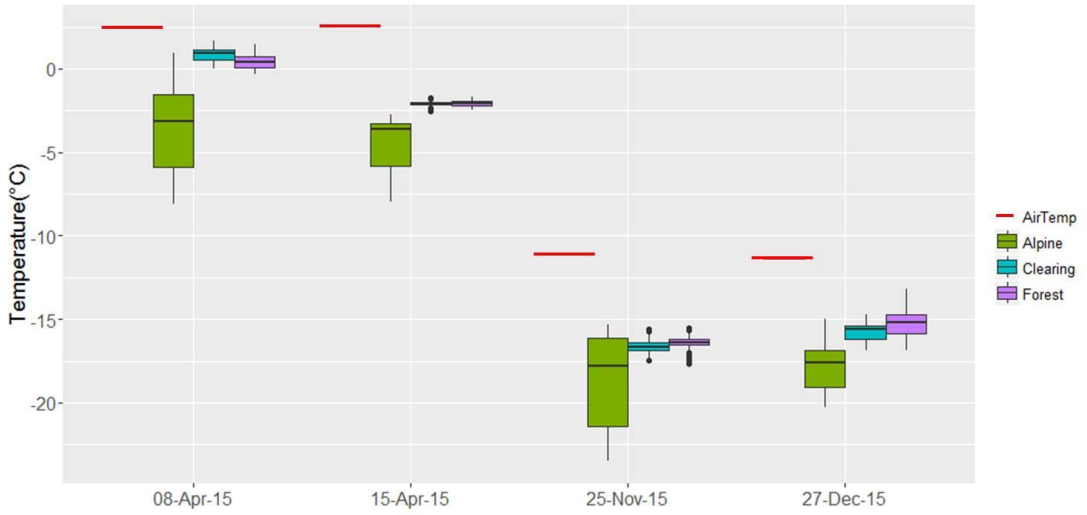

Figure 3-9. Comparison of Landsat derived land surface temperature for forest, clearings, snow covered alpine and measured air temperature for four selected dates.

Figure 3-10 shows the comparison of *in situ* measured forest canopy temperature and its nearby open-ground, snow-covered surface and air temperature on days that the canopy was snowcovered (April 26) and snow free (April 21) at FMSL. On April 26 with no canopy snow, the temperature of forest canopy was higher than air temperature most of the time with an average difference of 0.9 °C. However, the open ground snow surface temperature was much less than air temperature and the temperature of canopy with mean differences of -12.9 °C and -13.8 °C, respectively. When snow was intercepted by the canopy, the temperature of forest canopy was constantly around the freezing point, which was much lower than air temperature. The difference between canopy and air temperature was -3.6 °C. The presence of snow makes the canopy temperature close to the temperature of the open ground snow surface with a mean difference of 3.1 °C. The canopy temperature reached its peak around 1400h to 1430h on both days. The canopy temperature increased from 8.8 °C to 17.2 °C from 0930h to 1430h on April 21 while the canopy temperature only increased 0.6 °C during the same period on April 26. The presence of snow on the canopy also decreased the daily variation in canopy temperature. The standard deviations of daily canopy temperature for April 21 and 26 were 2.47 °C and 0.42 °C, respectively.

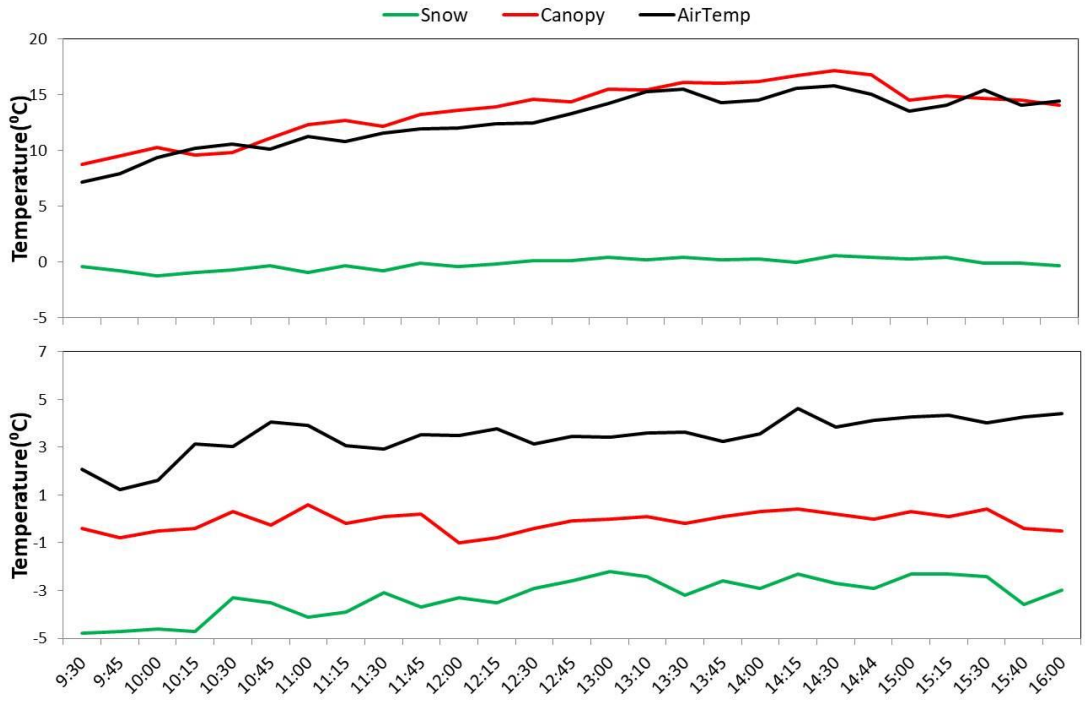

Figure 3-10. Comparison of measured canopy and open ground snow surface temperature with air temperature for April 21 2016 (snow-free canopy, upper panel) and April 26 2016 (snowcovered canopy, lower panel) at the Fortress Mountain Snow Laboratory.

3.4.5 Canopy snow estimation

Canopy snow clearly increases albedo under various forest and illumination conditions. However, its value is highly influenced by forest conditions, SEA, and illumination conditions. Snow on the canopy influences canopy temperature and this influence varies by time of day and year, elevation, cloud condition, and other factors. Thus, further research needs to be done before using satellite derived LST as an indicator of canopy snow. Among four indices, NDSI is the most sensitive to the presence of canopy snow as it had the greatest change. NDSI's response to canopy snow is also very stable as the NDSI for a snow-covered canopy was close in different forest conditions and seasons. However, it only provides information about snow conditions and no information about the forest. Prior knowledge of forests must be gathered when using it as a stand-alone indicator. NDVI is not as sensitive and stable as NDSI to canopy snow, but it provides forest information. Therefore, a combination of NDSI and NDVI were chosen as indicators of canopy snow in needleleaf forests as a result of the previous mentioned concerns.

Figure 3-11 shows the relationship between NDSI and NDVI for samples from different landscapes. Because large clearings with small trees have similar reflectance characteristics as snow intercepted intact forests, the samples from clearings were excluded in this analysis. NDSI is well correlated to NDVI in the forest region when

the forest floor was covered by snow. Samples from different scenarios were clustered in different regions. For samples from alpine areas, NDSI was usually higher than 0.4 and NDVI rarely exceed 0.1. Samples from summer forests were clustered in the upper left corner of the relationship with NDSI and NDVI largely ranging from -0.7 to -0.4 and 0.7 to 0.9, respectively. For winter forests (snow accumulated on the forest floor), NDSI is negatively correlated to NDVI with NDSI ranging from -0.9 to 0.8 and NDVI distributed from 0.1 to 0.9. It is noteworthy that some winter forest samples have even lower NDSI values than summer samples. The extremely low NDSI was largely caused by low SEA (13.58 º) and shading effect during winter satellite measurement. The low SEA and complex mountain terrain made it rare for sunlight to reach the forest floor and some samples in mixed forests were located in shade that significantly reduced reflectance. There is a clear divide between scenarios of snowcovered and snow-free canopies. Samples of snowcovered canopies were concentrated on the upper right corner of the relationship with NDSI and ranged largely from 0.4 to 0.8 while NDVI was mainly distributed from 0.1 to 0.5. Because NDSI and NDVI of snowcovered canopy are seldom lower than 0.4 and 0.1, respectively. Thus, the area covered by the blue polygon in Figure 3-11 is proposed as the region for detecting canopy snow. This means all the pixels are classified into two categories: snow-covered canopy located in the polygon and others (snow-free canopy and open areas) located inside and outside of the polygon.

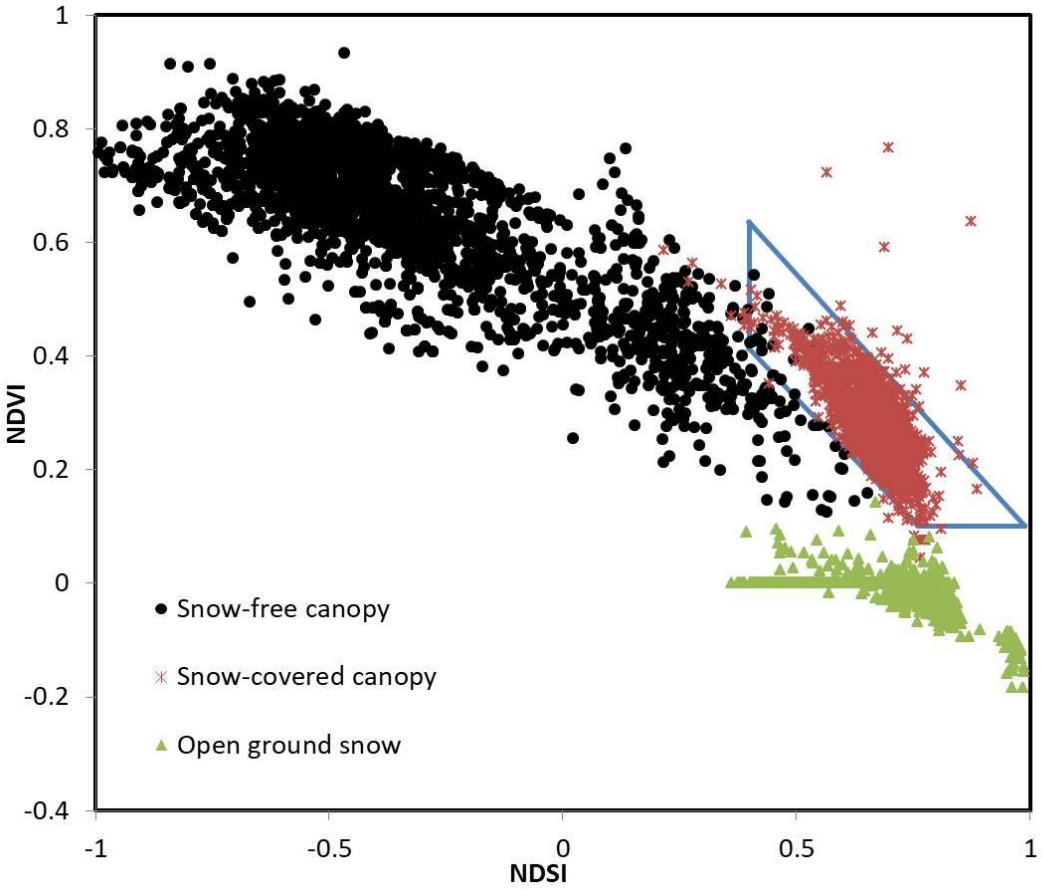

Figure 3-11. NDSI and NDVI relationships for different landscape and forest canopy conditions. Red stars and black dots depict snow-covered canopy and snow-free canopy (with snow below the canopy) respectively. Green triangles plot fully snow covered open areas. The blue polygon is the proposed area for measuring forests with a snow-covered canopy.

The remaining 52 Landsat 5 and Landsat 8 scenes in the study area were classified according to this approach and the results were compared to CRHM snow coverage simulations. CRHM-simulated hourly snow interception information was validated by using time-lapse camera images from March 11 2015 to June 9 2016 before comparison to remote sensing classifications. The results indicated that the CRHM canopy snow simulations agreed with time-lapse derived canopy snow coverage 89.8% of the time and, hence, it is reasonable to compare it to the classification results.

Figure 3-12 shows the comparison of the classification and CRHM model simulation for two selected days. On November 28, 2013, according to the model simulation, there was no snow on the canopy over the entire basin. This classification agreed well with model simulations at most of the hydrological response units (HRUs) except for some of the large clearings and forest edges. Because samples from large clearings were excluded from the NDSI-NDVI relationship, it is not surprising that this approach does not work well in those places. The forest edges have the situation that pixels are a mix

of forest and open ground, which make the reflectance characteristics similar to a snowcovered forest canopy. Therefore, some pixels in these areas were misclassified as snow-covered canopy. On November 28, 2013, most of the forest canopies were covered by 5 to 15.4 mm of snow according to CRHM simulation. This classification agreed very well to the simulation in most of the continuous forest types, but less well in sparse forests that were either artificially treated (CC) or a mix of deciduous and coniferous trees. In the model parameterization, the LAI of large clearings were set as 0. This is why the model simulated no snow interception at those places. However, the approach misclassified the large clearing as a snowcovered canopy because of fresh tree growth.

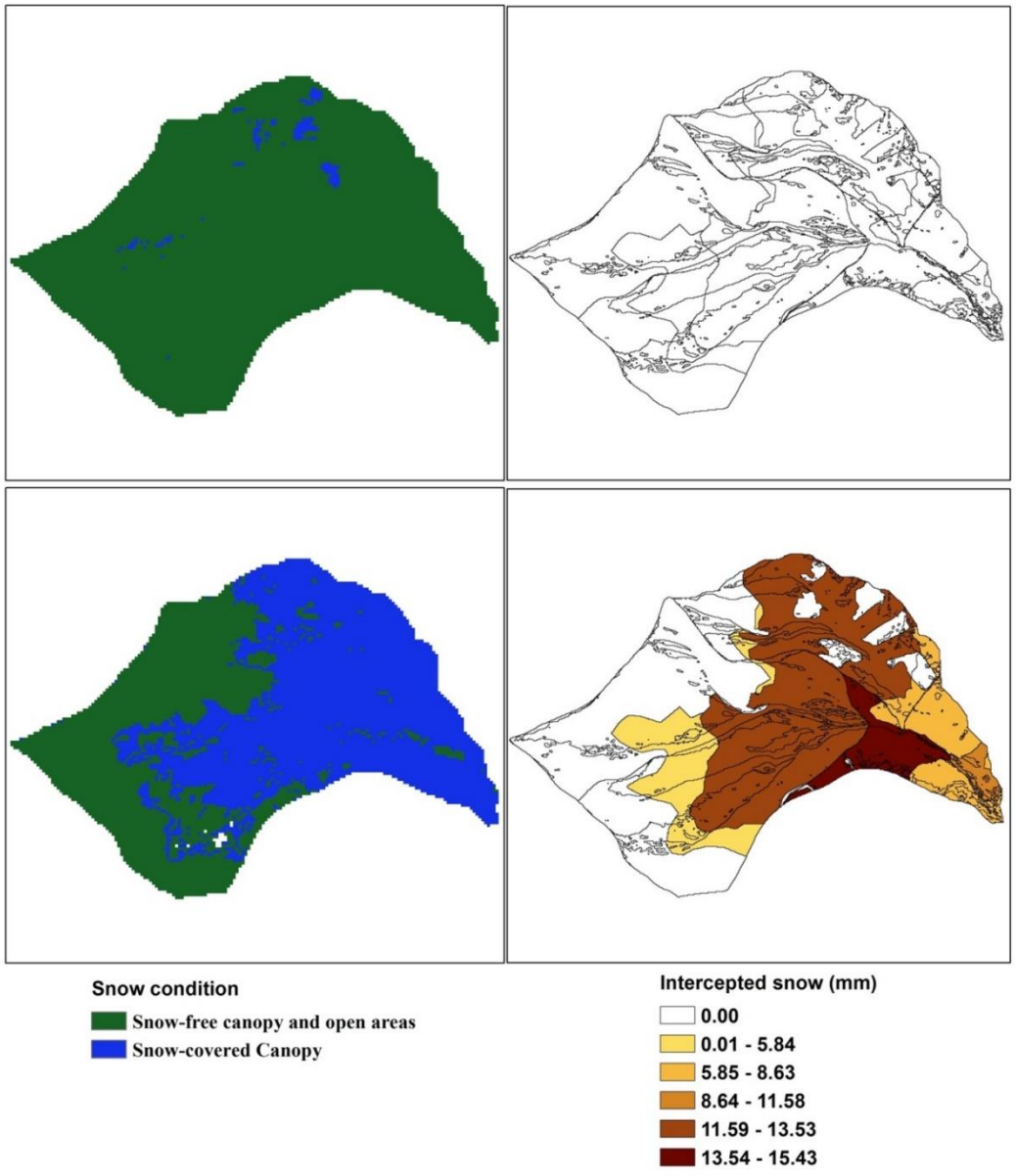

Figure 3-12. Comparison of canopy detection classification results (left) and CRHM simulated canopy snow interception (right) for November 28, 2013 (upper panel) and December 01, 2014 (lower panel).

The forty-five HRUs were classified into four landscapes according to their characteristics: Alpine (No trees), Clearing (large clearings with small re-growing trees), Sparse Forest (forests with circular cut clearings or the forests mixed of ever green trees and deciduous trees or shrubs), and intact forests (intact ever green forests with no treatment). Classification omission error (percentage of pixels that classified as snow-fee canopy or open ground while snow was covered on the canopy according to model simulation), commission error (percentage of pixels that classified as snowcovered canopy while canopies were snow-free according to model simulation), and total accuracy (percentage of pixels that classified correctly according to the model simulation) were analyzed in all four landscapes.

Table 3-4 shows the results of the comparison between CRHM simulations and classification of all 52 remaining Landsat 5 and Landsat 8 images from 2007 to 2016. In general, the approach worked very well in alpine areas. It classified 1.5% and 2.96% of the pixels from alpine areas into snowcovered canopy for Landsat 5 and Landsat 8 images, respectively. Alpine had the highest total accuracy (98.1%) between classification and model simulation among all four landscapes. This indicates that the combined threshold of NDVI and NDSI can easily distinguish non-forest area from forest. This approach works less well in clearings. It classified 28.1% and 34.3% clearings as snow-covered canopies for Landsat 5 and Landsat 8, respectively. The consistency between classification and model simulation in clearings was 70.1%, which is the lowest amongst the four landscapes. For sparse forests, the error classification rate was much lower than that in clearings, but the classification omission error was relatively high. The model only classified 10.9% and 42.7% of the Landsat 5 and Landsat 8 pixels into snowcovered canopy when model simulated canopy snow interception was greater than zero. The pattern was similar in intact forests. Although it had very low commission error in continuous forests, the classification omission error was 75.1% and 29.3% for Landsat 5 and Landsat 8, respectively. The high classification omission of Landsat 5 images may be explained by the differences in sensors used in Landsat 5 and Landsat 8. The classification approach was developed using Landsat 8 images, so some adjustment may have to be made when using data from other data sources. Even in intact forests, Landsat 8 still has 29.3% of classification omission error. The basic simulation unit of CRHM is the HRU. There are only 36 HRUs in MCRB while there are approximately 10452 pixels in each Landsat image in MCRB. In model simulations, each HRU only has one value for snow interception while there may be hundreds of pixels in each HRU. Due to various factors, canopy snowcover may be not homogeneous in one HRU. This may explain the relatively high classification omission error for sparse and intact forests. In all, the classification results were consistent with CRHM simulations in all landscapes with the accuracy of 98.1%, 70.1%, 72.1%, and 82.6% in alpine, clearing, sparse forests, and continuous forests, respectively. Thus, this approach is capable of detecting canopy snow interception in the study area.

Table 3-4. Comparison of CRHM-simulated and Landsat image-detected canopy snow cover of 52 Landsat 5 and Landsat 8 images from 2007 to 2016. Commission error (Com. %) refers to percentage of pixel was classified as snowcovered canopy while model simulated interception equals zero. Omission error (Omi. %) refers to percentage of pixel was classified as snow-free canopy while model simulated interception larger than zero. Accuracy (Acc. %) refers to classification results that agree with model simulation.

	Alpine			Clearing			Sparse Forests			Intact Forests		
	Com.	Omi.	Acc.	Com.	Omi.	Acc.	Com.	Omi.	Acc.	Com.	Omi.	Acc.
Landsat5	1.50	N/A	98.50	28.14	N/A	71.86	6.42	89.07	71.79	4.29	75.10	81.12
Landsat8	2.96	N/A	97.04	34.26	N/A	65.74	10.13	57.26	72.70	7.11	29.32	85.96
ALL	1.93	N/A	98.07	29.88	N/A	70.12	7.45	77.04	72.07	5.07	56.67	82.61

3.5 Discussion

This research evaluated the influence of canopy snow on several indices available from Landsat images and discovered the potential to use these indices to detect intercepted snow on a coniferous forest canopy. Canopy snow dramatically increased the forest NDSI to a level close to the NDSI for open areas. The increase varied amongst forest conditions, which is a reflection of canopy cover and topography. The NDSI increase was positively related to canopy cover, a result that is consistent with the research of Heinilä et al. (2014). A common method to retrieve ground fractional snowcover amongst remote sensing researchers is to use the relationship with NDSI (Salomonson and Appel, 2004; Salomonson and Appel, 2006). Because canopy snow could significantly increase the forest NDSI, attention should be paid when retrieving fractional snowcover in forests using the relationship developed by Salomonson and Appel (2004) as the NDSI may not only represent the snow on the ground but also contains information on canopy snow. No relationship was found between the time-lapse camera measured canopy snow-coverage index and NDSI because of the forest floor snow fraction difference caused by the variation of forest canopy coverage. So, it is not possible to use NDSI to quantitatively measure canopy snow without prior knowledge of forest canopy coverage. Canopy snow also decreased the NDVI for forests because the presence of snow on canopy blocked the green vegetation reflectance. The decrease in NDVI was relatively lower than the increase in NDSI, consistent with the research of Heinilä et al. (2014).

The land surface albedo increased considerably with snow interception but not to levels expected for open snowfields. The increase was found to be highly influenced by SEA and topography, which was supported by the research of Pomeroy and Dion (1996) and Pirazzini (2004). The forest canopy snow-free albedo (0.10 for Lodgepole Pine and 0.09 for mixed forest, on average) retrieved from Landsat images in this research was similar to surface observations (Harding and Pomeroy, 1996; Pomeroy and Dion, 1996). The relatively high canopy snow-coverage index needed to trigger an increase in

canopy albedo is consistent with research from Pomeroy and Dion (1996) who measured no albedo increase for relatively small snow loads in Canadian boreal forests and Nakai et al. (1999) who measured albedo increases for very high canopy snow loads in Japanese mountain forests

The measured canopy temperature was higher than air temperature at most times of the day in FMSL when canopies were snow-free (Figure 3-10). This coincides with the measurements of Pomeroy et al. (2009) and Musselman and Pomeroy (2017) in MCRB and elsewhere. In their research, the temperature of canopy needles was always higher than the sub-canopy temperature in daytime. However, here, Landsat derived LST in forests was lower than air temperature even when canopies were snow-free. This is presumably due to measurement scale differences. In the thermal camera measurement in FMSL and the data of Pomeroy et al. (2009) and Musselman and Pomeroy (2017), only the temperature of canopy needles was measured. However, the Landsat thermal sensor measures the thermal radiance of whole land surface, which is a mixture of forest canopy and understory snow. The temperature of snow surface on the ground is usually much lower than that of canopy and of the air temperature (Pomeroy et al., 2016a). Thus the measured LST for the whole pixel was lower than temperature of canopy and may explain the relatively low LST even when canopies were snow-free.

The relationship between forest NDSI and NDVI in Figure 3-11 shows that the NASA/GSFC SNOWMAP algorithm is not working for this high latitude, mountainous basin with complex topography. When canopies were snow-free, most pixels have negative NDSI values and are located outside of the region proposed by Klein et al. (1998) for snow classification in forest regions even though the forest floor was fully snow-covered. Therefore, more attention should be paid when classifying the snowcover of these forests. The canopy snow detection approach from Figure 3-11 was developed using Landsat 8 data (excluding data in clearings with small trees). The accuracy of Landsat 5 images was relatively low when using this approach due to the sensor differences with Landsat 8. Thus, an adjustment of this relationship is needed when using other satellite data. Clearly, the ability to detect canopy snow in sparse forests is limited. This is because the spectral characteristics of clearings with small trees and snow-covered canopies are similar. Thus, this approach is not suitable for the detection of canopy snow in sparse evergreen forests. Using the NDSI and NDVI relationship in Figure 3-11, the accuracy in mixed needleleaf and deciduous forests were relatively low (Table 3-4). This indicates that this method may need to be modified for these forests. No obvious difference was found in results for pure mature Pine forest (LPP) and the mature mixed coniferous forests (MF) of Spruce, Fir, and Pine using this method. To determine the effectiveness of this method for other forests with different coniferous tree species and status, further study is needed.

Because of limitations of *in situ* canopy snow measurement, this research can only detect snow presence on the canopy. With enough *in situ* snow interception and spectra

measurement, a quantitative measure of snow interception might be developed in the future. The canopy snow information derived from this research for the first time makes large-scale canopy snow interception model performance validation possible. Also, this information could be used as input for large scale hydrological data assimilation to hopefully improve the simulation of snow accumulation in coniferous forests. Because of the low repeat frequency of the Landsat satellite and cloud effects, there were only about 10 usable images of the study area each year. This may not be sufficient for hydrological model validation and data assimilation. One possible solution is to fill the gaps with data from other satellites, such as Sentinel 2 and MODIS Terra and Aqua. Although Sentinel 2 has just launched few years ago, it has higher spatial and temporal resolution than Landsat 8 and has been used in the snow related research (Wayand et al., 2018). MODIS has a lower spatial resolution, but it can provide two images each day for the study area and this can significantly increase data availability.

3.6 Conclusion

Four regular indices that are typically available from optical and thermal remote sensors were chosen in this research to study both the influence of canopy snow on reflectance and the potential for canopy snow detection. The results indicate that canopy snow dramatically increased NDSI and decreased NDVI and these changes in magnitude varied among forest conditions. When snow was present on a canopy, the increase of albedo was relatively small compared to changes in NDSI and NDVI, nevertheless, it was detectable. The magnitude and rate of increase of albedo were highly influenced by SEA, forest canopy coverage, and topography. Canopy snow reduced the LST of forests and clearings and enlarged the temperature difference between the forest canopy and air temperature. The temperature of canopies was closer to ground snow surface temperature when they were snowcovered. Canopy temperature was closer to air temperature when canopies were snow-free. However, canopy temperature is also highly influenced by illumination conditions and time of the day. Further research is needed to confirm LST use as an indicator of canopy snow.

A canopy snow detection case study was conducted in MRCB using both NDSI and NDVI thresholds. The results were compared to a simulation using CRHM forest canopy snow interception algorithms. The detection classification results agreed with model simulations 82.6% of the time in continuous forests while the agreement in sparse forests and clearings with small trees was relatively lower (72.1% and 70.1 %). Therefore, NDSI and NDVI are recommended as canopy snow detection indices. The new source of canopy snow interception information available from these indices may provide future methods to validate or assimilate to land surface snow prediction models.

CHAPTER 4: Assimilation of snow interception observations into a cold regions hydrological model

Status: submitted to Hydrological Processes on July 05, 2019

Citation: Lv, Z., and Pomeroy, J.W., 2019. Assimilation of snow interception observations into a cold regions hydrological model. Hydrological Processes. in review.

Author Contributions: Zhibang Lv conceptualized this research, performed simulations and analysis, and wrote the manuscript. John Pomeroy provided data and guidance to conceptualization, analysis and interpretation, and reviewed and revised the manuscript.

4.1 Preface

After developing a remote sensing snow interception detection approach in the previous chapter, the next step is to assimilate these observations to a hydrological model. Snow interception is a crucial hydrological process in cold regions needleleaf forests, but it is rarely measured directly. Indirect estimates of snow interception can be made by measuring the difference in the increase in snow accumulation between the forest floor and a nearby clearing over the course of a storm. Pairs of automatic weather stations with ultrasonic snow depth sensors provide an opportunity to estimate this, if snow density can be estimated reliably. Data assimilation can merge the advantages of snow interception observation and modelling to provide an optimal snow interception estimation. This research is aiming to: 1) determine how automatically measured snow depth in the forest and clearing can be used to quantify snow interception loss in the forest, and 2) examine the influence of assimilating ground measured and remotely sensed snow interception information to snow interception simulations.

4.2 Introduction

Snow is a critical, temporary land surface component in cold regions controlling water cycling and energy budget through stored precipitation and relatively high albedo than other, background surfaces. The processes governing snow residence in cold regions needleleaf forests, which cover more than 20% of the Earth's land surface, are much different from open areas because forest canopy alters snow and energy distribution (Pomeroy and Gray, 1995; Pomeroy et al., 2008; Suzuki and Nakai, 2008). In needleleaf forests, part of snowfall is usually first intercepted by the forest canopy followed only later by unloading, melt, evaporation or sublimation (Pomeroy and Goodison, 1997). Snow interception and release from tree crowns are mainly controlled by snowfall amount, air temperature, wind speed, canopy structure, and topography (Hedstrom and Pomeroy, 1998b; Pomeroy et al., 2002). Snow interception leads to the snow water equivalent (SWE) on the forest floor being notably different from nearby open areas. Many studies have reported that up to 60% annual snowfall can be intercepted by the canopy and two thirds of them never reach the ground because of the sublimation (Kuz'min, 1960; Pomeroy and Schmidt, 1993; Storck et al., 2002). Due to snow's high albedo and low thermal conductivity, it affects energy partitioning in and beneath the canopy (Suzuki and Nakai, 2008). Therefore, accurately determining the magnitude and timing of snow interception both play an important role in land surface or hydrological modelling and water management in cold regions evergreen forests.

Many methods have been developed by researchers during the past few decades to quantitatively or qualitatively measure intercepted snow (c.f., Friesen et al., 2015). Mass budgeting, which examines the difference between snow accumulations under the forest canopy and in nearby open areas over the course of a snowstorm or snow season, is the most common indirect approach for quantitatively estimating snow interception. Precipitation or snow accumulation can be measured by using traditional precipitation gauges (Koivusalo and Kokkonen, 2002), artificial boards (e.g., Floyd and Weiler, 2008; Lundberg et al., 1998), or snow surveys (Hedstrom and Pomeroy, 1998). The annual loss caused by sublimation of intercepted snow can be obtained by differences in peak SWE between an adjacent forest and open area (Lundberg et al., 1998; Pomeroy and Schmidt, 1993; Winkler et al., 2005). The direct approach for measuring snow interception on a single tree or branch always involves a lysimeter or compression sensor that connects to a cut, a live tree or branch to measure weight change during and after a snow storm (Hedstrom and Pomeroy, Lundberg et al., 1998; Martin et al. 2013; 1998; Pomeroy and Schmidt, 1993; Schmidt and Pomeroy, 1990; Suzuki and Nakai; 2008;). Although these approaches can provide accurate interception measures, they all have drawbacks. For example, a cut hanging tree (branch) dries out through time making its tare weight change. The compression senor method is still experimental. Images from ground based digital cameras (Floyd and Weiler, 2008; Garvelmann et al.

2013; Pomeroy and Schmidt, 1993) or an optical remote sensing satellite (Lv and Pomeroy, 2019a) have been used to detect canopy snow presence based on the high reflectance of snow. Some of these studies have developed a method to calculate the snowcovered area of the canopy, however, the actual amount of intercepted snow has remained elusive. Snow mass budgeting is laborious or requires regular observations to determine field SWE changes. Automatic SWE measurement is not readily available or possible under forest canopies in most cold regions (Kinar and Pomeroy, 2015). Nevertheless, automatic, ultrasonic snow depth sensors are usually included in meteorological stations. Such snow depth measurements have been used to derive precipitation (Mair et al., 2016), snow density (Helfricht et al., 2018), and SWE (Egli et al., 2009), and have been used to compare water balance between forests and clearings (Bales et al., 2011). But, to date its use for quantitatively determining snow interception is needed to be further explored.

Many models have been developed to simulate snow interception and unloading in forests (e.g. Bartlett et al., 2006; Hedstrom and Pomeroy, 1998; Niu and Yang, 2004). In these models, interception is usually determined by the initial snow load, snowfall rate, and the maximum snow storage capacity of the canopy, which is determined by air temperature, fresh snow density, and canopy coverage. The unloading of intercepted snow is usually determined by wind speed and time since the snowfall. The intercepted snow changes albedo, canopy temperature and hence the shortwave and longwave radiation around the canopy. All these factors rely on high quality climate data for simulating snow interception and release to achieve desirable accuracy. Because canopy intercepted snow is relatively less than snow on the ground and usually only stays for few hours to days, the modelling of canopy snow is more sensitive than ground snowpack to the quality of the forcing data that run the model. However, because of the sparse meteorological observation system in cold regions forests, climate model outputs that have relatively low accuracy are the only available source of data to model snow interception in most areas. Hence, the need for data assimilation (DA) to allow better simulation of snow interception.

Snow observations and models both have drawbacks in estimating hydrological properties. Observations are usually limited by small spatial coverage (e.g., automatic station) or sparse repeat frequency (e.g., satellite remote sensing), or both (e.g., manual survey). Models are simplified representations of real world physical processes and their simulation accuracy is greatly influenced by the quality of parameterization and input data. To optimize estimation of hydrological properties, DA has been introduced to hydrological models since it combines advantages of observation (e.g., relatively higher accuracy) and modelling (e.g. low cost and consistent at reasonable spatial and temporal scales).

Many DA methods have been developed in environmental science that differ in how they treat observations and model simulation error covariance (Liu et al., 2012). A

simple insertion method assumes that observations are perfect and only modelling contains error. Hence, modeled state variables are directly replaced by observations whenever there is an observation available. Other data assimilation approaches that have adopted improved sophisticated algorithms to determine model and observational uncertainty and are being used by many cold regions hydrologists. The most common are the Kalman filter (KF) family (traditional KF, EKF, EnKF), Particle Filter (PF), and four-dimensional variational data assimilation (4DVAR). Cold regions hydrologists have used these approaches to assimilate both *in situ* observations and remotely sensed data, including snow cover fraction (Andreadis and Lettenmaier, 2006; Clark et al., 2006; De Lannoy et al., 2012; Liu et al. 2013; Rodell and Houser 2004; Slater and Clark 2006; Stigter et al., 2017), snow depth (Hedrick et al., 2018; Kumar et al., 2014; Kumar et al., 2017; Liu et al. 2013; Lv and Pomeroy, 2019b; Magnusson et al., 2017; Stigter et al., 2017), and SWE (Andreadis and Lettenmaier, 2006; Bergeron et al., 2016; Franz et al., 2014; Huang et al., 2017; Liston and Hiemstra, 2007; Lv and Pomeroy, 2019b), into the hydrological models. However, to authors' knowledge, the assimilation of snow interception information has yet to be explored.

Snowmelt runoff from the Canadian Rockies contributes to the headwaters of major rivers that provide essential water supply for large portions of western Canada and the northwestern United States. Needleleaf forests cover much of the Canadian Rockies, and so accurate determination of the magnitude and timing of snow interception plays an important role in regional water management.

This research studied the use of automatically measured snow depth from adjacent forest and clearing sites to quantitatively estimate snow interception in a headwater basin in the Canadian Rocky Mountains. This snow interception data, along with a weighed, hanging tree and time-lapse camera measured snow interception information, were assimilated into a physically based, process-hydrology Cold Regions Hydrological Modelling platform (CRHM) model using EnKF and rule based direct insertion to assess the influence of DA on snow interception simulation. The specific objectives of research are to determine how automatically measured snow depth in the forest and clearing can be used to quantify snow interception loss in the forest, and to examine the influence of assimilating ground measured and remotely sensed snow interception information to snow interception simulations.

4.3 Study area and data

4.3.1 Marmot Creek Research Basin

This study took place in the Upper Forest (UF) and Upper Clearing (UC) sites at the Marmot Creek Research Basin (MCRB). MCRB is located in the Front Ranges of the Canadian Rockies in Alberta, Canada (Figure 4-1). It is about 9.4 km^2 with an elevation

range from 1700 to 2825 m. At low to middle elevations, continuous stands of Lodgepole Pine, Engelmann Spruce, and Douglas Fir are the dominant land covers. Upper elevations are dominated by Larch, Engelmann Spruce, Sub-alpine Fir, shrubs, and grasses. The highest elevations are covered largely by talus and exposed rock. The main precipitation type in the basin is snow (up to 75% in high elevations) with mean annual precipitation varying by elevation from 660 to 1140 mm. Approximately 65% of basin is covered by forest. Snow interception by the forest canopy and sublimation of intercepted snow both control snow accumulation such that up to 60% of the annual snowfall never reaches the ground under the needleleaf forests (Ellis et al., 2010). In the 1970s, six large and thousands of small clearings were cut to study the influence of deforestation on local hydrology (Rothwell et al., 2016). UC is located in one of the middle elevation (1840 m) clearings with a diameter of approximately 60 m. Forty years after deforestation, the main vegetation type in UC is short grass and natural forest regeneration with young trees less than 2 m high. The UF site is located in a relatively level mature mixed forest stand of Spruce, Fir and Pine that is approximately 30 m from the northwest edge of UC.

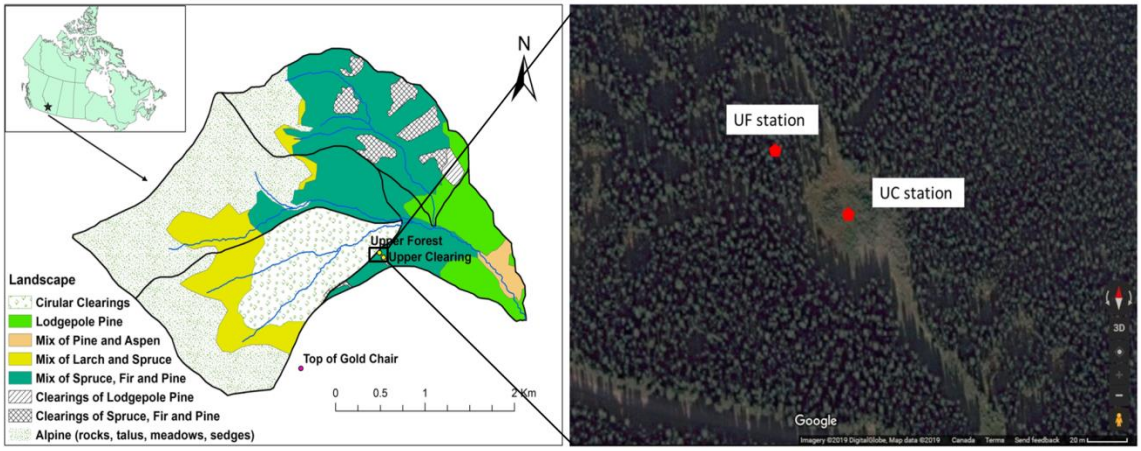

Figure 4-1. Landcover of Marmot Creek Research Basin, Alberta, Canada (left) and a close-up of upper forest and upper clearing sites (right, photo from Google Map).

4.3.2 Data collection

Two meteorological stations were mounted in UC and UF to continuously measure climate data at 15- minute intervals beginning in 2005. A Campbell SR50 sensor is mounted on each of the meteorological stations to measure snow depth. An Alter-shielded Geonor weighing precipitation gauge was used to measure precipitation at UC. Precipitation data are corrected for wind-induced undercatch (Smith, 2009). Hourly air temperature, relatively humidity, soil temperature, wind speed, short- and longwave radiation, snow depth, and precipitation data until September 2017 were collected at both sites. A tree was suspended at UF to quantitatively measure snow interception on forest canopy from January 2016 to June 2017. A time-lapse camera (Wingscapes

TimelapseCam) was mounted on the Gold chair-lift at the Nakiska Ski Resort beside MRCB from March 2015 to June 2016 to take pictures of the forest canopy in the basin. Hourly images were processed following Lv and Pomeroy (2019a) to determine the time of intercepted snow on the forest canopy. Snow surveys were conducted one to three times each month at both sites from November to June of each hydrological year from 2006 to 2017. The survey follows designed transects near the sites with at least 25 snow depth measures and one snow density measure among every five depth measurements using the ESC30 snow tube. In addition to locally observed meteorological data, the Environment and Climate Change Canada Global Environmental Multiscale (GEM) model 2.5 km grid product from November 2014 to August 2017 was used to run the CRHM model for DA experiments. Four grids of GEM data were needed to cover the entire MCRB basin. GEM outputs were hourly air temperature, relative humidity, wind speed, incoming shortwave radiation, incoming longwave radiation, and precipitation. These outputs were not bias corrected. The 2.5 km GEM data were downscaled to Hydrological Response Unit (HRU, which is the basic simulation unit in CRHM) scale before forcing CRHM. Precipitation and air temperature for each HRU were adjusted based the observed elevation lapse rate in MCRB. Other forcing variables of each HRU were assigned to the value of the closest GEM grid cell.

4.4 Methods

4.4.1 Snow interception estimation

4.4.1.1 Snow depth data filtering

SR50-measured fixed point snow depth data usually contains error and noise and is unable to represent landscape mean (Neumann et al., 2006; Ryan et al., 2008). Therefore, the data were error corrected, smoothed, and upscaled following the methods in Lv and Pomeroy (2019b). Because air temperature influences the speed of sound, temperature compensation was conducted on SR50 ultrasonic sensor reading according the following formula provided by Campbell Scientific (2009):

$$S_c = S_r\sqrt{\frac{T_a}{273.15}} \tag{4.1}$$

where S_c is the compensated snow depth, S_r is the raw sensor reading, and the T_a is air temperature in Kelvin.

After compensation, snow depth data still contains noise. “Noisy” data were removed by applying a three-hour moving average following Ryan et al. (2008). Fixed point snow depth measurements usually systematically over- or under-estimate areal means because of heterogeneity in snow accumulation, redistribution, and ablation caused by

topography, vegetation and wind (Pomeroy and Gray, 1995). Therefore, these were upscaled using a "scaling equation" developed using the relationship between temperature compensated as well as noise removed SR50 data and snow depth data from snow surveys at each site. For details of these "scale equations" refer to Lv and Pomeroy (2019b).

4.4.1.2 Fresh snow density estimation

Three methods were used to estimate fresh snow density to obtain SWE from the SR50 snow depth data. Because of popular air-borne snow depth measurements, many studies have combined these measurements with snowpack model-simulated snow density to estimate SWE in cold regions (Hedrick et al., 2018; Painter et al., 2016). In the present research, the first method used the physically based energy-balance Snobal module in CRHM running local observed meteorological data to simulate the snowpack density. However, Snobal can only simulate the density for the entire snowpack. Pomeroy and Gray (1995) reported that the different snow densities should be applied to fresh and old snow. Concomitant increases of simulated SWE and snow depth during snowfall events were used to calculate fresh snow density. The second method is described in Equation 4.2, proposed by Hedstrom and Pomeroy (1998) that uses air temperature to calculate freshly fallen snow density (the Hedstrom-Pomeroy method hereafter).

$$\rho_{fs} = 67.9 + 51.3\ e^{T/2.6} \tag{4.2}$$

where ρ_{fs} is the fresh fallen snow density, T is the air temperature at 2 m in ºC.

The third method is described by Equation 4.3, developed by Jordan et al. (1999), that uses air temperature and wind speed to estimate freshly fallen snow density (the Jordan et al. method hereafter).

$$\begin{cases} \rho_{fs} = 500\left[1 - 0.951e^{\left(-1.4\left(278.15-(T+273.15)\right)^{-1.15} - 0.008u^{1.7}\right)}\right] & -13 < T \leq 2.5\ ℃ \\ \rho_{fs} = 500\left[1 - 0.904e^{\left(-0.008u^{1.7}\right)}\right] & T \leq -13\ ℃ \end{cases} \tag{4.3}$$

where u is the 10-m wind speed in m/s.

Because the snowpack densification rate in cold and sheltered environments is usually as low as 25 kg/m^3 per month during the winter (Pomeroy et al., 1998a), all three methods assumed that the densification of lower old snowpack is negligible during snowfall events and the change of snowpack depth is contributed by fresh snow accumulation alone. The second and the third methods assume that fresh snow densities in the clearing and the forest are same during the snowtorm.

Snowfall events with mixed precipitation types (snow and rain) can affect the accuracy of snow density estimation. Thus data from these storms were excluded from the analyses and only data from pure snowstorms were analyzed. The precipitation phase of an event was determined following the method proposed by Harder and Pomeroy (2013).

Measured snowfall amount from a shielded weighing precipitation gauge and snow depth increase were used to estimate the actual fresh snow density of each storm. These data were used to validate the calculated fresh snow density using root mean square error (RMSE, Equation 4.4) and Model Bias (MB, Equation 4.5).

$$RMSE = \sqrt{\frac{\sum_{i=1}^{n}(Xo_i - Xs_i)^2}{n}} \quad (4.4)$$

$$MB = \frac{\sum Xs}{\sum Xo} - 1 \quad (4.5)$$

where x_s and x_o are simulated and observed fresh snow density, respectively.

4.4.1.3 Interception estimation

Forest canopy snow interception at the UF site was determined by the difference between SWE increases in UC and UF during each snow event using Equation 4.6:

$$\text{Int} = \Delta\text{SWE}_{\text{UC}} - \Delta\text{SWE}_{\text{UF}} \quad (4.6)$$

where Int is the snow interception amount for a snowfall event in UF, ΔSWE_{UC} and ΔSWE_{UF} denote the SWE increase during the snow fall for UC and UF, respectively.

The estimated snow interception from the three methods was compared to the snow interception measured by the suspended weighed tree at UF from January 2016 to June 2017 to determine the optimal method for snow interception estimation in the study site. The best method for estimating snow interception was used to scale the weighed tree data.

4.4.2 CRHM

The Cold Regions Hydrological Model platform (CRHM) was used to create a model to simulate snow interception and release from the forest canopy the UF site. CRHM is designed to assemble hydrological models that are suitable for cold regions. Researchers can create projects by choosing from a wide range of basin configurations, spatial and temporal resolutions, and hydrological process modules based on their research interests, data availability, and research scale. The CRHM library contains many modules that can be used to interpolate meteorological data, to simulate rainfall

and snowfall interception, wind redistribution, sublimation, albedo decay, canopy transmittance, snow energy and mass balance, evaporation, melt, snowcover depletion, infiltration, soil moisture, flow and storage of surface and subsurface, and streamflow routing. Detailed information about CRHM and the modules are given in several recent publications (Ellis et al., 2010; Fang et al., 2013; Fang and Pomeroy, 2016; Pomeroy et al., 2007; Pomeroy et al., 2016b).

The canopy module used in this study was initially developed by Parviainen and Pomeroy (2000) and later modified by Ellis et al. (2010). The main parameters of this module are canopy snow-free albedo, leaf area index (LAI), maximum canopy snow interception load, ice bulb temperature that controls snow unloading as solid or liquid, and the measurement height of air temperature and wind speed. These parameters were set according to field measurements or following the research of Ellis et al. (2010) and Pomeroy et al. (2012).

The Snobal module (DeBeer and Pomeroy, 2010; Marks et al., 1998) was used to simulate the mass - energy balance of snowpack and the snow density on the ground. Snobal assumes fresh fallen snow density as 100 kg/m^3. It divides the snowpack into two layers (active and lower) that are the same density if snowpack depth is greater than 10 cm. The active layer has a maximum thickness of 10 cm following Marks et al. (2008). The forcing data for the model are locally observed or GEM produced air temperature, relative humidity, soil temperature, wind speed, incoming shortwave radiation, and precipitation. The model is flexible but in this case was run at an hourly time step. When observations become available, model runs stop at 1 a.m. and a state file is exported. This state file contains values of all necessary state variables and fluxes at that moment. After the assimilation, this file is updated and set as the initial condition for next model run.

4.4.3 Snow interception assimilation

4.4.3.1 Ensemble Kalman Filter

The Ensemble Kalman Filter (EnKF) was used to assimilate continuous snow interception data obtained by snow depth measurements and weighted tree at the UF site. EnKF was chosen because it is easy to implement and it has been successfully used to assimilate other snow properties into hydrological models in many studies over the world (e.g., Franz et al., 2014; He et al., 2012; Kumar et al., 2009). EnKF is a sequential assimilation approach that can be used to update model state variable(s) when an observation is available. The updating amount is determined using the Kalman gain (K, Equation 4.8), which is determined by the error covariance of ensemble model simulation and observations, and the difference between simulated and observed state variable using the following equation:

$$x_{i,j}^{u} = x_{i,j}^{s} + K_i(y_{i,j} - H_i x_{i,j}^{s}) \quad (4.7)$$

where $x_{i,j}$ and $y_{i,j}$ denote the j^{th} (j=1, 2, …, N, N is ensemble size) ensemble model state and observation vector at time step i (i =1, 2, …, M, M is number of observations); superscripts u and s denote the updated and simulated model state vector; H_i is the operator that relates the model vector to the observed vector and it is a unit factor in this study. The Kalman gain K_i in i^{th} time step is calculated by:

$$K_i = P_i^s/(H_i P_i^s + R_i) \quad (4.8)$$

where P_i^s and R_i are the error covariances of model forecast and observation at time step i, respectively. Model forecast error covariance is estimated from the ensemble model simulations covariance. Observation error covariance is obtained by perturbation of observations with a presumed standard deviation.

In the EnKF DA, model simulation uncertainty is assumed to be primarily caused by uncertainty in forcing climate data in the present research. As a result, ensemble model simulations were run by Monte Carlo perturbed forcing data following earlier research (Kumar et al., 2014; Liu et al., 2013; Reichle et al., 2002). For incoming shortwave radiation and precipitation, multiplicative perturbation with a mean value of 1 was performed to avoid unreasonable outcomes such as positive incoming short-wave radiation at night or negative precipitation. Additive perturbation with a mean value of zero was run for other driving forces (Table 4-1). For model state variable – canopy snow load, multiplicative perturbation was conducted, with standard deviation set at 0.05. Because forcing variables are frequently related, such as precipitation resulting in low incoming shortwave radiation, a cross correlation was imposed to all variables except wind speed using established relationships (De Lannoy et al., 2012; Riechle et al., 2007) (Table 4-1). Theoretically, more ensemble simulations in EnKF DA means higher accuracy. However, in consideration of computational efficiency, twenty was chosen as ensemble number following on previous research (Kumar et al., 2009; Kumar et al., 2014). Using EnKF, snow interception data derived from SR50 measurement was assimilated for each snow storm detected from November 2014 to August 2017 (hereafter DA_SR50). The hanging tree measured snow interception was assimilated daily from January 2016 to June 2017 (hereafter DA_Tree).

Table 4-1. Model driving and state variables with perturbation parameters.

Variables	Perturbation Type	standard deviation	Cross correlations with Perturbations					
forcing variables			AT	RH	u	SW	LW	P
Air temperature (AT)	Additive	5 ℃	1	-0.3	-	0.3	0.6	-0.1
Relative humidity (RH)	Additive	10	-0.3	1	-	-0.8	0.5	0.8
Wind spread (u)	Additive	2 m/s	-	-	1	-	-	-
incoming short-wave radiation (SW)	Multiplicative	0.3	0.3	-0.8	-	1	-0.3	-0.5
incoming long-wave radiation (LW)	Additive	50 (W/m^2)	0.6	0.5	-	-0.3	1	0.5
Precipitation (P)	Multiplicative	0.5	-0.1	0.8	-	-0.5	0.5	1
CRHM state variables			SWE					
Intercepted SWE	Multiplicative	0.05	1					

4.4.3.2 Rule based direct insertion

Although snow interception data derived from the time-lapse camera (TLC) and satellite images is not able to determine the magnitude of interception, it provides the timing of interception. In particular, the data from time-lapse camera not only provides the initiation of interception, but also the duration of snow interception storage on the canopy. To assimilate this information into CRHM, a rule based simple insertion method inspired by the satellite measured snowcover information assimilation research of Rodell and Houser (2004) and Liu et al. (2013), was proposed in the present research. The TLC-derived snow interception information was assimilated daily (hereafter DA_TLC). Simulated snow interception was compared to the TLC information at end of each day. If the model-simulated snow interception was less than 1 mm and TLC information indicated there was snow on the canopy, the snow interception was adjusted to a minimum value (3 mm). In contrast, if model-simulated snow interception was greater than 1 mm but TLC information showing there was no snow on the canopy, the simulated snow was adjusted to 0. Assimilation can be only conducted at the midnight of each day in CRHM, but TLC can only show interception information during daylight. So, there were always several hours of lag between the observation and assimilation times. In addition, snowfall and intercepted snow unloading can happen at night. Therefore, only days with obvious midnight snow interception information were assimilated. On such days, canopy snow interception information was consistent before sunset of the first day and after sunrise of the second day. Therefore, days with unknown midnight snow interception information, indicated by no snow on the canopy in the evening but snow present on the canopy the following day, were omitted from the assimilation process. Two control experiments without DA were conducted to be compared to the DA experiments to assess the influence of DA on simulation of interception. One was forced by GEM data (OL) and the other was forced by local observed meteological data (ObsMet).

4.5 Results

4.5.1 Snow depth in forest and clearing

According to SR50 measurements, snow depth in the clearing was frequently higher than that in the forest (Figure 4-2). For the 12 hydrological years of observations, annual peak snow depths in the clearing and forest were correlated to each other (r^2=0.91, P<0.05). Peak snow depth in the forest was 26.5 – 54.1% (mean: 45.8%) less than that in the clearing. At the end of the snow season, the snowpack on the ground lasted 0 to 8 days (mean: 4.4 days) longer in the forest than in the clearing. Snow survey data indicated that the snowpack density in the clearing and forest were correlated, but not strongly (r^2=0.5, P<0.05; Figure 4-3 a) and the snowpack density distribution and mean value at the two sites were similar (Figure 4-3 b). A T-test for two data sets illustrated that there was no significant difference between two sample means (data not shown). This indicated that the snow depth ratio was close to the SWE ratio between sites.

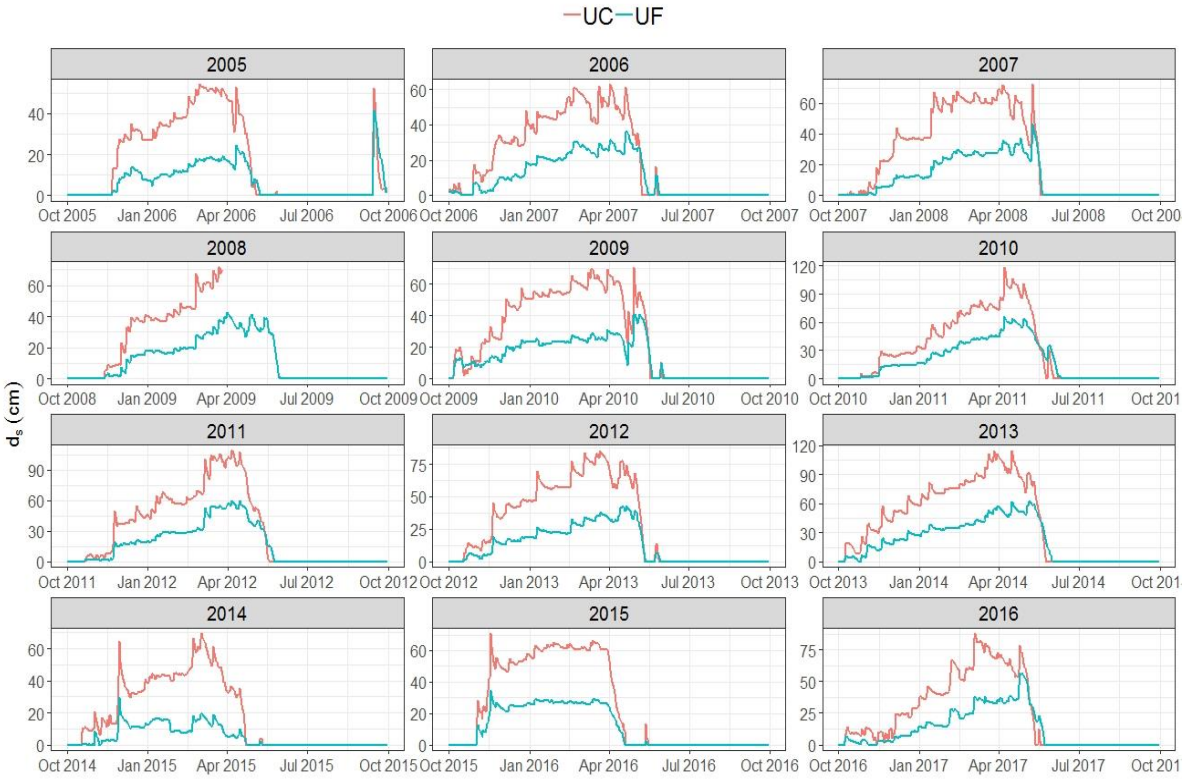

Figure 4-2. SR50 measured snow depth at upper clearing (UC) and upper forest (UF) sites in the Marmot Creek Research Basin.

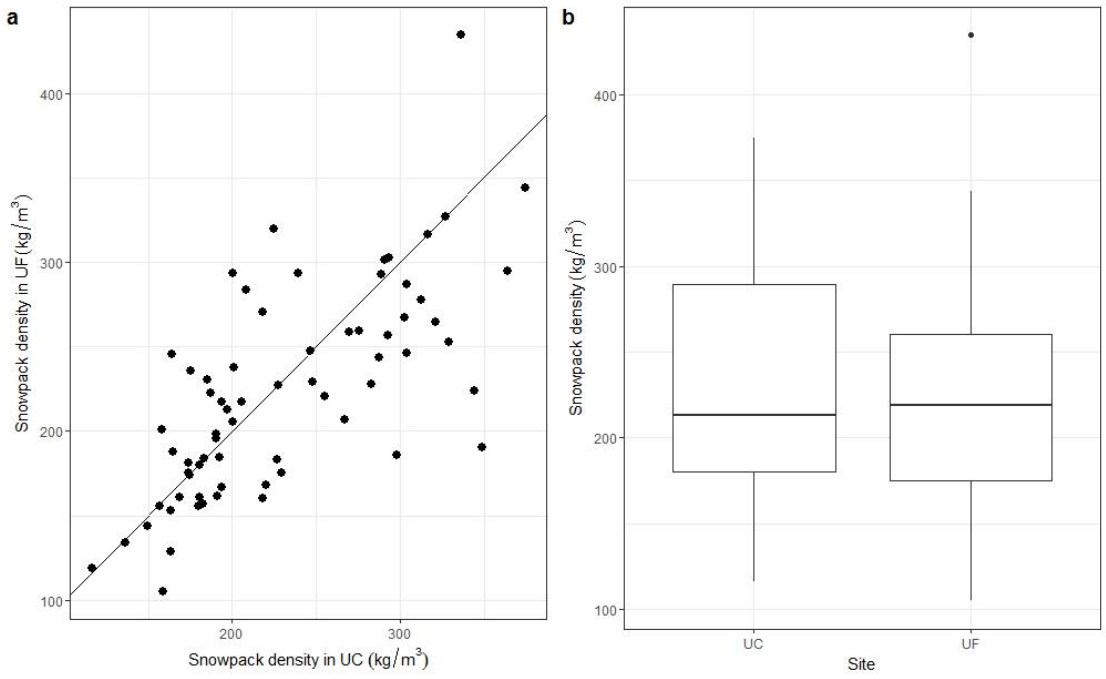

Figure 4-3. Comparison of observed snowpack densities at the upper clearing (UC) and upper forest (UC) sites in Marmot Creek Research Basin. a) UF density versus UC density and a 1:1 line for comparison, b) box plots of the distribution and mean of snowpack densities for UF and UC sites.

Snow depth increases during snowfall events in UC and UF were strongly correlated (r^2=0.9, P<0.05). The linear relationship between the snow depth increases was significant (Figure 4-4). On average, snow depth increases in the forest were approximately 47.6% lower than those in the clearing. For several small events, the snow depth changes in the forest were negative even though there was a snow depth increase in UC. This can be explained by a high interception efficiency for low snowfall amounts such that there was only very small accumulation below the canopy. Minor densification (< 3 cm) also impacts the old snowpack depth on the forest floor during the event. Almost all the events with heavy snow (snow depth increase higher than 30 cm in UC) were located above the correlation line, demonstrating that the snow interception efficiency decreases whilst snowfall amount increases.

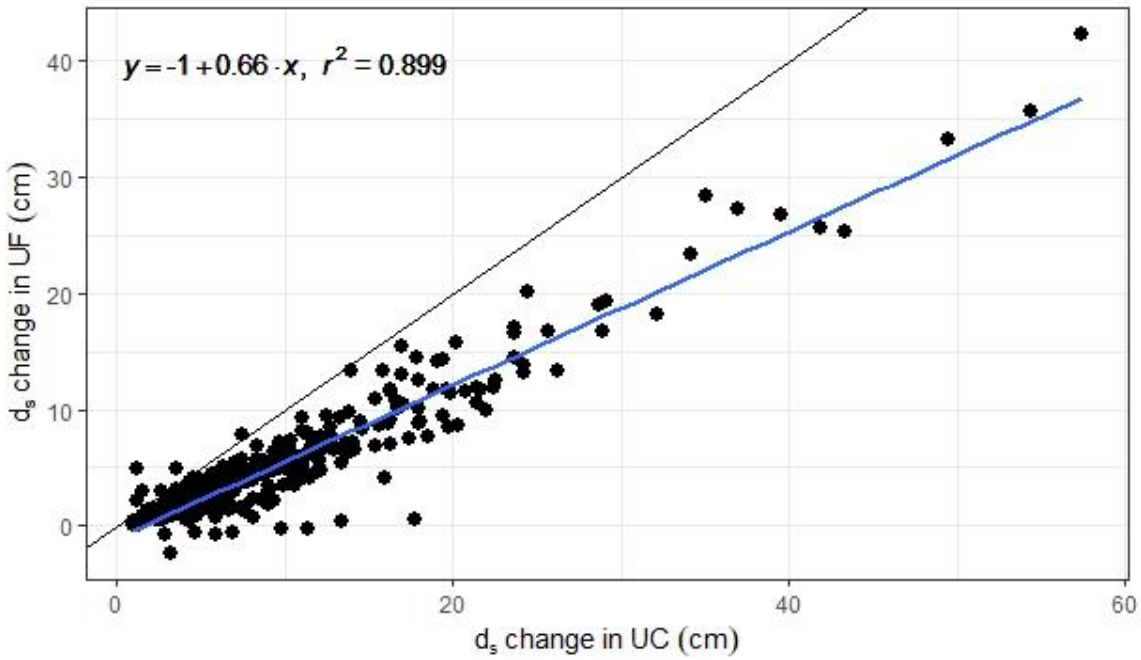

Figure 4-4. Comparison of snow depth (d_s) increase from upper forest (UF) and upper clearing (UC) during each snowfall event. Black line shows the 1:1 ratio and blue line shows indicates the best linear regression.

4.5.2 Fresh snow density estimation

Snobal-simulated snowpack density was compared to directly observed snowpack density in UC and UF from 2005 to 2017. The model simulation frequently overestimated observed snowpack density at both forest and clearing sites (Figure 4-5). The overestimation rate was especially high in the early snow season of each hydrological year. On average, the model overestimated snowpack density by 43% and 44% at UC and UF, respectively. The RMSE of model simulated snowpack density in UC and UF was 129.7 kg/m^3 and 141.5kg/m^3, respectively.

Model simulated fresh snow density was frequently larger than that observed, resulting in the modelled snow depth increase being much smaller than that observed (Figure 4-6). Therefore, using the model simulated snowpack density and observed snow depth leads to the overestimation of SWE at both sites. The calculated fresh snow density using Hedstrom-Pomeroy method was close to observation most of the time while the Jordan et al. method underestimated the fresh snow density for both events.

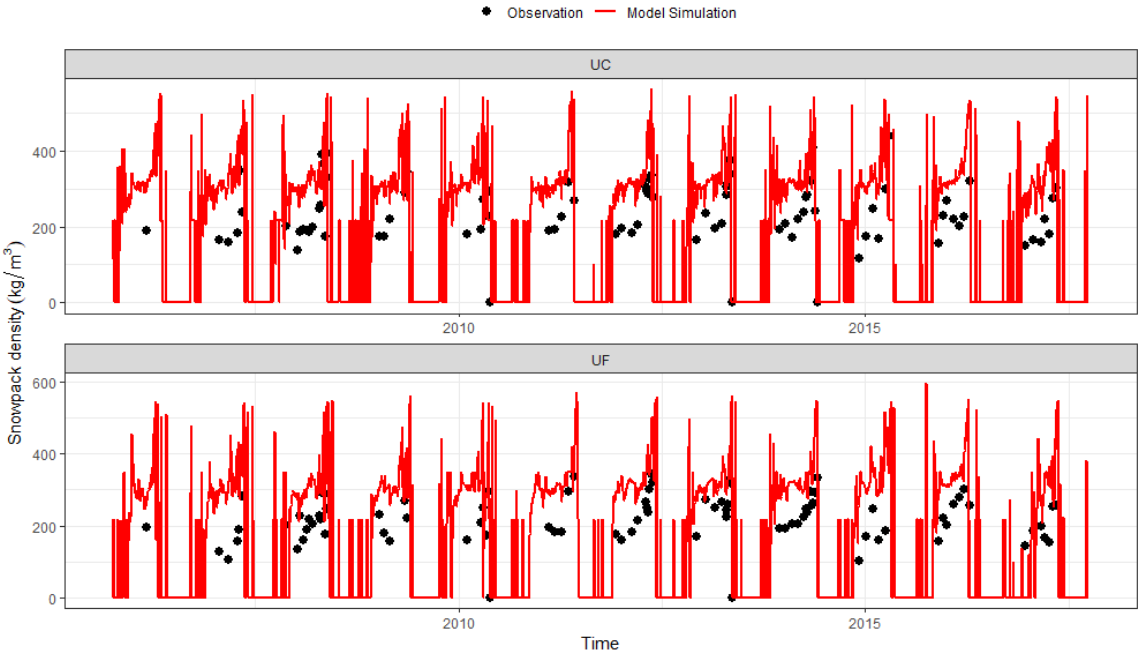

Figure 4-5. Time-series of Snobal simulated and observed snowpack density in the upper clearing (top) and upper forest (bottom) in Marmot Creek Research Basin.

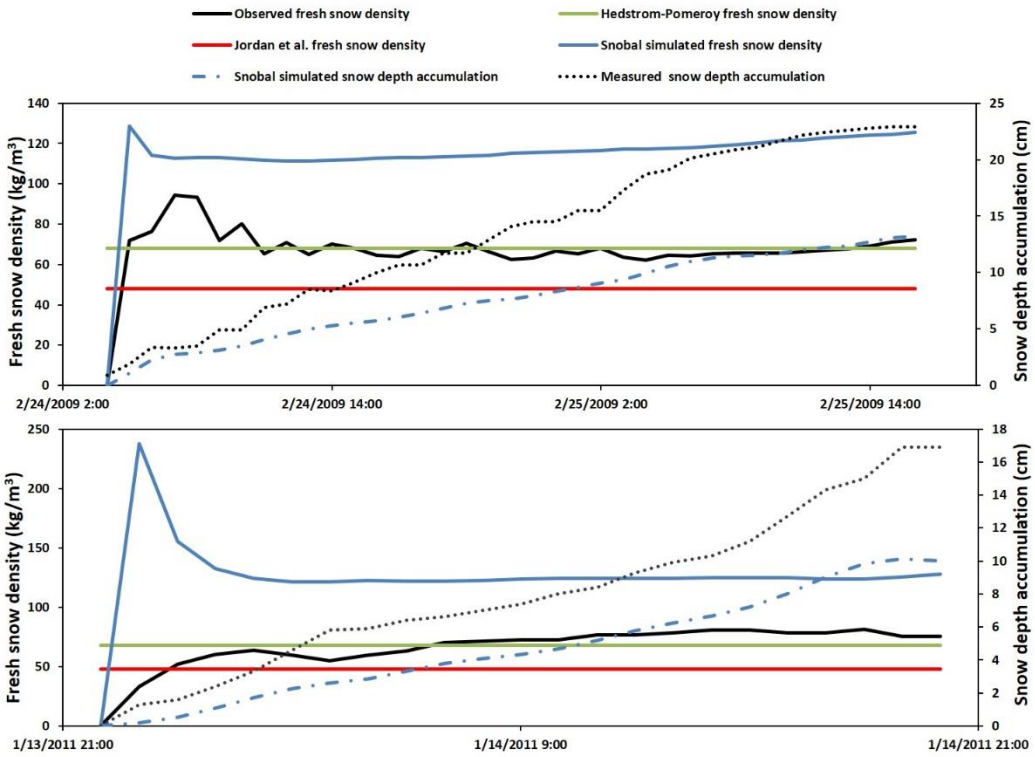

Figure 4-6. Time-series of simulated, calculated, and observed fresh snow density and simulated and observed snow depth accumulation during two snow storms at upper clearing site in Marmot Creek Research Basin.

The comparison between calculated and observed fresh snow density for all snowfall events from 2005 to 2017 is shown in Figure 4-7. The coefficients of determination (r^2) between observed and calculated fresh snow density were lower than 0.4 for both methods. The RMSE of the Hedstrom-Pomeroy equation calculated fresh snow density was 14.7 kg/m^3, while the RMSE of the Jordan et al. equation was slightly higher (21.5 kg/m^3). There was small underestimation trend for both Jordan et al. method and Hedstrom-Pomeroy method as their MB value were −0.02 and −0.08, respectively. The mean value for observed fresh snow density at the UC site was 83.7 kg/m^3, which is slightly higher than the average value calculated using both methods (82.2 kg/m^3 and 77 kg/m^3 for Hedstrom-Pomeroy and Jordan et al., respectively). The lower limit of calculated fresh snow density, which is the result of low air temperature, was around 68 kg/m^3 and 48 kg/m^3 for Hedstrom-Pomeroy and Jordan et al., respectively. This resulted in calculated fresh snow density values for many snowfall events being the same or around the lower limit value. This partially contributed to the relatively low r^2 values for both methods.

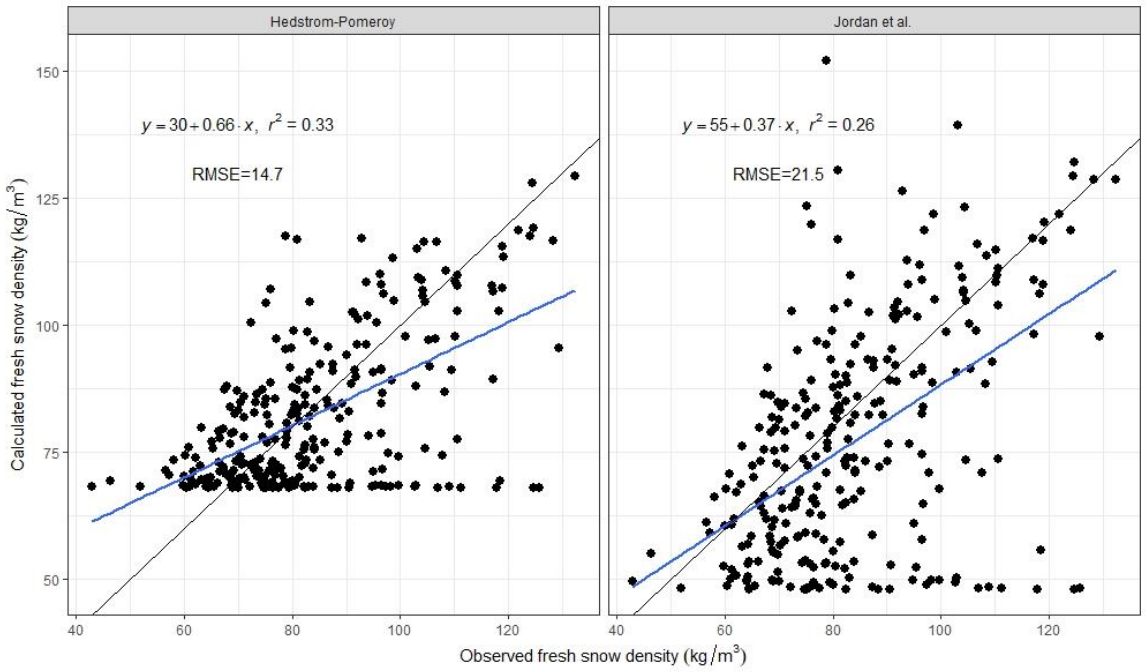

Figure 4-7. Comparison of measured and calculated fresh snow density using Hedstrom-Pomeroy equation (left) and Jordan et al., equation (right) without any fresh snow densification at the upper clearing site in Marmot Creek Research Basin. A 1:1 line (black) is plotted for comparison. The regression line (blue) is only shown to display the fitted relationship for the regression.

The difference between observed and calculated fresh snow density was determined and plotted against the snow event duration (Figure 4-8 a). For the Hedstrom-Pomeroy method, the average differences were negative when the snowstorm duration was less than 12 hours. When the snowstorm duration was longer than 12 hours, the difference became positive, increasing with longer snow event duration. This value peaked at 57

kg/m^3 when snow event duration was 53 hours. With the Jordan et al. method, average difference values were frequently positive and increasing with increasing snow event duration. This indicated that fresh snow densification exists and varies among snow events. This study and the predictive algorithms tested, assumed that the densification of fresh snow during snow events at sheltered study sites is negligible; an assumption not validated in many cold regions (Goodison et al., 1981). However, according to the calculated and observed fresh snow density, the densification rate was frequently less than 1 kg/m^3 per hour, indicating that the assumption of only a very small fresh snow densification is valid at present research sites. The densification rate is well correlated to the snow storm duration (Figure 4-8 b). Therefore, a small densification rate was added to the calculated fresh snow density for both methods for all snow storms according to the relationship between snow storm duration and densification rate that show in Figure 4-8 b. In all, the Hedstrom-Pomeroy equation worked better than the Jordan et al. equation at the study sites. In sheltered environments, fresh snow density can be effectively estimated using air temperature and a small densification rate.

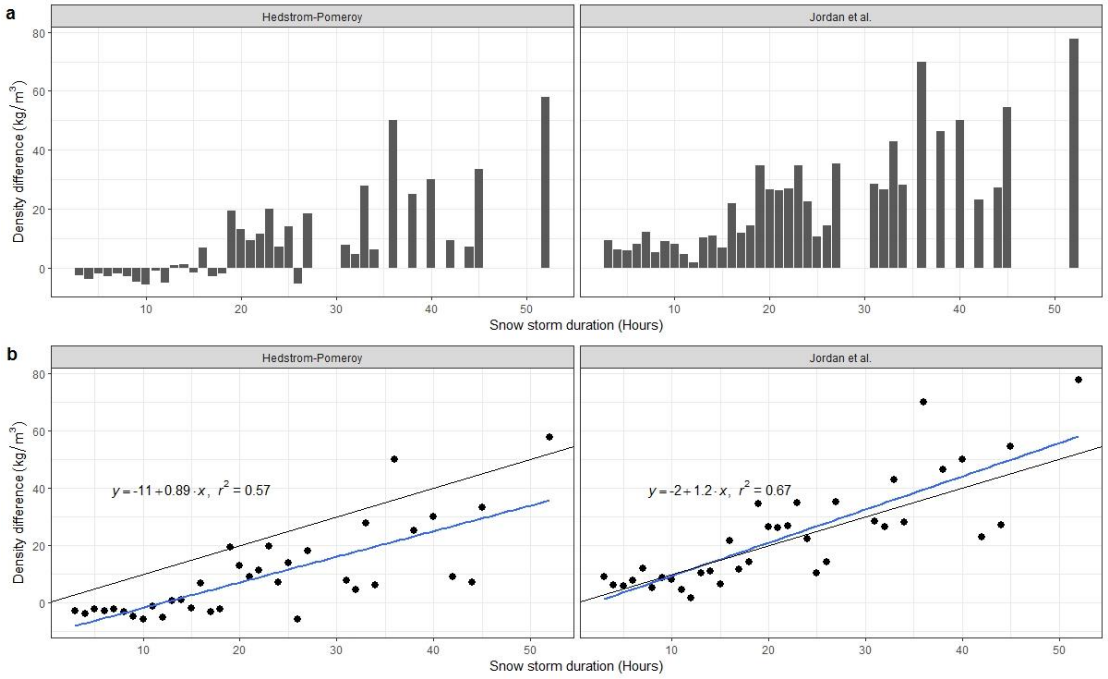

Figure 4-8. Comparison of snow storm duration (hours) to the difference between measured and calculated fresh snow density using two methods at the upper clearing site in Marmot Creek Research Basin. a). Average difference between measured and calculated fresh snow density among different snow storm durations. b). Comparison of average difference between measured and calculated fresh snow to snow storm durations (hours). A 1:1 line (black) is plotted for comparison. The regression line (blue) is only shown to display the fitted relationship for the regression.

4.5.3 Validation of interception estimation methods

The calculated snow interception using three methods from 2016 to 2017 was validated using interception data measured by the weighed tree at UF (Figure 4-9). The Snobal method showed poor accuracy in estimating snow interception with a high RMSE of 21.4 mm and low r^2 (0.21). The correlation between calculated and observed interception was weak. This may be caused by the fact that Snobal largely overestimated the fresh snow density and hence the SWE at both sites as it assumes the density of fresh snow is 100 kg/m^3. The two methods which use calculated fresh snow density and observed snow depth increase to estimate SWE change showed higher accuracy. The RMSE of both methods are low (2.0 mm and 2.6 mm for Hedstrom-Pomeroy and Jordan et al., respectively). The r^2 between calculated and observed snow interception for Hedstrom-Pomeroy method was 0.72, while the value for Jordan et al. was 0.66. The Hedstrom-Pomeroy method worked best amongst all methods so it was selected to estimate snow interception at UF. This indicates that continuously measured snow depth data are capable of quantifying snow interception.

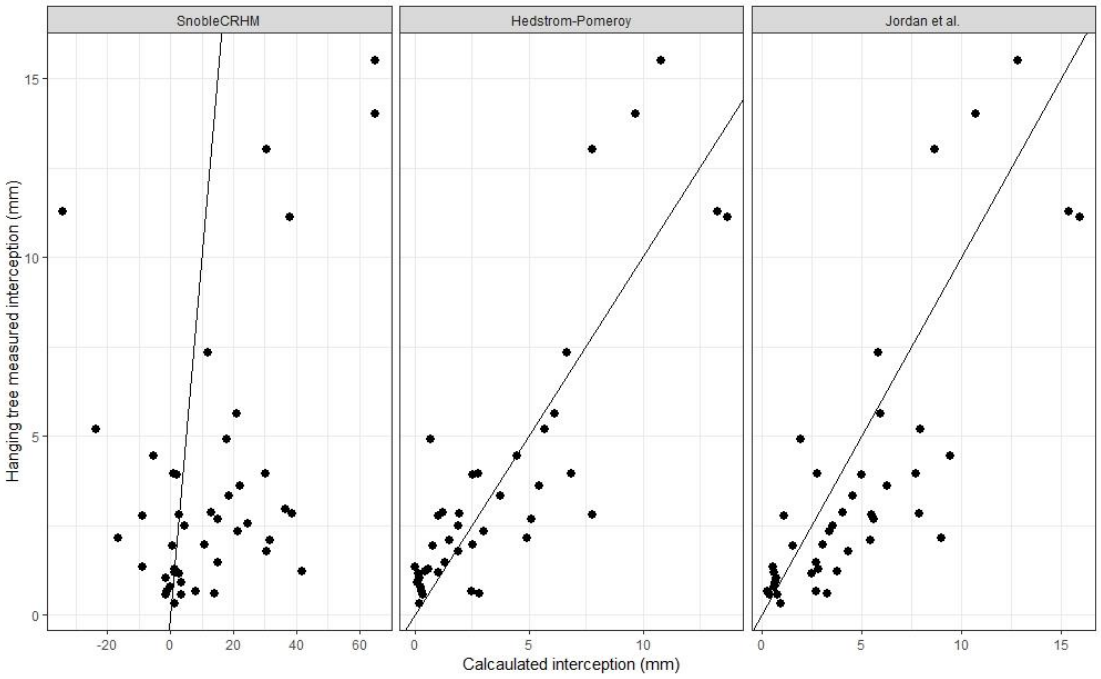

Figure 4-9. Comparisons between snow interception estimated by three methods and weighted tree observations at upper forest site in Marmot Creek Research Basin. A 1:1 comparison line is shown for reference.

4.5.4 Snow interception assimilation

Assimilation results were evaluated using weighed tree measurements and time-lapse camera photos from January to June 2016. These two data sets were both available only

during this period. ObsMet-simulated interception magnitude and timing were often close to observations (Figure 4-10). But the OL simulated snow interception did not agree with measurements most of the time, while three DA experiments improved interception simulation in varying degrees (Figure 4-10).

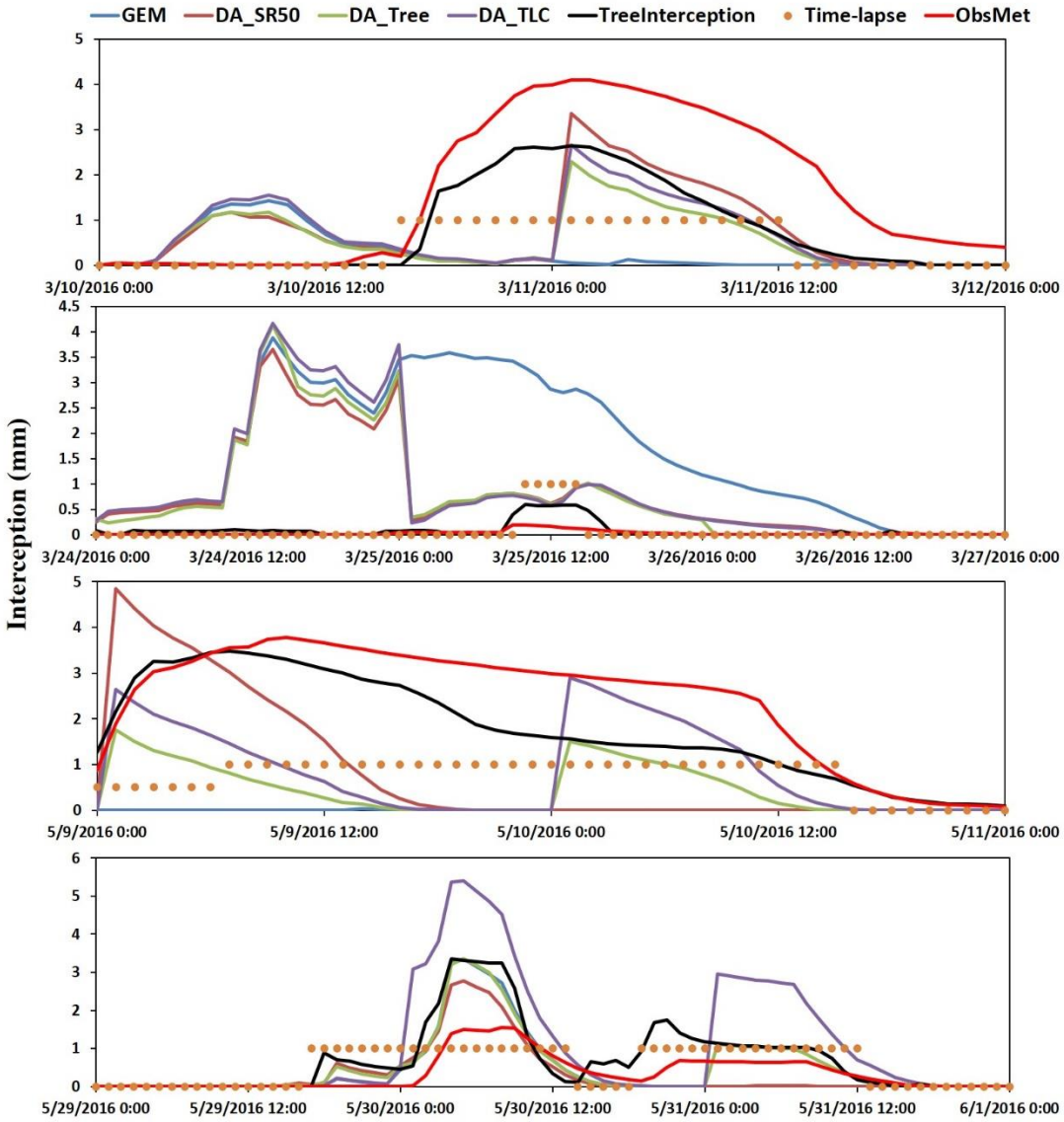

Figure 4-10. Time series of CRHM simulated snow interception from different DA experiments driven by GEM data (GEM, DA_SR50, DA_Tree, DA_TLC, unit: mm) and CRHM simulation driven by observed meteorological data (ObsMet, unit: mm), the hanging tree measured snow interception (TreeInterception, unit: mm), and the time-lapse camera derived canopy snow cover timing (Time-lapse, yellow dot, 0, 1, and 0.5 denote canopy snow free, canopy snow covered, and unknown, respectively).

The snowfall event shown in Figure 4-10 a, the OL simulated interception began 12 hours earlier than the observation and disappeared before the observed interception began. The ObsMet simulation slightly overestimated the magnitude and timing of snow interception when compared to observations. All three DA experiments improved

the simulation on March 11th and the simulated snow interceptions were closer to observations than ObsMet simulation. However, because assimilation time is midnight, the incorrect interception in the morning of March 10th was not removed and the interception before the midnight was not simulated by all three DAs.

During the event shown in Figure 4-10 b, observations indicated there were only a few hours of snow interception around noon of March 25th. The ObsMet simulation agreed with the observation in interception timing but slightly underestimated the interception magnitude. OL simulated snow interception was continuous from March 24th to 26th while the all three DAs did not detect interception at the beginning of March 25th. Simulations of all DAs agreed well with observations for the rest of detected events. However, like OL, all three DAs simulated interception following the afternoon of March 24th and there was no improvement in the simulated interception predictions for all three DA experiments on this day.

For the event shown in Figure 4-10 c, snow was observed continuously landing on the canopy. The ObsMet simulation agreed well with observation of interception timing while slightly overestimating the intercepted snow amount. The OL simulation did not capture the interception from May 9th to 10th at all. After assimilation, all three DA experiments added some snow to the canopy at the beginning of May 9th, but the canopy snow completely ablated in the afternoon that day due to the high sublimation that was simulated. At the beginning of the May 10th, DA_Tree and DA_TLC added some snow to the canopy again and the simulated canopy snow disappeared earlier than was observed that day. DA_SR50 did not add snow to the canopy on May 10th because this method only assimilates snow interception amount during a single event without information of how long the snow stays on the canopy.

There were two events shown in Figure 4-10 d. Like previous snowfall events, the ObsMet-simulated the timing of interception well but not the magnitude. The OL simulated the first event's interception well but missed the second. DA_SR50 and DA_Tree have good simulation results but DA_TLC greatly overestimated the interception for the first event. Because model-simulated snow interception was less than 1 mm at the beginning of May 30th, DA_TLC adjusted the snow interception to 3 mm according to assimilation rules. However, because the snowfall occurred after midnight, this contributed to the overestimation in DA_TLC. For the second small event, DA_Tree effectively simulated interception and DA_TLC again overestimated interception. The DA_SR50 simulation did not add any snow to the canopy because the storm was small and the SR50 interception estimation method did not catch this event.

Figure 4-11 shows the results of DA experiments for the entire validation period. These results show that the weighed tree measurements agreed well with the time-lapse camera data with 93% consistency and ObsMet simulation overestimated interception duration by 4%. However OL only agreed with the time-lapse camera information about

57% of the time. After data assimilation, this rate increased to 61%, 68%, and 76% for DA_SR50, DA_Tree, and DA_TLC, respectively. The improvement of DA_SR50 was small and believed to be caused by the low assimilation frequency. The DA_TLC had the best results indicating that assimilating the time-lapse camera snow interception information based on the simple rule based method can greatly contribute to predicting interception timing. The RMSE of OL was 0.84 mm and data assimilation improved the accuracy by varying amounts. DA_Tree (RMSE = 0.68 mm) achieved the best results among all DAs and this is likely contributed to its relatively high DA frequency and better input data quality. The improvement in the other two DAs was relatively small, particularly in the case of DA_TLC that only improved accuracy by 0.06 mm. This indicated that although DA_TLC can improve the predictions of interception timing, its contribution to the simulation magnitude is small.

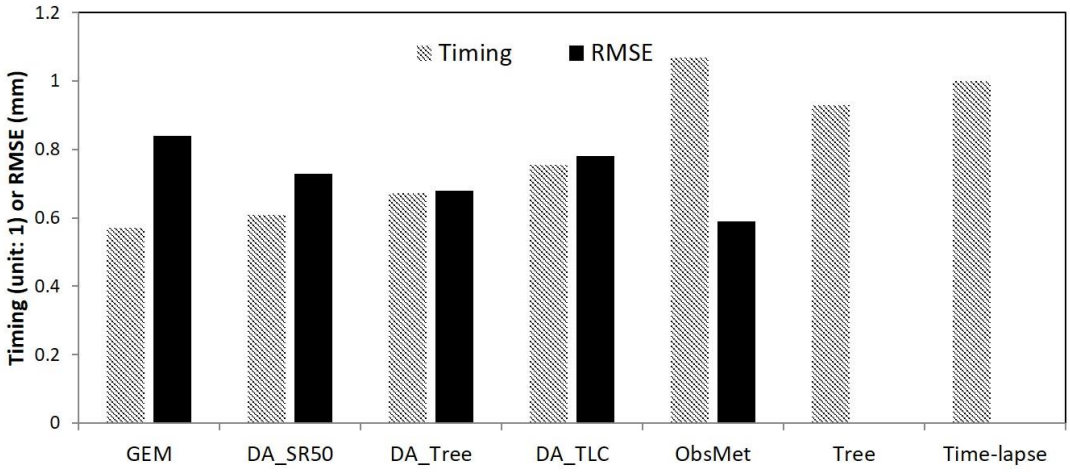

Figure 4-11. Normalized snow interception timing of DA experiments driven by GEM data (OL, DA_SR50, DA_Tree, DA_TLC), CRHM simulation driven by observed meteorological data (ObsMet), and tree measurements (Tree) to time-lapse camera (Time-lapse) derived snow interception information (shaded bars, unit: 1), and RMSE of snow interception from ObsMet simulation and different DA experiments when compared to hanging tree measurement (dark bars, unit: mm).

Although the three DA experiments that were forced using GEM data did not achieve the same results as ObsMet simulation that was forced using local meteorological observations, they all improved the interception magnitude and timing in comparison to the OL GEM-driven simulation. This indicated that assimilating interception information derived from automatic snow depth measurements and time-lapse cameras into a model that is forced by numerical weather model outputs can obtain results that are similar to those from a model driven by comprehensive locally observed forcing data (without assimilation). As comprehensive meteorological stations are sparse in cold regions forests, this assimilation strategy can benefit interception simulation in these areas.

4.6 Discussion

In this study, automatically measured snow depth data from a needleleaf forest and adjacent clearings were used to quantify snow interception in a forest canopy. Interception observations were assimilated into a physically based hydrological model to better simulate snow interception. Three methods were used to calculate snow density. All were used, along with depth observations, to quantify SWE change during snowfall events in a forest and a clearing using observed meteorological data. The Hedstrom-Pomeroy fresh snow density equation, using only air temperature to calculate fresh snow density, outperformed other methods. This agreed with the research of Mair et al. (2016) and Brazenec (2005). Freshly fallen snow densification can occur immediately after snowfall at a rate of 8–13 kg/m^3 per hour (up to 12h) during snow events in Ontario (Goodison et al., 1981). Gray et al. (1970) also found that the densification rate of snowpack in the Canadian Prairies can reach 9 kg/m^3 per hour over the course of a blowing snow storm. In the present research, no further densification factor was applied to fresh fallen snow during snowfall events but the calculated fresh snow density agreed well with observations. Although there was evidence of fresh snow densification when snowfall duration was longer than 12 hours, the densification rate was as low as <1 kg/m^3 per hour. This is much less than was found by Gray et al. (1970) and Goodison et al. (1981). This is almost certainly due to the fact that the study sites in the present research are located in sheltered environments where wind has a minor influence on snow densification and where cold conditions prevail during snowfall events.

All three DA experiments contribute to better modelling of canopy snow interception. Assimilation of time-lapse camera derived canopy snow information can greatly improve the simulation of canopy snow coverage timing. However, because snow interception is difficult to reliably quantify, improvements to interception magnitude are limited. Overall, the DA_Tree achieved the best results in simulating interception among all three DA experiments. However, the continuous measurement of snow interception amounts from a weighed, suspended tree is not normally available for the cold regions forests (there is only one other weighed tree like this in Western Canada), and when it is, data are confined to a point scale. Assimilating snow interception information that was derived from continuous snow depth measurements gave a reasonable result but with one drawback; this method provides the snow interception amount at the end of a snowfall event but not information on canopy snow coverage duration. This method has a lower DA frequency and no control on the snow unloading process compared to the other two DAs.

All three methods share a constraint that originates with the CRHM model. Because CRHM can only export and read the state file in the beginning of each day, the highest assimilation frequency is a 24 hour return period. This is not a big problem in for surface snowpack assimilation (Lv and Pomeroy, 2019b), but significantly influences canopy snow estimation. Unlike the surface snowpack that remains on the ground from weeks

to months, snow intercepted in forest canopies lasts only from hours to tens of days. If canopy snow storage is ephemeral, then the daily assimilation period is too infrequent to obtain useful information (c.f., Figures 4-10 a, b, and d). Therefore, higher assimilation frequencies at sub-daily or even hourly rates are preferable for canopy intercepted snow data assimilation.

Due to canopy snow interception processes, the data assimilation result sometimes may not be desirable even if one assimilated a reliable interception measurement. Compared to snow on the ground, canopy intercepted snow quantities are small and coverage is transitory, persisting for a shorter time and making it very sensitive to meteorological conditions. In modelling deep surface snowpacks, a minor error in the forcing data such as temperature and humidity, usually does not alter results significantly. However, canopy snow interception storage is usually less than 10 mm. Thus, forcing data errors can significantly influence simulation results, reducing the benefits of data assimilation. For example, in the simulation in depicted in Figure 4-10c, even the canopy snow interception was rapidly updated in the DA_Tree experiment. But the canopy snow quickly disappeared after assimilations in both days. Figure 4-12 shows an extreme example of how error in the forcing data can jeopardize assimilation results. This figure shows a comparison of canopy snow interception in the ObsMet simulation that is forced by observed meteorological data, to an open loop simulation forced by GEM data; the DA_Tree simulation forced by GEM data, and weighed tree measurements. According to the weighed tree measurements, intercepted snow covered the canopy continuously from January 1st to 17th 2017 and the removal of canopy snow was trivial until January 16th. The open loop simulation frequently underestimated canopy snow interception and its simulated interception was not continuous. After assimilation, the DA_Tree simulated interception agreed well with observations at the beginning of each day. However, the model constantly removed the canopy snow by unloading and sublimation after the daily assimilation time until the next assimilation. The ObsMet simulation captured unloading timing well with little error in the interception magnitude. The daily amount of released canopy snow through sublimation and unloading was compared between ObsMet and DA_Tree. The error in GEM forcing data caused a constantly higher ablation rate, mostly due to sublimation, in DA_Tree. This indicates that although data assimilation can improve interception simulations during the assimilation time, or shortly afterwards, this improvement would be short-lived if the model is run using poor quality forcing data.

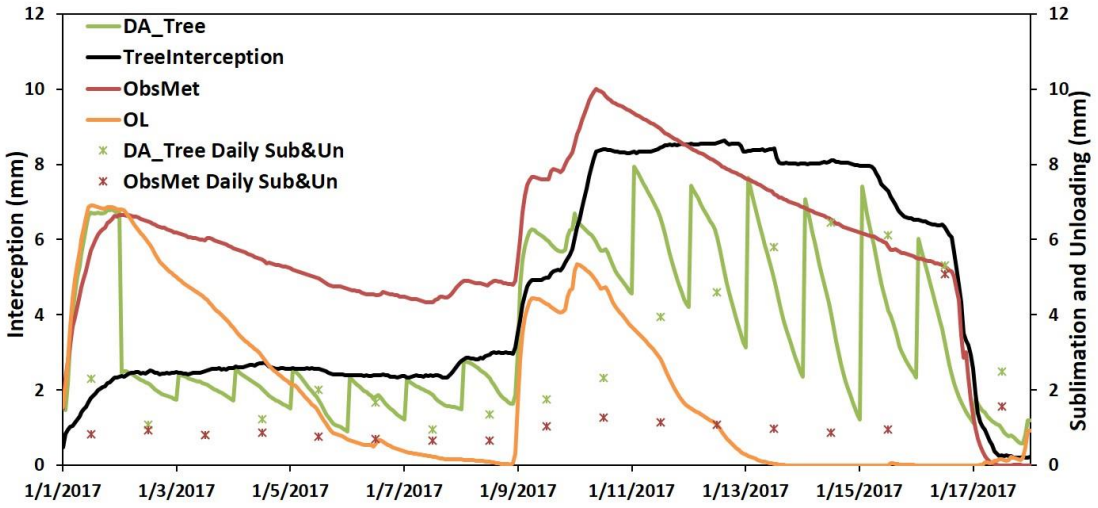

Figure 4-12. Comparison of ObsMet (observation driven), OL (GEM driven), and DA_Tree (GEM driven) simulated canopy interception to weighed tree measured snow interception (unit: mm). Stars show the accumulated daily unloading and canopy snow sublimation from DA_Tree and ObsMet simulation (unit: mm).

4.7 Conclusions

Automatically measured snow depth data from an adjacent needleleaf forest and clearing were analyzed to quantify losses due to forest canopy snow interception. Peak snow depth in the forest was 45.8% lower than in the clearing on average. During snowfall events, snow accumulation (peak SWE) under the forest canopy was approximately 47.6% less than that in the clearing. Three fresh snow density estimation methods were tested with results indicating that the Hedstrom-Pomeroy equation using air temperature to calculate fresh snow density worked best. Combining measured snow depth data with calculated fresh snow density, snow interception was determined for each snow event. Calculated snow interception using this technique was validated using measurements from a weighed, suspended tree with results indicating that model predictions agreed well with observations. This indicated that automatically measured snow depths from adjacent forests and clearings are suitable for estimating snow interception in the forest canopy. The calculated snow interception, along with weighed tree and time-lapse camera measured snow interception information, were assimilated into the Cold Regions Hydrological Model, driven by GEM atmospheric model outputs, using the EnKF or rule-based direct insertion approaches. The results were compared to the CRHM model driven by locally observed meteorological data. Although the simulations after DA were not as accurate as models driven by locally observed meteorology, they all improved the simulation accuracy of snow interception amount and timing. Snow interception data assimilation is greatly influenced by the assimilation frequency and quality of forcing data. Daily assimilation frequency can achieve accurate results, but sub-daily or hourly frequency is more suitable for intercepted snow data assimilation.

CHAPTER 5: Assimilation of ground observed SWE and snow depth data into a Cold Regions Hydrological Model

Status: submitted to Water Resources Research on May 16, 2019

Citation: Lv, Z., and Pomeroy, J.W., 2019. The influence of snow data assimilation on the performance of a coupled numerical weather forecast and physically based cold regions hydrological model. Water Resources Research. in review.

Author Contributions: Zhibang Lv conceptualized this research, designed and performed simulations, conducted analysis, and wrote the manuscript. John Pomeroy provided data, helped with the idea formulation and interpretation of results and provided useful comments with regards to the content, structure and writing of the manuscript.

5.1 Preface

As assimilation of snow interception observations benefited the simulation of intercepted snow on the canopy, the next step is to extend the benefit of data assimilation to basin snowpack and basin streamflow simulations. Accurate snowpack and streamflow estimation in snow dominated regions are crucial for local water management. Data assimilation (DA) can be used to improve simulations by merging uncertainty in model forcing data and observed snowpack information. The potential influence of DA on multilayer, physically based models that contain a full suite of snow redistribution and ablation processes still needed to be explored. The goal of this research is to: 1) determine the optimal method to assimilate in situ measures into CRHM, 2) evaluate how well assimilation of point and transect snow observations improves of basin snowpack prediction, and 3) assess the contribution of transect based SWE assimilation to reducing uncertainty in streamflow simulations.

5.2 Introduction

Snow is a crucial, seasonal component of the land surface in cold regions. It influences land surface energy balance with low thermal conductivity, high albedo, long duration and wide spatial distribution. It also contributes considerably to local, seasonal stream runoff (Moradkhani, 2008; Rodell and Houser, 2004). Snowmelt runoff provide an essential summer water supply for agriculture, industry, and domestic use over a large portion of the Earth's surface (Barnett et al., 2008). Due to the sensitivity of snow to temperature, the time and magnitude of snowcover and snowmelt runoff have faced or will face great changes with climate change (Bavay et al., 2009; Horton et al., 2006; Krogh and Pomeroy, 2018; Stewart, 2005; Musselman et al., 2017; Rasouli et al., 2014; Rasouli et al., 2015). This will become a major concern of the future global water security.

Accurate estimation of snow properties (e.g., SWE, depth, density, and distribution) has great weight in determining water and energy budgets in cold regions (Sheffield et al., 2003). Manual or automatic monitoring of the state of the snowpack can provide accurate data, but can be costly. As a result, it is usually not available apart from point observations or specialized airborne LiDAR campaigns over river basins that supply water to high populations (Painter et al., 2016). Modelling is an alternative tool to monitor hydrology as it can be used to estimate past, present, and future snow properties and stream flow at multiple spatial scales. However, simulation accuracy is greatly affected by model structure, meteorological forcing data, and parameterization. Indeed, one of the dominant challenges in snow hydrological modeling is the accuracy and scale of the forcing meteorological data. Observed forcing data from weather stations has relatively high accuracy. But stations are sparse even in some of the most heavily monitored locations, necessitating upscaling. Although the output of climate models show continuous cover over a wide geographic range, they have relatively low accuracy and are often of lower spatial resolution than the hydrological models they run.

Data assimilation (DA) can have great utility to hydrological management as it combines the advantages of snow property observation (relatively higher accuracy) with modelling (consistent at spatial and temporal scales). Hence, it offers optimal snow properties and streamflow estimation (Clark et al., 2006; Liston and Hiemstra, 2007; Liu et al., 2012). Several DA methods have been used to assimilate information both *in situ* observations and remotely sensed data, such as snowcover fraction (Andreadis and Lettenmaier, 2006; Clark et al., 2006; De Lannoy et al., 2012; Liu et al. 2013; Rodell and Houser 2004; Slater and Clark 2006; Stigter et al., 2017), snow depth (Hedrick et al., 2018; Kumar et al., 2014; Kumar et al., 2017; Liu et al. 2013; Magnusson et al., 2017; Stigter et al., 2017), and SWE (Andreadis and Lettenmaier, 2006; Bergeron et al., 2016; Franz et al., 2014; Huang et al., 2017; Liston and Hiemstra, 2007), into the

hydrological models. Assumptions differ amongst DA methods in how they treat the error covariance of observations and model simulations. The direct insertion method assumes that snow observations are perfect while model simulations contain errors so that whenever there is an observation, the simulated model state variable is replaced by the observation directly (Hedrick et al., 2018; Liston et al., 1999; Rodell et al., 2004). The direct insertion method is time saving and easy to implement, however, its assumption of error-free observations is far from reality much of the time. Therefore, other data assimilation approaches that have adopted improved, sophisticated algorithms to determine model and observational uncertainty are being used by many cold regions hydrologists.

Traditional Kalman filters update model state variables when an observation is shown by explicit computation of error covariances (using additional matrix equations) error propagation information from one-time step to the next (Reichle, 2008). This method performs well when model and observational error both follow Gaussian distributions. But the model needs to be linear. The nonlinear version of the Kalman filter is the extended Kalman filter (EKF), which can be used in nonlinear models. However, EKF cannot be used in large study areas because its error covariance integration requires huge computational capacity (Reichle et al. 2002). An alternative method is the ensemble Kalman filter (EnKF, Evenson, 1994; 2003) that has been shown to improve performance. It avoids the complex integration of the state error covariance matrix by propagating an ensemble of states with a Monte Carlo approach from which the required covariance information is obtained at the time of the update (Reichle et al. 2002). In addition, EnKF is easier to implement than other, more sophisticated assimilation methods such as four-dimensional variational data assimilation (4DVAR). This makes the EnKF the most popular assimilation method in cold regions hydrological community.

Many snow DA studies have been conducted with the simpler models (Bergeron et al., 2016; Franz et al., 2014; Slater and Clark, 2006; Stigter et al, 2017). Indeed, the potential influence of DA on multilayer physical models still needed to be researched (Magnusson, et al., 2017). The snow melt runoff from the Canadian Rockies forms headwaters for few major rivers that provides essential water supply for large portion of western Canada. However, due to the complex topography and large geographic cover, the sparse terrestrial weather monitoring system cannot provide accurate critical forcing data for hydrological modelling in this region. The results from weather prediction models become the only choice to force hydrological model at most of the location and time. However, due to the questionable accuracy of these weather prediction model results, data assimilation become critical to hydrological modelling for achieving the reasonable snowpacks and streamflow simulations. This research studied a mountain headwaters basin in the Canadian Rockies with abundant surface observations, ground manual observed SWE from once or twice monthly snow surveys and daily snow depth (d_s) observations from sonic ranging sensors. These were

assimilated into the physically based, process-hydrology Cold Regions Hydrological Modelling platform (CRHM) by using EnKF to assess the influence of DA on basin snowpack properties and streamflow simulation. CRHM includes a full suite of snow redistribution by wind and vegetation, sublimation, energy balance snowmelt and complex terrain downscaling algorithms along with most other hydrological processes and so provides a unique opportunity to explore assimilation into a comprehensive simulation of the mountain hydrological cycle. The specific objectives of research were to determine the optimal method to assimilate *in situ* measures into CRHM, evaluate how well assimilation of point and transect snow observations improves of basin snowpack prediction and evaluate the contribution of transect based SWE assimilation to reducing uncertainty in streamflow simulations.

5.3 Study area, data, and model

5.3.1 Marmot Creek Research Basin (MCRB)

MCRB (50°57`N, 115°09`W) is located in the Front Ranges of the Canadian Rockies, Alberta, Canada (Figure 5-1). It has an area of approximately 9.4 km^2 and elevation range from 1450 m to 2825 m. It includes three upper sub-basins: Cabin Creek, Middle Creek, and Twin Creek as well as a lower confluence sub-basin. The main landcovers are dense coniferous lodgepole pine in the lower elevations, deciduous alpine larch, shrubs, grasses, needleleaf Engelmann spruce, and sub-alpine fir in the middle upper elevations; talus and bare rocks occupy in the high alpine region (DeBeer and Pomeroy, 2009). The basin has had both large clearcuts and small forest clearings in the coniferous forest zone from forest management in the 1970s and 1980s (Ellis et al., 2013; Rotherwell et al., 2016). There are substantial snow interception losses from coniferous forests (Ellis et al., 2010) and wind redistribution of snow from alpine ridges and windward slopes to sheltered slopes and treeline forests (MacDonald et al., 2010). The annual precipitation in MCRB has an average value of 900 mm, and increases with elevation reaching 1140 mm at the areas above treeline. Snow is the dominant precipitation type, accounting for approximately 60–75% of annual precipitation (DeBeer and Pomeroy, 2009). Snow usually accumulates from November to March and starts to melt in later April or early May.

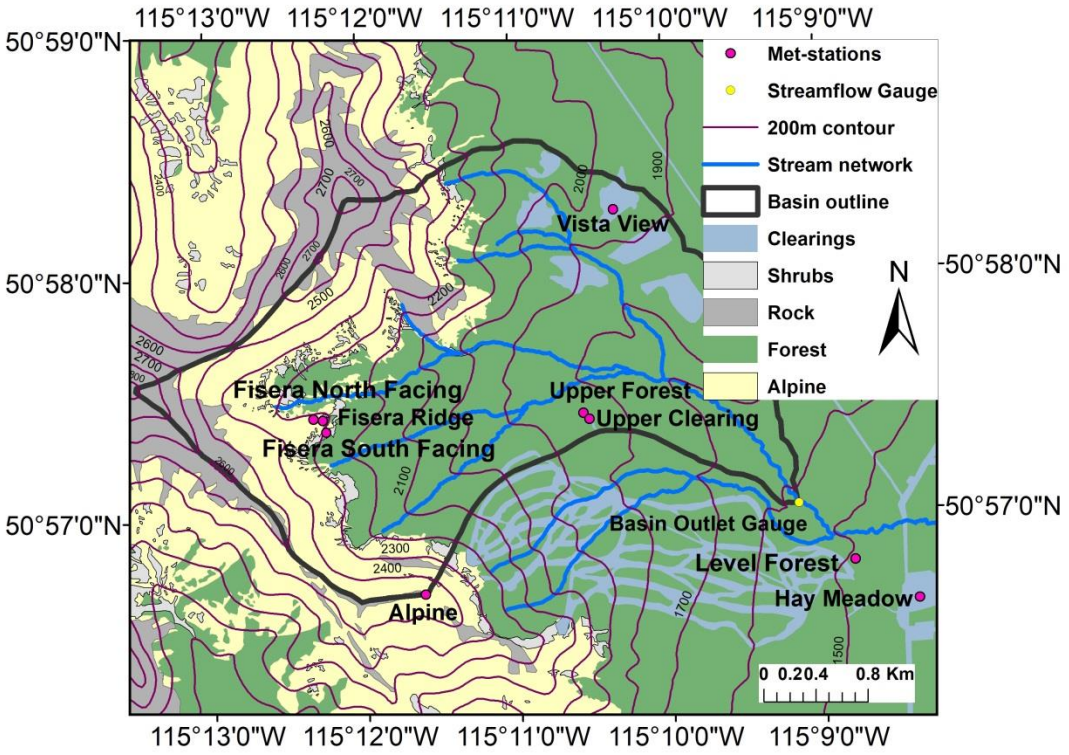

Figure 5-1. Landscape condition and local observation stations at the Marmot Creek Research Basin, Alberta, Canada.

5.3.2 Observations

Seven permanent hydrometeorological stations were located to observe in various elevation bands and landscapes (Figure 5-1) in MCRB beginning in 2005. These stations are Hay Meadow (HM), Vista View (VV), Level Forest (LF), Upper Forest (UF), Upper Clearing (UC), Alpine (Al) and Fisera Ridge (FR) and continuously collect short-wave and long-wave radiation, air temperature, soil temperature, relative humidity, and wind speed. Precipitation is measured with an Alter-shielded Geonor weighing precipitation gauge at the HM, UC, and FR stations and is corrected for wind-induced undercatch (Smith, 2009). Five Campbell SR50 sensors were mounted at sites UC (June 2005 – Present), UF (June 2005 – Present), Fisera Ridge Top (FRRT, June 2005 – Present), Fisera Ridge South Facing (FRSF, November 2008 – September 2014), and Fisera Ridge North Facing (FRNF, November 2008 – September 2014) to measure snow depth at 15 minute intervals. UC and UF are located in the mixed forests of Spruce, Fir and Pine with elevation around 1845 m and snow interception in the forest canopy controls the snow accumulation at UF. UC station located in the middle of a 50 m diameter clearcut surrounded by the forest, UF station is in a forest approximately 20 m from the UC clearing edge. Fisera Ridge is in the open alpine tundra at 2323 m elevation. Wind redistribution controls the local snow patterns. Snow usually blows from a source area on the north-facing slope, across the ridgetop to a sink area on the south-facing slope over the snow season. MCRB basin seasonal (1 May – 31 October)

daily mean streamflow data was collected by a long-term streamflow gauge (05BF016) at the basin outlet operated by the Water Survey of Canada (Environment and Climate Change Canada). Snow surveys have been conducted monthly or semi-monthly at the UC, UF, VV, FR, LF, and HM sites through the winter and spring of each year since 2007. The survey follows designated transects near the meteorological stations with at least 25 snow depth measurements and snow densities measured every fifth depth measurement using a ESC30 gravimetric snow tube and weighing scale. In addition to locally observed meteorological data, the Environment and Climate Change Canada Global Environmental Multiscale (GEM) model 2.5 km grid product from November 2014 to August 2017 were also used to run the CRHM model for DA experiments. Four grids of GEM data needed to cover the whole MCRB basin and GEM outputs were air temperature, relative humidity, wind speed, incoming short-wave radiation, incoming long-wave radiation, and precipitation. To downscale the 2.5 km GEM data to Hydrological Response Units (HRU, which is the basic simulation unit in CRHM) scale, precipitation and air temperature for each HRU were adjusted based on the elevation and observed elevation lapse rate for precipitation and air temperature in MCRB. The rest of the forcing variables of each HRU was assigned to the closest GEM grid cell's values.

5.3.3 SR50 data processing

SR50 snow depth raw data contains errors and noise need to be removed before using. Because air temperature influences the speed of sound, temperature corrections were applied to the SR50 sensor reading according the following formula (Equation 5.1, Campbell Scientific, 2009):

$$S_c = S_r\sqrt{\frac{T_a}{273.15}} \tag{5.1}$$

where S_c is the compensated snow depth, S_r is the raw sensor reading, and the T_a is air temperature in K. To reduce or smooth noise, a three-hour moving average was applied to the compensated snow depth data (Ryan et al., 2008).

The final, fixed-point snow depth measurement cannot be directly used to estimate snow depth over a large area because the areal average depth is prone to heterogeneity in accumulation, redistribution, and ablation caused by topography, vegetation, and wind (Pomeroy and Gray, 1995). However, repeating patterns in snow redistribution and ablation as governed by vegetation and topography mean that locally calibrated empirical formula can be used for upscaling over small areas. For example, Neumann et al. (2006) found the in each site of their Canadian boreal forest study area, the fixed-point automatic snow depth measurement consistently over- or under-estimated the landscape mean. As a result, a simple "scaling equation" can be developed for each site to improve the local spatial representation of the fixed-point automatic snow depth

measures. In the present research, the mean snow depth value from snow surveys conducted around each SR50 sensor was used to both build the "scaling equation" and adjust the SR50 data to a large scale. The details of this calculation are shown in Section 5.5.1.

5.3.4 CRHM

The CHRM platform is a system to assemble hydrological models developed for Canadian and other cold and temperate environments. It can create spatially distributed physically based hydrological models that use the concept of internally uniform HRU to discretize the basin as the basis for application of energy and mass balances and flux calculations. HRUs are conceptual landscape groups that are subdivisions of the basin based on the elevation, slope, aspect, vegetation cover, soils and other hydrological or biophysical characteristics. Each HRU has a unique set of parameters that govern hydrological process calculations. CRHM has various modules to simulate the snow and hydrological processes of each HRU. Users can construct their own model by selecting modules from the CRHM library, with selection based on input data availability, research scale and the predictive variable of interest. These modules can be used to interpolate meteorological data over complex terrain and to simulate rainfall and snowfall interception, wind redistribution, sublimation, albedo decay, canopy transmittance, snow energy and mass balance, evapotranspiration, melt, snowcover depletion, infiltration, detention, depressional storage, soil moisture, flow and storage of surface and subsurface water, and streamflow routing. The full description of CRHM is provided by Pomeroy et al. (2007). Updates and details on the modules used, model setup and parameterization of this research are described in several recent publications (Fang et al., 2013; Fang and Pomeroy, 2016; Pomeroy et al., 2016b). Here, the Snobal module (Marks et al., 1998) was used to simulate the mass and energy balance of snowpack. It divides the snowpack into two layers (active and lower) if snowpack depth higher than 10 cm. The active layer has the fixed thickness of 10 cm and the lower layer depth equals the snowpack depth minus active layer depth. The two layers share the same snowpack density but have different temperatures.

5.4 Methodology

5.4.1 Ensemble Kalman Filter

In this research, EnKF was used as assimilation method following previous, successful examples (Franz et al., 2014; He et al., 2012; Kumar et al., 2009). EnKF is a sequential assimilation approach that updates model state variable(s) when an observation is available based the Kalman gain (K, Equation 5.2) that is determined by the error covariance of ensemble model simulation and observation (Equation 5.3).

$$x_{i,j}^{u} = x_{i,j}^{s} + K_i(y_{i,j} - H_i x_{i,j}^{s}) \quad (5.2)$$

where $x_{i,j}$ and $y_{i,j}$ denote the jth (j=1, 2, …, N, N is ensemble size) ensemble model state and observation vectors at time step i (i =1, 2, …, M, M is number of observations); superscripts u and s represent the updated and simulated model state vector; H_i is the operator that relates the model vector to the observed vector and it is a unit factor in this research. The Kalman gain K_i in i^{th} time step is calculated by:

$$K_i = P_i^s/(H_i P_i^s + R_i) \quad (5.3)$$

where P_i^s is the model forecast error covariance and R_i is the observation error covariance at time step i. Model forecast error covariance is calculated from the ensemble model simulation covariance. Observation error covariance is derived by perturbation of observations with a presumed standard deviation.

5.4.2 Application of EnKF to CRHM

In this study, model simulation uncertainty is assumed to be mainly caused by the uncertainty of forcing data (Huang et al., 2017). As a result ensemble model simulations were run by Monte Carlo perturbation of the driving forces following the suggestions of early studies (Kumar et al., 2014; Liu et al., 2013; Reichle et al., 2002). For incoming shortwave radiation and precipitation, the multiplicative perturbation with a mean value of 1 was conducted to avoid unreasonable outcomes such as positive incoming short-wave radiation at night or negative precipitation. Additive perturbation with a mean value of zero was run on other driving forces (Table 5-1). For model state variables, multiplicative perturbations were conducted, and a 0.05 standard deviation was set for all three variables as indicated by measurement instrument error. Further, because these forcing variables are usually related to each other, such as precipitation often resulting in low incoming short-wave radiation. This is also true for the snowpack state variables, such as higher SWE usually lead to higher d_s. Therefore, a cross correlations were imposed to all variables except wind speed (Riechle et al., 2007; De Lannoy et al., 2012) (Table 5-1). In EnKF, model simulation error covariance is represented by that of ensemble members. Theoretically, an infinite number of ensembles could perfectly represent the real model error covariance. However, more ensemble members lead to more computational cost. Therefore, an ensemble number of twenty was chosen according to the previous research (Kumar et al., 2009; Kumar et al., 2014) and the authors' experience.

Table 5-1. Model driving and state variables with their perturbation parameters.

Variables	Perturbation Type	Standard deviation	Cross correlations with Perturbations					
Forcing variables			AT	RH	u	SW	LW	P
Air temperature (AT)	Additive	5 (C°)	1	-0.3	-	0.3	0.6	-0.1
Relative humidity (RH)	Additive	10	-0.3	1	-	-0.8	0.5	0.8
Wind spread (u)	Additive	2 (m/s)	-	-	1	-	-	-
Incoming short-wave radiation (SW)	Multiplicative	0.3	0.3	-0.8	-	1	-0.3	-0.5
Incoming long-wave radiation (LW)	Additive	50 (W/m^2)	0.6	0.5	-	-0.3	1	0.5
Precipitation (P)	Multiplicative	0.5	-0.1	0.8	-	-0.5	0.5	1
CRHM state variables			SWE	d_s	ρ			
SWE	Multiplicative	0.05	1	0.9	0.9			
Snow depth (d_s)	Multiplicative	0.05	0.9	1	0.9			
Snowpack density (ρ)	Multiplicative	0.05	0.9	0.9	1			

Although CRHM can be run hourly, it can only export and read the state file just after midnight of each day. Therefore, the minimum assimilation frequency for CRHM is limited to daily frequency. When an observation is available, model runs will stop at 1 a.m. of that day and a state file will be exported and updated. Then the updated state file will reset to initial conditions for the next time step model running. To maintain water balance in the model, during the state file updating process, 15 state variables may have to be updated in addition to the assimilated state vectors (e.g., SWE and snow depth). These state variables are: snowcover presence, average snowpack density, snow depth, SWE, snowpack layer count, active layer snow depth, lower layer snow depth, active layer specific mass, lower layer specific mass, snowpack temperature, active layer temperature, lower layer temperature, snowpack cold content, active layer cold content, lower layer cold content. There are issues with how Snobal handles snowpack temperature, active layer temperature, and lower layer temperature variables for shallow and ephemeral snowpacks. Snobal sets the temperature of a snowpack layer that has no snow to −74.99 °C. If a snowpack grows such that the layer SWE is updated from zero during the run, but the snowpack layer temperature(s) are not adjusted, then the snowpack temperature will stay extremely low and the snowpack can have an unreasonable cold content. This degrades the model simulation of subsequent melt and results in the modelled snowpack accumulating more snow than in reality. This feature of Snobal has implications for and introduces challenges for data assimilation.

Taking assimilation of SWE alone as an example, Figure 5-2 shows the details of how these 15 state variables were updated. SWE was updated to the calculated SWE_a (SWE after update, subscript a means the state variable was after update) from EnKF (Equation 5.2). If SWE_a was equal to 0, then the rest of the 14 variables were set to 0 or -74.99 °C (three temperature variables). If SWE_a was greater than 0, the rest of 14 variables were updated according to the rules showing in Figure 5-2.

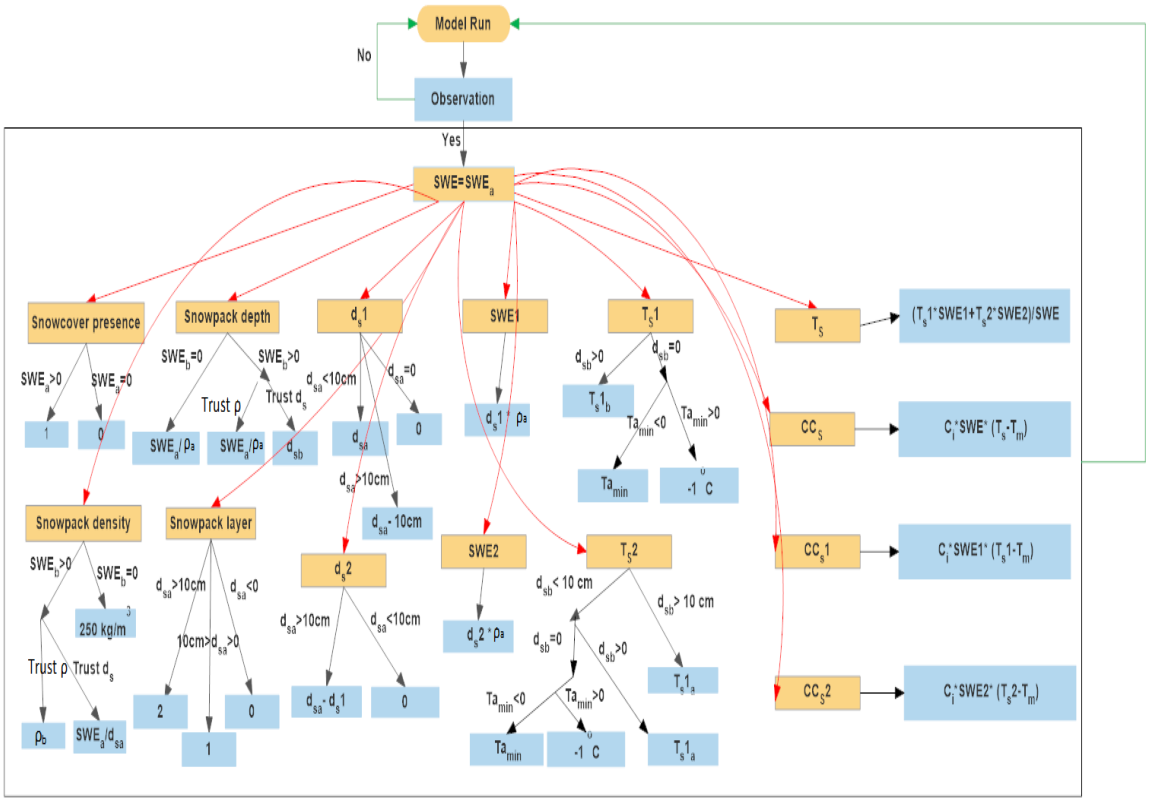

Figure 5-2. Rules for updating the state variables in CRHM during data assimilation. SWE is the whole snowpack snow water equivalent. Subscript a means the state variable value that after update. Subscript b denotes the state variable value that before update. d_s is the whole snowpack depth. d_s1 is the active layer snowpack depth, d_s2 is the lower layer snowpack depth. ρ is the snowpack density. SWE1 is the active layer specific mass. SWE2 is the lower layer specific mass. T_s is the snowpack temperature. T_s1 is the active layer temperature. T_s2 is the lower layer temperature. CCs is the snowpack cold content. CCs1 is the active layer cold content. CCs2 is the lower layter cold content. Ta_{min} is the lowest air temperature of the previous day. C_i is the specific heat of ice (2102 J /kg*°C). T_m is the melting temperature of snow (0 °C).

5.4.3 Experiment design

5.4.3.1 SWE and snow depth assimilation influence on snow pack properties

To evaluate the influence of SWE and d_s assimilation on primary snowpack properties and find the optimal DA scheme, several DA experiments were conducted by assimilating d_s and SWE separately, together, or with historical snowpack density (Figure 5-3). For assimilation of d_s alone, there were two experiments conducted based on the methods updating SWE and snowpack density. To balance the relationship between d_s, SWE and snowpack density (Equation 5.4), one has to update one or both of SWE and snowpack density while updating d_s.

$$SWE = d_s \times \rho \quad (5.4)$$

where SWE is in mm when d_s is in m and snowpack density ρ is in kg/m^3.

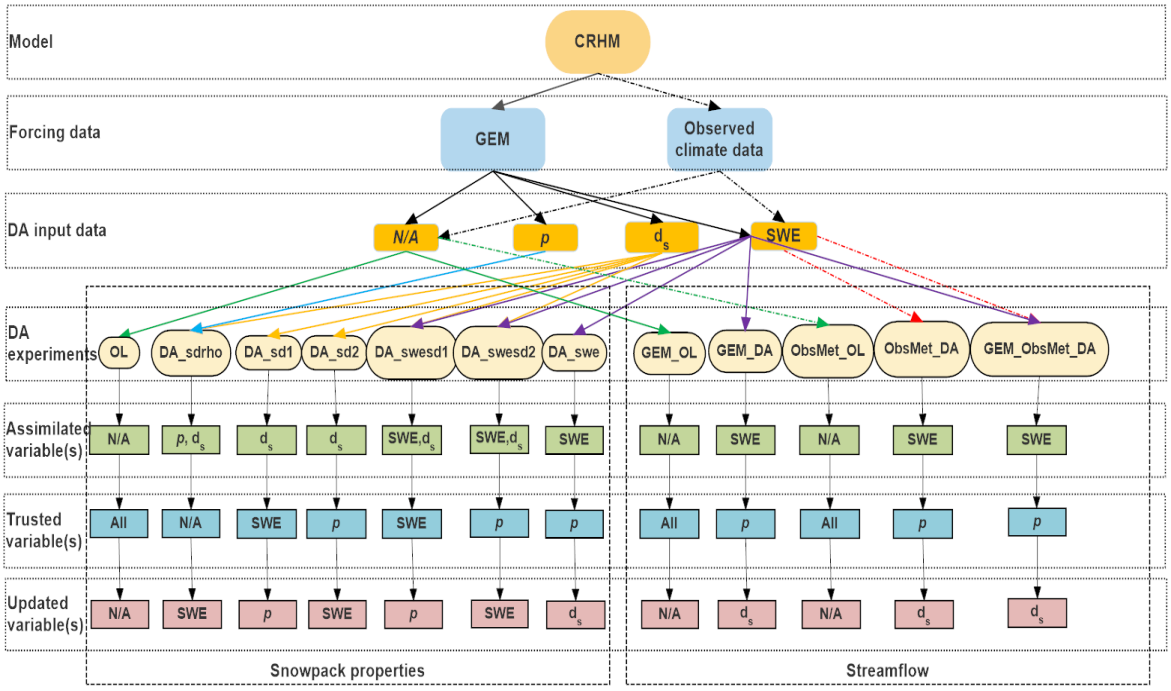

Figure 5-3. Forcing data, input data, and variable (s) that assimilated, trusted, and updated for different DA experiments.

In experiment a), d_s was assimilated alone and the model simulated SWE was trusted so that the snow density was updated according to model simulated SWE and updated d_s was updated based on Equation 5.4. In this experiment, SWE was updated only if simulated SWE equaled zero but updated d_s was non-zero. Under this condition, the snowpack density was assumed as 200 kg/m^3 and the SWE was updated accordingly. This DA experiment will be referred to as DA_sd1.

In experiment b), d_s was assimilated alone and modelled snowpack density was trusted so that SWE was updated according to model simulated snowpack density and updated d_s. If simulated snowpack density equals zero but not the updated d_s, the snowpack density was adjusted to 200 kg/m^3. This DA experiment will be referred to as DA_sd2.

In experiment c), d_s and historical snowpack density were assimilated together into the model. Therefore, SWE was updated according to the updated d_s and snow density. In this experiment, the updated d_s has the highest confidence, which means if updated d_s and snow density did not agree with each other on the matter of snow presence in the HRU, snow density was adjusted according to d_s value. In other words, if updated

snowpack density equals zero but not the updated d_s, snowpack density was adjusted to 200 kg/m^3. However, if updated d_s equal zero but not the updated snowpack density, snow pack density was adjusted to zero. This DA experiment will be referred to as DA_sdrho.

In experiment d), SWE was assimilated into the model alone when SWE observations were available. d_s was simultaneously updated by using the simulated snowpack density and updated SWE. This DA experiment will be referred to as DA_swe.

In experiment e) and f), SWE and d_s were assimilated together. Because SWE and d_s data had different data frequency (once or twice a month vs. daily), the model was run hourly, d_s was updated daily while SWE was updated whenever the observation was available. When SWE and d_s were both assimilated in the same day, snowpack density was updated based on the updated SWE and d_s. However, there were few d_s values assimilated alone between two consecutive SWE assimilations. Hence, the confidence level problem of SWE and snowpack density arose again in this situation. In experiment e), when d_s assimilated alone, model simulated SWE had higher confidence so that the snowpack density was updated based on the simulated SWE and updated d_s. This DA experiment will be referred to as DA_swesd1.

In experiment f), in contrast to DA_swesd1, model simulated snowpack density had higher confidence so that the SWE was updated based on simulated snowpack density and updated d_s when assimilating d_s alone. This DA experiment will be referred to as DA_swesd2.

Experiment g) is a simulation forced by 20 forced ensembles perturbed from GEM data without any data assimilation. This open loop (OL) simulation was used as a control to determine the improvement of other experiments on snowpack properties and simulation accuracy. This DA experiment will be referred to as OL.

All the DA experiments forced by GEM data started from November 13, 2014 and ended on August 31, 2017. A CRHM model forced by local observations was run from October 1, 2005 to November 12, 2014 to generate a state file. The data from this state file were used as the initial conditions to start the model run of DA experiments.

The influence of SWE and ds assimilation on snow pack properties was evaluated at the Upper Forest and Fisera Ridge sites because of data availability and the fact that these sites can represent the majority topography and snow redistribution and ablation processes in MCRB. Assimilation in Upper Forest and Upper Clearing sites was forced by the GEM data from November 2014 to August 2017. At Fisera Ridge, however, because the SR50 data were not available in north facing and south facing slopes after August 2014, the assimilation was run by local observed meteorological data from November 2008 to August 2014.

5.4.3.2 SWE assimilation influence on streamflow simulation

To evaluate the influence of SWE assimilation on streamflow simulation, experiments were conducted to assimilate SWE with different schemes (Figure 5-3). The snow survey SWE from 10 sites in MCRB were interpolated to 36 HRUs over the whole basin based on linear regressions between SWE and elevation, slope, aspect, vegetation cover (LAI), wind index. These linear relationships were built daily as the snow accumulation and ablation are highly influenced by time of year. These interpolated SWE were then assimilated into CRHM. Assimilations were forced by GEM data and local *in situ* forcing data either separately or combined. This was aimed to evaluate the importance sensitivity of streamflow simulation to forcing data and SWE assimilation. Kumar et al. (2017) indicated that when using two or more sets of forcing data in one data assimilation experiment, the EnKF method led to better simulation results in assimilated state variables than using a single forcing data resource. In this case, two sets of forcing data would led to a better simulation of SWE, which was assimilated into the model using EnKF. Therefore, an assimilation driven by combined forcing data was conducted to evaluate if better SWE assimilation can improve streamflow simulation.

In experiment h), the model was run by 20 forced ensembles perturbed from GEM data without data assimilation. This DA experiment will be referred to as GEM_OL.

In experiment i), SWE were assimilated into the model run by 20 forced ensembles perturbed from GEM data. This DA experiment will be referred to as GEM_DA.

In experiment j), the model was run by 20 forced ensembles perturbed from local observed forcing data without data assimilation. This DA experiment will be referred to as ObsMet_OL.

In experiment k), SWE were assimilated into the model with 20 ensemble simulations forced by perturbation from local observed forcing data. This DA experiment will be referred to as ObsMet_DA.

In experiment l), SWE were assimilated into the model with 20 ensemble simulations forced by combined perturbation from GEM and local observed forcing data. There were 10 ensembles by perturbation of GEM forcing data while the remaining 10 ensembles were forced by the perturbation of local observed forcing data. This DA experiment will be referred to as GEM_ObsMet_DA.

5.4.4 Evaluation of DA experiments results

Evaluation of DA research sometimes can be difficult as some researchers assimilate all of the observations into the model, leaving no observations for validation (Clow et

al. 2012). In the present study, snow surveys are the only reliable data source for SWE and are already assimilated into some of the DA experiments. Due to lack of other independent SWE observations, snow survey SWE data were used to evaluate SWE simulations from all DA experiments. However, in the SWE-involved DA experiments, such as DA_swe, DA_swesd1, and DA_swesd2, two SWE measures were randomly excluded from assimilation in each year as an independent validation data. This independent validation was aimed to assess the effect of these DAs in SWE simulation in the interval between two assimilation time steps. Because only d_s measures from SR50 were assimilated into the model, the d_s measures from snow surveys were reliable independent data for assessing the impact of various DAs on d_s accuracy. In this study, snowpack density was not directly assimilated into the model but included as historical snowpack density (DA_sdrho) or updated by the assimilated SWE and d_s (DA_swesd1 and DA_swesd2), so snowpack density from snow surveys was a reliable, independent data source for snowpack density evaluation for all DA. However, in DA_swesd1 and DA_swesd2, both SWE and d_s were assimilated at the time when both data sets were available. This resulted in snowpack density also being indirectly assimilated. Therefore, another independent validation for snowpack density was conducted in these two DAs using the excluded data to assess their ability to simulate snowpack density between assimilation time steps.

The results of designed experiments were evaluated though several metrics. Root mean square error (RMSE, Equation 5.5) was used to evaluate the difference between simulated and observed variables. Normalized root mean square error (NRMSE, Equation 5.6) is RMSE divided by mean of observation data. Model Bias (MB, Equation 5.7) was used to assess the ability of the experiment to reproduce the measured variables. A positive MB means the simulation overestimates observations while a negative MB means underestimation. Nash-Sutcliffe efficiency (NSE, Equation 5.8) was used to test the consistency between simulation and observation across time scales. The closer the NSE is to 1, the more accurate the simulation is, with 1 being a perfect match.

$$RMSE = \sqrt{\frac{\sum_{i=1}^{n}(Xo_i - Xs_i)^2}{n}} \tag{5.5}$$

$$NRMSE = \frac{RMSE}{\overline{X_o}} \tag{5.6}$$

$$MB = \frac{\sum Xs}{\sum Xo} - 1 \tag{5.7}$$

$$NSE = 1 - \frac{\sum(X_o - X_s)^2}{\sum(X_o - \overline{X_o})^2} \tag{5.8}$$

where Xs and Xo are values of simulated and observed variables, respectively, $\overline{\text{Xo}}$ is the average of observed variables. In this present research RMSE and MB were used to evaluate the main snow pack properties (e.g. SWE, d_s, Snowpack density) whilst

streamflow was assessed by RMSE, MB, and NSE.

5.5 Results

5.5.1 Spatial representation of SR50 point snow depth measures

To evaluate the spatial variation of snow depth in MCRB snow survey sites, the standard deviation (SD) and coefficient of variation (CV) were calculated for every snow survey at each site. Figure 5-4 shows the SD and CV of areal snow depth from each snow survey for five MCRB sites from November 2007 to June 2018. In the blowing snow transport-dominated Fisera Ridge sites, snow depth SD usually increases initially as snow accumulates and then decreases when snow ablation begins. However, in the sites where wind plays a minor role (UC and UF), SD values increase consistently as the snow season progresses. Amongst the three FR sites, FRSF has the highest SD value as the site with the highest annual snow accumulation. Amongst all five sites, UC has the lowest SD as wind and vegetation have minimal influence on snow accumulation, redistribution, and ablation. Although UF has low annual snow accumulation, it has higher SD than UC because canopy interception exacerbates spatial variation as found by Faria et al. (2000) in the boreal forest. The CV of all five sites show the same pattern, decreasing with snow accumulation, peaking before ablation begins, then decreasing as the snowpack melts. In the forest sites, the clearing – UC (CV=0.25) has a lower areal snow depth variation than the forested area – UF (CV=0.62). In open sites, the blowing snow sink area – FRSF (CV=0.45) has the much lower snow depth variation than the source area – FRNF (CV=0.82) and FRRT (CV=0.8).

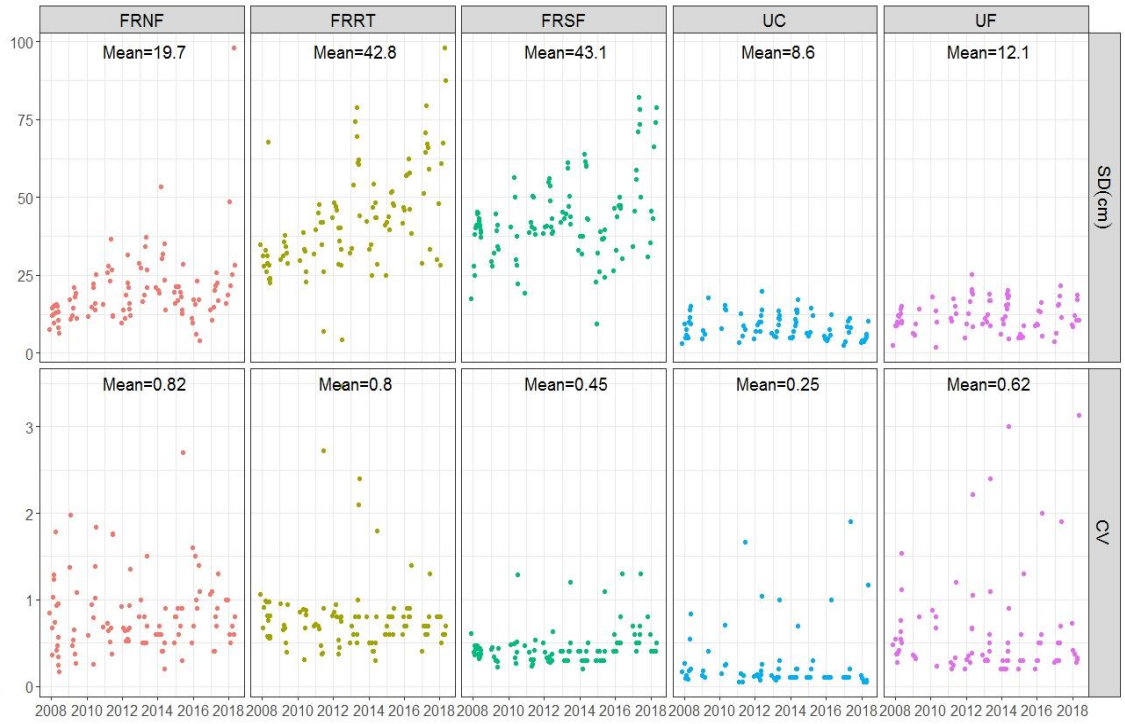

Figure 5-4. Aerial snow depth standard deviation (SD) and coefficient of variation (CV) from snow survey data at five sites at the Marmot Creek Research Basin, Alberta, Canada.

The ability to represent the areal mean snow depth of SR50 varies amongst the five sites (Figure 5-5). In sites that have relatively low snow depth variation – FRSF and UC, the SR50 measurement agreed well with the snow survey mean value. The best fit lines of both sites were close to the 1:1 ratio line as the slopes of the linear regression equation were close to 1 and the intercepts were small (0.02 and 0.0007). The SR50 measurement at the UC site, where wind and vegetation have a minor influence on snow accumulation and redistribution, agreed best with the areal mean with the lowest NRMSE (0.09) and MB (−0.03). FRSF also had a low NRMSE (0.15) and MB (0.05) especially considering the high annual accumulation at this site. In other three sites, the SR50 point observation consistently either under- or over-estimated the areal mean value. In FRNF and FRRT, which are the blowing snow source areas, the SR50 observation underestimated the areal mean by 35% and 45% on average and with a high NRMSE (0.45 and 0.51). In UF, where areal snow variation is mainly influenced by forest cover, the SR50 observation overestimated the areal mean with an MB of 0.41 and NRMSE of 0.56. In addition, the coefficient of determination values of all sites were higher than 0.74. This indicated that the linear relationship between SR50 point snow depth and snow survey snow depth areal mean can be used to adjust the SR50 point measurement to allow upscaling.

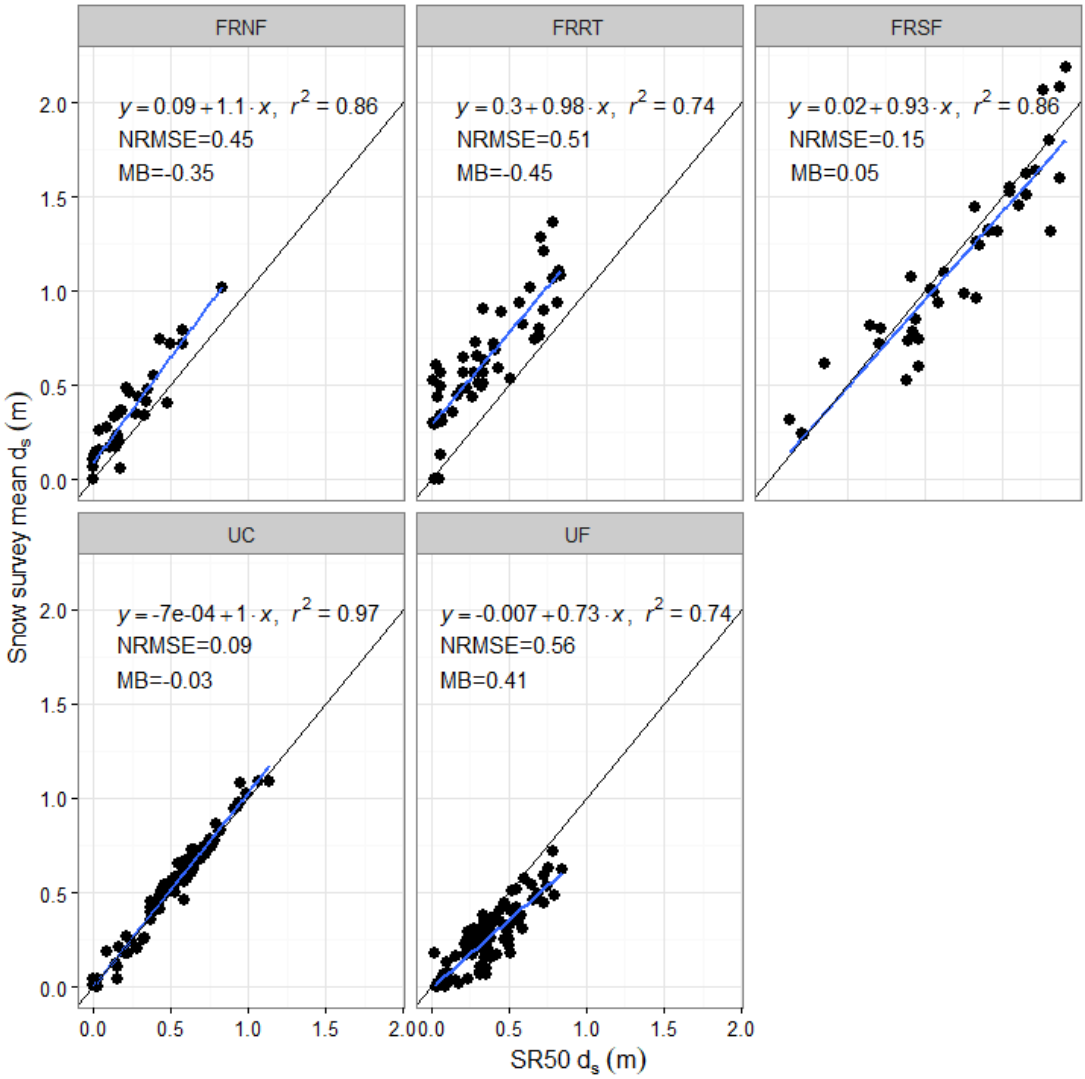

Figure 5-5. Comparison of point SR50 snow depth measurements and landscape average from snow surveys at five sites at the Marmot Creek Research Basin, Alberta, Canada. Blue lines show the best fit and black lines denote the 1:1 line.

Figure 5-6 shows the comparison of observed area mean snow depth from snow surveys, fixed-point SR50, and unscaled snow depth from SR50 according to the linear relationship from Figure 5-5 for each site in MCRB. The results indicated that upscaling largely improved the ability of SR50 to represent the areal mean value at most sites at MCRB. The unscaled snow depth agreed with snow survey data much better at sites FRNF, FRRT, and UF. Upscaling decreased the RMSE in these sites by 40% to 50%. The improvement in UC and FR was low because fixed-point SR50 observation already had a high accuracy. Upscaling improved the RMSE of FRSF by only 5% and the unscaled SR50 was almost identical to the snow survey measurements.

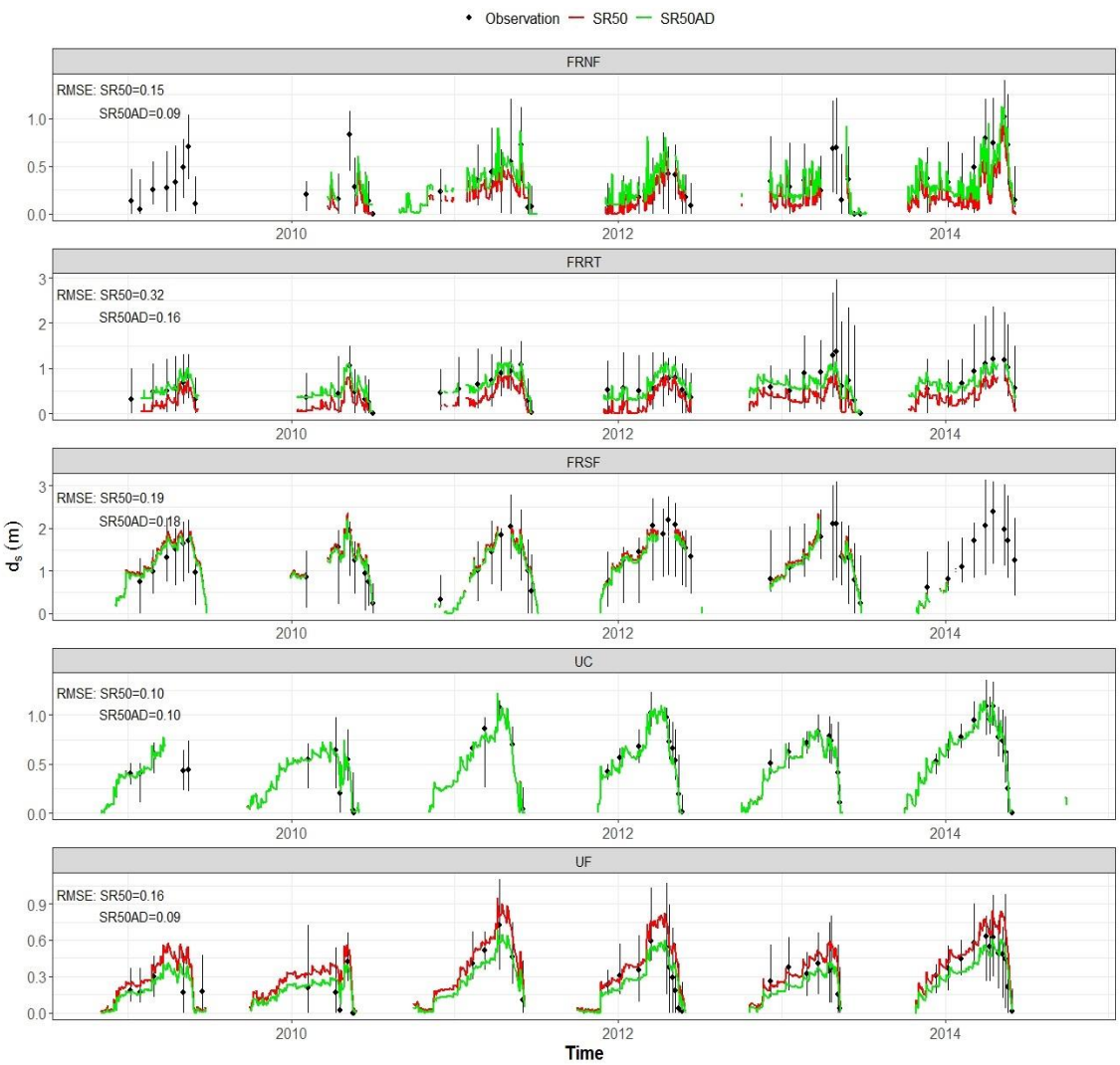

Figure 5-6. Time series of snow depth from snow survey observed areal means, fixed-point SR50 measurements, and upscaled SR50 measurements at the Marmot Creek Research Basin, Alberta, Canada. Error bar shows the data range of the snow depth observation.

5.5.2 SWE and snow depth assimilations influence on snowpack properties at middle elevations forest sites

The open loop simulation largely underestimated SWE and snowpack duration when compared to observations in every year at site UF (Figure 5-7). At UC, although the open loop simulated snowpack duration was close to observations in most years, it largely underestimated SWE in hydrological year (HY) 2014 while overestimating SWE in 2016 (Figure 5-7). The open loop simulation overestimated snowpack density by 34% to 84% annually at both sites. This resulted in snow depth being underestimated at both sites most of the time. After the assimilation, different DA experiments influenced snowpack properties differently and were sensitive to the time of the year, simulation year, location, and CRHM model performance.

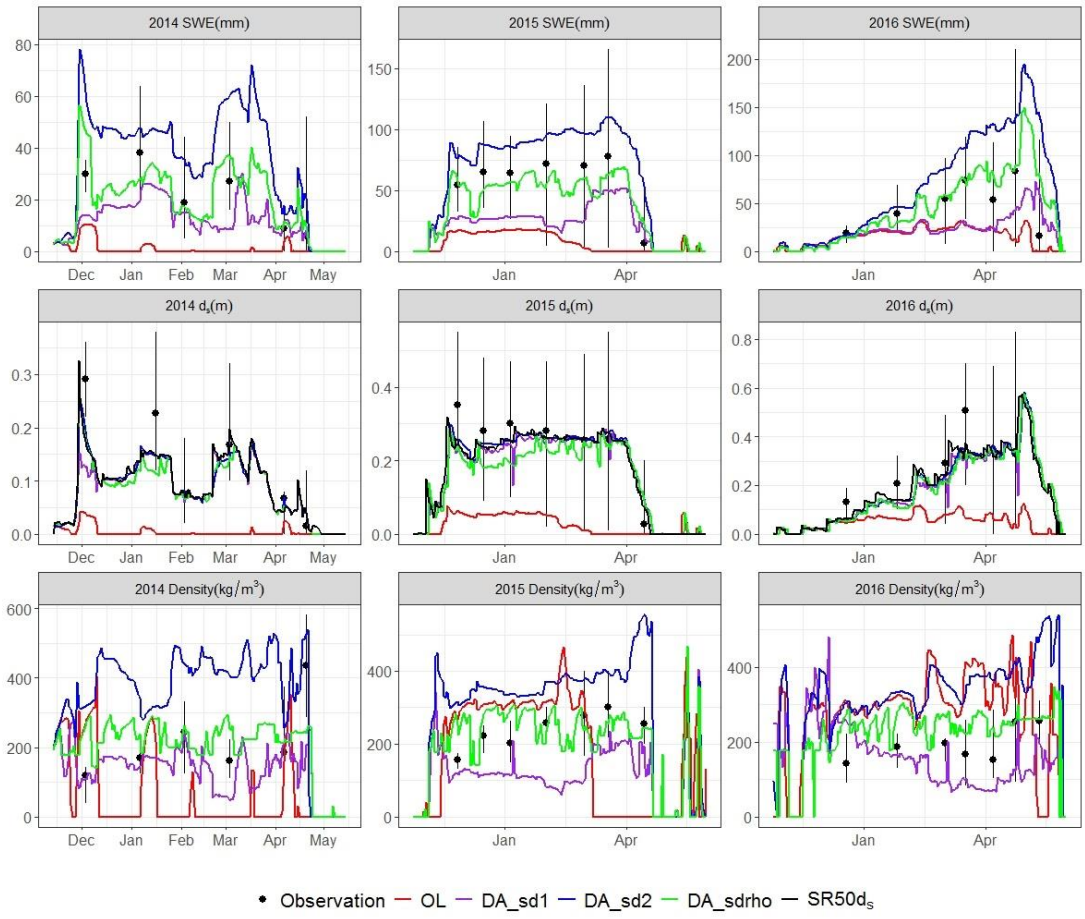

Figure 5-7. Comparisons of d_s assimilation experiments simulated SWE (upper panel), d_s (Middle panel), and snowpack density (lower panel) to observation at upper forest sites at the Marmot Creek Research Basin, Alberta, Canada. Error bars show the data range and the points show the mean values of the snow survey observations. SR50d_s denotes the upscaled SR50 snow depth measurement.

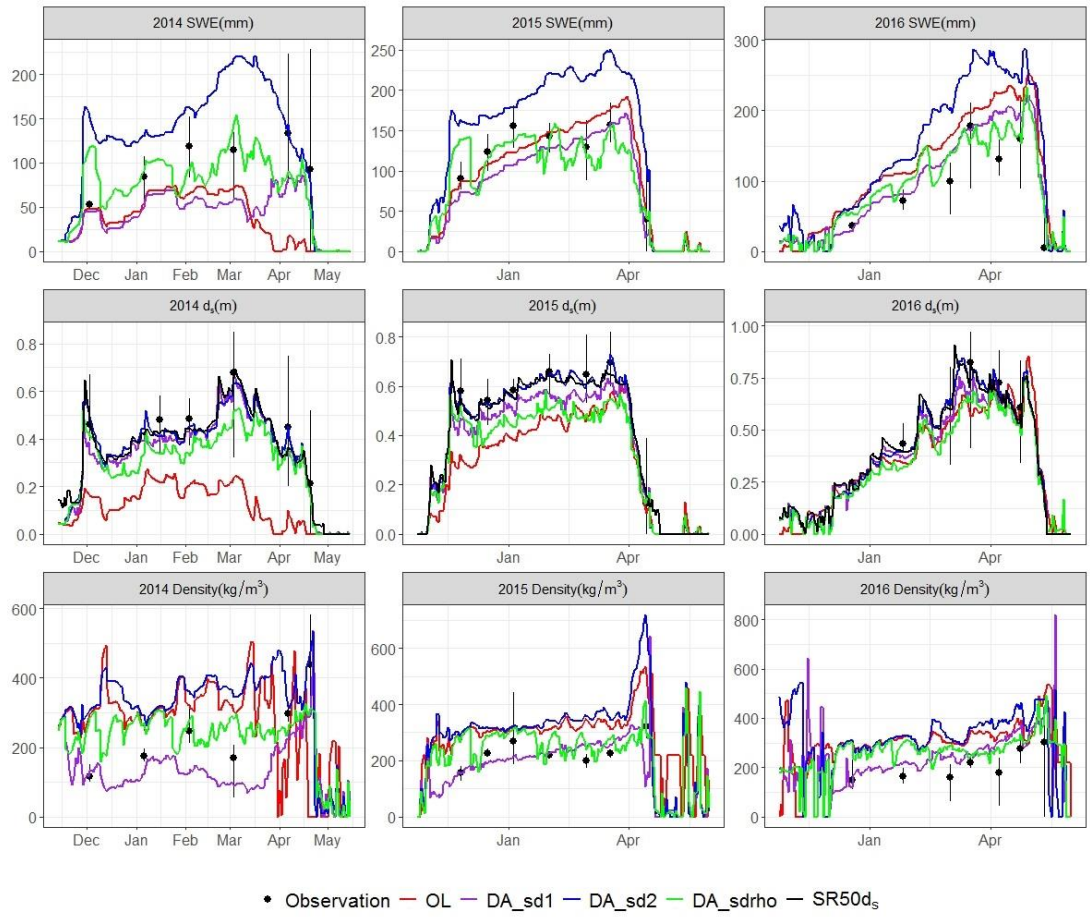

Figure 5-8. Comparisons of d_s assimilation experiments simulated SWE (upper panel), d_s (Middle panel), and snowpack density (lower panel) to observation at upper clearing sites at the Marmot Creek Research Basin, Alberta, Canada. Error bars show the data range and points show the mean values of the snow survey observations. SR50d_s denotes the upscaled SR50 snow depth measurement.

Assimilating d_s alone generally improved the timing of snowpack simulation (Figures 5-7, 5-8). The simulated snowpack duration (positive SWE days) agreed well with d_s observations at both sites (Table 5-2). The improvement is particularly large in the HY 2014 site UF where DA_sd1 and DA_sd2 both improved modeled snowpack duration to 160 days from open loop simulated 49 days when observed snow pack duration was 161 days.

Table 5-2. Duration (days) of observed and DA experiment simulated snowpack measures at forested sites at the Marmot Creek Research Basin, Alberta, Canada.

	2014		2015		2016	
	UF	UC	UF	UC	UF	UC
Observation	161	167	169	175	190	199
OL	49	156	124	186	186	198
DA_sd1	162	166	168	174	189	193
DA_sd2	162	164	168	174	189	190
DA_sdrho	162	162	168	174	189	194
DA_swe	102	165	156	173	188	188
DA_swesd1	159	167	167	174	185	190
DA_swesd2	160	163	168	174	191	196

DA_sd1 significantly improved d_s simulation accuracy. Compared to OL, DA_sd1 decreased RMSE for d_s from 0.22 m and 0.22 m to 0.07 m and 0.08 m for sites UF and UC independently (Table 5-3). The open loop simulation largely underestimated d_s at both sites by −80 to −93% (UF) and −16 to −67% (UC) annually (Table 5-4). After the assimilation, the annual MB was improved from −0.27 to −0.09 and −0.16 to −0.12 for sites UF and UC, respectively (Table 5-4). DA_sd1 improved the SWE simulation MB in most of years at both sites and slightly decreased the SWE simulation RMSE to 29.9 mm and 38.0 mm from 40.4 mm and 54.9 mm at sites UF and UC respectively. However, this improvement was mainly observable in early snow accumulation and late depletion periods. One exception was the at UF site during the 2014 HY when the annual snow peak was low and open loop simulated snowpack was not continuous. Because snowpack density was updated according to assimilated d_s and simulated SWE, which improved little, the enhancement of DA_sd1 on snowpack density simulation was also small.

Table 5-3. RMSE of DA experiments when compared to *in situ* observations at forested sites in the Marmot Creek Research Basin, Alberta, Canada. Bold font shows the lowest RMSE simulation among DA experiments at each site. Numbers before the division slash show the RMSE of the whole evaluation while the ones after the division slash show the RMSE of independent evaluations.

	SWE (mm)		d_s (m)		ρ (kg/m^3)	
	UF	UC	UF	UC	UF	UC
OL	40.37	54.86	0.22	0.22	193.92	162.75
DA_sd1	29.94	37.95	0.07	0.08	106.18	86.30
DA_sd2	42.39	77.54	0.07	**0.04**	171.37	161.11
DA_sdrho	18.16	31.20	**0.05**	0.13	**83.99**	95.97
DA_swe	14.97/20.30	35.56/51.12	0.15	0.24	184.22	162.62
DA_swesd1	**8.71/15.78**	**23.79/43.11**	0.07	0.10	96.23	**71.70**
DA_swesd2	61.63/87.63	40.95/67.48	0.07	0.05	157.66	103.79

Table 5-4. Model Bias (unit:1) of DA experiments when compared to *in situ* observation at forested sites at the Marmot Creek Research Basin, Alberta, Canada. Bold font shows the lowest MB simulation among DA experiments at each site. Numbers before the division slash show the MB of whole evaluation while the ones after the division slash show the MB of independent evaluations.

			OL	DA_sd1	DA_sd2	DA_sdrho	DA_swe	DA_swesd1	DA_swesd2
SWE	UF	2014	-0.89	-0.12	1.80	0.69	-0.55/-0.78	**0.09**/0.44	0.51/2.02
		2015	-0.83	-0.43	1.04	0.22	-0.22/-0.27	**-0.03**/**-0.08**	0.31/0.67
		2016	-0.65	-0.25	1.61	0.35	-0.23/-0.34	**-0.14**/**-0.33**	0.57/1.14
	UC	2014	-0.57	-0.43	0.48	**-0.02**	-0.41/-0.57	-0.20/-0.46	0.21/**0.21**
		2015	0.01	-0.15	0.56	**0.002**	-0.02/-0.07	-0.004/-0.05	0.22/0.32
		2016	0.59	0.29	0.89	0.22	0.04/0.04	**-0.01**/**-0.03**	0.42/0.72
SD	UF	2014	-0.93	0.08	0.14	**-0.04**	-0.73	0.13	0.10
		2015	-0.87	0.26	0.30	**0.02**	-0.48	0.12	0.27
		2016	-0.80	0.11	0.10	**-0.07**	-0.59	-0.16	0.10
	UC	2014	-0.67	-0.16	**-0.06**	-0.24	-0.57	-0.19	-0.06
		2015	-0.31	-0.13	**-0.01**	-0.21	-0.34	-0.11	-0.03
		2016	-0.16	-0.12	**-0.08**	-0.22	-0.42	-0.15	-0.08
Density	UF	2014	0.41	-0.38	0.80	0.23	-0.40	-0.25/**0.09**	**0.03**/0.72
		2015	0.38	-0.55	0.61	0.17	0.50	-0.19/**0.02**	**-0.06**/0.36
		2016	0.84	-0.38	0.94	0.31	0.96	**-0.05**/**0.04**	0.25/0.62
	UC	2014	0.34	-0.32	0.46	0.16	0.41	**-0.01**/**-0.17**	0.27/0.24
		2015	0.48	-0.12	0.65	-0.36	0.46	**0.07**/**0.19**	0.20/0.33
		2016	0.72	0.34	0.81	0.49	0.76	**0.25**/**0.28**	0.27/0.72

The DA_sd2 simulation achieved similar results as DA_sd1 to predict d_s (Figures 5-7, 5-8). It decreased RMSE by 0.15 m and 0.18 m at sites UF and UC. However, due to CRHM largely overestimating snowpack density with annual MB from 0.46 to 0.91, DA_sd2 simulated SWE clearly deviated from observations. DA_sd2 overestimated SWE with an annual MB of 0.47 to 0.91 and 0.48 to 0.89 for sites UF and UC respectively. The SWE simulation RMSE of DA_sd2 was 42.4 mm and 77.5 mm for UF and UC, separately, which was even higher than the OL. DA_sd2 simulated snowpack density closely matched the DA_OL except in the early accumulation and late melt period when DA_OL simulated a SWE of zero. This slightly decreased the snowpack density RMSE at both sites by 22.6 kg/m^3 and 1.65 kg/m^3.

By introducing historical snowpack density assimilation along with d_s, DA_sdrho achieved much better SWE predictions than DA_sd1 and DA_sd2 (Figures 5-7, 5-8). DA_sdrho decreased the SWE RMSE by 22.2 mm and 23.7 mm at sites UF and UC respectively. MB estimates in each simulation year were also improved (Table 5-4). The

RMSE of simulated d_s decreased from 0.22 m and 0.22 m to 0.05 m and 0.13 m for sites UF and UC independently. Simulated d_s MB also improved every year at both sites and MB was lower than ±0.29 for all years. DA_sdrho for the most part increased the accuracy of snowpack density simulations, decreasing the RMSE by 109.9 kg/m^3 and 66.8 kg/m^3 at UF and UC, separately, and improving the MB by 0.16 to 0.53.

Assimilating SWE alone generally improved SWE simulation accuracy (Figures 5-9, 5-10). The SWE simulation RMSE decreased to 15.0 mm and 35.6 mm from 40.4 mm and 54.9 mm at sites UF and UC, independently (Table 5-3). The simulation MB was also decreased in most years by 0.16 to 0.61 (Table 5-4). However, due to sparse SWE data availability and the nature of EnKF, there were several drawbacks for assimilating SWE alone. First, the assimilation result was poor during a dry year at site UF. In HY 2014, the DA_swe simulated SWE at UF site was not continuous (Figure 5-9), which did not match with SR50 observations that showed the snowpack was continuous from November 13, 2014 to April 27, 2015. There were six SWE measurements at these sites in this year of which four were assimilated into the model and two were excluded as independent validation data. The model reacted well to the assimilation during the first two time steps and SWE was improved but the snowpack disapeared a few days after assimilations. At the third and fourth assimilation time steps (March 3 and April 20, 2015), the model did not respond at all to assimilation. This is because model simulated SWE ensembles were all equal to zero before the update so that the model simulation error covariance (P_i^s in Equation 5.3) equaled zero at these two time steps. This resulted in the Kalman gain K (Equation 5.2) equaling zero as well and hence there were no updates at these two time steps. Therefore, although the simulation snowpack duration increased to 102 from 49 days (OL), it was still much less than the observed snowpack duration – 168 days in this year at site UF. Second, although DA_swe can greatly improve SWE simulation in the middle of the snow season, its influence can be limited in the early accumulation and late depletion periods in some years due to SWE data sparsity. One example was that in 2015 at site UF, the snowpack started few days later and disapeared a few days earlier than SR50 snow pack duration. Third, although assimilating SWE alone greatly improved SWE simulation accuracy, it only enhanced model simulated d_s and snowpack density accuracy to a small extent. DA_swe greatly overestimated snowpack density at most times of the year at both sites, as DA_OL did, and this led to it simulating d_s lower than observed (Figures 5-9, 5-10). The RMSE and MB for DA_swe simulated d_s and snowpack density were only slightly improved or even worsened over most of the year at both sites (Tables 5-3, 5-4).

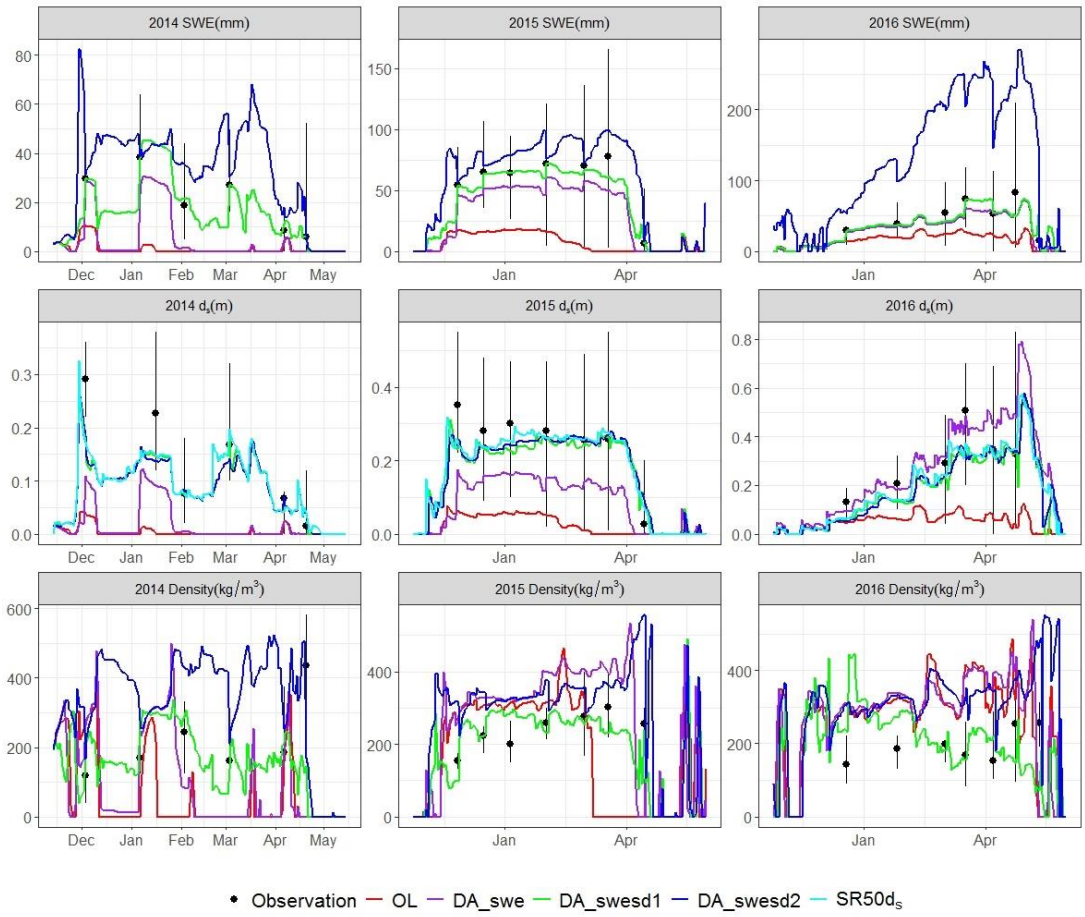

Figure 5-9. Comparisons of SWE assimilation experiments simulated SWE (upper panel), d_s (Middle panel), and snowpack density (lower panel) to observation at upper forest sites at the Marmot Creek Research Basin, Alberta, Canada. Error bars shows the data range and points show the mean values of the snow survey observations. SR50d_s denotes the upscaled SR50 snow depth measurement.

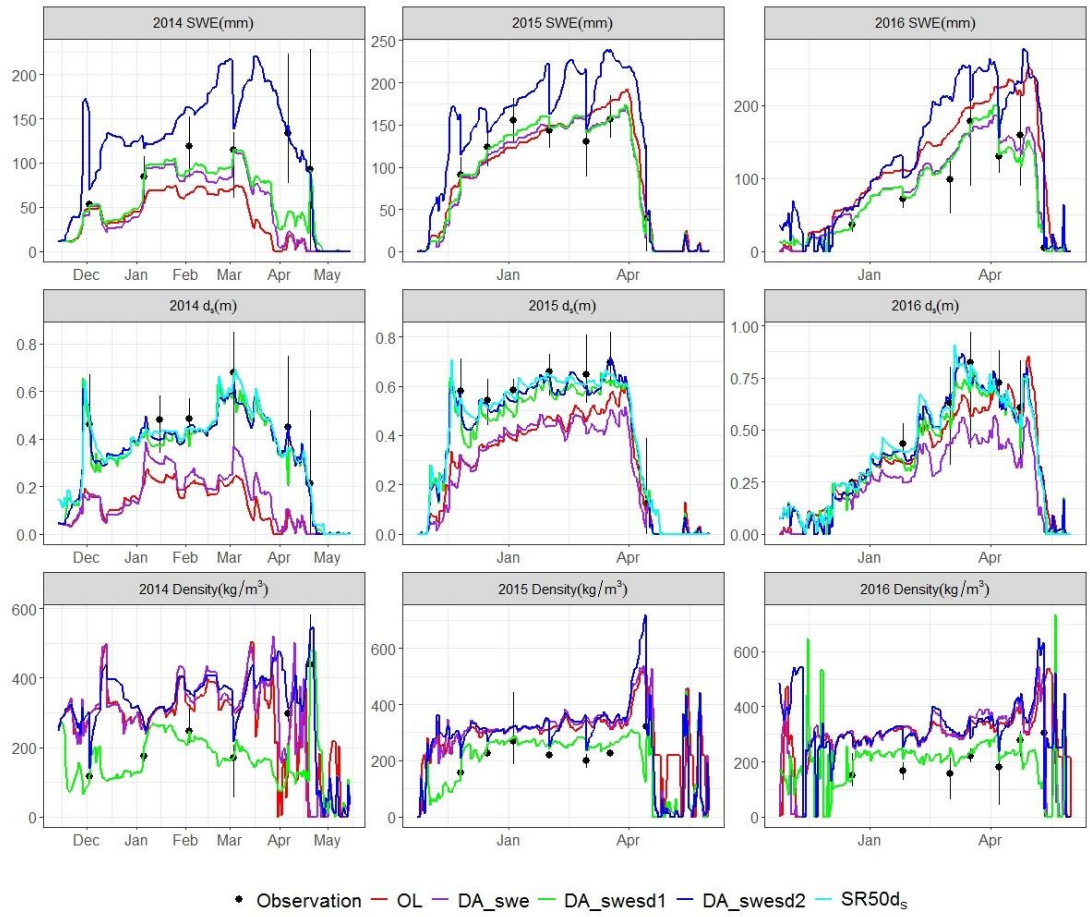

Figure 5-10. Comparisons of SWE assimilation experiments simulated SWE (upper panel), d_s (Middle panel), and snowpack density (lower panel) to observation at upper clearing sites at the Marmot Creek Research Basin, Alberta, Canada. Error bars shows the data range and points show the mean values of the snow survey observations. SR50d_s denotes the upscaled SR50 snow depth measurement.

By assimilating daily measured automatic d_s data along with SWE, DA_swesd1 resulted in the best snowpack estimates amongst all DA experiments (Figures 5-9, 5-10). DA_swesd1 decreased the SWE simulation RMSE to 8.7 mm and 23.8 mm for UF and UC, respectively, which was the lowest RMSE value among all DA experiments. Annual MB values from most years were close to zero and all of them were less than or equal to ±0.2. DA_swesd1 also outperformed in the independent validation among SWE involved DAs most of the time (Tables 5-3, 5-4). DA_swesd1 also avoided the three drawbacks when SWE was assimilated alone. Because the daily d_s information was also assimilated into the model, the DA_swesd1 simulated snowpack was continuous in each year leading to the model reacting to SWE assimilation at each time step. d_s also provided detailed snowpack duration information, and this enhanced the ability for SWE to simulate early accumulation and late depletion. Therefore, The DA_swesd1 simulated snowpack durations were improved to a close match level to the observations in all the years at both sites (Table 5-4). Simultaneously assimilating SWE and d_s provided reliable SWE information and high temporal resolution d_s information.

This resulted in a DA_swesd1 simulated snowpack density that was closely matched to most observations. However, this close match was limited to the time of assimilation at the beginning of each day. Density always increased gradually immediately after the assimilation time because CRHM tends to overestimate the snowpack density at these sites. Figure 5-11 shows the detailed response of SWE, d_s, and snowpack density to DA_swesd1 assimilation at hourly time steps at sites UF and UC from January 30 to March 1, 2016. Snow depth was updated at beginning of each day and snowpack density was updated based on simulated SWE and updated d_s. However, because CRHM tends to overestimate snowpack density at both sites, snowpack densification started immediately after the time of assimilation and the snowpack density can increase as much as 70 kg/m^3 within one day. The simulated d_s decreased accordingly and became much smaller than observed until the next assimilation time. This confirmed the necessity of assimilating d_s every day or at an even higher frequency, if possible, to keep simulating a reasonable snowpack density at sites like UF and UC.

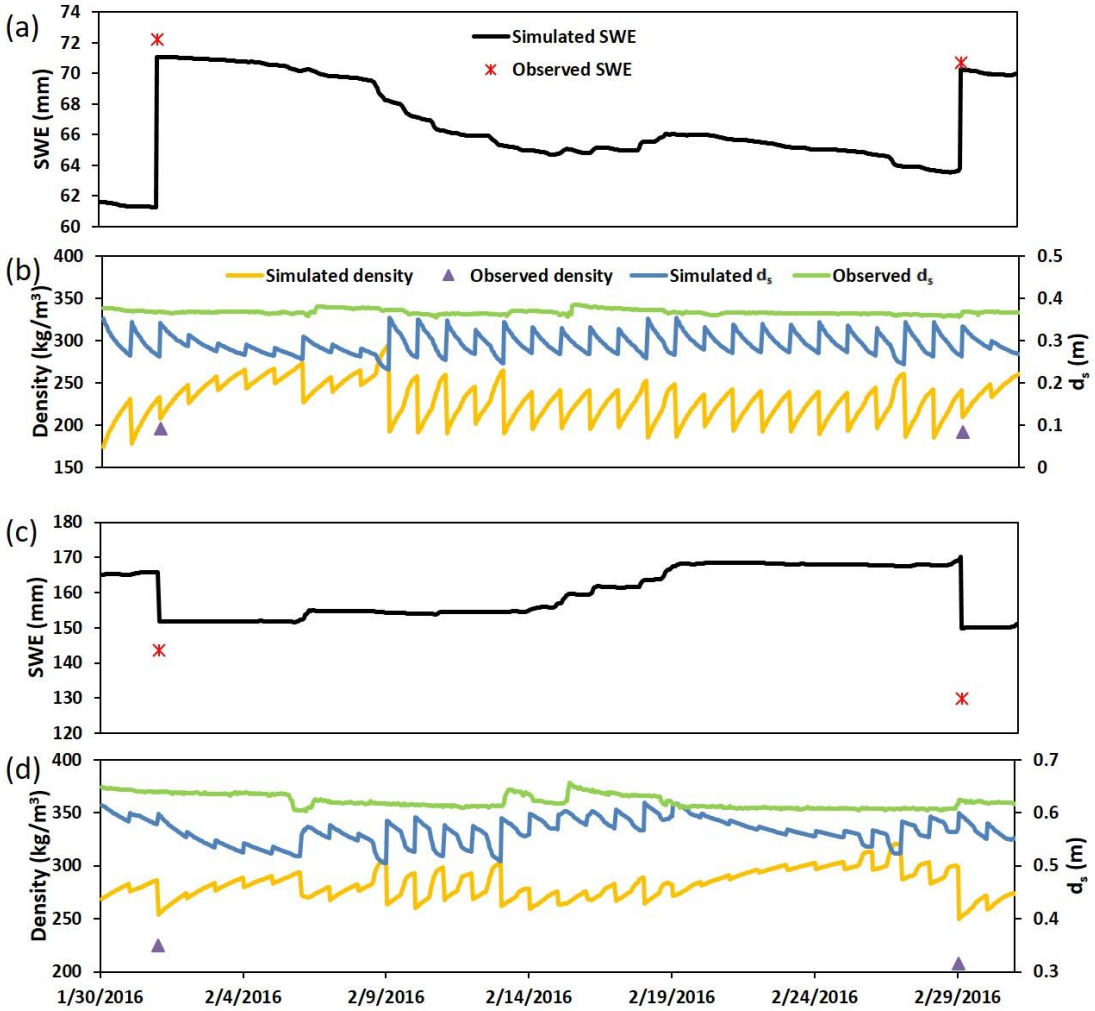

Figure 5-11. Reaction of main snow properties (SWE, d_s, and snowpack density) to DA_swesd1 assimilation at upper forest (a, b) and upper clearing (c, d) sites in Marmot Creek Research Basin, Alberta, Canada.

DA_swesd2 simulated SWE agreed with observations at the SWE assimilation time steps. However, SWE was largely overestimated the rest of time because the model consistently overestimated snowpack density. Independent validation indicated that RMSE between simulated and observed SWE was 87.63 mm and 67.48 mm at sites UF and UC respectively. This was the highest among all the SWE involved DAs. Like other DA experiments with d_s assimilation, DA_swesd2 simulated d_s agreed with observations most of the time with low RMSE (0.07 m and 0.05 m) and MB (−0.22 to −0.03 annually). Although the snowpack density was close to observed at time steps when both SWE and d_s observations were available, the snowpack densified gradually after these assimilations. This resulted in the simulated snowpack density being 24% to 72% higher than observed, resulting in the overestimation of SWE at both sites.

5.5.3 SWE and ds assimilation influences on snowpack properties in open alpine sites

Figure 5-12 shows the SWE from snow survey and several DA experiments at the windblown Fisera Ridge sites. Compared to OL, all DA experiments improved SWE simulation accuracy to varying degrees. At the FRNF site, OL largely overestimated SWE in all simulation years with a MB of 1.16. All DAs produced similar results, decreasing MB to between 0 and 0.2 with a decreased RMSE of simulated SWE from 148.3 mm (OL) to between 22.4 and 69.4 mm (Table 5-5). The SWE-involved DAs (DA_swe, DA_swesd1, and DA_swesd2) performed better than assimilating snow depth alone (DA_sd1 and DA_sd2) or together with historical snow density data (DA_sdrho). Amongst SWE involved DAs, improvements were similar while DA_swesd1 gained a slightly higher accuracy (around 1 mm) than DA_swe and DA_swesd2. For the non-SWE DAs, DA_sdrho had between 1 and 31 mm higher accuracy than DA_sd2 and DA_sd1, respectively. At site FRRT, as in FRNF, OL overestimated SWE in most years with a MB of 0.49 dropping to between −0.19 and 0.15 after assimilation. The SWE involved DAs had much better performance than non-SWE DAs. The SWE involved DAs decreased the RMSE from 122.4 mm (OL) to between 18.6 and 48.0 mm with DA_swe outperforming DA_swesd1 and DA_swesd2. DA_sd1, DA_sd2, and DA_sdrho also improved SWE simulation accuracy but with relatively higher RMSE (62.2, 55.9, and 71.7 mm). OL overestimated SWE at site FRRT, however after the assimilation, DA_sd2 and DA_sdrho underestimated SWE. This is partially due to the adjusted SR50 observation underestimating snow depth at this site in most years. The open loop running at site FRSF had the highest RMSE (152.5 mm) but lowest MB (0.12) among the three sites. Considering the high annual snow accumulation at this site, the OL simulated the snowpack the best at FRSF. After assimilations, the MB of the designed experiments improved to between −0.11 and 0.06. DA_swe, DA_swesd1, and DA_swesd2 improved RMSE by 113.5, 102.2, and 81.4 mm, respectively, whilst the improvements from DA_sd1, DA_sd2 and DA_sdrho were only 25.4, 69.8 and 24.9 mm, respectively. Although the whole validation showed that assimilating SWE alone can be better than simultaneously assimilating SWE and d_s,

independent validation shows that DA_swesd1 outperformed at sites FRRT and FRSF while DA_swesd2 achieved its best result at site FRNF (Table 5-6).

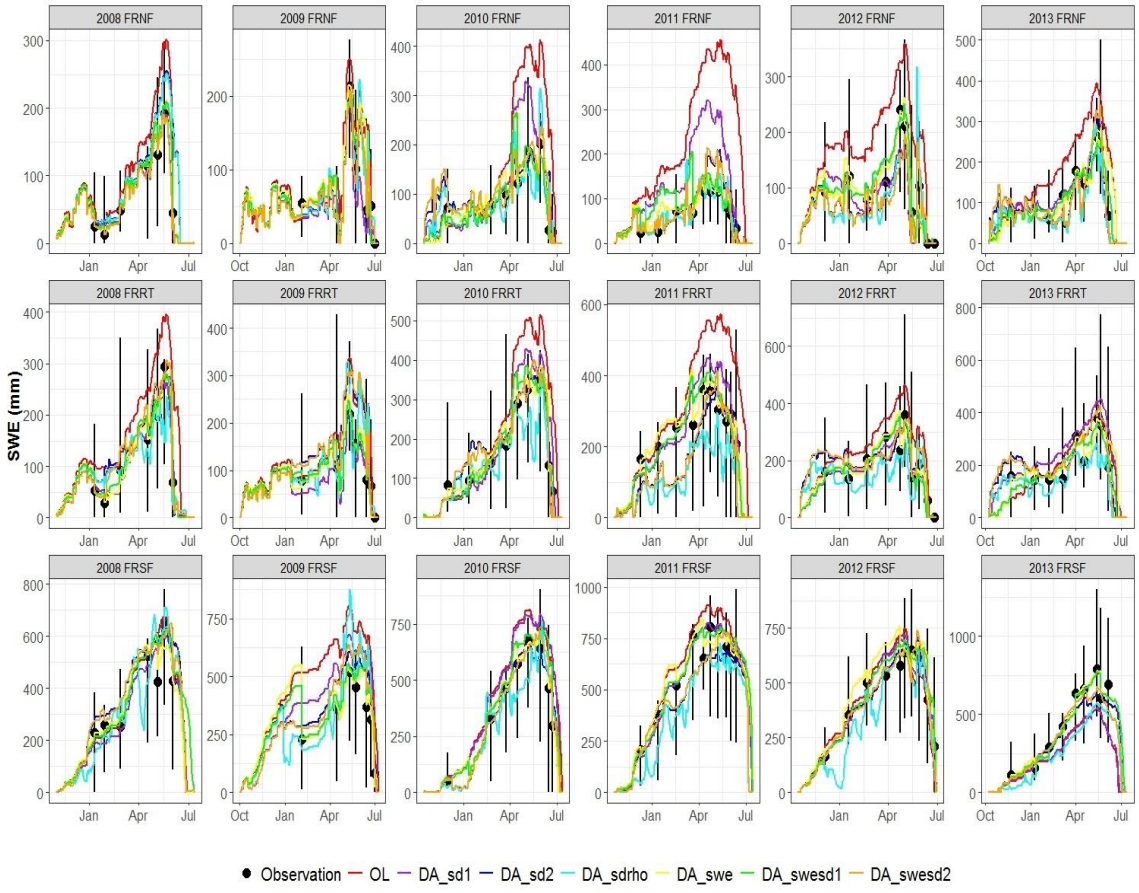

Figure 5-12. Comparison of observed and simulated SWE in DA experiments at Fisera Ridge sites at the Marmot Creek Research Basin, Alberta, Canada. Error bars shows the data range and points show the mean values of the snow survey observations.

Table 5-5. RMSE and MB of DA experiments simulating SWE, snow depth, and snowpack density at Fisera Ridge sites in Marmot Creek Research Basin, Alberta, Canada.

	OL		DA_sd1		DA_sd2		DA_sdrho		DA_swe		DA_swesd1		DA_swesd2	
	RMSE	MB	RMSE	MB	RMSE	MB	RMSE	MB	RMSE	MB	RMSE	MB	RMSE	MB
							SWE (mm)							
FRNF	148.25	1.16	69.38	0.20	39.25	0.12	38.29	0.01	23.05	0.04	22.40	0.03	23.57	0.00
FRRT	122.35	0.49	62.21	0.15	55.94	0.06	61.70	-0.19	18.64	0.02	26.16	0.02	47.95	0.04
FRSF	152.49	0.12	127.11	0.06	82.72	0.01	127.55	-0.11	39.01	0.02	50.31	0.04	71.12	0.01
							d_s (m)							
FRNF	0.42	0.87	0.11	-0.10	0.09	-0.02	0.10	-0.07	0.09	-0.09	0.09	-0.04	0.10	-0.10
FRRT	0.42	0.36	0.16	-0.06	0.15	-0.06	0.19	-0.19	0.19	-0.08	0.15	-0.05	0.15	-0.07
FRSF	0.51	0.17	0.28	-0.04	0.19	-0.02	0.35	-0.12	0.23	0.03	0.20	0.00	0.19	-0.04
							ρ (kg/m^3)							
FRNF	83.93	0.16	180.73	0.25	80.45	0.14	74.88	0.07	82.47	0.15	93.56	0.08	99.29	0.09
FRRT	123.90	0.10	130.67	0.19	127.50	0.16	101.39	-0.02	123.03	0.15	103.11	0.11	137.49	0.16
FRSF	76.23	-0.04	109.55	0.14	63.93	0.04	54.10	-0.02	62.87	0.00	57.97	0.03	60.11	0.05

Table 5-6. RMSE and MB of independent validation of DAs simulated SWE and snowpack density at Fisera Ridge sites in Marmot Creek Research Basin, Alberta, Canada. Bold font shows the lowest RMSE or MB simulation among DA experiments at each site.

	OL		DA_swe		DA_swesd1		DA_swesd2	
	RMSE	MB	RMSE	MB	RMSE	MB	RMSE	MB
				SWE (mm)				
FRNF	139.79	1.11	47.93	0.15	41.41	0.08	**32.62**	**0.02**
FRRT	100.16	0.42	37.39	0.07	**29.51**	**0.01**	57.02	0.03
FRSF	164.60	0.09	74.69	0.04	**59.25**	0.04	98.47	**0.02**
				ρ (kg/m^3)				
FRNF	**86.83**	**0.16**	104.88	0.22	105.67	0.26	115.59	0.25
FRRT	**82.08**	**0.07**	107.89	0.16	128.26	0.12	115.78	0.21
FRSF	64.22	-0.09	63.69	-0.02	**39.74**	**0.01**	44.83	0.05

Similar to SWE, the OL overestimated d_s by 17−87% with an RMSE of 0.42 to 0.51 m (Figure 5-13). All assimilations improved model accuracy. After assimilating d_s alone, DA_sd1 and DA_sd2 simulated d_s agreed better to observations with MB lower than ±0.06 and RMSE from 0.09 to 0.28 m. The results from assimilating SWE and d_s together were similar to assimilating d_s alone in d_s simulations and the performances of DA_swesd1 and DA_swesd2 were close. DA_swe achieved even better results than DA_sdrho. This is likely due to DA_swe improving SWE simulations and CRHM having reasonable accuracy in snow density simulations. Hence, the d_s updated

consistently with updated SWE and simulated snowpack density improved even though no d_s data was assimilated into the model directly.

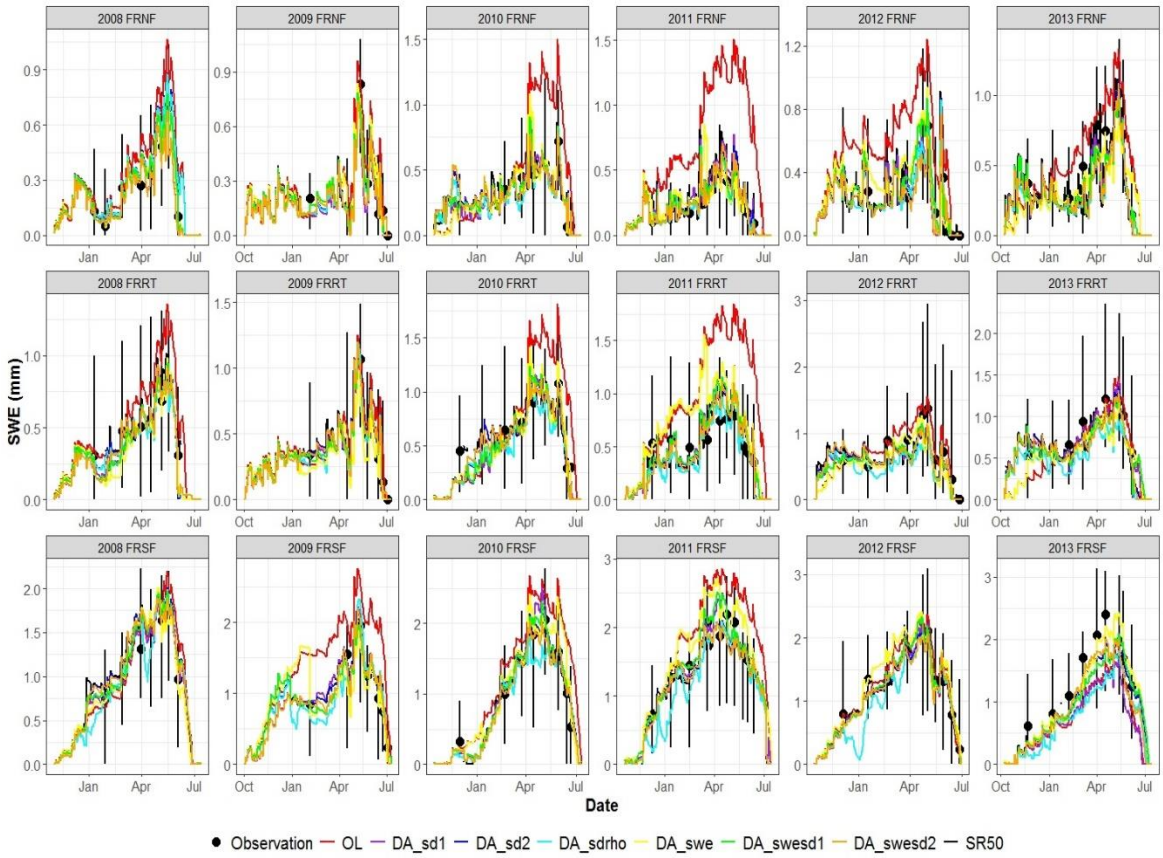

Figure 5-13. Comparison of observed and simulated snow depth by DA experiments at Fisera Ridge sites in Marmot Creek Research Basin, Alberta, Canada. Error bars shows the data range and points show the mean values of the snow survey observations.

The OL had relatively small over- or underestimation rates (−4% to 16%) in snowpack density simulations and the RMSE values between observations and simulation were 76.2 to 123.9 kg/m^3. The DA experiments improved little or not at all at the Fisera Ridge sites (Figure 5-14). DA_sd1 increased the RMSE and MB at all three sites and DA_sd2 slightly improved the accuracy in two of three sites. DA_swe increased the simulation accuracy with little improvement of RMSE (0.87 to 13.4 kg/m^3). DA_swesd1 decreased the RMSE in two of the three sites and DA_swesd2 only decreased at one of the sites. The DA_sdrho achieved its best results among all DA experiments by decreasing the MB to within ±0.07 and the RMSE by 9 to 22.5 kg/m^3. Validation observations show that the SWE-involved DAs increased the RMSE and MB at all sites with one exception: DA_swesd1 on a south-facing slope (Table 5-6). These results indicated that, at FR sites, assimilations of SWE and d_s in these experiments have very limited potential to improve the accuracy of snowpack density estimation.

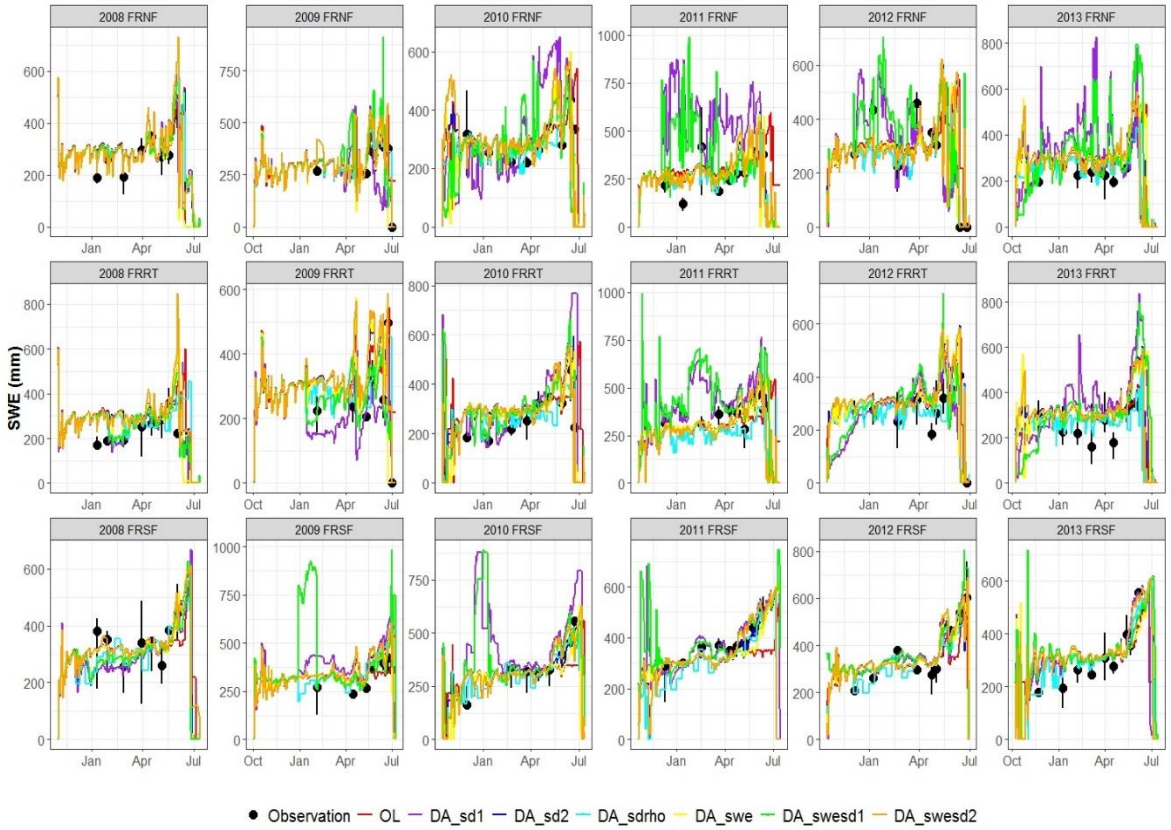

Figure 5-14. Comparison of observed and simulated snowpack density by DA experiments at Fisera Ridge sites in Marmot Creek Research Basin, Alberta, Canada. Error bars shows the data range and points show the mean values of the snow survey observations.

In all, the DAs assimilated SWE outperformed the DAs assimilated d_s alone or together with historical snow density at FR sites. This indicated that assimilating snow survey SWE data is better than assimilating point scale d_s in general, even though d_s has a much higher collection frequency. This differs from the finding at the UC and UF sites, where assimilating SWE and d_s together did always achieve better results than assimilating SWE alone when simulating SWE. Rather, DA_swesd1 had higher RMSE than DA_swe at two of three sites in FR. This is likely caused by several factors. The first is the high SWE and its consistency throughout the winter at these sites. At sites UC and UF, annual snow accumulation is small which makes OL simulated SWE discontinuous throughout the snow season in some years (Figure 5-7). Assimilating d_s under this condition significantly benefits SWE assimilation. At the FR sites, however, the snowpack is continuous throughout the snow season in all years for OL so that the benefits of assimilating d_s are small. Second, the SR50 observations did not provide enough information at the beginning and end of each snow season due to data gaps. At UC and UF, one reason DA_swesd1 outperformed DA_swe was that the former simulated SWE better at the beginning and end of the snow season. At FR, however, adjusted SR50 measurements only provided clear information about the beginning and end of the snow season in a few years (Figure 5-6). For the independent validation, the

DA_swesd1 outperformed the DA_swesd2 in two of the three FR sites (Table 5-6). This indicates that one can trust SWE more than snowpack density when assimilating SWE and d_s together even if the model is reasonably accurate in snowpack density simulation. At FR, amongst all DAs, DA_sdrho had the second worst performance, in contrast to results from the forest zone UC and UF sites. This can be explained by differences in CRHM's ability to predict snow density. CRHM tended to overestimate snow density at all sites where snow surveys are available. However, the degree of overestimation decreases with increasing elevation (Figure 5-15). At low elevations, such as at site LF, the overestimation rate can reach 69%. At middle elevations, such as at sites UC and UF, the rate decreased to between 47 and 49%. At high elevations (Fisera Ridge), this rate dropped to between 10 and 22%. At the forest zone sites UF and UC, because CRHM greatly overestimates snow density, incorporating a more reliable snow density measure can greatly improve SWE simulation accuracy. Although CRHM still has errors in simulating snow density at FR sites, the overestimation rate is low and modelled density is better than assimilating the ten-day average historical snow density.

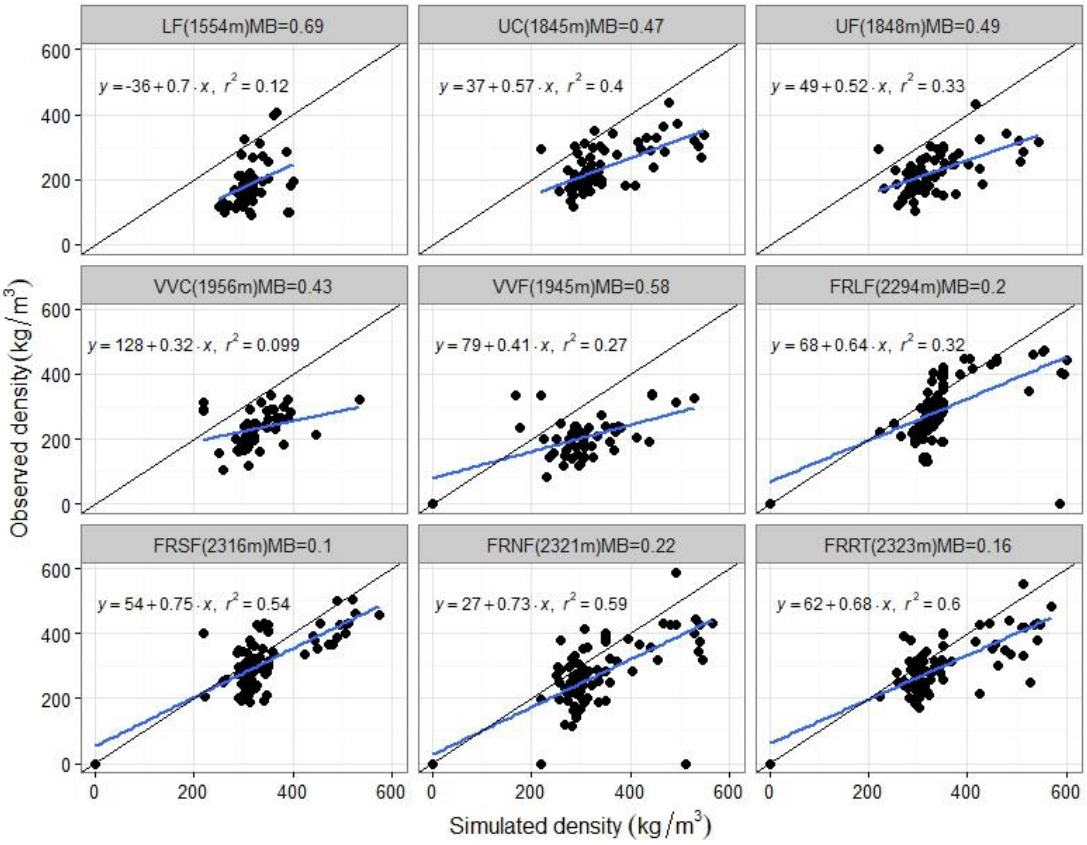

Figure 5-15. Comparison of observed and simulated snow density at all sites in Marmot Creek Research Basin, Alberta, Canada from 2007 to 2018. Black line shows the 1:1 relationship and the blue line shows the best fit.

5.5.4 SWE assimilation impacts on streamflow simulation

GEM_OL tended to overestimate streamflow by 66% to 109% annually and the overall RMSE was 0.24 m^3/s (Table 5-7). Simulated peak streamflow was 2 to 3 times higher than observations (Figure 5-16). SWE assimilation had a modest impact on the streamflow simulation when driving the model with GEM forcing data. The overall RMSE, MB, and NSE all improved slightly after SWE assimilation. GEM_DA only slightly improved the stream simulation in HY 2014 and 2015. RMSE, MB, and NSE changed very little and the annual peak flow was slightly improved when compared to the open loop simulation in these years. The improvement in HY 2016 was significant enough that the simulated discharge closely matched observations in magnitude and timing, with a low RMSE (0.1 m^3/s) and MB (−0.07), and a higher NSE (0.65). In HY 2014 and 2015, improvement in late summer streamflow estimates were insignificant because rainfall was a major source of summer streamflow. However, in HY 2016, predictive improvements occurred throughout the season because there was little rainfall in that summer (Figure 5-16). This indicated that snow data assimilation can only impact late season streamflow simulation in dry summers when rainfall is at a minimum.

Table 5-7. RMSE, MB, and NSE of simulated daily streamflow (m^3/s) from DA experiments in Marmot Creek Research Basin, Alberta, Canada. Bold font shows the best simulation among DA experiments.

	GEM_OL	GEM_DA	ObsMet_OL	ObsMet_DA	GEM_ObsMet_DA
			RMSE		
2014	0.18	0.13	0.09	**0.07**	0.10
2015	0.25	0.19	0.09	**0.07**	0.11
2016	0.27	0.10	0.11	0.10	**0.08**
All seasons	0.24	0.15	0.10	**0.08**	0.10
			MB		
2014	0.66	0.59	0.32	**0.15**	0.512
2015	1.09	0.88	0.23	**0.09**	0.592
2016	0.61	-0.07	**-0.05**	-0.33	-0.160
All seasons	0.78	0.45	0.15	**-0.04**	0.294
			NSE		
2014	-3.50	-1.28	-0.11	**0.30**	-0.34
2015	-9.72	-5.22	-0.30	**0.23**	-1.16
2016	-1.61	0.65	0.61	0.66	**0.78**
All seasons	-3.19	-0.58	0.35	**0.53**	0.29

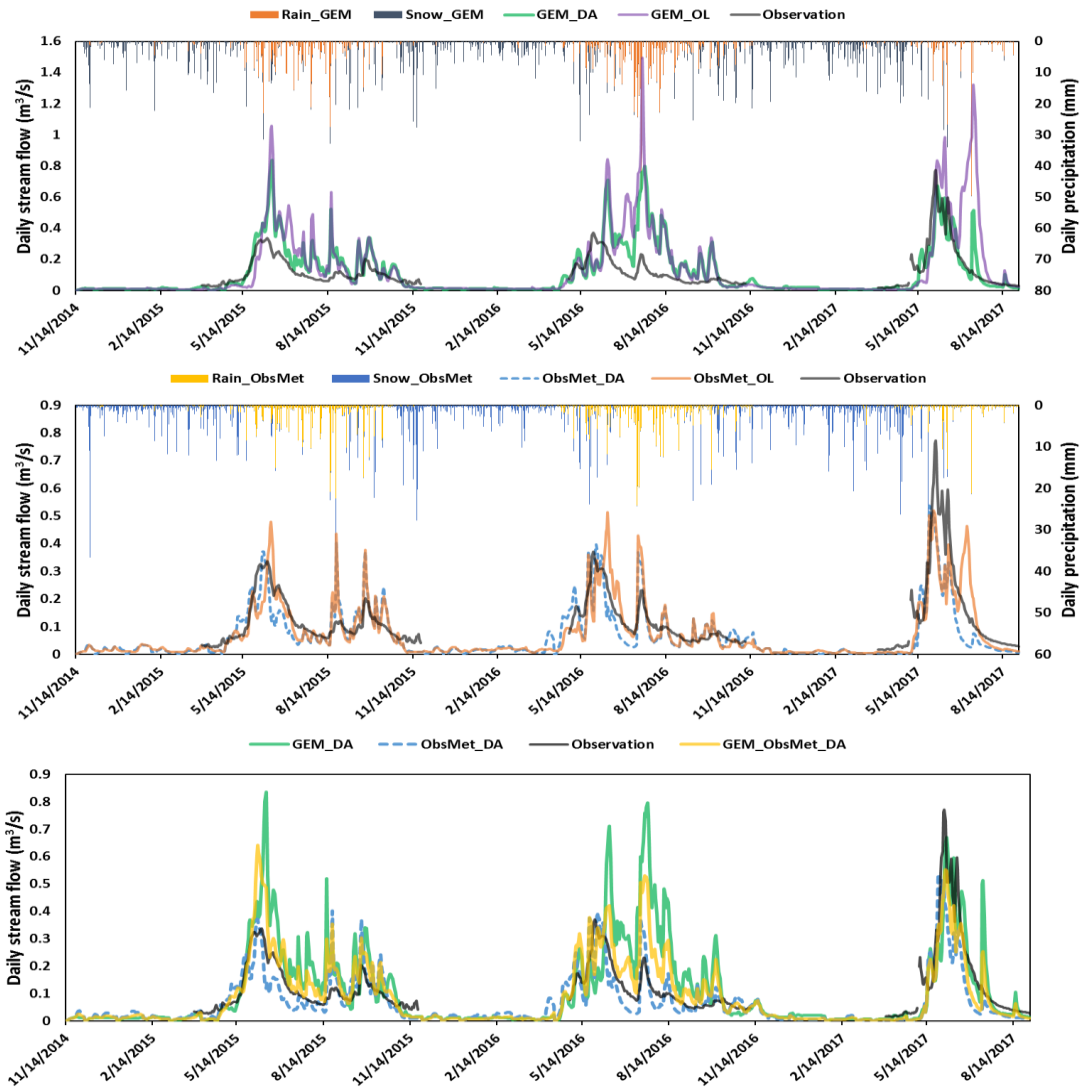

Figure 5-16. Comparisons between several DAs simulated basin daily stream flow and the measured stream flow at the outlet of Marmot Creek Research Basin, Alberta, Canada. (Daily rainfall and snowfall from GEM and local observed precipitations are included to show the timing and type of precipitation)

The open loop simulation using locally observed meteorological data as forcing performed better than GEM_OL and GEM_DA with an overall RMSE of 0.094 m^3/s and MB of 0.15. The ObsMet_OL simulated annual peak streamflow still differed from observations in magnitude and timing, but was, nevertheless, an improvement over GEM_OL and GEM_DA. ObsMet_OL simulated streamflow matched observations well in the early season. Differences grew in the late season when precipitation type shifted from snowfall to rainfall. After SWE assimilation, the ObsMet _DA simulated streamflow improved considerably. Annual peak streamflow simulations agreed well with observations in timing and magnitude. The overall RMSE and MB decreased to 0.08 m^3/s and −0.04 respectively. The NSE also improved, reaching positive values in each year while the overall NSE increased to 0.53. However, this improvement was mainly evident in the early season whilst the impact of SWE assimilation on late season

streamflow was insignificant. This was due to the overwhelming effect of rainfall on late season streamflow generation in every year of simulation except for 2016 which was exceptionally dry.

GEM_ObsMet_DA performed better than GEM_DA but worse than GEM_ObsMet. Estimates of magnitude and timing of peak flow by GEM_ObsMet_DA improved in all simulation years when compare to GEM_OL and GEM_DA. The RMSE, MB, and NSE of GEM_ObsMet_DA simulated streamflow in the first two years were greatly improved when compared to GEM_OL and GEM_DA but not when compared to ObsMet_OL and ObsMet_DA simulations (Table 5-7). However, GEM_ObsMet_DA achieved the best results in the third year, generating the lowest RMSE and highest NSE among all DAs. This is believed to be because of low rainfall from both forcing data sets that summer. This indicates that, although DA can improve streamflow estimates, reliable forcing data are still more important. In the combined forcing data assimilation experiment, snowpack SWE provided better results than single forcing data. However, streamflow simulations forced with combined data cannot be as accurate as simulations forced from observations, as the timing and magnitude of streamflow in the Canadian Rockies rely heavily on the basin-wide mass and energy flux and not only a snapshot of snowpack state.

5.6 Discussions

This research uncovered an approach to assimilating ground observed SWE and d_s into a physically based, cold regions hydrological model that included snow redistribution and ablation processes. The influence of different assimilation schemes on snowpack properties and streamflow simulation were detailed.

Snow survey-derived SWE and automatically measured, high-frequency d_s were assimilated separately or together into models to evaluate the influence of assimilation on snowpack properties (SWE, d_s, and ρ). The results show that, although snowpack property simulations can be improved to some degree when assimilating SWE or d_s alone, there are clear drawbacks to using these approaches. Due to the limited availability of SWE measurements, assimilation may sometimes influence SWE simulations too little in the early and late snow season. The snow ablation season is a particularly important hydrological period as it controls snowmelt runoff estimates. Because of the nature of EnKF, the model may not respond to assimilation at critical times (snow season onset, snow season end, dry years) when model simulated SWE equals zero for all ensembles. This leads to a zero Kalman gain and no model updates. Kumar et al. (2009) proposed a method that used multiple sources of forcing data in one ensemble member set to increase model simulation error covariance. This approach generally enhances assimilation performance, and particularly in the early and late snow season. Assimilating observations of daily snow depth data alone can greatly improve the snow depth estimates, but its contribution to simulated SWE is entirely

dependant on the performance of modelled snowpack density. It has been shown elsewhere that d_s assimilation can improve SWE estimates (Liu et al., 2013; Magnusson et al., 2017). Here however, the assimilation of d_s alone did little to improve SWE estimates and in some cases made those estimates worse at the middle elevation sites. This is attributed to the Snobal module in CRHM tending to overestimate snowpack density. CRHM tends to overestimate snowpack density across the basin and overestimates are particularly high at low to middle elevations. Models of high elevation sites (Fisera Ridge) showed that assimilating d_s alone achieved results close to SWE involved assimilation. At middle elevation sites (UC and UF), however, these models performed only slightly better and sometimes worse. This reveals the importance of reliable snowpack density estimates prior to assimilating d_s into hydrological models.

Most snow data assimilation research has assimilated either SWE or d_s alone while updating the unincorporated variable based on modelled snowpack density (e.g., Clark et al., 2006; Liu et al. 2013; Magnusson et al. 2017; Slater and Clark, 2006). Knowing that snowpack density estimates from CRHM in study area were poor, this research assimilated monthly or semi-monthly SWE data from snow survey and daily snow depth measurements together into the model. Instead of trusting modelled snowpack density, snow density was adjusted based on updated SWE and d_s in one experiment. At middle elevation sites, where CRHM greatly overestimates snowpack density, this experiment achieved its best results with three main snowpack properties (SWE, d_s, and ρ). A comparable result was obtained by assimilating historical snowpack density along with d_s data into the model. Reliable automatic and manual SWE measures are costly and not available in most cold regions. Hence, assimilating automatically measured d_s and a reliable ρ together is more feasible for hydrological modeling than assimilating d_s into a snow model that inadequately estimates snowpack density. A reliable ρ can be obtained by involving another snow density estimation algorithm based on meteorological data, topography, day of the year and other parameters (c.f., Jones et al., 2009; Meløysund et al., 2007; Sturm et al., 2010). At the Fisera Ridge sites, where CRHM simulated the snowpack density relatively well, incorporating the historical snowpack density did not always produce better results than by assimilating d_s alone. This indicated that when model simulated ρ is reliable, assimilating d_s alone is the better choice because introducing another ρ estimation method always increases uncertainty. The results suggest that the flexible CRHM platform should employ other snowpack module options than Snobal for application in the Canadian Rockies.

In the second part of this research, monthly or semi-monthly snow survey SWE data from several sites were interpolated to the whole basin scale and then assimilated into the model to evaluate its influence on streamflow simulation. Three parallel experiments were designed by forcing the model using climate model output or locally observed meteorological data, both separately or together. All three experiments improved streamflow estimates in the study area. The best result was achieved by using

observed forcing data. The simulation using mixed forcing data outperformed that using atmospheric model output alone. This indicated that SWE DA can improve streamflow simulation, but the influence is mainly during the snowmelt season. Forcing data plays a more important role than SWE assimilation for these simulations. Although including multiple forcing data can improve the simulation of SWE, better SWE simulation alone does not necessarily lead to better streamflow estimates (Liu et al., 2013). Magnusson et al. (2017) assimilated snow depth into a snow model, comparing the results of two experiments using observations and reanalysis data as model forcing. Their model achieved similar SWE and snow depth estimation accuracy, but the snowpack runoff accuracy was much higher when using observations rather than reanalysis data as forcing.

Although fixed-point snow depth measurements used in the research are cheaper and more common in the field than SWE measurements, they are still not available in many remote cold regions. As well, the low sample site density creates issues in upscaling to the basin scale. Airborne remote sensing technology has made available ever more snow depth measurements with high spatial and temporal resolution (Harder et al., 2016; Painter et al., 2016). Assimilation of these snow depth measurements may contribute to a more accurate snow distribution and streamflow estimates and forecasting at regional or basin scales.

5.7 Conclusions

This research assessed the influence of data assimilation on snowpack properties and basin streamflow simulations of a coupled numerical weather forecast and physically based cold regions hydrological model in a headwater basin in the Canadian Rockies. Manual snow survey data and automatic snow depth measurement were assimilated into the coupled model using the EnKF method and simulation results were validated using local observations. Results showed that the snowpack module Snobal, in hydrological model, CRHM, tended to overestimate snowpack density. The overestimation rate decreased with increasing elevation suggesting that different assimilation strategies should be applied at different elevations to achieve the best results for SWE simulation. At low to middle elevations, where annual snow accumulation is low and CRHM heavily overestimates snowpack density, assimilating d_s or SWE independently provides little or no improvement for the SWE simulation in some years. The best results were obtained by assimilating SWE or d_s together. A similar result was achieved by assimilating ds and historical snow density estimates. At high elevation sites where annual snow accumulation is high and CRHM only slightly overestimates the snowpack density, assimilating SWE or d_s alone can achieve a close or even better result compared to assimilating SWE and d_s together. Introducing another snowpack density source is not necessary as it may not provide better results but increases uncertainty. SWE from annual snow surveys or automatic stations are not cost

effective nor available in most cold regions compared to automatic snow depth measurements that are relatively inexpensive and more common. Assimilating automatic measured snow depth is a better choice. However, the findings show that attention must be paid to the reliability of snowpack density estimates in snow models. If models cannot simulate densities well, then assimilating d_s with other, more reliable density data will be necessary. Alternative snowpack modules in CRHM in the future might provide more reliable density calculations and permit greater reliance on snow depth assimilation alone.

Snow survey SWE data were assimilated into the coupled model with results showing that assimilation of snow information can improve streamflow estimates during the snowmelt period but not generally late in the hydrological year. Another two experiments in which the hydrological model was forced by observations or mixed forcing data showed that using observations achieved much better results than using numerical weather forecasts or mixed forcing data. This indicated that assimilation of SWE can improve streamflow simulation, but the quality of forcing data also plays an important role.

CHAPTER 6: Conclusions

6.1 Overall conclusions

This research advances the understanding of observation, modelling, and data assimilation for cold regions hydrological properties and processes. With intensive data collection, data analyses, and modelling, novel snow interception measurement approaches were developed to provide input data for DA, and the roles of model structure, model input data, assimilation input data, and assimilation strategy of DA systems were analyzed to provide a better understanding of DA. These findings can advance the estimation of snow properties and snowmelt runoff in the cold regions.

The SWE product of the SNODAS system was validated in western Canadian environments (boreal forests, prairie, and mountains) for the first time, and its error sources were analyzed (Chapter 2). SNODAS overestimated SWE in all three environments, most of the time. By mimicking and then diagnosing the SNODAS system, the overestimation was found to be caused by errors in the input data for the snow model and by missing important snow redistribution processes in the model structure. Including the missing snow redistribution processes of blowing snow transport and snow interception by forest canopy can generally improve the accuracy of SNODAS SWE data. Therefore, this research recommends that these two processes be included in the SNODAS snow model.

The ability to detect canopy intercepted snow using data from optical and thermal satellite remote sensors was demonstrated for the first time (Chapter 3). The influence of canopy intercepted snow on four indices (NDSI, NDVI, albedo, LST) was analyzed. Intercepted snow clearly increases the magnitudes of NDSI and albedo, whereas it decreases those of NDVI, LST and the daily variation of canopy temperature. NDSI and NDVI together were recommended to detect intercepted snow on the canopy as they are more sensitive to the snow on the canopy than the other two indices. Using NDSI and NDVI together also avoids the prior knowledge of land cover information. This work makes the validation of snow interception modelling on a large-scale possible and provides more input data for snow interception DA.

Quantification of snowfall interception by the forest canopy using automatic snow depth measurements from an adjacent forest and clearing and the influence of DA on snow interception simulation were explored (Chapter 4). With a reliable fresh snow density estimation method, the snow depth measured from adjacent forest and clearing is able to indirectly determine snow interception quantitatively using a mass budget approach. The snow interception load estimated in this manner agreed well with the *in situ* directly measured snow interception. Indirectly estimated, directly measured, and remotely sensed (Chapter 3) snow interception information was assimilated into a

physically based snow interception, unloading, drip and sublimation routine in a cold regions hydrology model. The results indicated that these assimilations can improve the time and magnitude of snow interception simulation. The improvements are strongly influenced by the assimilating frequency and quality of forcing data for the hydrology model. This work explores using automatic snow depth measurements to quantify snowfall interception and demonstrates the benefit of snow interception DA.

Effective approaches were developed for assimilating *in situ* measured SWE and snow depth data into a physically based hydrological model to improve the simulations of snowpack properties and streamflow (Chapter 5). Assimilation of SWE and snow depth generally improves the simulation of snowpack properties and streamflow, but the results can be undesirable under certain circumstances. First, assimilating low-frequency (monthly or semi-monthly) SWE measurements alone in the shallow snowpack areas does not always improve the simulation of snowpack properties, especially in the beginning and the end of the snow season. This can be improved upon by assimilating automatically measured high-frequency snow depth data together with SWE into the model. Second, the result of assimilating snow depth data alone depends on the ability of the snow model to simulate snowpack density. Assimilating reliable snowpack density data together with snow depth can solve this problem. Third, assimilating SWE data can improve the accuracy of snowpack property simulations, but a better SWE simulation does not always lead to the better prediction of streamflow as the streamflow is also heavily influenced by the quality of meteorological forcing data, including rainfall, that drives the hydrological model. This work improves the understanding of snow DA and helps hydrologists to better design the DA framework.

6.2 Synthesis and discussion

The snowmelt runoff from the mountain areas is the main early summer water resource for many rivers in the world and hence provides critical water supply for large of the population over the surface of the Earth. With the complex topography and land over, ground snowpack observations are rare or confined in the small scale and the remote sensing data either contains substantial error or lacks of enough temporal or spatial coverage. The hydrological modelling results are always not desirable because lack of accurate meteorological forcing data as ground climate stations are sparse and weather model outputs usually have low accuracy. In a small headwater basin in the Canadian Rockies with dense snowpack and climate observations, the ground based and remotely sensed snow information was assimilated into a CRHM platform created physically base hydrological model that forcing by numerical weather prediction (GEM) outputs to achieve the better simulation of snow properties on the ground or the canopy and basin scale streamflow. This research demonstrates how to use DA to obtain optimal hydrological simulations in the mountain areas that have sparse weather stations.

The main theme of this research is to reduce the uncertainty in estimation of cold

regions hydrological processes where there is redistribution of snow by wind and forest cover, through using DAs. To achieve this goal, several studies have been conducted in two major fields throughout the present study. The first one developed novel snow property measuring techniques to provide new input data for DA (Chapter 3 and 4). The second one helped to better understand DA through analyzing DA systems that were developed by other researchers (Chapter 2) and contributing a new one (Chapter 4 and 5).

A novel approach was proposed in this research to measure snow interception on a large scale qualitatively using satellite remote sensing (Chapter 3). Using automated snow depth measurements from adjacent forest and clearing sites to quantify the snow interception on a small scale was explored (Chapter 4). Many approaches have been developed to measure snow interception qualitatively and quantitatively from single-tree to catchment scales (Friesen et al., 2015). However, measuring snow interception at a regional or larger scales was not possible before this research. Chapter 3 demonstrated that optical satellite sensors are promising tools for detecting the presence of canopy intercepted snow. This makes the validation of snow interception simulation on a large scale possible for the first time. This research should initiate further studies of snow interception measurement using satellite remote sensing in the cold regions hydrological research community. The snow interception detected using satellite data was not used in the latter DA research in Chapter 4 for two reasons. First, the data frequency was too low as there were only 56 measurements from 2007 to 2016. Second, there was no validation data for this kind of assimilation as ground-based time lapse photo derived basin-scale snow interception was only available for 2015 spring to 2016 summer. However, the ground-based time lapse photo derived snow interception was assimilated into the model at a HRU scale, and it improved simulations of the timing of snow interception. This encourages the assimilation of satellite data into the snow interception models in the future. Chapter 4 demonstrated, evaluated and clarified how automatic snow depth measurements from adjacent forest and clearing can be used to quantify snow interception magnitude in a forest. Before this research, snow interception was typically measured using direct methods using weighted, suspended whole trees; tree branches; or other artificial objects (Floyd and Weiler, 2008; Pomeroy and Schmidt, 1993; Schmidt et al., 1988; Schmidt and Gluns, 1991; Storck et al., 2002) or indirect budgeting methods that different SWE increases that measured through snow surveys (Hedstrom and Pomeroy, 1998; Gelfan et al., 2004; Pomeroy et al., 2008b) or precipitation gauges (Koivusalo and Kokkonen, 2002) between adjacent forest and clearing during the snow storm. These methods either require high maintenance or are costly. However, with a reliable fresh snow density estimation method, Chapter 4 proposed using automatic snow depth sensor, which is usually included in weather stations and is relatively cheap and requires minimum maintenance, to quantify snow interception for snow storm. The snow interception determined in this way agreed well with the measurements from a weighed, suspended tree. Although this method only provides the maximum interception for each snow storm, it improved the timing and

magnitude of snow interception simulation by assimilating these data into the snow interception model (Chapter 4).

An analysis of the performance of the SNODAS system found that it is missing important snow processes in the snow model. This along with errors in input forcing data for the snow model triggered the overestimation of SNODAS SWE data in western Canada (Chapter 2). With low assimilation frequency, missing snow processes in model have an important effect on the accuracy of SNODAS products in western Canadian environments. Error in the input data for the snow model is hard to avoid at this point. However, the missing processes could be incorporated into the snow model since many models have been developed to simulate snow interception in the forests (e.g., Hedstrom and Pomeroy, 1998) and blowing snow transport in the open areas (e.g., Pomeroy and Li, 2000). Although incorporating these processes can increase the computational cost of the DA system, it is still cheaper than collecting more observations as input data for data assimilation. Many researchers indicated that these two processes are crucial for the snow accumulation and redistribution at many regions in the U.S. (e.g., Clow et al., 2012; Miller, 1964; Montesi et al., 2004). Therefore, with limited observation for assimilation, development of a more comprehensive model should be a top priority for any DA system. Based on these findings, all the important processes were included in the model of the assimilation system used in this research (Chapters 4 and 5). Although assimilation of snow information improved simulations of snow properties on the ground and on the canopy and of streamflow, two major drawbacks were found in the DA system. The first one is that the Snobal module in the CRHM hydrological model tended to overestimate snowpack density at low to middle elevations in the Canadian Rockies (Chapter 5). Although high-quality snow depth data were assimilated alone into the model at some experiments, the SWE simulation at the middle elevation sites was degraded by DA. This indicates that researchers have to pay more attention to their models' snowpack density algorithms before assimilating snow depth into the models. The second drawback is that the highest assimilation frequency to CRHM-created models is limited to daily. This might have not affect ground snowpack properties assimilation much, but it influenced the results of canopy snow assimilation (Chapter 4). Compared to snow on the ground, intercepted snow only stays on the canopy for few hours to tens of days. Daily assimilation frequency can sometimes be too low to obtain a desirable result. Overall, DA is a useful tool, but it has its limits. The input data for DA are always limited. To better estimate the hydrological properties, researchers have to pay more attention to both their model structure and assimilation strategies when designing their DA systems.

6.3 Future work

Based on the research results of this thesis, some research opportunities have been found, and recommendations for future research are given as follows.

As shown in Chapter 2, missing processes (snow interception in the forests and blowing snow transport in open areas) in the snow model of SNODAS largely affects the accuracy of its snow products. Therefore, it is recommended that the SNODAS team include these processes in their snow model. Also, researchers have to pay more attention to their hydrological models structure when designing their DA system. In other words, researchers have to incorporate all the important hydrological processes in their models to obtain the optimal simulation of hydrological properties.

This research discovered the possibility of using satellite remote sensing to detect the presence of intercepted snow on a forest canopy. Because of lack of sufficient *in situ* data, the present study cannot measure the quantity of canopy intercepted snow using remote sensing data at this point. Although the timing of interception is important, the magnitude of interception is of the greatest interest to cold region hydrologists. Using ground snow interception magnitude to compare with the change of existing remote sensing indices such as NDSI or NDVI is one approach to quantifying snow interception. Measuring the snow interception magnitude for large areas as ground truth data for satellite data is not possible in the near future. However, the research at a single-tree scale is a good start. A weighed, hanging tree to measure the interception magnitude and a spectrometer can be used to measure the reflectance of that tree canopy during and after the snow interception process. These data can be used to study the influence of snow interception magnitude on these indices. The relationship between the changes of intercepted snow magnitude and these indices can be used to determine the intercepted snow magnitude using remote sensing data. Another direction is to develop a new index based on the theory of determining the LAI using remote sensing data. LAI shows the leaf area in a canopy. With snow on the canopy, the area of the projected canopy can be modified; hence, LAI will be changed. With the theory of LAI and *in situ* snow interception measurements, statistical (or empirical) and physical approaches can be developed to determine the quantity of snow interception using remote sensing data.

Owing to the low data availability, the satellite remote-sensing-derived snow interception information from Chapter 3 was not included in the DA in Chapter 4. The data gaps can be filled by introducing more satellite data, such as MODIS or Sentinel 2, in the future DA research. Assimilation of these satellites' data could improve the simulation accuracy of snow interception on a large scale. In Chapter 4, the snow depth data were only used to quantify snow interception magnitude and these data were assimilated into the model to update the snow interception state. Another way of using these snow depth data is to assimilate them directly into the model to adjust the precipitation through reverse modeling. This will not only benefit the snow interception simulation but also contribute to the simulation of snowpack on the ground.

Due to strong winter winds, drone-based snow measurements are sparse in the research basin for the current study. Therefore, Chapter 5 only assimilated the HRU-scale SWE

and snow depth data into the model. Although the results are promising, better results can be obtained if basin-scale snow measurements are available for assimilation. With the development of airborne remote sensing technology, more and more areal snow measurements are available (Harder et al., 2016; Paiter et al., 2016). Assimilating these observations into a hydrological model could improve the snow properties and streamflow simulation. Before assimilating these snow depth data, researchers have to make sure the snowpack density algorithm is able to simulate density with reasonable accuracy. For example, the snowpack density algorithm in the Snobal needs to be upgraded for future DA work.

New snow data assimilation systems need to be built for operational use. These systems should include snow interception and redistribution processes and take advantage of advances in remote sensing and surface observation found in this thesis. Snow interception can be detected using remote sensing. Interception losses can be estimated using remote sensing and surface observations of fresh snow depth if fresh snow density can be estimated accurately. These data should be included in the input data set for new DA systems to improve the simulation accuracy of snow interception on the forest canopy and snowpack on the forest floor. Snow data assimilation can be improved by using high frequency snow depth along with low frequency SWE observations, if snowpack density can be estimated accurately. More accurate snow density algorithm should be developed for the purpose of assimilating snow depth data considering more and more areal snow depth observations are available from LiDAR or other meaurements. However, snow DA alone cannot overcome poor forcing data for streamflow prediction, even in snowmelt dominated mountain basins. Therefore, there is need for more accurate climate model products for better simulation of stream flow through DA.

Reference

Abbott, M.B., Bathurst, J.C., Counge, J.A, O'Connell, P.E., and Rasmussen, J., 1986. An introduction to the European Hydrological System - System Hydrologique Europeen 'SHE': 2. Structure of the physically based, distributed modeling system. Journal of Hydrology, 87, 61-77.

Anderson, B., 2011. Spatial distribution and evolution of a seasonal snowpack in complex terrain: an evaluation of the SNODAS modeling product. Master's Thesis. Boise State University, Boise Idaho, United States.

Anderson, E.A., 1973. National weather service river forecast system—snow accumulation and ablation model. NOAA Technical Memorandum. NWS HYDRO-17, 217 pp.

Andreadis, K.M., Storck, P., and Lettenmaier, D.P., 2009. Modeling snow accumulation and ablation processes in forested environments. Water Resources Research, 45, W05429. doi:10.1029/2008WR007042.

Andreadis, K.M. and Lettenmaier, D.P., 2006. Assimilating remotely sensed snow observations into a macroscale hydrology model. Advances in Water Resources, 29, 872–886.

Artan, G.A., Verdin, J.P., and Lietzow, R., 2013. Large scale snow water equivalent status monitoring: comparison of different snow water products in the upper Colorado Basin. Hydrology and Earth System Sciences, 17, 5127–5139. doi:10.5194/hess-17-5127-2013.

Ayers, H.D., 1959. Influence of soil profile and vegetation characteristics on net rainfall supply to runoff. In: Proceedings of Hydrology Symposium No. 1: Spillway Design Floods. National Research Council Canada, Ottawa, pp. 198 – 205.

Azar, A.E., Ghedira, H., Romanov, P., Mahani, S., Tedesco, M., and Khanbilvardi, R., 2008. Application of satellite microwave images in estimating snow water equivalent. Journal of the American Water Resources Association, 44, 1347–1362. doi: 10.1111/j.1752-1688.2008.00227.x

Baldocchi, D.D., Vogel, C.A., and Hall, B., 1997. Seasonal variation of energy and water vapour exchange rates above and below a boreal jack pine forest canopy. Journal of Geophysical Research, 102 (D24), 28,939–28,951.

Bales, R.C., Hopmans, J.W., O'Geen, A.T., Meadows, M., Hartsough, P.C., Kirchner, P., Hunsaker, C.T., and Beaudette, D., 2011. Soil moisture response to snowmelt and rainfall in a Sierra Nevada mixed-conifer forest. Vadose Zone Journal, 10, 786 – 799. doi:10.2136/vzj2011.0001.

Barlage, M., Chen, F., Tewari, M., Ikeda, K., Gochis, D., Dudhia, J., Rasmussen, R., Livneh, B., Ek, M., and Mitchell, K., 2010. Noah land surface model modifications to improve snowpack prediction in the Colorado Rocky Mountains. Journal of Geophysical Research, 115. doi: 10.1029/2009JD013470.

Barr, A.G., Black, T.A., Hogg, E.H., Kljun, N., Morgenstern, K., and Nesicm, Z., 2004. Inter-annual variability in the leaf area index of a boreal aspen-hazelnut forest in relation to net ecosystem production. Agricultural and Forest Meteorology, 126, 237–255. doi: 10.1016/j.agrformet.2004.06.011.

Barr, A.G., van der Kamp, G., Black, T.A., McCaughey, J.H., and Nesic, Z., 2012. Energy balance closure at the BERMS flux towers in relation to the water balance of the White Gull Creek watershed 1999–2009. Agricultural and Forest Meteorology, 153, 3–13.

Barrett, A.P., 2003. National Operational Hydrologic Remote Sensing Center SNOw Data Assimilation System (SNODAS) products at NSIDC. Number 11 special report of National Snow and Ice Data Center.

Barnett, T.P., Pierce, D.W., Hidalgo, H.G., Bonfils, C., Santer, B.D., Das, T., Bala, G., Wood, A.W., Nozawa, T., Mirin, A.A., Cayan, D.R., and Dettinger, M.D., 2008. Human-induced changes in the hydrology of the western United States. Science, 319(5866), 1080–1083.

Barsi, J.A., Barker, J.L., and Schott, J.R., 2003. An atmospheric correction parameter calculator for a single thermal band earth-sensing instrument. In: Proceedings of the IEEE International Geoscience and Remote Sensing Symposium, (IGARSS'03), Toulouse, France, 21 – 25 July, pp. 3014 – 3016.

Bartlett, P.A., MacKay, M.D. and Verseghy, D.L., 2006. Modified snow algorithms in the Canadian land surface scheme: Model runs and sensitivity analysis at three boreal forest stands. Atmosphere-Ocean, 44(3), 207-222.

Bavay, M., Lehning, M., Jonas, T., and Löwe, H., 2009. Simulations of future snow cover and discharge in Alpine headwater catchments, Hydrological Processes, 23(1), 95–108.

Bergeron, J.M., Trudel, M., and Leconte, R., 2016. Combined assimilation of streamflow and snow water equivalent for mid-term ensemble streamflow forecasts in snow-dominated regions. Hydrology and Earth System Sciences, 20, 4375–4389. doi:10.5194/hess-20-4375-2016.

Beven, K., Warren, R., and Zaoui, J., 1980. SHE: towards a methodology for physically-based distributed forecasting in hydrology. In: Hydrological Forecasting, Proc. Symposium International Association of Hydrological Sciences, Oxford. IAHS Publ. No. 129, pp. 133-137.

Boon, S., 2009. Snow ablation energy balance in a dead forest stand. Hydrological Processes. doi:10.1002/hyp.7246.

Boyle, D.P., Barth, C., and Bassett, S., 2014. "Towards Improved Hydrologic Model Predictions in Ungauged Snow-Dominated Watersheds Utilizing a Multi-Criteria Approach and SNODAS Estimates of SWE," in Putting PUB (Predictions in Ungauged Basins) into Practice, edited by J. Pomeroy, C. Spence, and P. Whitfield, Red Book monograph published by the International Association of Hydrological Sciences and the Canadian Water Resources Association.

Brazenec, W.A., 2005. Evaluation of ultrasonic snow depth sensors for automated surface observing systems (ASOS). Thesis (MS). Colorado State University, Fort Collins, Colorado, 124 pp.

Cambell Scientific, 2009. SR50A sonic ranging sensor, instruction manual. Logan, UT: Campbell Scientific Canada Corp., 42 pp.

Carroll, T., Cline, D., Fall, G., Nilsson, A., Li, L., and Rost, A., 2001. NOHRSC operations and the simulation of snow cover properties for the conterminous U.S. Proceedings of the 69th Annual Meeting of the Western Snow Conference, 1-14.

Carroll, T.R., Cline, D.W., Olheiser, C., Rost, A., Nilsson, A., Fall, G., Bovitz, C., and Li, L., 2006. NOAA's national snow analyses. Proceedings of the 74th Annual Meeting of the Western Snow Conference, 74, 13.

Chow, V.T., 1964. Handbook of Applied Hydrology. McGraw-Hill, Inc, New York.

Clark, M.P., Slater, A.G., Barrett, A.P., Hay, L.E., McCabe, G.J., Rajagopalan, B., and Leavesley, G. H., 2006. Assimilation of snow covered area information into hydrologic and land-surface models. Advances in Water Resources, 29, 1209-1221.

Clark, M.P., Rupp, D.E., Woods, R.A., Zheng, X., Ibbitt, R.P., Slater, A.G., Schmidt, J., and Uddstrom, M.J., 2008. Hydrological data assimilation with the ensemble Kalman

filter: Use of streamflow observations to update states in a distributed hydrological model. Advances in Water Resources, 31, 1309–1324.

Clow, D.W., Nanus, L., Verdin, K.L., and Schmidt, J., 2012. Evaluation of SNODAS snow depth and snow water equivalent estimates for the Colorado Rocky Mountains, USA. Hydrological Processes. doi: 10.1002/hyp.9385.

DeBeer, C.M., and Pomeroy, J.W., 2009. Simulation of the snowmelt runoff contributing area in a small alpine basin. Hydrology and Earth System Sciences, 14 (7), 1205–1219.

DeBeer, C.M., and Pomeroy, J.W., 2010. Simulation of the snowmelt runoff contributing area in a small alpine basin. Hydrology and Earth System Sciences, 14, 1205–1219.

DeBeer, C.M., Wheater, H.S., Quinton, W., Carey, S.K., Stewart, R., MacKay, M., and Marsh, P., 2015. The Changing Cold Regions Network: Observation, diagnosis and prediction of environmental change in the Saskatchewan and Mackenzie River Basins, Canada. Science China Earth Sciences, 58, 46-60. doi: 10.1007/s11430-014-5001-6.

Dechant, C. and Moradkhani, H., 2011. Radiance data assimilation for operational snow and streamflow forecasting. Advances in Water Resources, 34, 351–364.

De Lannoy, G.J.M., Reichle, R.H., Arsenault, K.R., Houser, P.R., Kumar, S., Verhoest, N.E.C., and Pauwels, V.R.N., 2012. Multiscale assimilation of Advanced Microwave Scanning Radiometer-EOS snow water equivalent and Moderate Resolution Imaging Spectroradiometer snow cover fraction observations in northern Colorado. Water Resources Research, 48, W01522. doi:10.1029/2011wr010588.

D'Eon, R., 2004. Snow depth as a function of canopy cover and other site attributes in a forested ungulate winter range in Southeast British Columbia. BC Journal of Ecosystems and Management, 3, 1 – 9.

Derksen, C., Walker, A., and Goodison, B., 2003. A comparison of 18 winter seasons of in situ and passive microwave derived snow water equivalent estimates in western Canada. Remote Sensing of Environment, 88, 271–282.

Doesken, N.J. and Judson, A., 1996. The Snow Booklet: A Guide to the Science, Climiatology, and Measurements of Snow in the United States. 2nd ed. Fort Collins, Colorado: Colorado Climate Center.

Dornes, P.F., Pomeroy, J.W., Pietroniro, A., Carey, S.K., and Quinton, W.L., 2008. Influence of landscape aggregation in modelling snow-cover ablation and snowmelt

runoff in a sub-arctic mountainous environment. Hydrological Sciences Journal, 53, 725 – 740.

Dozier, J., 1989. Remote sensing of snow in visible and near infrared wavelengths. In: Asrar, G. (Ed.), Theory and Applications of Optical Remote Sensing, pp. 527 – 547 (New York).

Dozier, J., Bair, E.H., and Davis, R.E., 2016. Estimating the spatial distribution of snow water equivalent in the world's mountains. WIREs Water, 3, 461-474. doi:10.1002/wat2.1140.

Durand, M., Kim, E.J., and Margulis, S.A., 2009, Radiance assimilation shows promise for snowpack characterization. Geophysics Research Letters, 36, L02503. doi:10.1029/2008GL035214.

Egli, L., Jonas, T., and Meister, R., 2009. Comparison of different automatic methods for estimating snow water equivalent. Cold Regions Science and Technology, 57 (2–3), 107–115. doi:10.1016/j.coldregions.2009.02.008.

Elder, K., Dozier, J. and Michaelsen, J., 1991. Snow accumulation and distribution in an alpine watershed. Water Resources Research, 27, 1541-1552.

Ellis, C.R., Pomeroy, J.W., Brown, T., and MacDonald, J.P., 2010. Simulation of snow accumulation and melt in needleleaf forest environments. Hydrology and Earth System Sciences, 14, 925-940. doi: 10.5194/hess-14-925-2010.

Ellis, C.R., Pomeroy, J.W., Link, T.E., 2013. Modeling increases in snowmelt yield and desynchronization resulting from forest gap-thinning treatments in a northern mountain headwater basin. Water Resources Research, 49, 936–949. doi:10.1002/wrcr.20089.

Essery, R.L.H., Pomeroy, J.W., Parviainen, J., and Storck, P., 2003. Sublimation of snow from coniferous forests in a climate model. Journal of Climate, 16, 1855 – 1864.

Evensen, G., 1994. Sequential data assimilation with a nonlinear quasi- geostrophic model using Monte Carlo methods to forecast error statistics. Journal of Geophysical Research, 99, 10 143–10 162.

Evensen, G., 2003. The Ensemble Kalman Filter?: theoretical formulation and practical implementation. Ocean Dynamics, 53, 343–367. doi:10.1007/s10236-003-0036-9.

Fall, G., Olheiser, C., and Rost, A., 2014. SNODAS Assimilation from 2004-2014: Qualifications as a Reference Analysis. 1st Annual Satellite Snow Products Intercomparison Workshop. Available online:

http://calvalportal.ceos.org/documents/10136/404316/Greg_Fall_ISSPI_20140722_brief.pdf

Fang, X. and Pomeroy, J.W., 2009. Modelling blowing snow redistribution to Prairie wetlands. Hydrological Processes, 23, 2557–2569. doi:10.1002/hyp.7348.

Fang, X. and Pomeroy, J.W., 2016. Impact of antecedent conditions on simulations of a flood in a mountain headwater basin. Hydrological Processes, 30, 2754-2772.

Fang, X., Pomeroy, J.W., Ellis, C.R., MacDonald, M.K., DeBeer, C.M., and Brown, T., 2013. Multi-variable evaluation of hydrological model predictions for a headwater basin in the Canadian Rocky Mountains. Hydrology and Earth System Sciences, 17, 1635–1659. doi:10.5194/hess-17-1635-2013.

Fang, X., Pomeroy, J.W., Westbrook, C., Guo, X., Minke, A., and Brown, T., 2010. Prediction of snowmelt derived streamflow in a wetland dominated prairie basin. Hydrology and Earth System Sciences, 14, 991–1006.

Faria, D., Pomeroy, J.W. and Essery, R.L.H., 2000. Effect of covariance between ablation and snow water equivalent on depletion of snow-covered area in a forest. Hydrological Processes, 14, 2683-2695.

Floyd, W. and Weiler, M., 2008. Measuring snow accumulation and ablation dynamics during rain-on-snow events: innovative measurement techniques. Hydrological Processes, 22, 4805–4812. doi: 10.1002/ hyp.7142.

Franz, K.J., Hogue, T.S., Barik, M., and He, M., 2014. Assessment of SWE data assimilation for ensemble streamflow predictions. Journal of Hydrology, 519, 2737–2746.

Frei, A., Tedesco, M., Lee, S., Foster, J., Hall, D.K., Kelly, R., and Robinsonf, D.A., 2012. A review of global satellite-derived snow products. Advances in Space Research, 50, 1007–1029.

Friesen, J., Lundquist, J., and Van Stan, J.T., 2015. Evolution of forest precipitation water storage measurement methods. Hydrological Processes, 29, 2504–2520.

Friesen, J., Van, B.C., Selker, J., Savenije, H.H.G., and van De Giesen, N., 2008. Tree rainfall interception measured by stem compression. Water Resources Research, 44, 1 – 5.

Garnier, B.J. and Ohmura, A., 1970. The evaluation of surface variations in solar radiation income. Solar Energy, 13, 21-34.

Garvelmann, J., Pohl, S., and Weiler, M., 2013. From observation to the quantification of snow processes with a time-lapse camera network. Hydrology and Earth System Sciences, 17, 1415–1429.

Gelfan, A.N., Pomeroy, J.W., and Kuchment, L.S., 2004. Modeling forest cover influences on snow accumulation, sublimation, and melt. Journal of Hydrometeorology, 5, 785– 803.

Golding, D., and Swanson, R., 1986. Snow distribution patterns in clearings and adjacent forest. Water Resources Research, 22 (13), 1931 – 1940.

Gomez-Landsea, E. and Rango, A., 2002. Operational snowmelt runoff forecasting in the Spanish Pyrenees using the snowmelt runoff model. Hydrological Processes, 16, 1583–1591.

Goodell, B.C., 1959. Management of forest stands in western United States to influence the flow of snow-fed streams. International Association of Scientific Hydrology, Publication 48, 49–58.

Goodison, B.E., Ferguson, H.L., and McKay. G.A., 1981. 'Measurement and data analysis', in Gray. D.M. and Male. D.H. (eds), Handbook of snow: Principles, Processes, Management and Use. Pergamon Press. New York, pp. 191-274.

Granger, R.J., and Gray, D.M., 1989. Evaporation from natural nonsaturated surfaces. Journal of Hydrology, 111, 21 – 29.

Granger, R.J., and Gray, D.M., 1990. A new radiation model for calculating daily snowmelt in open environments. Nordic Hydrology, 21, 217 – 234.

Granger, R.J., and Pomeroy, J.W., 1997. Sustainability of the western Canadian boreal forest under changing hydrological conditions – 2 – Summer energy and water use. In: Rosjberg, D., Boutayeb, N., Gustard, A., Kundzewicz, Z., Rasmussen, P. (Eds.), Sustainability of Water Resources under Increasing Uncertainty. IAHS Publication No. 240 IAHS Press, Wallingford, UK, pp. 243 – 250.

Gray, D.M., and Landine, P.G., 1988. An energy budget snowmelt model for the Canadian Prairies. Canadian Journal of Earth Sciences, 25, 1292-1303.

Gray, D.M. and Male, D.H., 1981. Handbook of Snow: Principles, Processes, Management and Use. Pergamon Press, Toronto.

Gray. D.M., Norum, D.I., and Dyck. G.E., 1970. 'Densities of prairie snowpacks', Proc.

38th Annual Meeting Western Snow Conference. pp. 24-30.

Groisman, P.Y., and Davies, T.D., 2001. Snow cover and the climate system, in Snow Ecology, edited by H. G. Jones et al., pp. 1 – 44, Cambridge Univ. Press, New York.

Grünewald, T., Stötter, J., Pomeroy, J.W., Dadic, R., Moreno Baños, I., Marturià, J., Spross, M., Hopkinson, C., Burlando, P., and Lehning, M., 2013. Statistical modelling of the snow depth distribution in open alpine terrain. Hydrology and Earth System Sciences, 17, 3005-3021. doi:10.5194/hess-17-3005-2013.

Gubler, H. and Rychetnik, J., 1991. Effects of forests near the timberline on avalanche formation. In. Snow, Hydrology and Forests in High Alpine Areas proceedings of the Vienna Symposium, August, 199 1). IAHS Publ. No. 205. IAHS Press, Wallingford, UK. 19-38.

Hall, D.K., Riggs, G.A., and Salomonson, V.V., 1995. Development of methods for mapping global snow cover using moderate resolution imaging spectroradiometer data. Remote Sensing of Environment, 54, 127 – 140.

Harder, P., Helgason, W.D., and Pomeroy, J.W., 2018. Modelling the snow-surface energy balance during melt under exposed crop stubble. Journal of Hydrometeorology, 19, 1191 – 1214. doi:10.1175/JHM-D-18-0039.1.

Harder, P. and Pomeroy, J.W., 2013. Estimating precipitation phase using a phycrometric energy balance method. Hydrological Processes, 27, 1901–1914. doi:10.1002/hyp.9799.

Harder, P., Schirmer, M., Pomeroy, J., and Helgason, W., 2016. Accuracy of snow depth estimation in mountain and prairie environments by an unmanned aerial vehicle. The Cryosphere, 10, 2559-2571. doi: 10.5194/tc-10-2559-2016.

Harding, R.J., and Pomeroy, J.W., 1996. The energy balance of a winter boreal landscape. Journal of Climate, 9, 2778 – 2787.

Harer, S., Bernhardt, M., Corripio, J.G., and Schulz, K., 2013. PRACTISE – photo rectification and classification software (v.1.0). Geoscientific Model Development, 6(3), 837 – 848.

Harshburger, B. J., Humes, K. S., Walden, V. P., Blandford, T. R., Moore, B. C., and Dezzani, R. J., 2010. Spatial interpolation of snow water equivalency using surface observations and remotely sensed images of snow-covered area. Hydrological Processes, 24, 1285– 1295. doi:10.1002/hyp.7590.

He, M., Hogue, T.S., Margulis, S.A., and Franz, K.J., 2012. An integrated uncertainty and ensemble-based data assimilation approach for improved operational streamflow predictions. Hydrology and Earth System Sciences, 16(3), 815–831. doi:10.5194/hess-16-815-2012.

Hedrick, A.R., Marks, D., Havens, S., Robertson, M., Johnson, M., Sandusky, M., Marshall, H-P., Kormos, P.R., Bormann, K.R., and Painter, T.H., 2018. Direct insertion of NASA Airborne Snow Observatory-derived snow depth time series into the iSnobal energy balance snow model. Water Resources Research, 54. doi:10.1029/2018WR023190.

Hedrick, A., Marshall, H.P., Winstral, A., Elder, K., Yueh, S., and Cline, D., 2015. Independent evaluation of the SNODAS snow depth product using regional-scale lidar-derived measurements. The Cryosphere, 9, 13-23. doi:10.5194/tc-9-13-2015.

Hedstrom, N.R., and Pomeroy, J.W., 1998. Measurement and modelling of snow interception in the boreal forest. Hydrological Processes, 12, 1611 –1625.

Heinila, K., Salminen, M., Pulliainen, J., Cohen, J., Metsamaki, S., and Pellikka, P., 2014. The effect of boreal forest canopy to reflectance of snow covered terrain based on airborne imaging spectrometer observations. International Journal of Applied Earth Observation and Geoinformation, 27, 31 – 41.

Helfricht, K., Hartl, L., Koch, R., Marty, C., and Olefs, M., 2018. Obtaining sub-daily new snow density from automated measurements in high mountain regions. Hydrology and Earth System Sciences, 22(5), 2655.

Hogg, E.H., Black, T.A., den Hartog, G., Neumann, H.H., Zimmerman, R., Hurdle, P., Blanken, P.D., Nesic, Z., Yang, P.C., Staebler, R.M., McDonald, K.C., and Oren, R., 1997. A comparison of sap flow and eddy fluxes of water vapour from a boreal deciduous forest (BOREAS Special Issue). Journal of Geophysical Research, 102 (D24), 28,929–28,937.

Horton, P., Schaefli, B., Mezghani, A., Hingray, B., and Musy, A., 2006 Assessment of climate-change impacts on alpine discharge regimes with climate model uncertainty. Hydrological Processes, 20(10), 2091–2109.

Huang, C.C., Newman, A.J., Clark, M.P., Wood, A.W., and Zhang, X., 2017. Evaluation of snow data assimilation using the ensemble Kalman filter for seasonal streamflow prediction in the western United States. Hydrology and Earth System Sciences, 21, 635–650.

Jimenez-Munoz, J.C., Sobrino, J.A., Skokovic, D., Mattar, C., and Cristobal, J., 2014.

Land surface temperature retrieval methods from Landsat-8 thermal infrared sensor data. IEEE Transactions on Geoscience and Remote Sensing. 11, 1840 – 1843.

Jonas, T., Marty, C., and Magnusson, J., 2009. Estimating the snow water equivalent from snow depth measurements in the Swiss Alps. Journal of Hydrology, 378, 161–167.

Jordan, R., 1990. User's Guide for USACRREL One-Dimensional Snow Temperature Model (SNTHERM.89). U.S. Army Cold Regions Research and Engineering Laboratory, Hanover, New Hampshire.

Jordan, R.E., Andreas, E.L., and Makshtas, A.P., 1999. Heat budget of snow-covered sea ice at North Pole 4. Journal of Geophysical Research, 104 (C4), 7785–7806. doi:10.1029/1999JC900011.

Kays, R.W., Gompper, M.E., and Ray, J.C., 2008. Landscape ecology of eastern coyotes based on large-scale estimates of abundance. Ecological Applications, 18, 1014–1027.

Ke, Y., Im, J., Park, S., and Gong, H., 2016. Downscaling of MODIS one kilometer evapotranspiration using Landsat-8 data and machine learning approaches. Remote Sensing, 8, 215.

Kittredge, J., 1953. Influence of forests on snow in the ponderosa-sugar pine-fir zone of the central Sierra Nevada. Hilgardia, 22, 1– 96.

Kinar, N.J., and Pomeroy, J.W., 2015. Measurement of the physical properties of the snowpack. Reviews of Geophysics, 53, 2, 481–544.

Klein, A.G., Hall, D.K., and Riggs, G.A., 1998. Improving snow cover mapping in forests through the use of a canopy reflectance model. Hydrological Processes, 12, 1723 – 1744.

Knoche, M., Fischer, C., Pohl, E., Krause, P., and Merz, R., 2014. Combined uncertainty of hydrological model complexity and satellite-based forcing data evaluated in two data-scarce semi-arid catchments in Ethiopia. Journal of Hydrology, 519, 2049–2066. doi:10.1016/j.jhydrol.2014.10.003

Koivusalo, H. and Kokkonen, T., 2002. Snow processes in a forest clearing and in a coniferous forest. Journal of Hydrology, 262(1–4), 145–164. doi:10.1016/S0022-1694(02)00031-8.

Krogh S.A. and Pomeroy J.W., 2018. Recent changes in the hydrological cycle of an Arctic basin at the tundra-taiga transition. Hydrology and Earth System Sciences, 22, 3993-4014. doi: 10.5194/hess-22-3993-2018.

Kuchment, L.S, Gelfan, A.N, and Demidov, V.N., 2000. A distributed model of runoff generation in the permafrost regions. Journal of Hydrology, 240, 1–22.

Kuchment, L.S., Romanov, P., Gelfan, A.N., and Demidov, V.N., 2010. Use of satellite-derived data for characterization of snow cover and simulation of snowmelt runoff through a distributed physically based model of runoff generation. Hydrology and Earth System Sciences, 14, 339–350.

Kumar, S.V., Dong, J., Peters-Lidard, C.D., Mocko, D., and Gómez, B., 2017. Role of forcing uncertainty and background model error characterization in snow data assimilation. Hydrology and Earth System Sciences, 21(6), 2637–2647.

Kumar, S., Koster, R., Crow, W., and Peters-Lidard, C., 2009. Role of subsurface physics in the assimilation of surface soilmoisture observations. Journal of Hydrometeorology, 10, 1534–1547. doi:10.1175/2009JHM1134.1.

Kumar, S., Peters-Lidard, C., Mocko, D., Reichle, R., Liu, Y., Arsenault, K., Xia, Y., Ek, M., Riggs, G., Livneh, B., and Cosh, M., 2014. Assimilation of remotely sensed soil moisture and snow depth retrievals for drought estimation. Journal of Hydrometeorology, 15, 2446–2469. doi:10.1175/JHM-D-13-0132.1.

Kuusinen, N., Kolari, P., Levula, J., Porcar-Castell, A., Stenberg, P., and Berninger, F., 2012. Seasonal variation in boreal pine forest albedo and effects of canopy snow on forest reflectance. Agricultural and Forest Meteorology, 164, 53 – 60.

Kuz'min, P.P., 1960. Formirovanie Snezhnogo Pokrova i Metody Opredeleniya Snegozapasov. Gidrometeoizdat: Leningrad. Published 1963 as Snow Cover and Snow Reserves. [English Translation by Israel Program for Scientific Translation, Jerusalem]. National Science Foundation: Washington, DC. 139.

Leonard, R.E., and Eschner, A.R., 1968. Albedo of intercepted snow. Water Resources Research, 4, 931 – 935.

Liang, S., 2000. Narrow to broadband conversion of land surface albedo I: algorithms. Remote Sensing of Environment, 76, 213 – 238.

Liston, G.E., Haehnel, R.B., Sturm, M., Hiemstra, C.A., Berezovskaya, S., and Tabler, R.D., 2007. Simulating complex snow distributions in windy environments using SnowTran-3D. Journal of Glaciology, 53, 241–256.

Liston, G.E. and Hiemstra, C.A., 2007. A simple data assimilation system for complex snow distributions (SnowAssim). Journal of hydrometeorology, Oct, 989-1004.

Liston, G.E., Pielke Sr., R.A., and Greene, E.M., 1999. Improving first-order snow related deficiencies in a regional climate model. Journal of Geophysical Research, 104, 19559– 19567.

Liu, Y., Peters-Lidard, C., Kumar, S., Foster, J., Shaw, M., Tian, Y., and Fall, G., 2013. Assimilating satellite-based snow depth and snow cover products for improving snow predictions in Alaska. Advances in Water Resources, 54, 208–227. doi:10.1016/j.advwatres.2013.02.005.

Liu, Y., Weerts, A.H., Clark, M., Hendricks Franssen, H.-J., Kumar, S., Moradkhani, H., Seo, D.-J., Schwanenberg, D., Smith, P., van Dijk, A.I.J.M., van Velzen, N., He, M., Lee, H., Noh, S.J., Rakovec, O., and Restrepo, P., 2012. Advancing data assimilation in operational hydrologic forecasting: progresses, challenges, and emerging opportunities. Hydrology and Earth System Sciences, 16, 3863–3887. doi:10.5194/hess-16-3863-2012.

López-Moreno, J. I. and Stähli, M., 2008. Statistical analysis of the snow cover variability in a subalpine watershed: Assessing the role of topography and forest interactions. Journal of Hydrology, 348(3–4), 379-394. doi:10.1016/j.jhydrol.2007.10.018.

Lundberg, A., 1993. Measurement of intercepted snow-review of existing and new measurement methods. Journal of Hydrology, 151, 267 – 290.

Lundberg, A., Calder, I., and Harding, R., 1998. Evaporation of intercepted snow – measurements and modelling. Journal of Hydrology, 206, 151–163.

Lundberg, A. and Halldin, S., 1994. Evaporation of intercepted snow: Analysis of governing factors. Water Resources Research, 30(9): 2587– 2598.

Lundquist, J.D., and Lott, F., 2008. Using inexpensive temperature sensors to monitor the duration and heterogeneity of snow-covered areas. Water Resources Research, 44, W00D16. doi:10.1029/2008WR007035.

Lv, Z. and Pomeroy, J.W., 2019a. Detecting intercepted snow in the coniferous forest by using satellite remotely sensed data. Remote Sensing of Environment, 231. doi:10.1016/j.rse.2019.111222.

Lv, Z., and Pomeroy, J.W., 2019b. The influence of snow data assimilation on the performance of a coupled numerical weather forecast and physically based cold regions hydrological model. Water resources research. Under review.

Magnusson, J., 2006. Snow interception measurements using impulse radar. Master's Thesis. Uppsala University, Uppsala, Sweden.

Magnusson, J., Winstral, A., Stordal, A. S., Essery, R., and Jonas, T., 2017. Improving physically based snow simulations by assimilating snow depths using the particle filter. Water Resources Research, 53, 1125–1143. doi:10.1002/2016WR019092.

MacDonald, M.K., Pomeroy, J.W., and Pietroniro, A., 2010. On the importance of sublimation to an alpine snow mass balance in the Canadian Rocky Mountains. Hydrology and Earth System Sciences, 14, 1401-1415. doi: 10.5194/hess-14-1401-2010.

Magnusson, J., Winstral, A., Stordal, A.S., Essery, R., and Jonas, T., 2017. Improving physically based snow simulations by assimilating snow depths using the particle filter. Water Resources Research, 53, 1125–1143. doi:10.1002/2016WR019092.

Mair, E., Leitinger, G., Della Chiesa, S., Niedrist, G., Tappeiner, U. and Bertoldi, G., 2016. A simple method to combine snow height and meteorological observations to estimate winter precipitation at sub-daily resolution. Hydrological Sciences Journal, 61(11), 2050-2060. doi: 10.1080/02626667.2015.1081203

Marks, D., Kimball, J., Tingey, D., and Link, T., 1998. The sensitivity of snowmelt processes to climate conditions and forest cover during rain-on-snow: a case study of the 1996 Pacific Northwest flood. Hydrological Processes, 12, 1569-1587.

Marks, D., Reba, M., Pomeroy, J.W., Link, T.E., Winstral, A., Flerchinger, G. and Elder, K. 2008. Comparing Simulated and Measured Sensible and Latent Heat Fluxes over Snow under a Pine Canopy to Improve an Energy Balance Snowmelt Model. Journal of Hydrometeorology, 9, 1506-1522. doi: 10.1175/2008JHM874.1

Marsh, C.B., Pomeroy, J.W., and Spiteri, R., 2012. Implications of mountain shading on calculating energy for snowmelt using unstructured triangular meshes. Hydrological Processes, 26, 1767 – 1778. doi:10.1002/hyp.9329.

Martin, K.A., Van Stan, J.T., Dickerson-Lange, S.E., Lutz, J.A., Berman, J.W., Gersonde, R., and Lundquist, J.D., 2013. Development and testing of a snow interceptometer to quantify canopy water storage and interception processes in the rain/snow transition zone of the North Cascades, Washington, USA. Water Resources Research, 49, 3243– 3256.

McLaughlin, D., O'Neill, A., Derber, J., and Kamachi, M., 2005. Opportunities for enhanced collaboration within the data assimilation community. Quarterly Journal of the Royal Meteorological Society, 131, 3683-3693.

McNay, R., Peterson, L., and Nyberg, B., 1988. The influence of forest stand characteristics on snow interception in the coastal forests of British Columbia. Canadian Journal of Forest Research, 18, 566 – 573.

Meloysund, V., Leira, B., Hoiseth, K.V., and Liso, K.R., 2017. Predicting snow density using meteorological data. Meteorological Applications, 14 (4), 413–423.

Miller, D.H., 1964. Interception processes during snow storms. Tech. Rep. PSW-18, Pac. Southwest For. and Range Exp. Stn., For. Serv., U.S. Dep. of Agric., Berkeley, Calif, 24 pp.

Millington, J.D.A., Walters, M.B., Matonis, M.S., and Liu, J., 2010. Effects of local and regional landscape characteristics on wildlife distribution across managed forests. Forest Ecology and Management, 259, 1102–1110. doi: 10.1016/j.foreco.2009.12.020

Moeser, D., Stähli, M., and Jonas, T., 2015. Improved snow interception modeling using canopy parameters derived from airborne LiDAR data. Water Resources Research, 51, 5041–5059. doi:10.1002/2014WR016724.

Momeni, M., and Saradjian, M., 2007. Evaluating NDVI-based emissivities of MODIS bands 31 and 32 using emissivities derived by day/night LST algorithm. Remote Sensing of Environment, 106, 190 – 198.

Montesi, J., Elder, K., Schmidt, R.A., and Davis, R.E., 2004. Sublimation of intercepted snow within a subalpine forest canopy at two elevations. Journal of Hydrometeorology, 5, 763–773.

Moradkhani, H., 2008. Hydrologic remote sensing and land surface data assimilation. Sensors, 8, 2986-3004.

Muniz, P.R., de Araujo Kalid, R., Cani, S.P.N., and da Silva Magalhaes, R., 2014. Handy method to estimate uncertainty of temperature measurement by infrared thermography. Optical Engineering, 53, 074101. doi:10.1117/1.OE.53.7.074101.

Musselman, K.N., Clark, M.P., Liu, C., Ikeda, K., and Rasmussen, R., 2017. Slower snowmelt in a warmer world. Nature Climate Change, 7(3), 214–219.

Musselman, K.N., and Pomeroy, J.W., 2017. Estimation of needleleaf canopy and trunk temperatures and longwave contribution to melting snow. Journal of Hydrometeorology. doi:10.1175/JHM-D-16-0111.1.

Naglar, T., Rott, H., Malcher, P., and Muller, F., 2008. Assimilation of meteorological

and remote sensing data for snowmelt runoff forecasting. Remote Sensing of Environment, 112, 1408–1420.

Nakai, Y., Sakamoto, T., Terajima, T., Kitahara, H., and Saito, T., 1994. Snow interception by forest canopies: weighing a conifer tree, meteorological observation and analysis by the Penman-Monteith formula, Snow and Ice Covers: Interactions with the Atmosphere and Ecosystems (Proceedings of Yokohama Symposia J2 and J5, July 1993). IAHS Publ. no. 423.

Nakai, Y., Sakamoto, T., Terajima, T., Kitamura, K., and Shirai, T., 1999a. Energy balance above a boreal coniferous forest: a difference in turbulent fluxes between snow-covered and snowfree canopies. Hydrological Processes, 13, 515–529.

Nakai, Y., Sakamoto, T., Terajima, T., Kitamura, K., and Shirai, T., 1999b. The effect of canopy-snow on the energy balance above a coniferous forest. Hydrological Processes, 13, 2371–2382.

Neumann, N.N., Derksen, C., Smith, C., and Goodison, B., 2006. Characterizing local scale snow cover using point measurements during the winter season. Atmosphere Ocean, 44(3), 257 – 269.

Nichol, C.J., Huemmrich, K.F., Black, T.A., Jarvis, P.G., Walthall, C.L., Grace, J., and Hall, F.G., 2000. Remote sensing of photosynthetic-light-use efficiency of boreal forest. Agricultural and Forest Meteorology, 101, 131 -142.

Niemi, K., Metsamaki, S., Pulliainen, J., Suokanerva, H., Bottcher, K., Lepparanta, M., and Pellikka, P., 2012. The behaviour of mast-borne spectra in a snow-covered boreal forest. Remote Sensing of Environment, 124, 551 ‑ 563.

Niu, G-Y, and Yang, Z-L., 2004. Effects of vegetation canopy processes on snow surface energy and mass balances. Journal of Geophysical Research, 109: D23111. doi: 10.1029/2004JD004884.

Nolin, A.W., 2010. Recent advances in remote sensing of seasonal snow. Journal of Glaciology, 56 (200), 1141–1150.

Painter, T.H., Berisford, D.F., Boardman, J.W., Bormann, K.J., Deems, J.S., Gehrke, F., et al., 2016. The Airborne Snow Observatory: Fusion of scanning lidar, imaging spectrometer, and physically-based modeling for mapping snow water equivalent and snow albedo. Remote Sensing of Environment, 184, 139–152. doi:10.1016/j.rse.2016.06.018.

Painter T. H., Rittger, K., McKenzie, C., et al., 2009. Retrieval of subpixel snow covered

area, grain size, and albedo from MODIS. Remote Sensing of Environment, 22, 1-14.

Pan, M., Sheffield, J., Wood, E.F., Mitchell, K.E., Houser, P.R., Schaake, J.C., Robock, A., Lohmann, D., Cosgrove, B., Duan, Q., and Luo, L., 2003. Snow process modeling in the North American Land Data Assimilation System (NLDAS): 2. Evaluation of model simulated snow water equivalent. Journal of Geophysical Research: Atmospheres, 108, 8850. doi:10.1029/2003JD003994.

Papesch, A.J.G., 1984. Wind and its Effects on Canterbury Forests. University of Canterbury, Christchurch, New Zealand, pp. 156 – 157 (p. 181ff., PhD thesis).

Parajka, J., Haas, P., Kirnbauer, R., Jansa, J., and Blöschl, G., 2012. Potential of time-lapse photography of snow for hydrological purposes at the small catchment scale. Hydrological Processes, 26, 3327–3337.

Parviainen, J. and Pomeroy, J.W., 2000. Multiple-scale modelling of forest snow sublimation: initial findings. Hydrological Processes, 14, 2669-268.

Peterson, N., and Brown, A., 1975. Accuracy of snow measurements. Proceedings of the Western Snow Conference, 43, 1-9.

Pietroniro, A., Fortin, V., Kouwen, N., Neal, C., Turcotte, R., Davison, B., Verseghy, D., Soulis, E. D., Caldwell, R., Evora, N., and Pellerin, P., 2007. Development of the MESH modelling system for hydrological ensemble forecasting of the Laurentian Great Lakes at the regional scale. Hydrology and Earth System Sciences, 11, 1279–1294. doi:10.5194/hess-11-1279-2007.

Pirazzini, R., 2004. Surface albedo measurements over Antarctic sites in summer. Journal of Geophysical Research, 109, D20118. doi:10.1029/2004JD004617.

Pomeroy, J.W., and Dion, K., 1996. Winter radiation extinction and reflection in a boreal pine canopy: measurements and modelling. Hydrological Processes, 10, 1591 – 1608.

Pomeroy, J.W., Essery, R.L.H., and Helgason, W.D., 2016a. Aerodynamic and radiative controls on the snow surface temperature. Journal of Hydrometeorology, 17, 2175 – 2189. doi:10.1175/JHM-D-15-0226.1.

Pomeroy, J.W., Fang, X., and Ellis, C., 2012. Sensitivity of snowmelt hydrology in Marmot Creek, Alberta, to forest cover disturbance. Hydrological Processes, 26, 1891 – 1904.

Pomeroy, J.W., Fang, X. and Marks, D.G., 2016b. The cold rain-on-snow event of June

2013 in the Canadian Rockies - characteristics and diagnosis. Hydrological Processes, 30, 2899-2914. doi: 10.1002/hyp.10905.

Pomeroy J.W. and Goodison B.E., 1997. Winter and snow. In The Surface Climates of Canada, Bailey WG, Oke TR, Rouse WR (eds). McGillQueen's University Press: Montreal, Quebec; 68–100.

Pomeroy, J.W. and Granger, R.J., 1997. Sustainability of the western Canadian boreal forest under changing hydrological conditions - I- snow accumulation and ablation In (eds. D. Rosjberg, N. Boutayeb, A. Gustard, Z. Kundzewicz and P Rasmussen) Sustainability of Water Resources under Increasing Uncertainty (IAHS Publ No. 240) 237 - 242p. IAHS Press, Wallingford, UK.

Pomeroy, J.W. and Gray, D.M., 1995. Snowcover: Accumulation, Relocation, and Management. National Hydrology Research Institute, Saskatoon, Canada, NHRI Science Report, 7, Saskatoon, 144 pp.

Pomeroy, J W., Gray, D.M., Brown, T., Hedstrom, N.R., Quinton, W.L., Granger, R.J., and Carey, S.K., 2007. The cold regions hydrological process representation and model: a platform for basing model structure on physical evidence. Hydrological Processes, 21, 2650–2667.

Pomeroy, J.W., Gray, D.M., Hedstrom, N.R., and Janowicz, J.R., 2002. Prediction of seasonal snow accumulation in cold climate forests. Hydrological Processes, 16(18), 3543–3558. doi:10.1002/hyp.1228.

Pomeroy, J.W., Gray, D.M. and Landine, P.G., 1993. The Prairie Blowing Snow Model: characteristics, validation, operation, Journal of Hydrology, 144, 165-192.

Pomeroy, J.W., Gray, D.M., Shook, K.R., Toth, B., Essery, R.L.H., Pietroniero, A., and Hedstrom, N., 1998a. An evaluation of snow accumulation and ablation for land surface modelling. Hydrological Processes, 12, 2339–2367.

Pomeroy, J.W., and Li, L., 2000. Prairie and Arctic areal snow cover mass balance using a blowing snow model. Journal of Geophysical Research, 105, 26619–26634.

Pomeroy, J.W., Marks, D., Link, T.E., Ellis, C.R., Hardy, J., Rowlands, A., and Granger, R.J., 2009. The impact of coniferous forest temperature on incoming longwave radiation to melting snow. Hydrological Processes, 23, 2513 – 2525.

Pomeroy, J.W., Parviainen, J., Hedstrom, N.R., and Gray, D.M., 1998b. Coupled modeling of forest snow interception and sublimation. Hydrological Processes, 12, 2317–2337.

Pomeroy, J.W., Rowlands, A., Hardy, J., Link, T.E., Marks, D., Essery, R.L.H., Sicart, J.E. and Ellis, C.R., 2008. Spatial variability of shortwave irradiance for snowmelt in forests. Journal of Hydrometeorology, 9, 1482-1490.

Pomeroy, J.W. and Schmidt, R.A., 1993. The use of fractal geometry in modeling intercepted snow accumulation and sublimation. Proceedings of the Eastern Snow Conference, 50, 1 – 10.

Pomeroy, J.W., Shook, K., Fang, X., Dumanski, S., Westbrook, C., Brown, T., 2014. Improving and testing the prairie hydrological model at Smith Creek Research Basin. Centre for Hydrology Report No. 14. May 2014.

Priestley, C.H.B., and Taylor, R.J., 1972. On the assessment of surface heat flux and evaporation using large-scale parameters. Monthly Weather Review, 100, 81 – 92.

Pulliainen, J, and Hallikainen, M., 2001. Retrieval of regional snow water equivalent from spaceborne passive microwave observations. Remote Sensing of Environment, 75, 76–85.

Rasouli, K., Pomeroy, J.W., Janowicz, J.R., Carey, S.K. and Williams, T.J., 2014. Hydrological sensitivity of a northern mountain basin to climate change. Hydrological Processes. doi: 10.1002/hyp.10244.

Rasouli, K., Pomeroy, J.W., and Marks, D., 2015 Snowpack sensitivity to perturbed climate in a cool mid-latitude Mountain Catchment. Hydrological Processes. 29, 3925-3940. doi:10.1002/hyp.10587.

Reichle, R.H., 2008. Data assimilation methods in the Earth sciences. Advances in Water Resources, 31, 1411–1418.

Reichle, R.H., Koster, R.D., Liu, P., Mahanama, S.P.P., Njoku, E.G., Owe, M., 2007. Comparison and assimilation of global soil moisture retrievals from the Advanced Microwave Scanning Radiometer for the Earth Observing System (AMSR-E) and the Scanning Multichannel Microwave Radiometer (SMMR). Journal of Geophysical Research, 112 (D9) Art. Nb. D09108.

Reichile, R.H., Walker J.P., Koster R.D., and Houser P.R., 2002. Extended versus Ensemble Kalman Filtering for Land Data Assimilation. Journal of hydrometeorology, 3, 728-740.

Rittger, K., Kahl, A., and Dozier, J., 2011. Topographic distribution of snow water equivalent in the Sierra Nevada. Proceedings of the Western Snow Conference, 79, 37–

46.

Rodell, M., Houser, P.R., Jambor, U., Gottschalck, J., Mitchell, K., Meng, C.J., Arsenault, K., Cosgrove, B., Radakovich, J., Bosilovich, M., Entin, J.K., Walker, J.P., Lohmann, D., and Toll, D., 2004. The global land data assimilation system. Bulletin of the American Meteorological Society, 85, 381-394.

Rodell, M. and Houser, P.R., 2004. Updating a land surface model with MODIS-derived snow cover. Journal of hydrometeorology, 5, 1064-1075.

Roth, T.R. and Nolin, A.W., 2019. Characterizing maritime snow canopy interception in forested mountains. Water Resources Research. doi: 10.1029/2018WR024089.

Rothwell, R., Hillman, G., and Pomeroy, J.W., 2016. Marmot creek experimental watershed study. The Forestry Chronicle, 92, 32 – 36. doi:10.5558/tfc2016-010.

Roy, D.P., Wulder, M.A., Loveland, T.R., Woodcock, C.E., Allen, R.G., Anderson, M.C., Helder, D., Irons, J.R., Johnson, D.M., Kennedy, R., Scambos, T.A., Schaaf, C.B., Schott, J.R., Sheng, Y., Vermote, E.F., Belward, A.S., Bindschadler, R., Cohen, W.B., Gao, F., Hipple, J.D., Hostertt, P., Huntington, J., Justice, C.O., Kilic, A., Kovalskyy, V., Lee, Z.P., Lymburner, L., Masek, J.G., McCorkel, J., Shuai, Y., Trezza, R., Vogelmann, J., Wynne, R.H., and Zhu, Z., 2014. Landsat-8: science and product vision for terrestrial global change research. Remote Sensing of Environment, 145, 154 – 172.

Rutter, A.J., Kershaw, K.A., Robins, P.C. and Morton, A.J., 1971. A predictive model of rainfall interception in forests, 1. Derivation of the model from observations in a plantation of Corsican pine. Agricultural and Forest Meteorology, 9, 367-384.

Ryan, W.A., Doesken, N.J., and Fassnacht, S.R., 2008. Evaluation of ultrasonic snow depth sensors for US snow measurements. The Journal of Atmospheric and Oceanic Technology, 25(5), 667–684.

Salomonson, V.V., and Appel, I., 2004. Estimating the fractional snow covering using the normalized difference snow index. Remote Sensing of Environment, 89, 351 – 360.

Salomonson, V.V., and Appel, I., 2006. Development of the Aqua MODISNDSI fractional snow cover algorithm and validation results. IEEE Transactions on Geoscience and Remote Sensing, 44 (7), 1747 – 1756.

Salvatori, R., Plini, P., Giusto, M., Valt, M., Salzano, R., Montagnoli, M., Cagnati, A., Crepaz, G., and Sigismondi, D., 2011. Snow cover monitoring with images from digital camera systems. Italian Journal of Remote Sensing, 43, 137 – 145. doi:10.5721/ItJRS201143211.

Satterlund, D.R. and Haupt, H.F., 1967. Snow catch by conifer crowns. Water Resources Research, 3, 1035-1039.

Schmidt, R.A., 1991. Sublimation of snow intercepted by an artificial conifer. Agricultural and Forest Meteorology, 54, 1 –27.

Schmidt, R.A. and Gluns, D.R., 1991. Snowfall interception on branches of three conifer species. Canadian Journal of Forest Research, 21, 1262-1269.

Schmidt, R.A., Jairell, R.L., and Pomeroy, J.W., 1988. Measuring snow interception and loss from an artificial conifer. Proceedings of the 56th Western Snow Conference, pp. 166–169.

Schmidt, R.A. and Pomeroy, J.W., 1990. Bending of a conifer branch at subfreezing temperatures: implications for snow interception. Canadian Journal of Forest Research, 20, 1250-1253.

Schneiderman, E., Matonse, A., Zion, M., Lounsbury, D., Mukundan, R., Pradhanang, S., and Pierson, D., 2013. Comparison of approaches for snowpack estimation in New York City watersheds. Hydrological Processes, 27, 3050–3060. doi:10.1002/hyp.9868.

Sesnie, S.E., Dickson, B.G., Rosenstock, S.S., and Rundall, J.M., 2011. A comparison of Landsat TM and MODIS vegetation indices for estimating forage phenology in desert bighorn sheep (Ovis canadensis nelsoni) habitat in the Sonoran Desert, USA. International Journal of Remote Sensing, 33, 276 – 286.

Sheffield, J., Pan, M., Wood, E.F., Mitchell, K.E., Houser, P.R., Schaake, J.C., Robock, A., Lohmann, D., Cosgrove, B., Duan, Q., Luo, L., Higgins, R.W., Pinker, R.T., Tarpley, J.D., and Ramsay, B.H., 2003. Snow process modeling in the North American Land Data Assimilation System (NLDAS):1. Evaluation of model-simulated snow cover extent. Journal of Geophysical Research, 108(D22): 8849. doi: 10Ð1029/2002JD003274.

Shuai, Y., Masek, J.G., Gao, F., and Schaaf, C.B., 2011. An algorithm for the retrieval of 30-m snow free albedo from Landsat surface reflectance and MODIS BRDF. Remote Sensing of Environment, 115, 2204 – 2216.

Sicart, J.E., Pomeroy, J.W., Essery, R.L.H., and Bewley, D., 2006. Incoming longwave radiation to melting snow: observations, sensitivity and estimation in northern environments. Hydrological Processes, 20, 3697 – 3708. doi:10.1002/hyp.6383.

Slater, A.G. and Clark, M.P., 2006. Snow data assimilation via an ensemble Kalman

filter. Journal of Hydrometeorology, 7, 478–493. doi:10.1175/jhm505.1.

Smith, C.D., 2007. Correcting the wind bias in snowfall measurements made with a Geonor T-200B precipitation gauge and alter wind shield. Proc. 87th American Meteorology Society Annual Meeting, San Antonio, Texas.

Smith, C.D., 2009. The relationship between snowfall catch efficiency and wind speed for the Geonor T-200B precipitation gauge utilizing various wind shield configurations. Proceedings of the 77th Western Snow Conference, pp. 115 – 121, Canmore AB.

Sobrino, J.A., Jimenez-Munoz, J.C., and Paolini, L., 2004. Land surface temperature retrieval from Landsat TM 5. Remote Sensing of Environment, 90, 434 – 440.

Stähli, M., Jonas, T., and Gustafsson, M.D., 2009. The role of snow interception in winter-time radiation processes of a coniferous sub-alpine forest. Hydrological Processes, 23. 2498–2512. doi: 10.1002/hyp.7180.

Steppuhn, H., and Dyck, G.E., 1974. Estimating true basin snowcover, in: Advanced Concepts and Techniques in the Study of Snow and Ice Resources, US National Academy of Sciences, Washington, DC, 304–313.

Stewart, I.T., Cayan, D.R., and Dettinger, M.D., 2005. Changes toward earlier streamflow timing across Western North America. Journal of Climate, 18(8), 1136–1155.

Stigter, E.E., Wanders, N., Saloranta, T.M., Shea, J.M., Bierkens, M.F.P., and Immerzeel, W.W., 2017. Assimilation of snow cover and snow depth into a snow model to estimate snow water equivalent and snowmelt runoff in a Himalayan catchment. The Cryosphere, 1647-1664.

Storck, P., Lettenmaier, D.P., and Bolton, S., 2002. Measurement of snow interception and canopy effects on snow accumulation and melt in mountainous maritime climate, Oregon, USA. Water Resources Research, 38, 1223–1238.

Sturm, M., Taras, B., Liston, G.E., Derksen, C., Jonas, T., and Lea, J., 2010. Estimating snow water equivalent using snow depth data and climate classes. Journal of Hydrometeorology, 11, 1380–1394.

Sukyer, A.E., Verma, S.B., and Arkebauer, T.J., 1997. Season-long measurement of carbon dioxide exchange in a boreal fen. Journal of Geophysical Research. 102(D24), 29,021–29,028.

Sun, S., Jin, J., and Xue, Y., 1999. A simple snow-atmosphere-soil transfer model.

Journal of Geophysical Research, 104, 19,587–19,597.

Sun, C., Walker, J.R., and Houser, P.R., 2004. A methodology for snow data assimilation in a land surface model. Journal of Geophysical Research, 109, D08108. doi:10.1029/2003JD003765.

Suzuki, k and Nakai, Y., 2008. Canopy snow influence on water and energy balances in a coniferous forest plantation in northern Japan. Journal of Hydrology, 352, 126 – 138.

Tait, A.B., 1998. Estimation of snow water equivalent using passive microwave radiation data. Remote Sensing of Environment, 64, 286–91.

Tarboton, D.G., and Luce, C.H., 1996. Utah Energy Balance Snow Accumulation and Melt Model (UEB). Utah Water Research Laboratory, Utah University and USDA Forest Service, Intermountain Research Station. 41 p.

Tedesco, M. and Narvekar, P., 2010. Assessment of the NASA AMSR-E SWE product. IEEE Journal of Selected Topics in Applied Earth Observations and Remote Sensing, 3(1), 141–159.

Tennyson, L.C., Ffolliott, P.F., and Thorud, D.B., 1974. Use of time-lapse photography to assess potential interception in Arizona Ponderosa Pine. Water Resources Bulletin, 10, 1246–1254.

Toure, A.M., Goïta, K., Royer, A., Kim, E.J., Durand, M., Margulis, S.A., and Lu, H., 2011. A case study of using a multilayered thermodynamical snow model for radiance assimilation. IEEE Transactions on Geoscience and Remote Sensing, 49, NO. 8.

Valor, E., and Caselles, V., 1996. Mapping land surface emissivity from NDVI: application to European, African, and South American areas. Remote Sensing of Environment, 57, 167 – 184.

Van de Griend, A., and Owe, M., 1993. On the relationship between thermal emissivity and the normalized difference vegetation index for natural surfaces. International Journal of Remote Sensing, 14, 1119 – 1131.

Verseghy, D.L., 1991. CLASS-A Canadian land surface scheme for GCMs. I. soil model. The International Journal of Climatology, 11, 111-133.

Vrugt, J.A., ter Braak, C.J.F., Clark, M.P., Hyman, J.M., and Robinson, B.A., 2008. Treatment of input uncertainty in hydrologic modeling: Doing hydrology backward with Markov chain Monte Carlo simulation. Water Resources Research, 44, W00B09. doi:10.1029/2007WR006720.

Vuyovich, C.M., Jacobs, J.M., and Daly, S.F., 2014. Comparison of passive microwave and modeled estimates of total watershed SWE in the continental United States. Water Resources Research, 50. doi:10.1002/2013WR014734.

Wang, X., Wang, J., Jiang, Z., Li, H., and Hao, X., 2015. An effective method for snow-cover mapping of dense coniferous forests in the upper Heihe River basin using Landsat operational land imager data. Remote Sensing, 7, 17246 – 17257.

Wang, X., Wang, J., Che, T., Huang, X., Hao, X., and Li, H., 2018. Snow cover mapping for complex mountainous forested environments based on a multi-index technique. IEEE Journal of Selected Topics in Applied Earth Observations and Remote Sensing, 11, 1433 – 1441.

Warren, S.G., 1982. Optical properties of snow. Reviews of Geophysics, 20, 67 – 89.

Watt, A., and Watt, M., 1992. Advanced Animation and Rendering Techniques: Theory and Practice. ACM Press, New York.

Wayand, N.E., Marsh, C.B., Shea, J.M., and Pomeroy, J.W., 2018. Globally scalable alpine snow metrics. Remote Sensing of Environment, 213, 61 – 72.

Wigmosta, M.S., Vail, L.W., and Lettenmaier, D.P., 1994. A distributed hydrology-vegetation model for complex terrain. Water Resources Research, 30(6), 1665-1679.

Winkler, R.D., Spittlehouse, D.L., and Golding, D.L., 2005. Measured differences in snow accumulation and melt among clearcut, juvenile, and mature forests in southern British Columbia. Hydrological Processes, 19(1), 51 – 62.

Wood, E.F., Lettenmaier, D.P., and Zartarian, V.G., 1992. A land-surface hydrology parameterization with subgrid variability for general circulation models. Journal of Geophysical Research, 97, D3, 2717-2728.

Woods, S., Ahl, R., Sappington, J., and McCaughey, W., 2006. Snow accumulation in thinned lodgepole pine stands, Montana, USA. Forest Ecology and Management, 235, 202 – 211.

Yamazaki, T., Fukabori, K., and Kondo, J., 1996. Albedo of forest with crown snow (in Japanese). Journal of the Japanese Society of Snow and Ice, 58, 11 – 18.

Yu, X., Guo, X., and Wu, Z., 2014. Land surface temperature retrieval from Landsat 8 TIRS—comparison between radiative transfer equation-based method, split window algorithm and single channel method. Remote Sensing, 6, 9829 – 9852.

Zaitchik, B.F. and Rodell, M., 2009. Forward-looking assimilation of MODIS-derived snow-covered area into a land surface model. Journal of hydrometeorology, 10, 130-148.

Zhang, Z., Kane, D.L., and Hinzman, L.D., 2000. Development and application of a spatially-distributed Arctic hydrological and thermal process model (ARHYTHM). Hydrological Processes, 14, 1017–1044.

Zhao, L., and Gray, D.M., 1999. Estimating snowmelt infiltration into frozen soils. Hydrological Processes, 13, 1827 – 1842.

Zreda, M., Shuttleworth, J.W., Zeng, X., Zweck, C., Desilets, D., Franz, T., Rosolem, R., and Ferre, T.P.A., 2012. COSMOS: the COsmic-ray soil moisture observing system. Hydrology and Earth System Sciences, 16, 4079 – 4099.

Appendix A

This section presents some images and data, which are not shown in Chapter 3, to provide more details of this research. Figure A.1 presents two selected time-lapse photos that taken on the date with no snow on the canopy (left, Apr. 08th 2015) and with snow on the canopy (right, Apr. 15th 2015). These images illustrate the different look in RGB photos of snowcovered and snow-free canopies. Table A.1 shows the parameters that used in PRACTISE for processing these images. Most of these parameters were determined according to the field measurements or camera specifications except the target position (X and Y). Unlike the camera position, it is not possible to measure the target position for these images in this research. Therefore, it was determined using the ground control point module in PRACTISE using 18 GCPs. Figure A.2 provides the Landsat 8 images derived NDSI, NDVI, albedo, and LST for MCRB on two dates with snow and without snow on the forest canopies. From these images, one can clearly see how different these indices were when snow was covered or not on the canopies with just eyes. For all indices, the boundaries of the big clearings on the upper right side of the basin were much clearer when there was no snow on the canopies. This can be explained by the fact that canopy snow reduced the heterogeneity of these indices between forest canopy and ground snow surface in clearings. Table A.2 shows the multiple linear regression statistics among changes of NDSI, NDVI, and albedo and SEA, elevation (E), slope (S), aspect (A), and canopy coverage (C). The equations show the detailed influence of SEA, E, S, A, and C on the changes of NDSI, NDVI, and albedo from snow-free to snowcovered canopy.

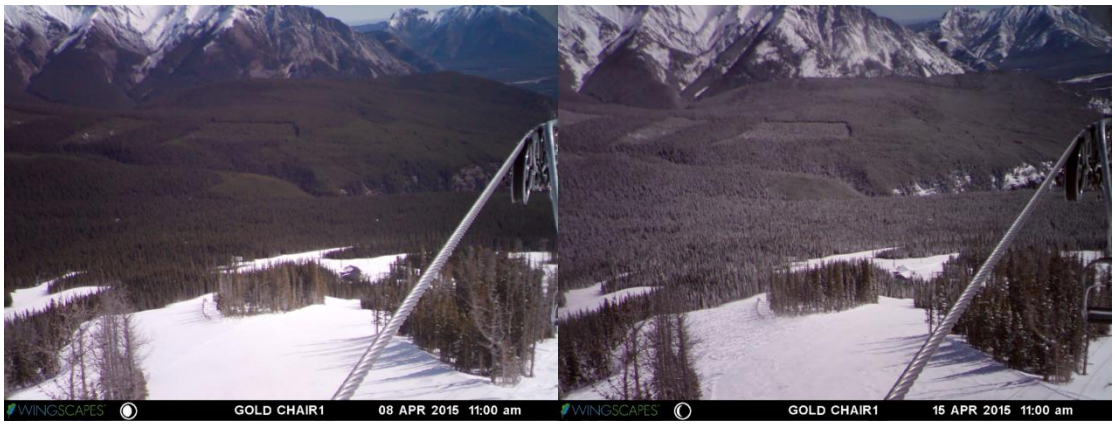

Figure A.1. RGB photos that taken by time-lapse camera on the date with no snow on the canopy (left, Apr. 08th 2015) and with snow on the canopy (right, Apr. 15th 2015) in Marmot Creek Research Basin, Alberta, Canada.

Table A.1. Parameters used in PRACTISE for processing RGB photos that taken by time-lapse camera in Marmot Creek Research Basin, Alberta, Canada.

Parameter name	Value
Camera position X	627245.5
Camera position Y	5645456.718
Target position X	628248.235
Target position Y	5646628.165
offset height	8
roll angle of camera	-4
focal length	0.055
camera sensor height	0.0315
camera sensor width	0.042
pixel rows	2448
pixel columns	3264

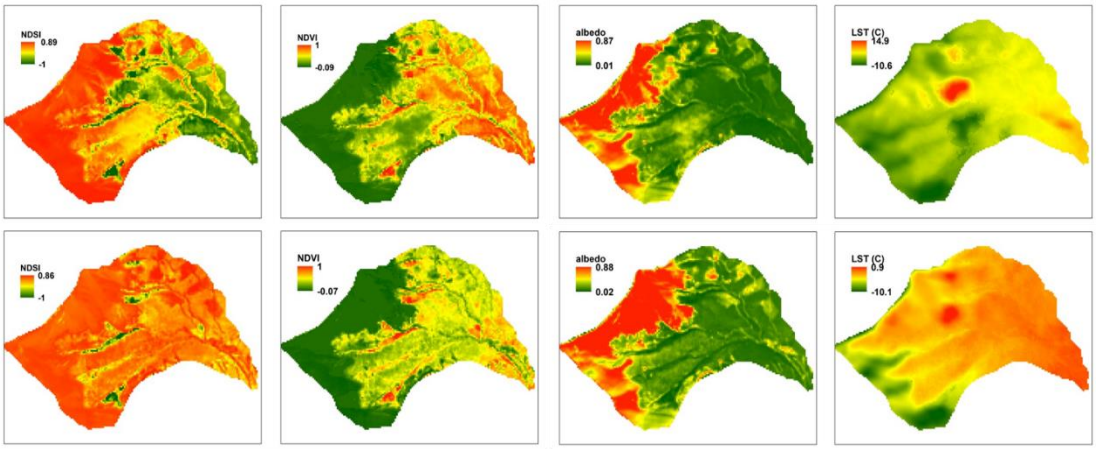

Figure A.2. Landsat 8 images derived NDSI, NDVI, albedo, and LST for Apr. 8th 2015 (upper) and Apr. 15th 2015 (lower) in Marmot Creek Research Basin, Alberta, Canada.

Table A.2. Multiple linear regression statistics among changes of NDSI, NDVI, and albedo and SEA, elevation (E), slope (S), aspect (A), and canopy coverage (C).

Parameter	R^2	Model	p-Value
NDSI			
E,S,A,C,SEA	0.62	Change=-0.0019E-0.0061S+0.1A+1.56C-0.0027SEA+3.81	<0.05
E,S,A,C	0.61	Change=-0.0019E-0.0061S+0.1A+1.56C+3.73	<0.05
E,S,A	0.30	Change=-0.004E+0.00063S+0.16A+8.3	<0.05
E,S	0.26	Change=-0.0038E+0.0029S+7.86	<0.05
E	0.25	Change=-0.0039E+8.1	<0.05
S	0.05	Change=0.017S+0.66	<0.05
A	0.02	Change=-0.0010768A-0.0290316	<0.05
C	0.56	Change=1.79C+0.045	<0.05
SEA	0.01	Change=-0.0027SEA+0.96	<0.05
NDVI			
E,S,A,C,SEA	0.50	Change=0.00067E+0.00037S-0.095A-0.44C-0.000025SEA-1.32	<0.05
E,S,A,C	0.49	Change=0.00067E+0.00037S-0.095A-0.44C-1.32	<0.05
E,S,A	0.32	Change=0.0013E-0.0015S-0.11A-2.6	<0.05
E,S	0.18	Change=0.0011E-0.0031S-2.3	<0.05
E	0.17	Change=0.0012E-2.56	<0.05
S	0.06	Change=-0.007S-0.25	<0.05
A	0.11	Change=-0.096A-0.29	<0.05
C	0.37	Change=-0.56C-0.086	<0.05
SEA	0.00	Change=-0.000025SEA+0.34	0.89
albedo			
E,S,A,C,SEA	0.49	Change=-0.00013E+0.0019S+0.037A-0.11C-0.00056SEA+0.34	<0.05
E,S,A,C	0.43	Change=-0.00013E+0.0019S+0.037A-0.11C+0.33	<0.05
E,S,A	0.26	Change=0.00002E+0.0015S+0.034A+0.0053	<0.05
E,S	0.06	Change=0.0000779E+0.002S-0.089	<0.05
E	0.00	Change=0.0000018E-0.075	0.9
S	0.06	Change=-0.0008518S+0.1006	<0.05
A	0.22	Change=0.035A+0.06	<0.05
C	0.08	Change=-0.064C+0.11	<0.05
SEA	0.06	Change=-0.00056SEA+0.096	<0.05

Appendix B

Data and code availability

Meteorological, snowpack, and streamflow data collected in Marmot Creek Research Basin, Alberta, Canada is available at: http://www.ccrnetwork.ca/outputs/data/index.php.

Thermal images for forest canopy and ground snow surface collected in Fortress Mountain Snow Laboratory Alberta, Canada and the time-lapse RGB images for forest snow conditions that collected in Marmot Creek Research Basin, Alberta are available through Zhibang Lv (Zhibang.lv@usask.ca).

SNODAS data used in Chapter 2 is available at: http://www.nohrsc.noaa.gov/nsa/.

Landsat data used in Chapter 3 is available United States Geological Survey (USGS) website: http://earthexplorer.usgs.gov/.

The CRHM platform is available at Centre for Hydrology, University of Saskatchewan website: http://www.usask.ca/hydrology/.

All the data assimilation works in this research were done by using MATLAB. The code for DA process is available through a GitHub repository found at: https://github.com/ZhibangLv